Analysis of Ubiquitin Signaling in the Human Mitochondrial Protein Import

Dissertation

Zur Erlangung des Grades

„Doktor der Naturwissenschaften“

(Dr. rer. nat.)

am Fachbereich Biologie

der Johannes Gutenberg-Universität Mainz

Nils Christian Krapoth

Geboren am 23.02.1995 in Heppenheim

Mainz, March 2026

Dean: Prof. Dr. Eckhard Thines

1st examiner:

2nd examiner:

Date of defense: 11.05.2026

Declaration

I, Nils Krapoth, declare that the work presented in this thesis is my own. AI-based language assistants (Perplexity and Claude) were used to obtain suggestions for rephrasing. All scientific content, interpretations, and final wording are my own and were critically reviewed and approved by me. I confirm that any information or data obtained from other sources are appropriately indicated in the thesis.

Abstract

Mitochondrial protein import is essential for eukaryotic organisms. Approximately 99% of mitochondrial proteins are imported from the cytoplasm, thereby ensuring proper mitochondrial function. Successful protein import is required for critical mitochondrial functions such as energy production, metabolism and immune signaling. Consequently, cells have developed a broad repertoire of mitochondrial import quality control mechanisms. Import defects are linked to several pathological conditions such as Alzheimer's and Parkinson's disease, and cancer, underscoring mitochondrial protein import quality control a topic of high medical and cell-biological relevance.

Ubiquitin, an essential eukaryotic modifier, appears to be central in the mitochondrial quality control in *S. cerevisiae*, but its role in human cells is poorly characterized. To address this gap of knowledge, a protein-based mitochondrial import clogging model was established in human cells, enabling protein engineering to study mitochondrial quality control. The mitochondrial quality control deals with the mitochondrial clogger by rapid degradation. The mitochondrial clogger is highly ubiquitylated, most likely leading to its degradation in a proteasome-dependent manner. In addition, proximity labeling was employed to characterize the interactome of both the mitochondrial clogger and the clogged mitochondrial surface. This provides an in-depth view on mitochondrial protein-protein interaction networks upon import stress in human cells. A cluster of proteins that regulate OXPHOS and mitochondrial gene expression was enriched in the proximity of the clogged mitochondrial surface. The interactome was unexpectedly enriched in nuclear speckle splicing factors whereas a cluster of proteins centered around the tumor suppressor BRCA1 decreased. Collectively these observations suggest that the mitochondrial surface under mitochondrial import stress defines a mitochondrial-nuclear signaling axis.

The analysis further reveals the potential role of atypical ubiquitylation of the mitochondrial clogger. However, tools to study atypical ubiquitylation *in vivo* remain limited. Therefore, the recently developed Ubiquiton system, which enables inducible ubiquitylation *in vivo,* was extended to include atypical linkages K6 and K11. This provides a perspective for future studies on ubiquitylation during mitochondrial import clogging.

In conclusion, this work connects two essential eukaryotic pathways, mitochondrial protein import and ubiquitin signaling and thereby contributes to a better understanding of the mitochondrial quality control which is crucial for cellular and organismic health.

Zusammenfassung

Der mitochondriale Proteinimport ist essenziell für eukaryotische Organismen. Etwa 99% der mitochondrialen Proteine werden aus dem Zytoplasma importiert. Dies ist Voraussetzung für zentrale mitochondriale Prozesse wie Energieproduktion, Stoffwechsel und Immunantwort. Zellen haben deshalb ein breites Repertoire an Kontrollmechanismen für den mitochondrialen Proteinimport entwickelt. Importdefekte sind mit verschiedenen Krankheiten wie Alzheimer, Parkinson und Krebs assoziiert und unterstreichen die hohe medizinische und zellbiologische Relevanz des mitochondrialen Proteinimports.

Ubiquitin, ein essenzieller eukaryotischer Modifikator, spielt eine zentrale Rolle in der mitochondrialen Qualitätskontrolle in *S. cerevisiae*, während seine Funktion in menschlichen Zellen in diesem Kontext bislang nur unzureichend charakterisiert ist. Dafür wurde ein proteinbasiertes Modell für die Blockierung des mitochondrialen Proteinimports in humanen Zellen etabliert. Dies ermöglicht Protein-engineering, um die mitochondriale Qualitätskontrolle zu untersuchen. Der mitochondriale „Clogger“ wurde in humanen Zellen stark ubiquitiniert, was zu einem rapiden proteasomalen Abbau geführt hat. Außerdem wurde eine Methode etabliert, um das Interaktom des „Cloggers“ und der mitochondrialen Oberfläche zu charakterisieren. Dadurch wird eine detaillierte Analyse von Protein-Protein-Interaktionen der direkten Umgebung des mitochondrialen „Cloggers“ und der mitochondrialen Oberfläche unter Importstress in humanen Zellen ermöglicht. In der direkten Umgebung der verstopften Oberfläche der Mitochondrien waren regulierende Proteine angereichert, die an der Regulation der Zellatmung und der mitochondrialen Genexpression beteiligt sind. Unerwarteterweise war das Interaktom zusätzlich mit RNA-bindenden Faktoren angereichert, während eine Gruppe von Proteinen in Verbindung mit dem Tumorsuppressor BRCA1 verringert war. Dies deutet darauf hin, dass die mitochondriale Oberfläche unter Importstress eine mitochondriale-nukleäre Signalachse definiert.

Ergebnisse dieser Arbeit deuten auf eine potenzielle Rolle atypischer Ubiquitinierung des mitochondrialen „Cloggers“ hin. Da Möglichkeiten zur Untersuchung atypischer Ubiquitinierung *in vivo* bisher begrenzt sind, wurde das Ubiquiton-System, um die atypischen K6- und K11-Ubiquitinketten erweitert. Dadurch wird eine induzierbare Ubiquitinierung mit diesen Verknüpfungen *in vivo* ermöglicht und eröffnet neue Perspektiven für zukünftige Studien zur Rolle der Ubiquitinierung von mitochondrialen Importdefekten.

Zusammenfassend verknüpft diese Arbeit zwei essenzielle eukaryotische Zellprozesse, die Ubiquitinierung von Proteinen mit dem Prozess des mitochondrialen Proteinimports. Dadurch trägt diese Arbeit zu einem besseren Verständnis der mitochondrialen Qualitätskontrolle bei, die von zentraler Bedeutung für die zelluläre und organismische Gesundheit ist.

Contents

List of figures

List of tables

1 Introduction

1.1. Mitochondria - origin, structure and function

Mitochondria also known as the “powerhouse of the cell” are double-membraned organelles carrying their own genomic DNA **(Fig. 1)**. They are essential for virtually all eukaryotic organisms, with the notable exception of protists in the genus *Monocercomonoides* which lack mitochondria entirely (Karnkowska et al., 2016). The name “powerhouse” goes back to their key function of adenosine triphosphate (ATP) synthesis through oxidative phosphorylation (OXPHOS). In addition, mitochondria fulfill critical roles in the cellular metabolism, and signaling, e.g. fatty acid oxidation (FAO), iron-sulfur (Fe-S)-biogenesis, calcium homeostasis and reactive oxygen species (ROS)-mediated pathways (A. J. Anderson et al., 2019). The mitochondrial size ranges between 0.5-10 µm and they can make up to 25% of the cells volume (Pizzorno, 2014). Mitochondrial numbers per cell vary by cell-type, cell cycle stage and energy demand, though precise counts are difficult to obtain partly due to the dynamic nature of the mitochondrial network. Estimations of mitochondrial numbers roughly reflect cell-type-specific energy demands ranging from hundreds in leukocytes, up to thousands in somatic cells such as cardiomyocytes and millions in neurons **(Table 1)** (Moura et al., 2025).

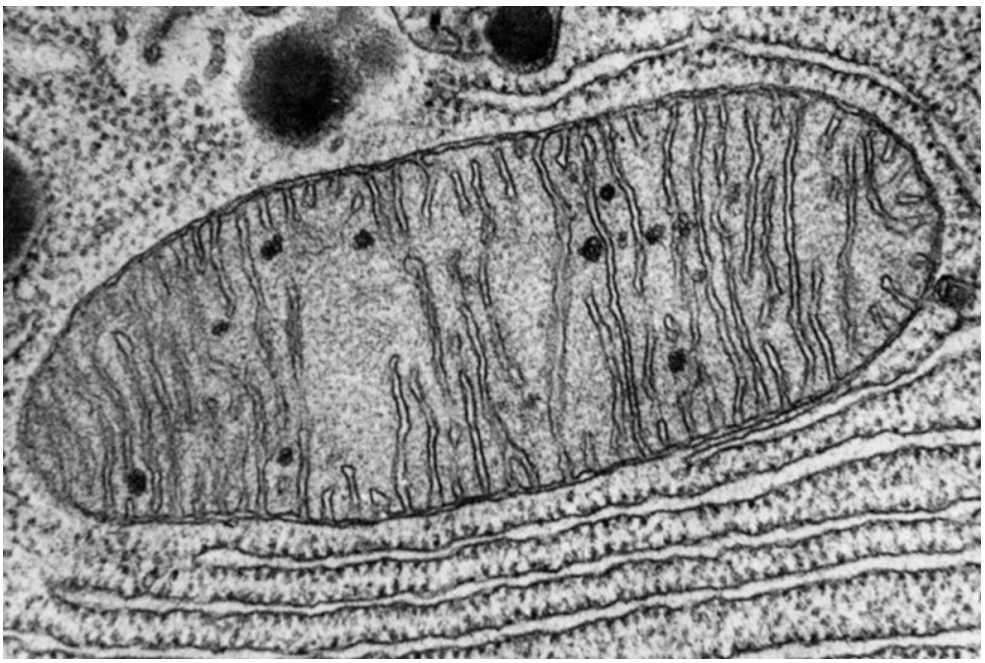

Figure 1 Electron microscopy of a mitochondrion from the bat pancreas. (Moura et al., 2025)

Table 1 Number of mitochondria in different mammalian cell types. Mitochondrial numbers are estimated either on mitochondrial DNA copy number or theoretical estimations (Moura et al., 2025).

Cell type	Number of mitochondria per cell
Cardiomyocytes	3000-8000
Hepatocytes	1000-1700
Skeletal muscle	120-160
Fibroblasts	200-350
Neurons	~2 × 10^6
Macrophages	100-700
Erythrocytes	0
Platelets	4-10
Spermatozoa	50-75
Mature oocyte	10^5
Female germ cells (excluding mature oocytes)	10-5000

1.1.1. The endosymbiotic origin of mitochondria

First, mitochondria have been discovered in 1857 by Rudolf Albert von Kölliker who described them as “strongly refractive granules” within the sarcoplasm of muscle fibers (Kölliker, 1856). Afterwards, Carl Benda was the first to introduce the term ‘mitochondria’ for these granular-like structures in 1898 (Benda, 1898). About 100 years ago, several mitochondrial key characteristics such as their ability to multiply by fission, their pleomorphism and their staining similarities with the same staining agents as bacteria, gave rise to the question of the mitochondrial origin (Wallin, 1927). First, in 1905, Mereschkowsky suggested the symbiotic origin of chloroplasts (C Mereschkowsky, 1905). Based on this idea, it was proposed by Ivan Wallin that mitochondria have arisen from bacterial ancestors in a symbiotic manner which is nowadays consensually accepted and believed to have occurred ~2 billion years ago (Dolezal et al., 2006; Wallin, 1927; Zimorski et al., 2014). Currently, mitochondria are believed to derive from an *α-proteobacterium* taken up by a relative of *Asgard archaea* (Roger et al., 2017). However, until now the specific species of that bacterium and host cell remain uncertain and the process of how a bacterium transitioned into the mitochondrion is still not fully understood (Zimorski et al., 2014).

One major requisite of the endosymbiotic event was the extensive gene transfer that outsourced much of the endosymbiont's genome to the host's nucleus (Raval et al., 2023). In *S. cerevisiae*, a single-celled fungal microorganism, also known as Brewer's yeast and humans approximately ~99% of the mitochondrial proteome is outsourced to the nucleus of the host cell (Badrie et al., 2024). The human mitochondrial DNA (mtDNA) encodes 13 proteins required for OXPHOS, 2 ribosomal RNAs (rRNA) and 22 transfer RNAs (tRNAs) involved in mitochondrial protein synthesis (S. Anderson et al., 1981). Thereby, mitochondria heavily rely on the host cell's protein synthesis and require membrane transporters that facilitate the cellular exchange between the host cell and the endosymbiont. Especially, the development of protein channels mediating the protein transport into and out of the mitochondria enabled the collaboration between host and endosymbiont. This protein import machinery partly consists of highly conserved protein complexes throughout all eukaryotes (Dolezal et al., 2006). Due to their double-membraned structure, mitochondria require a specialized machinery to span both the outer and inner membranes during protein import which will be addressed in the following sections.

1.1.2. Mitochondrial organization

Eukaryotic cells make use of compartmentalization to create specific cellular environments enabling different metabolic activities dependent on specific environments, gradients and polarization (Alberts et al., 2002). Mitochondria are a good example for compartmentalization. They are defined by two membranes: the outer mitochondrial membrane (OMM), which separates mitochondria from the cytoplasm, and the inner mitochondrial membrane (IMM), which forms two distinct internal compartments **(Fig. 2A)** (Roger et al., 2017). The intermembrane space (IMS) defines the space between the OMM and the IMM. The mitochondrial core lays behind the IMM and is called mitochondrial matrix (Suomalainen & Nunnari, 2024).

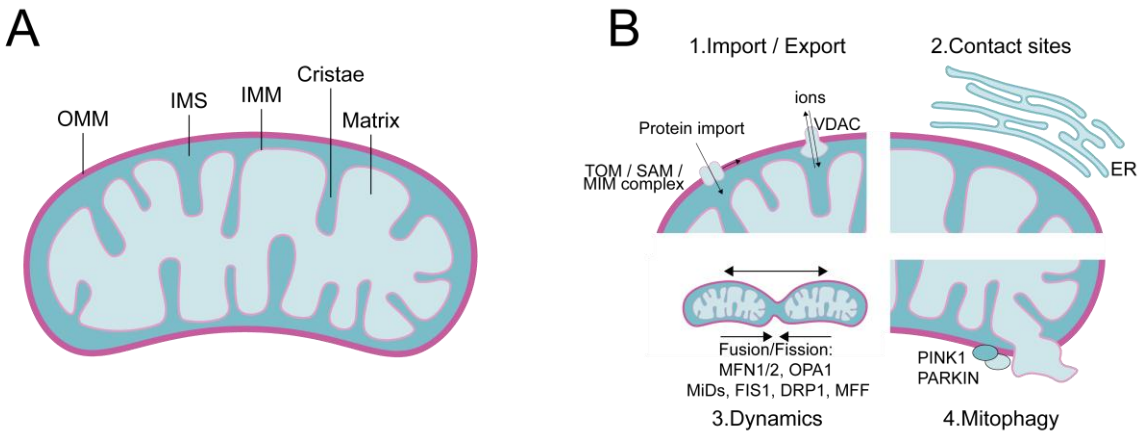

Figure 2 Mitochondrial organization. (A) schematic illustration of the mitochondrial compartmentalization; the outer mitochondrial membrane (OMM) separates mitochondria from the cytoplasm, while the inner mitochondrial membrane (IMM) forms the intermembrane space (IMS) and matrix, including mitochondrial cristae. **(B)** The OMM mediates ion, metabolite and protein import, contact sites with other cell organelles such as the ER, regulation of mitochondrial fusion and fission, and mitophagy signaling.

1.1.2.1. Outer mitochondrial membrane

The OMM mainly consists of lipids and proteins and facilitates the final exchange between mitochondria and the host cell. All OMM proteins are encoded in the nucleus (Muthukumar & Weissman, 2025). These proteins mediate important processes, including import/export of ions, metabolites and proteins; regulate mitochondrial dynamics, quality control and contact sites with other organelles **(Fig. 2B)** (Eaglesfield & Tokatlidis, 2021; Xian & Liou, 2021). Voltage dependent anion channels (VDACs) allow passive diffusion of ions, small peptides and metabolites such as ATP (Varughese et al., 2021). The translocase of the OMM (TOM) mediates the transport of mitochondrial precursor proteins through the OMM while the sorting and assembly machinery (SAM) and the mitochondrial intermembrane space import machinery (MIM) insert proteins into the OMM. Both processes will be described in more detail later **(chapter 1.2)**. Further, OMM proteins such as DRP1 regulate mitochondrial dynamics. Mitochondria undergo fission and fusion in a stress dependent manner (Xian & Liou, 2021). Under acute stress conditions, proteins on the OMM, e.g. PINK1, facilitate the induction of mitophagy **(chapter 1.3.2.3)**.

The OMM displays a hybrid between the ancestral membrane and the host cell. In *S. cerevisiae* the OMM mainly consists of phosphatidylcholine (44%), phosphatidylethanolamine (34%) and phosphatidylinositol (14%) which are typical for eukaryotic membranes. However, also cardiolipin (5%) a phospholipid, mainly found in the IMM and in bacteria are also present in the OMM (Sperka-Gottlieb et al., 1988). Analysis of the fluidity of the OMM and IMM further

revealed a higher dynamic of the OMM. Furthermore, ancestral β-barrel proteins are found in the OMM (Suomalainen & Nunnari, 2024).

1.1.2.2. Intermembrane space

The IMS is the smaller sub compartment of the mitochondria and is defined and surrounded by the OMM and the IMM. Thereby, the IMS serves as a bridging compartment between the OMM and the IMM. Thus the 51 proteins in yeast and 53 human proteins predominantly localizing to the IMS are involved in the protein import into the mitochondrial matrix and assist the cristae organization (Edwards et al., 2021). Furthermore, IMS proteins are involved in protein folding via the mitochondrial intermembrane space assembly (MIA) machinery, redox signaling and homeostasis, apoptosis regulation and metabolite exchange (Edwards et al., 2021). Additionally, proteins in the IMS fulfill the critical surveillance of the IMS by degradation of aggregated and wrongly imported proteins (Weith et al., 2025).

1.1.2.3. The inner mitochondrial membrane

The IMM is the second membrane which separates the mitochondrial matrix from the IMS. The major function of the IMM is the production of ATP. The IMM can be subdivided into the inner boundary membrane and the cristae membrane. The inner boundary membrane is in close contact with the OMM, which is required for signaling between those two membranes and required for accurate protein trafficking (Colina-Tenorio et al., 2020). Second, invaginations of the IMM by the mitochondrial contact site and cristae organizing system (MICOS) form the mitochondrial cristae (Colina-Tenorio et al., 2020). This membrane is called cristae membrane. Cristae rapidly increase the membrane surface which is required for optimal OXPHOS. Besides harboring respiratory chain complexes I, II, III and IV, cristae of the IMM also contain the ATP synthase (Giacomello et al., 2020). While respiratory chain complexes I, III and IV pump protons from the matrix into the intermembrane space, they generate a proton-motive force with two components: a pH gradient and the mitochondrial membrane potential ($\Delta\psi m$) (Geissler et al., 2000). The transfer of protons from the mitochondrial matrix to the IMS leads to a local increase of pH and positive charge in the IMS while the mitochondrial matrix exhibits a more alkaline and negatively charged environment. The ATP synthase now fulfills a dual function (Colina-Tenorio et al., 2020). During the production of ATP, the ATP synthase is fueled by a proton gradient from the IMS back into the mitochondrial matrix which was generated by the respiratory chain complexes (Jonckheere et al., 2012). Thereby, the ATP synthase not only provides energy in the form of ATP but is also required for the maintenance of the mitochondrial proton-motive force. The negative charge in the matrix resulting from $\Delta\psi m$ is required for the protein import into the matrix, acting as a force that pulls the positively charge mitochondrial targeting sequences (MTS) into the matrix (Geissler et al., 2000).

1.1.2.4. The mitochondrial matrix

The mitochondrial matrix not only harbors the mitochondrial genome but also creates the space as a metabolic hub for the synthesis of ATP, cofactors like NAD+, FAD, CoA and Fe-S clusters and regulates the ion homeostasis (Shen et al., 2022). The alkaline environment that is generated by the respiratory chain complexes is the optimal environment for the enzymatic activity in the matrix (A. J. Anderson et al., 2019). The following section will describe those metabolic processes in more detail.

1.1.3. Mitochondrial function

As described above, mitochondria are highly specialized multicompartmental organelles. Compartmentalization allows mitochondria to fulfill a broad palette of cellular functions priming mitochondria central for cellular function (L. Wang et al., 2025). This palette ranges from metabolism, signaling, cellular regulation and immunity **(Fig. 3)** (A. J. Anderson et al., 2019).

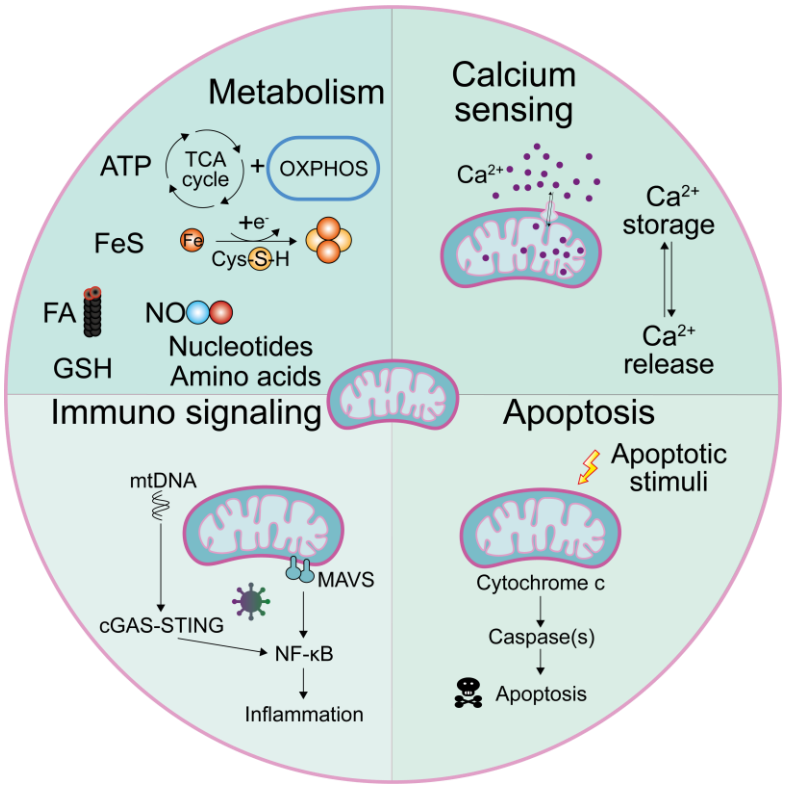

Figure 3 Central mitochondrial functions. Schematic overview of key mitochondrial roles in the cellular metabolism (top left), calcium sensing (top right), immune signaling (bottom left) and apoptosis (bottom right). Metabolic functions include ATP production via the TCA cycle and OXPHOS and the synthesis of metabolites such as fatty acids, Fe-S clusters, glutathione, nitric oxide, nucleotides, and amino acids. Mitochondria contribute to cellular calcium signaling by storage and release of Ca^{2+} ions. Mitochondria are involved in the inflammatory response via MAVS-cGAS-STING-NF-κB. Damaged mitochondria can induce apoptosis via cytochrome c release and caspase activation.

1.1.3.1. Mitochondria and metabolism

Mitochondria are best known for providing energy to the host cell. This is achieved by the combination of the tricarboxylic acid (TCA) cycle with OXPHOS (A. J. Anderson et al., 2019). The TCA cycle is used to deliver electrons to the respiratory chain complexes I-IV which use those electrons to pump protons from the mitochondrial matrix into the IMS. Later on, the ATP synthase uses the derived proton gradient for the ATP synthesis (Fillingame et al., 2003). Byproducts of OXPHOS are ROS which can cause damage to mitochondria and harm the host cell at high levels while also fulfilling essential signaling roles for the cellular homeostasis at physiological concentrations (Dan Dunn et al., 2015; Dizdaroglu & Jaruga, 2012; Finkel & Holbrook, 2000).

Besides providing fuel for the cell in form of ATP, mitochondria are also involved in the production of fatty acids, amino acids, nucleotides and co-factors such as Fe-S clusters (Freibert et al., 2021). The synthesis of some metabolites is utilized by the cell to sense and respond to environmental changes (Frezza, 2017).

1.1.3.2. Mitochondria in cell signaling

Another major mitochondrial role is the sensing and storage of Calcium (Ca). VDACs channel Ca^{2+} ions through the OMM. The IMM membrane calcium uniporter complex (MCU) allows Ca^{2+} uptake into the mitochondrial matrix while its export is facilitated by SLC8A3 (A. J. Anderson et al., 2019). Thereby, mitochondria can store Ca with concentrations approximately ~20x higher compared to the cytoplasm. This function plays an important role in neurotransmitter release, muscle contraction, and cell migration (Giorgi et al., 2018).

While mitochondria are important for cellular calcium signaling, they are also important for the cellular immune response. For example, the OMM protein MAVS facilitates RIG-I signaling upon RNA virus infection (Horner et al., 2011). Furthermore, MAVS is also targeted by a protease of the hepatitis C virus in order to support its infection (Meylan et al., 2005). Furthermore, both the release of ROS and mtDNA can lead to inflammasome activation linking mitochondria to the innate immunity, e.g. by the regulation of cGAS-STING dependent inflammatory response (A. J. Anderson et al., 2019; Zou et al., 2024).

Another important mitochondrial role is the regulation of cell progression and cell death. The metabolic mitochondrial functions further enable a regulatory role during cell-cycle by providing energy and nucleotides (A. J. Anderson et al., 2019). Among others, the mitochondrial protein MFN2 is involved in the proliferative RAS-RAF signaling (K.-H. Chen et al., 2014). Further, apoptosis can be initiated by Ca^{2+} overload and ROS demonstrating the important role of mitochondria to regulate programmed cell death (Vakifahmetoglu-Norberg et al., 2017). During apoptosis mitochondria are permeabilized by BAX-BAK oligomerization leading to the release

of pro-apoptotic proteins into the cytoplasm while VDAC2 seems to counteract apoptosis by sequestration of BAK (A. J. Anderson et al., 2019).

In conclusion, mitochondria fulfill critical functions for the eukaryotic host cell. To perform these diverse functions, mitochondria require the import of proteins from the cytoplasm, as the organelle has outsourced most of its genes (~99%) to the nuclear genome of the host cell.

1.2. Mitochondrial protein import

Mitochondria consist of a double membrane and 99% of the approximately ~1000 (1500^{hum}) mitochondrial proteins in yeast are encoded in the nucleus. Those proteins have to be transported to the mitochondria and imported through membranes to their desired location such as the mitochondrial matrix or the IMS **(Fig. 4)** (Schmidt et al., 2010). Research of the recent years mainly focused on the mitochondrial protein import in the model organism *S. cerevisiae* and this section therefore, mainly describes findings in yeast and mentions the human homologs in brackets, however the conservation of some of these pathways still need to be confirmed (Lithgow & Schneider, 2010). For consistency, yeast and human TOM complex and translocase of the inner membrane (TIM) subunits will be written capitalized in the following sections.

1.2.1. Mitochondrial targeting

Furthermore, two different modes of mitochondrial protein import can be distinguished. (i)The post-translation translocation describes the process of initial ribosomal translation followed by chaperon-guided protein transport and import into the mitochondria. (ii) The co-translational import refers to a translation-coupled protein import mediated via close contact of ribosomes and the mitochondrial surface (Becker et al., 2019). This section focuses on the post-translational mitochondrial protein import which seems to be the prevalent way for mitochondrial protein expression, while the co-translational protein import is described in more detail in the subsequent section **(chapter 1.2.8)** (Becker et al., 2019).

Nuclear encoded mitochondrial proteins are targeted towards mitochondria via MTS. Roughly ~60% of nuclear encoded mitochondrial proteins are targeted towards mitochondria via a short cleavable N-terminal MTS which is positively charged and amphiphilic (Becker et al., 2019); (Boob et al., 2025). Proteins without this canonical MTS contain non-cleavable MTS, for example proteins of the OMM, which are usually targeted via their transmembrane domain (Becker et al., 2019). The general characteristics of the MTS seem to be conserved among eukaryotes (Lithgow & Schneider, 2010).

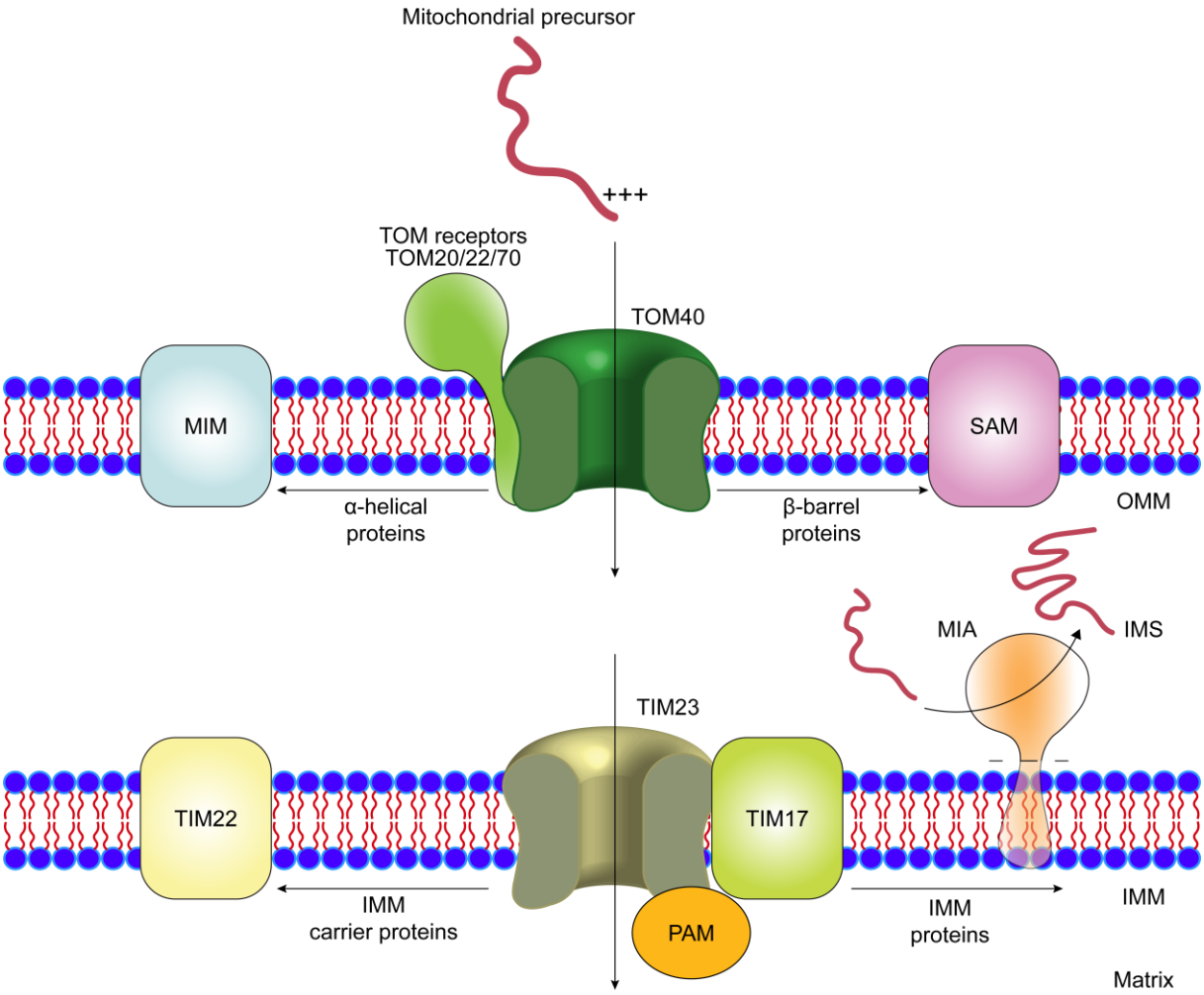

Figure 4 Mitochondrial protein import pathways. Cytosolic mitochondrial precursor proteins are recognized by TOM receptors (TOM20/22/70) and translocated through the OMM by TOM40. α-helical OMM proteins such as TOM20 and TOM70 are inserted via the MIM complex, whereas the SAM complex mediates the insertion of β-barrel proteins, e.g. TOM40. IMS proteins with cysteine motifs are oxidatively refolded by the MIA machinery; the dashed line indicates that the MIA machinery is anchored in the IMM in yeast while this membrane anchoring is lost in metazoans. The TIM22 complex mediates the insertion of IMM carrier proteins, and the TIM23 complex together with the translocase-associated motor PAM accomplishes translocation of matrix proteins and insertion of other IMM proteins.

1.2.2. Chaperon guidance from the cytoplasm to the OMM

After translation, proteins must be transported through the cytoplasm to mitochondria. This transport happens in a chaperon-guided manner to prevent aggregation in the cytoplasm and ensure the required unfolded state for the mitochondrial import (Matouschek et al., 1997). In *S. cerevisiae*, proteins of the chaperon family Hsp70 and Hsp90 either bind the mitochondrial precursor protein directly or are recruited and bind the precursor protein via so-called DnaJ-related cochaperones (J-proteins) in a semi-selective manner (Becker et al., 2019; Bykov et al., 2020; Hoseini et al., 2016; Jores et al., 2018). The delivery of the precursor protein to the mitochondrial membrane is further achieved by an interaction of the guiding chaperone(s) with

TOM receptors. For example, Hsp70 in *S. cerevisiae* and HSP70 and HSP90 in mammalian cells interact with the TOM receptor TOM70 which also exhibits a chaperon-like function (Yamamoto et al., 2009; Young et al., 2003). The co-chaperon Sti1 was found to bind TOM20 and TOM70 *in vitro* (Hoseini et al., 2016). Preferences of MTS to different chaperones and their preferences to different mitochondrial import receptors enable a complex regulation of the mitochondrial protein import. Upon binding to the TOM receptor, the mitochondrial precursor will either be imported through the TOM complex into the IMS or sorted into the OMM via the SAM or MIM complex which will be described in the following sections (Pfanner et al., 2025).

1.2.3. The mitochondrial entry gate: The TOM complex

Mitochondrial protein import through the OMM relies on the “main entry gate”, the TOM complex. Seven subunits form the TOM complex in yeast and mammalian cells (Araiso et al., 2022). High resolution structural analysis have revealed that the channel-forming TOM40 is surrounded by TOM5, TOM6, TOM7 and TOM22 which form a stable complex **(Fig. 5)** (Tucker & Park, 2019). The TOM receptors, TOM20 and TOM70 are associated with the TOM complex in a dynamic manner and can dissociated from the core complex (Ahting et al., 1999). Different oligomeric states of the TOM complex have been described and a trimer is suggested to be the major arrangement, while there is a dynamic exchange to a dimeric and monomeric state (Araiso et al., 2022). The other TOM subunits besides TOM40 can be grouped into two groups: the small TOMs and the receptors of the TOM complex. Both groups will be described in the following sections.

1.2.3.1. The small TOM proteins

TOM5, TOM6 and TOM7 are considered as the small TOMs. Their function is still elusive but recent research has revealed that TOM6 and TOM7 modulate the stability and dynamics of the TOM complex. TOM6 seems to stabilize TOM22 in the TOM complex and the formation of the trimeric state while TOM7 has a rather destabilizing effect (Hönlinger et al., 1996; Sakaue et al., 2019). In contrast to the complex modulating function of TOM6 and TOM7, TOM5 seems to be involved in the transfer of the precursor protein from the TOM receptors to TOM40 (Dietmeier et al., 1997).

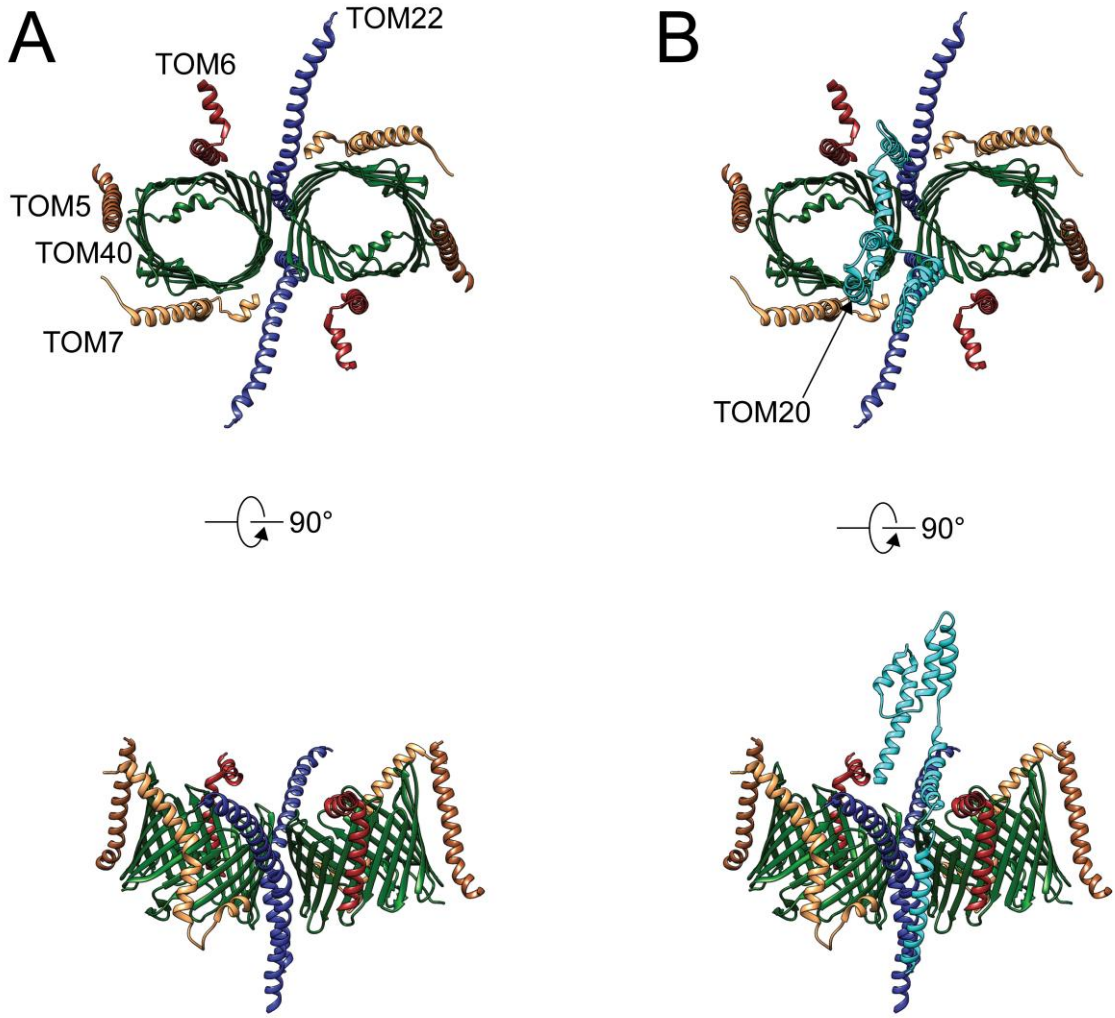

Figure 5 Structure of the human TOM complex. **(A)** Top and side view of the human dimeric core TOM complex composed of the channel forming TOM40 (dark green), and subunits TOM5 (sienna), TOM6 (brown) TOM7 (sandy brown) and TOM22 (medium blue). **(B)** Corresponding views of the TOM complex containing a single copy of the TOM receptor TOM20 (cyan) which can dissociate from the TOM complex (PDB: 8XVA).

1.2.3.2. Mitochondrial import sorting via TOM receptors TOM20, 22 and 70

Mitochondrial protein import relies on the recognition of the MTS by the TOM complex. This is facilitated by the TOM receptors TOM20, TOM22 and TOM70 (Araiso et al., 2022). While both TOM20 and TOM70 are inserted into the OMM via their N-terminal transmembrane domains, exposing their C-termini to the cytoplasm, TOM22 carries a transmembrane region in the middle of the protein exposing its N-terminus to the cytoplasm while C-terminus faces the IMS (Araiso et al., 2022). TOM20 is the major receptor for the recognition of MTS containing proteins and contains a hydrophobic groove that binds the amphiphilic helix of the MTS **(Fig. 6)** (Araiso et al., 2022; Yamano et al., 2008). In contrast to TOM20, TOM70 has a preference for aggregation prone precursor proteins and fulfills a chaperone-like function during the

recognition process (Yamamoto et al., 2009). While TOM22 stably associates with the TOM complex, TOM20 and TOM70 associate with the TOM complex dynamically and can dissociate from the TOM complex (Meisinger et al., 2001). Deletions of TOM20 and TOM22 demonstrate similarities within the precursor specificity of both receptors (Yamano et al., 2008). In addition to the precursor recognition function, TOM22 exhibits a docking site for TOM20 and TOM70. Thereby, TOM22 is involved in the bridging between the two TOM receptors and the channel forming subunit TOM40 as well as in TOM complex stability and formation (Pfanner et al., 2025).

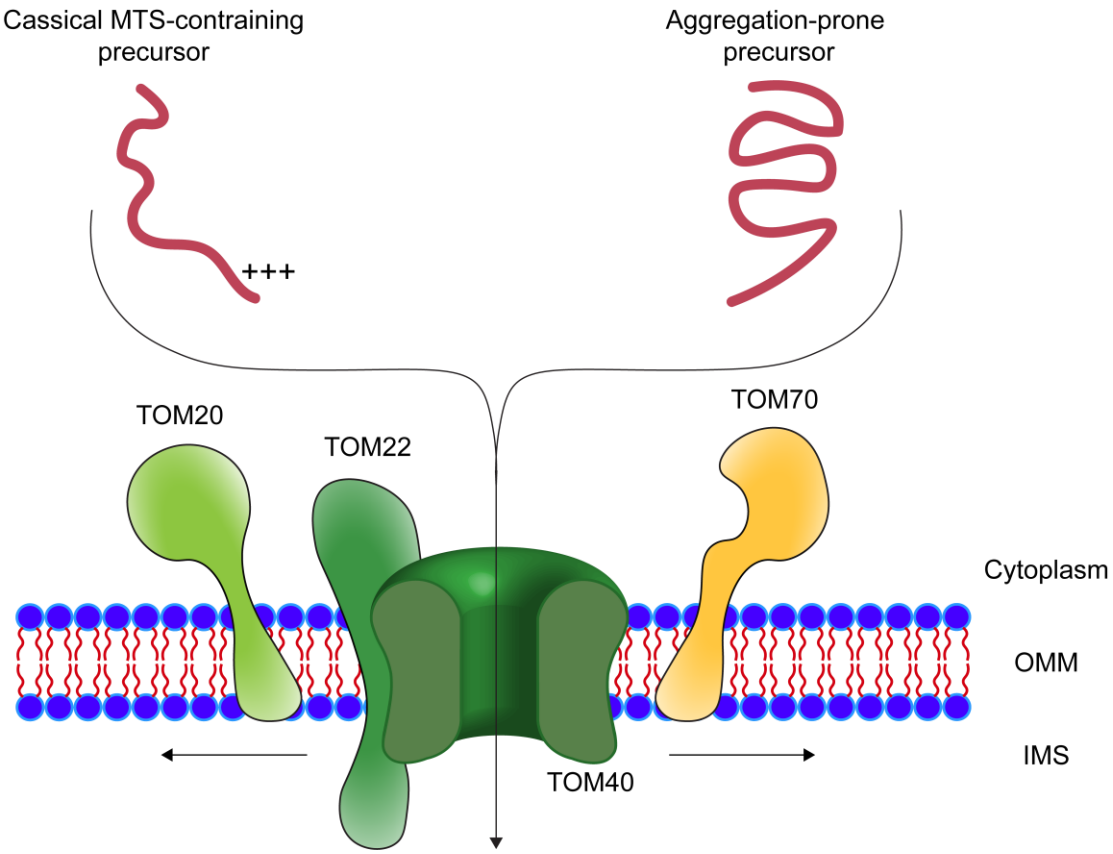

Figure 6 Precursor recognition by TOM20 and TOM70. Classical MTS-containing proteins targeted to the mitochondrial matrix or the IMS are recognized by the TOM complex receptor TOM20, whereas aggregation-prone hydrophobic precursors are recognized by TOM70, which additionally acts in a chaperone-like manner to prevent precursor aggregation. Both TOM20 and TOM70 can dissociate from the TOM complex after substrate delivery.

1.2.4. Protein sorting to the OMM via SAM and MIM

Mitochondrial function further requires the translocation of proteins into the OMM. Especially the insertion of the TOM complex into the OMM is required for the mitochondrial protein import of all other mitochondrial proteins (Ahting et al., 1999). Two different types of proteins are inserted into the OMM: α-helical proteins and β-barrel proteins. Both types are inserted in a

distinguishable manner. β-barrel proteins are first translocated via the TOM complex to the IMS where TIM chaperones guide the transport of the β-barrel protein to the SAM complex which inserts the protein into the OMM (Schmidt et al., 2010). In contrast, α-helical proteins such as the TOM receptors TOM20 and TOM70 are inserted into the OMM via the MIM complex. The MIM complex in *S. cerevisiae* consists of multiple copies of Mim1 and Mim2 that form a channel and translocate the α-helical protein into the OMM (Doan et al., 2020).

1.2.5. Protein import into the IMS

After translocation through the TOM complex, mitochondrial proteins are in the IMS. From here they either travel to the mitochondrial matrix, are inserted into the IMM or reside in the IMS. 53 human proteins mainly reside in the IMS (Edwards et al., 2021). Two major import routes for IMS proteins can be distinguished, both rely on the initial translocation through the TOM complex.

1.2.5.1. IMS import and refolding via MIA

Mitochondrial proteins undergo translocation through the TOM complex as a linearized polypeptide chain (Schmidt et al., 2010). This requires refolding in the IMS. Due to the oxidative environment in the IMS in comparison to the matrix and the cytosol, oxidative refolding is achieved by the MIA machinery **(Fig. 7)** (Endo & Wiedemann, 2025). IMS proteins are mostly targeted towards the IMS without a canonical MTS. Instead, they carry an IMS sorting signal that is recognized by Mia40 ($CHCHD4^{hum}$) (Sideris et al., 2009). Those proteins are translocated through the TOM complex in a TOM20, TOM22 and TOM70 independent manner (Gornicka et al., 2014). In yeast, Mia40 is anchored in the IMM, while in metazoa, Mia40 is a soluble protein in the IMS with close contact to the IMM (Edwards et al., 2021). The oxireductase Mia40 binds the IMS-directed protein upon translocation through TOM40 and forms a disulfide intermediate, ultimately leading to the formation of disulfide bonds of the IMS targeted protein (Endo & Wiedemann, 2025). The sulfhydryl oxidase Erv1 (ALR^{hum}) further recycles Mia40 by re-oxidation of Mia40.

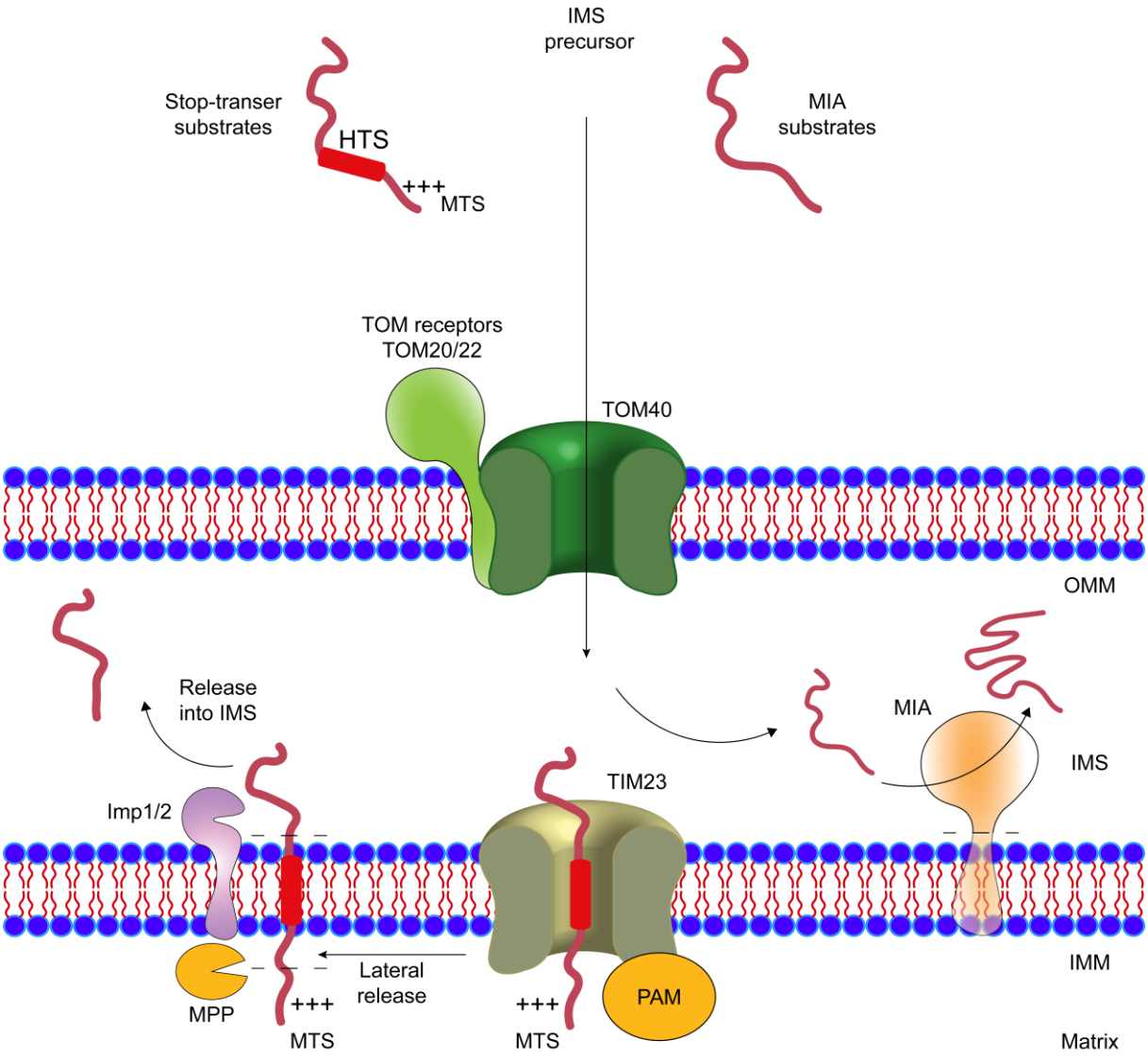

Figure 7 Mitochondrial protein import into the IMS. After translocation through the TOM complex, mitochondrial precursors lacking the canonical MTS are recognized by the MIA machinery via a cysteine containing IMS sorting signal. By contrast, proteins containing a canonical MTS and a hydrophobic transmembrane segment (HTS) are partially translocated through the TIM23 complex, where the HTS domain arrests in the channel, leading to the lateral release of the protein into the IMM, followed by removal of the MTS by MPP and subsequent processing by Imp1/2 which release the mature protein into the IMS.

1.2.5.2. IMS import through the stop-transfer pathway

Mitochondrial proteins that are sorted into the IMS via a stop-transfer pathway consist of a bipartite presequence **(Fig. 7)** (Edwards et al., 2021). This presequence starts with an N-terminal MTS which directs the precursor through the TOM complex towards the mitochondrial matrix. The second part of the presequence contains a hydrophobic transmembrane segment (HTS). The MTS translocates through TIM23, whereas the HTS arrests within the channel, leading to a stop of the transfer. The arrested precursor is thought to be released into the IMM via a lateral gate mechanism by the TIM23 channel, although this mechanism remains

incompletely understood (Edwards et al., 2021). After the lateral release, the matrix processing peptidase (MPP) removes the matrix standing MTS. The mature protein is released from the IMM into the IMS via a second cleavage by Imp1/Imp2 proteases.

1.2.6. Protein import into the IMM and matrix

Upon translocation into the IMS via the TOM complex, proteins are sorted either into the OMM as described above **(chapter 1.2.4)**, remain in the IMS or require further transport into the matrix and IMM. Central for both transport routes is the TIM complex. The TIM complex can be subdivided into the multi-subunit complexes TIM22 and TIM23, with each name derived from its respective central subunit **(Fig. 4)** (Schmidt et al., 2010).

The TIM23 complex facilitates both the import of mitochondrial matrix proteins as well as the insertion of IMM proteins with an IMM-sorting signal. While the TIM22 complex mediates the insertion of IMM carrier proteins with hydrophobic non-cleavable sorting signals such as TIM23 and TIM22 themselves, this process is referred to as “carrier import pathway” (Schmidt et al., 2010).

The TIM23 complex consists of the key and channel forming subunit TIM23 which adopts a dimeric structure, and the Δψm is the driving force for the presequence translocation through TIM23 across the IMM (Truscott et al., 2001). To fulfill both functions, the mitochondrial matrix protein import and the lateral release of transmembrane proteins into the IMM, TIM23 seems to adopt two different conformations which are thought to undergo dynamic alteration in order to facilitate the complexity of the protein import. The subspecies $TIM23^{SORT}$ inserts proteins into the IMM while a PAM associated species $TIM23^{PAM}$ mediates the translocation of mitochondrial matrix proteins (Chacinska et al., 2009). Both $TIM23^{SORT}$ and $TIM23^{PAM}$ consist of the main subunits TIM17, TIM23 and TIM50, but $TIM23^{SORT}$ additionally contains TIM21. In contrast, $TIM23^{PAM}$ lacks TIM21 but associates with PAM subunits (Callegari et al., 2020).

1.2.6.1. The core TIM23 subunits

TIM23 is the channel forming subunit of the TIM23 complex. Although TIM17 shares a high sequence similarity with TIM23, the subunit seems to be unable to form a channel but is required for the accurate pore formation of TIM23 in a dimeric manner (Callegari et al., 2020; Martinez-Caballero et al., 2007). Additionally, TIM17 seems to be involved in the tethering of the PAM complex subunit PAM18 to the TIM23 complex (Chacinska et al., 2005). Furthermore, both TIM21 and TIM50 fulfill dual functions. TIM50 is the main receptor of the TIM23 complex and contains two presequence binding sites. TIM50 binds the presequence containing protein, that is currently bound to a negatively charged IMS facing domain of TOM22. In contrast, TIM21 was found to interact with this domain of TOM22 stimulating the release of the

presequence containing protein to TIM50, guiding it to the TIM23 pore (Chacinska et al., 2009). Together with TIM21, TIM50 serves as a molecular bridge connecting the TOM and TIM23 complexes which delivers the presequence containing protein from the TOM to the TIM23 complex and even super complex formations between the TOM and the TIM23 complex are suggested (Gold et al., 2014). Additionally, TIM50 prevents leakage through TIM23 by closing the channel, and successful protein transfer from TIM50 to TIM23 results in the release of TIM50 from the TIM23 channel, thereby activating it for translocation (Callegari et al., 2020). Furthermore, an interaction between TIM21 and respiratory chain complexes was found (van der Laan et al., 2006). The role of the respiratory chain complexes in the formation of the Δψm indicates that TIM21 might regulate and locally increase this potential in order to accelerate the import via the TIM23 complex (Schmidt et al., 2010).

1.2.6.2. Protein insertion into the IMM via TIM23^{SORT}

The insertion of mitochondrial proteins via an IMM-sorting signal solely depends on the Δψm. The TIM23 complex must distinguish matrix proteins from proteins that should be released into the IMM. This sorting process is complicated and not fully understood but in *S. cerevisiae*, Mgr2 has been proposed as a gatekeeper distinguishing between matrix and IMM proteins based on their hydrophobicity (Kizmaz et al., 2024; Maruszczak et al., 2024). The insertion requires a stop of the translocation and a lateral release of the protein into the IMM which is called stop-transfer and requires a stop-transfer signal. The hydrophobic transmembrane segment seems to interact with hydrophobic domains of TIM17 and TIM23 and might induce the lateral release into the IMM (Rojo et al., 1998). However, the hydrophobic segment might not be sufficient for the stop-transfer and charged residues flanking the hydrophobic transmembrane domain are hypothesized to further assist the arrest of the translocation followed by the lateral release and C-terminal negatively charged residues are indicated to stop the translocation process (Kizmaz et al., 2024; Rojo et al., 1998).

1.2.6.3. Protein import into the mitochondrial matrix via TIM23^{PAM}

In contrast to the lateral release of mitochondrial proteins into the IMM, the translocation of MM proteins requires a second driving force in addition to Δψm, which is facilitated by the PAM complex which functions as ATP dependent motor (Schmidt et al., 2010). A third driving force seems to be the interaction of the presequence of the imported protein with TIM44, which also facilitates the recruitment and anchoring of Hsp70 and other PAM subunits to the TIM23 complex (Demishtein-Zohary & Azem, 2017). ATP hydrolysis by Hsp70 releases the Hsp70 bound precursor protein into the matrix. The cochaperone Mge1, TIM14 and TIM16 regulate the Hsp70 activity. TIM14 and TIM16 have a regulator function on the ATPase activity of Hsp70 while Mge1 is required for the recycling of Hsp70 by replacing ADP with ATP (Demishtein-Zohary & Azem, 2017).

1.2.6.4. Carrier import pathway via TIM22

Mitochondrial carrier proteins, that must be inserted into the IMM, contain multiple α-helical transmembrane segments and require an additional import system. Example carrier proteins are the above mentioned TIM23 and TIM17 subunits of the TIM23 complex and metabolite carriers. Their insertion into the IMM is mediated via the so-called TIM22 complex (Schmidt et al., 2010). Carrier proteins are aggregation prone, and their mitochondrial import is guided via chaperones and TOM70 through the TOM complex. Interestingly, carrier proteins maintain a loop-like structure and are not linearized during the import through the TOM complex (Wiedemann et al., 2001). In the IMS carrier proteins are shuttled to the TIM22 complex by two chaperone complexes TIM9-TIM10 and TIM8-TIM13 (Beverly et al., 2008). The TIM22 channel has an opening towards the lipid bilayer and inserts the carrier protein into the IMM (Nauerz et al., 2025).

1.2.6.5. Membrane insertion of OXPHOS complexes

Mitochondrial encoded respiratory chain complexes are translated in the mitochondrial matrix and are inserted directly via the so-called OXA machinery. Therefore, mitochondrial ribosomes interact with Oxa1 handing over the translated protein. Oxa1 contains a membrane-facing hydrophilic groove that leads to the insertion of the translated protein into the IMM (Endo & Wiedemann, 2025). Furthermore, Oxa1 assists TIM23 during the insertion of less hydrophobic IMM proteins where the stop-transfer mechanism is not involved (Endo & Wiedemann, 2025).

1.2.7. Presequence processing via MPP and IMP and other proteases

Mitochondrial protein import depends on targeting and sorting signals (Schmidt et al., 2010). Those targeting and sorting signals differ depending on the type of protein and the desired destination. However, ~70% of the mitochondrial proteins carry a canonical N-terminal MTS which is positively charged and amphiphilic (Mossmann et al., 2012). The MTS needs to be removed upon correct mitochondrial localization in order to avoid further sorting and refolding problems (Kunová et al., 2022). This is achieved by several specialized metalloproteases, especially by the essential mitochondrial processing peptidases (MPP) (Kutejová et al., 2013). MPP cleaves the MTS in the mitochondrial matrix and the resulting cleavage remnants can be further processed by mitochondrial intermediate peptidases (MIP) Oct1 (MIP^{hum}) and Icp55 (Kücükköse et al., 2021). In contrast to the canonical MTS, the HTS which also serves as a hydrophobic IMM targeting signal is cleaved by the so-called inner membrane processing peptidase (IMP, $IMMP2L^{hum}$) (Kunová et al., 2022). Some proteins, e.g. one of the model protein used in this thesis, cytochrome b2 (b2) are first processed by MPP to remove the N-

terminal targeting sequence before the IMP acts on the hydrophobic targeting signal **(chapter 1.5.4.3)** (Shiota et al., 2012).

1.2.8. Co-translational mitochondrial protein import

Approximately ~99% of all mitochondrial proteins are encoded in the nucleus and transported into the mitochondria. While ~80% of the mitochondrial proteins are thought to be imported in a post-translational way, the remaining ~20% are believed to be imported in a co-translational manner (Z. Zhu et al., 2025). Co-translational protein import describes a process which facilitates the protein translocation through TOM during ongoing translation. In *S. cerevisiae* this mechanism is proposed to prevent aggregation of proteins containing hydrophobic transmembrane domains, in the cytoplasm (Williams et al., 2014). However, in human cells, proteins subjected for mitochondrial co-translational import are characterized by large size, multiple domains and a high force required for unfolding (W. Li et al., 2014).This demonstrates that co-translation protein import also functions in the mitochondrial protein import quality control. The average co-translation import begins after translation of ~350 amino acids but can already start for some proteins after translation of ~200 amino acids. Examples of co-translation protein import are the mitochondrial IMS protease YME1L1^{hum}, DELE1^{hum} and PINK1^{hum} (W. Li et al., 2014).

1.3. Mitochondrial quality control

1.3.1. Molecular causes of mitochondrial import defects

Mitochondrial protein import is critical for mitochondrial functions and import defects can cause severe diseases in humans (MacKenzie & Payne, 2007). Mutations in protein sequences are central for mitochondrial defects. First of all, mutations in the mitochondrial import machinery can disrupt the import function, thus causing mitochondrial import defects (Jain et al., 2024). N-terminal mutations of non-mitochondrial proteins can imitate a MTS and induce mistargeting to the TOM complex (MacKenzie & Payne, 2007). Protein import of those mistargeted proteins can be problematic for the TOM complex, as translocation requires an unfolded state of the import protein. Mutations in the MTS of mitochondrial precursor proteins can lead to protein import deficiencies (MacKenzie & Payne, 2007). Interestingly, import defects through the IMM can also lead to impaired TOM complex translocation (Hasson et al., 2010). Furthermore, mutations in mitochondrial precursor proteins can lead to misfolding and stalling of the precursors in the translocation machinery of mitochondria, which is discussed to be associated with Alzheimer's disease (Coyne et al., 2023; Devi et al., 2006). As the described mitochondrial import defects have severe effects on cellular wellbeing, cells have developed several

mitochondrial quality control (MQC) mechanisms to overcome and prevent mitochondrial import defects.

1.3.2. Cellular response to mitochondrial import defects

Mitochondrial protein import is essential and requires tight quality control mechanisms (K. P. Baker & Schatz, 1991). Major cellular stressors are stalled mitochondrial precursors at the TOM complex which further lead to the accumulation of mitochondrial precursors in the cytoplasm. Several quality control mechanisms are known to date, most of them are based on the model organism *S. cerevisiae* (Pfanner et al., 2025). Furthermore, ubiquitylation plays an important role in activation and regulation of those mitochondrial import quality control (MIQC) mechanisms and is described in more detail in a later section **(chapter 1.5)**. MIQC can be divided into two groups. Group 1 acts on the clogged translocase, while group 2 takes care of accumulating precursor proteins in the cytoplasm. This section will describe both groups in more detail and tries to bridge our understanding from *S. cerevisiae* to mammalian cells.

1.3.2.1. The MIQC pathways mitoTAD and mitoCPR

Group 1 deals with translocation-arrested proteins. Those can arise from premature-folded proteins, mutated or damaged TOM complexes and defects in the membrane potential Δψm (Pfanner et al., 2025). Two main pathways are taking care of the clearance of clogged mitochondrial TOM complexes in *S. cerevisiae*: (i) mitochondrial protein translocation-associated degradation (mitoTAD), and (ii). mitochondrial compromised protein import response (mitoCPR) (Pfanner et al., 2025). The mitoTAD pathway observes TOM complexes under non-stress conditions, guaranteeing intact mitochondrial protein import **(Fig. 8)**. The Cdc48 (VCP^{hum}) adaptor protein Ubx2 ($FAF2^{hum}$) associates with the TOM complex exposing its UBX and UBA domains to the cytoplasm (Mårtensson et al., 2019). The UBA domain interacts with the ubiquitylated stalled precursor protein and the UBX recruits the Cdc48 (VCP^{hum}) complex containing Ufd1 and Npl4. This recruitment leads to extraction and proteasomal degradation of the precursor protein (Mårtensson et al., 2019).

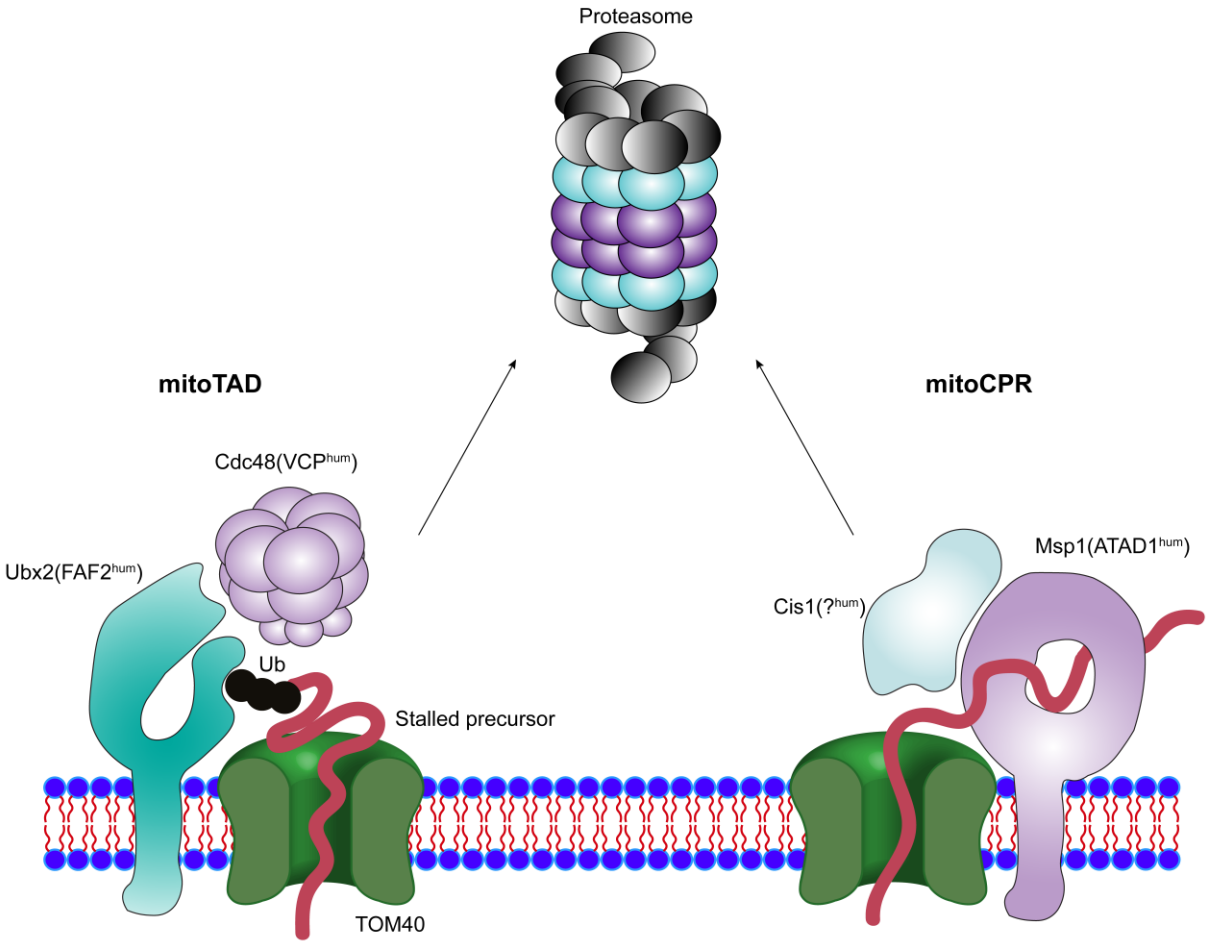

Figure 8 Cellular mechanisms for the removal of stalled mitochondrial precursors in yeast. In yeast, two pathways deal with clogged TOM complexes by removal of the stalled precursors. In the mitoTAD pathway, ubiquitylated precursors are recognized by Ubx2 which recruits Cdc48 to the stalled precursor leading to its subsequent extraction and proteasomal degradation. By contrast, in the mitoCPR pathway, the AAA-ATPase Msp1 is recruited to stalled precursors via Cis1 followed by subsequent precursor extraction.

While the MIQC pathway mitoTAD controls mitochondrial protein import under unchallenged conditions, the mitoCPR pathway is activated when cells encounter a higher load of mitochondrial import stress (Pfanner et al., 2025). Here, mitochondrial import stress leads to the upregulated expression of the cytosolic protein Cis1 dependent on the transcription factor Pdr3 (Weidberg & Amon, 2018). Cis1 forms a complex with TOM70 and Msp1 (ATAD1^{hum}) which extracts the stalled precursor proteins (Pfanner et al., 2025). While mitoTAD and mitoCPR are general repair mechanisms, other repair factors can also lead to the degradation of arrested precursor proteins. The ubiquitin ligase Rsp5 seems to be recruited to TOM70 for the ubiquitylation of stalled precursor proteins and Pth2 together with the ubiquilin Dsk2 lead to the degradation of precursor proteins via the ubiquitin-proteasome system (UPS) (Ishii et al., 2006).

Precursor proteins are aggregation-prone due to their MTS, and their enzymatic activity in the cytoplasm could interfere with the cellular metabolism (Pfanner et al., 2025). Thus, in a second layer, group 2 takes care of accumulated precursor proteins in the cytoplasm. One mechanism that was discovered in the absence of the proteasomal master regulator Rpn4 is the formation of so-called Mito-Stores. These cytosolic granules/inclusions contain accumulated mitochondrial precursor proteins and are formed by the small heat-shock protein Hsp42 (Krämer et al., 2022). Precursor proteins are temporary packed in Mito-Stores and with the help of the disaggregase Hsp104 they can be released from the inclusion and successfully imported into mitochondria upon translocase clearance (Krämer et al., 2022). Notably, expression of the mitochondrial model clogger b2-DHFR **(chapter 1.5.4.3)** increases the accumulation of mitochondrial precursor proteins with Hsp104. Furthermore, cells lacking Rpn4 and thereby exhibiting downregulated proteasomal degradation, are more resistant against clogger induced precursor accumulation due to the upregulation of Mito-Stores (Krämer et al., 2022). Mito-Stores prevent aggregation of retained mitochondrial precursors in the cytoplasm without primary degradation. In contrast, another pathway termed nuclear-associated mitoprotein degradation (mitoNUC) facilitates the degradation of mitochondrial precursor proteins in the nucleus. Non-imported precursor proteins are found in the nucleus and the ubiquitin ligases San1, Ubr1 and Doa10 are involved in the proteasome dependent degradation of those precursor proteins (Shakya et al., 2021). Precursor proteins seem to form nuclear protein aggregate compartments. Non-imported hydrophobic mitochondrial precursor proteins can also be redirected to the endoplasmic reticulum (ER) where they are handled by the UPR machinery of the ER (Pfanner et al., 2025).

1.3.2.2. Mitophagy-independent membrane clearance (MDVs, MDCs and SPOTS)

Cells can encounter multiple damage sources on the OMM e.g. misfolded proteins and clogged TOM complexes. While pathways such as mitoTAD or mitoCPR can remove stalled precursor at the TOM complex, mechanisms have evolved to remove whole membrane regions to deal with unwanted mitochondrial compartments (Uoselis et al., 2023). To date, three distinct mechanisms have been identified: (i) mitochondrial-derived vesicles (MDVs), (ii) mitochondrial-derived compartments (MDCs) and (iii) structures positive for OMM (SPOTs). This section will describe our current understanding of these three mechanisms.

1.3.2.2.1. MDVs

MDVs were originally identified as mitochondrial vesicles that facilitate cargo delivery and biogenesis of peroxisomes (Neuspiel et al., 2008). Later, it was shown that MDVs also participate in the vesicular transport from mitochondria to lysosomes (Soubannier, McLelland, et al., 2012). Thus MDVs are believed to fulfill a quality control mechanism that enables the bulk removal of whole membrane sections with misfolded membrane proteins (König &

McBride, 2024). MDVs are independent from the autophagy machinery, clearly separating them from mitophagy (König & McBride, 2024). Their size ranges from approximately 60-150 nm characterizing them smaller than MDCs and SPOTS. Two different types of MDVs are existing, type one describes MDVs that only contain the OMM while type two MDVs consist of both the OMM and the IMM (Soubannier, Rippstein, et al., 2012). Furthermore, MDVs are cargo selective and different subpopulations dependent on the cargo exist (Neuspiel et al., 2008).

One model describing the formation of MDVs includes the formation of thin, long membrane protrusions along microtubules budding away from mitochondria in a scission dependent manner (König et al., 2021). The machinery that is involved in the MDV formation can differ depending on the subtype of MDVs and is not fully understood. However, recent work has demonstrated, that at least a subset of MDVs are formed through MIRO1 and 2 (König et al., 2021). Both pull small membrane protrusions along microtubules. Here, DRP1 is recruited via MID49, MID51 and MFF for the scission of MDVs. While some studies suggest the involvement of PINK1 and PARKIN in the generation of MDVs, recent publications could not confirm the involvement of both proteins in the MDV biogenesis (König et al., 2021; Roberts et al., 2021; Ryan et al., 2020). Notably, MDV formation seems to be enhanced in the absence of the deubiquitylase (DUB) USP30 which is also linked to accumulation of stalled mitochondrial precursors (König et al., 2021).

1.3.2.2.2. MDCs

MDCs are mitochondrial compartments initially identified in *S. cerevisiae* with an average diameter of ~1 µm, thus approximately 10x larger than MDVs (Uoselis et al., 2023). MDCs contain and lead to the degradation of OMM and IMM proteins (Hughes et al., 2016). In contrast to mitophagy, MDCs remove membrane sections containing OMM and IMM proteins in a fission dependent manner without destruction of the remaining mitochondrion. Membrane proteins without MTS, e.g. mitochondrial carrier proteins are targeted into MDCs in an Dnm1 (DRP1), TOM70 and TOM71 dependent manner (Hughes et al., 2016). While MDCs can lead to the removal of membrane sections, they seem to rather maintain mitochondrial metabolic homeostasis than assisting the mitochondrial protein import (Uoselis et al., 2023). Notably, to my knowledge, MDCs have only been studied in *S. cerevisiae* and their existence and function in human cells need to be confirmed.

1.3.2.2.3. SPOTS

SPOTs are large spherical structure positive for OMM proteins, that have been identified six hours post *Toxoplasma* infection (X. Li et al., 2022). They are in average ~2.6 µm in diameter distinguishing them from smaller MDCs and MDVs. SPOT formation was shown to be independent of DRP1, MIRO1 and MIRO2 that are involved in the formation of MDVs (König

et al., 2021; X. Li et al., 2022). SPOT formation leads to the removal of OMM proteins under high overexpression of α-helical OMM proteins but not as a consequence of mitochondrial depolarization or mitochondrial import stress (X. Li et al., 2022). Thus, this mechanism allows mitochondrial membrane remodeling under mitochondrial stress conditions e.g. infections and accumulation of OMM proteins. However, the removal of OMM proteins by the formation of SPOTs could still indirectly modulate mitochondrial import through the removal of TOM complex subunits. Noteworthy, to my knowledge there is only one publication to date that identified SPOTs.

1.3.2.3. Mitochondrial removal via mitophagy

The cell has multiple quality control mechanisms to overcome mitochondrial stress such as mitochondrial precursor arrest at the TOM complex. If those quality control mechanisms fail to ensure mitochondrial function, not only an ATP and metabolite shortage arises but also an increase of ROS (Cadenas & Davies, 2000). High levels of ROS can lead to apoptosis which the cell tries to prevent by removal of malfunctioning mitochondria. Therefore, the cell uses a special form of macro-autophagy called mitophagy, which describes the lysosomal degradation of defective mitochondria (S. Wang et al., 2023). This mechanism serves as a last resort mechanism only under overwhelming conditions when other repair mechanisms are not sufficient to guarantee proper mitochondrial function (S. Wang et al., 2023). Mitophagy can be subdivided into PINK1-PARKIN dependent and independent pathways.

The PINK1-PARKIN mediated mitophagy pathway is a well-established ubiquitin dependent way of mitochondrial removal. Under normal conditions, PINK1 is degraded upon successful insertion into the IMM (Sekine & Youle, 2018). In malfunctioning mitochondria, PINK1 does not undergo translocation through the TOM complex and accumulates on the mitochondrial surface. This leads to autophosphorylation of PINK1 which leads to further phosphorylation of ubiquitin at residue serine 65 (Ub^{S65}) and phosphorylation of the ubiquitin-like (Ubl) domain of PARKIN. Binding of Ub^{S65} and phosphorylation releases PARKIN from an autoinhibited state into an activated state creating poly-Ub chains on multiple OMM proteins, e.g. MFN1 and MFN2 (Palikaras et al., 2018; S. Wang et al., 2023; Wauer et al., 2015). Those poly-ubiquitylated chains are further phosphorylated by PINK1 which leads to the recruitment of more PARKIN and results in a highly amplified mitophagy signal (S. Wang et al., 2023). This amplified ubiquitin signal is recognized by autophagy receptors OPTN, NDP52, NBR1. Binding of Sequestosome 1 (p62) and proteins of the microtubule associated protein 1 light chain 3 (LC3) family enable the formation of mitophagosomes leading to the degradation of damaged mitochondria (Khaminets et al., 2016; Picca et al., 2023). Binding of ULK1, WIPI1 and DFCP1 to NDP52 further enhances mitophagy. While PARKIN driven ubiquitylation promotes

mitophagy, USP30 counteracts mitophagy by removal of the ubiquitin signal (Khaminets et al., 2016).

PINK1-PARKIN independent mitophagy is induced by proteins that can recruit LC3 family proteins independent of PARKIN ubiquitylation. This includes proteins BCL1-interacting protein 3 (BNIP3), NIP-3-like protein X (NIX), FUN14 domain-containing protein (FUNDC1) and PHB2 and FKBP8 (Lim & Lim, 2017; Picca et al., 2023; Terešak et al., 2022).

1.3.2.4. MIQC mechanisms in human cells

In human cells, mitochondrial import defects activate the integrated stress response (ISR) via a mitochondrial-nuclear stress signaling axis. Mitochondrial stressed-induced cleavage of DELE1 by OMA1 and/or HTRA2 activates HRI, which phosphorylates the eukaryotic translation initiation factor 2 (eIF2α). This reduces eIF2α activity and results in decreased protein synthesis (Calais & Bertolin, 2025). In the meanwhile, eIF2α-phosphorylation results in enhanced expression of activating transcription factors (ATF) such as ATF4, ATF5 and CHOP (Calais & Bertolin, 2025). Together these transcription factors modulate the cellular response to mitochondrial stress and upregulate the mitochondrial unfolded protein response (mtUPR) (Horibe & Hoogenraad, 2007; X. Zhang et al., 2024).

Furthermore, several MIQC factors have been identified that act either at the level of stalled precursors or in maintaining the mitochondrial proteome during import stress **(Fig. 9)**. For instance, ATPase family AAA domain-containing protein 1 (ATAD1), the human ortholog of yeast Msp1, was recently shown to remove stalled precursor proteins from the TOM complex (J. Kim et al., 2024). In addition, ATAD1 is also involved in the removal of mistargeted tail-anchored proteins from the OMM.
While ATAD1 activity has not been linked to ubiquitin, it was shown that the mitochondrial E3 MARCH5, associates with the TOM receptor TOM70, and a role in the MIQC is suggested (Phu et al., 2020). The mitochondrial DUB USP30 seems to counteract MARCH5 and may likewise contribute to the MIQC. Moreover, a recent publication showed that arrested mitochondrial import intermediates can be resolved by proteolytic cleavage from the IMS side by the protease OMA1 (Krakowczyk et al., 2024). In this study, VCP and the proteasome were implicated in the cytoplasmic degradation of released precursor proteins.

In addition, several proteases protect the mitochondrial proteomic homeostasis during mitochondrial stress (M. J. Baker et al., 2025). Recently it was demonstrated that mitochondrial import clogging results in the degradation of TIM17A and TIM23 through YME1L1, a IMM-bound protease that faces the IMS (Hsu et al., 2025). Furthermore, YME1L1 also degrades unassembled OXPHOS subunits, and its protease activity is proposed to help in overcoming mitochondrial import stress (M. J. Baker et al., 2025). In addition to YME1L1, also the

mitochondrial disaggregase, caseinolytic peptidase B (CLPB), helps to maintain the IMS proteostasis through solubilization of protein aggregates (M. J. Baker et al., 2024).

Moreover, MDVs participate in the vesicular transport from mitochondria to lysosomes and may contribute to mitochondrial control mechanism enabling bulk removal of whole membrane sections with misfolded membrane proteins (König & McBride, 2024; Soubannier, McLelland, et al., 2012). While MDVs are independent of the autophagy machinery, as a last resort, whole malfunctioning mitochondria can be cleared via mitophagy (König & McBride, 2024; S. Wang et al., 2023).

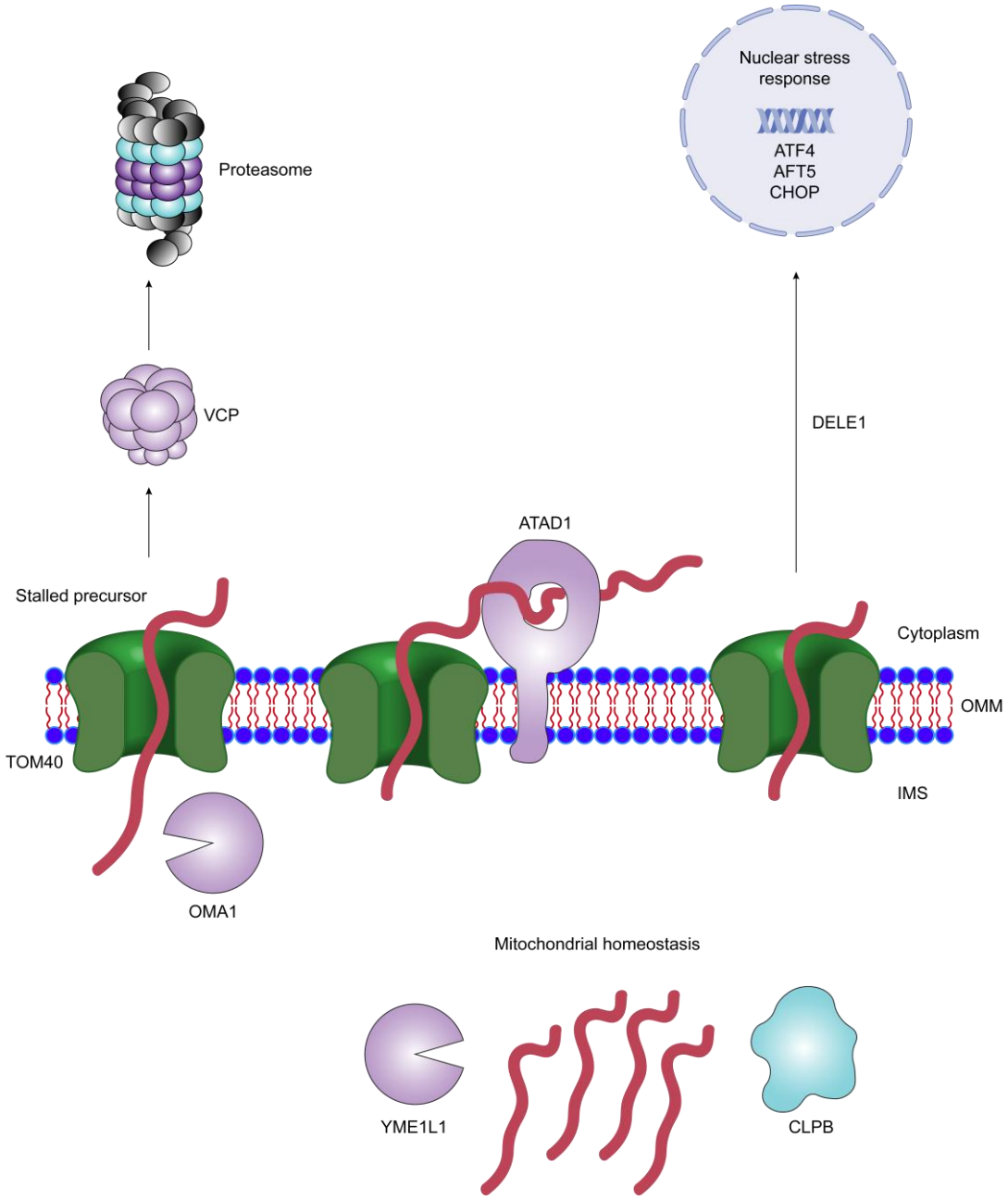

Figure 9 MIQC mechanisms in human cells. While the AAA-ATPase ATAD1 extracts arrested mitochondrial precursors from the TOM complex, recent work suggests that the mitochondrial protease OMA1 can cleave the stalled precursors from the IMS side, leading to the precursor release into the cytoplasm and subsequent VCP/proteasome dependent degradation. During mitochondrial import stress, factors such as YME1L1 and CLPB maintain mitochondrial protein homeostasis. In parallel, import stress dependent processing of DELE1 leads to the activation of the nuclear stress response involving ATF4/5 and CHOP.

1.4. Mitochondria in human disease

Mitochondrial dysfunction is associated with a broad spectrum of human disease. One can distinguish primary and secondary forms of mitochondrial disease (Niyazov et al., 2016). Primary mitochondrial diseases are often caused by pathogenic mutations in the mitochondrial DNA or in nuclear genes encoding mitochondrial OXPHOS-related proteins (Wen et al., 2025)(Valenti & Vacca, 2022). The disturbance of OXPHOS results in compromised cellular energy levels and increased oxidative stress and is frequently associated with a reduction or loss of Δψm which in turn impairs mitochondrial protein import (Wen et al., 2025). This ultimately contributes to the development of primary mitochondrial diseases that often manifest as myopathies and neuropathies, reflecting the high energetic demand of skeletal muscle and nerve cells.

Secondary mitochondrial diseases are defined by mitochondrial dysfunction caused through defects in genes not primarily encoding OXPHOS components, or from acquired environmental and metabolic factors (Niyazov et al., 2016). Given the diverse physiological roles of mitochondria, the precise underlying molecular mechanisms of dysfunction are highly context-dependent **(chapter 1.1.3)** (Zong et al., 2024). Typical examples are neurodegenerative diseases, e.g. Alzheimer's disease, Parkinson's disease, amyotrophic lateral sclerosis and Huntington's disease. In these examples it is still unclear if mitochondrial defects represent the primary cause or a secondary consequence of these diseases, nevertheless, mitochondrial dysfunction appears to exacerbate disease severity (Zong et al., 2024).

1.4.1. Mitochondrial import defects and human disease

Mitochondrial protein import is required to sustain diverse mitochondrial functions, including OXPHOS. Hence, persistent mitochondrial import impairment has been suggested to contribute to the above mentioned diseases (Calais & Bertolin, 2025). Recent research has focused on the mechanistic links between mitochondrial protein import and human disease.

TOM receptors are involved in the initial step of the mitochondrial protein import. They are required for the mitochondrial precursor recruitment to the TOM complex. Mutations of the TOM receptor TOM70 have been identified in patients with neurological phenotypes and OXPHOS deficiencies (Calais & Bertolin, 2025). Mutations in this TOM receptor resulted among others in anemia, lactic acidosis, developmental delays and ataxia. Furthermore, the pore-forming TOM complex subunit TOM40 has been linked to major depressive disorder (McFarquhar et al., 2014).

In addition, several TIM complex subunits, such as TIM8A and TIM14 also called DNAJC19, have been linked to diseases such as human deafness dystonia syndrome and dilated cardiomyopathy with ataxia (MacKenzie & Payne, 2007). Genetic alterations in TIM22 and TIM50 have been found in patients with neuromuscular phenotypes and sever encephalopathy (Nicolas et al., 2019).

Furthermore, upregulation of TOM and TIM complex subunits, such as TOM20, TOM70 , TOM40, TIM9 and TIM17 have been linked to multiple cancer types and their progression (Calais & Bertolin, 2025). Overexpression of TOM70, TIM9 and TIM17 was observable in breast cancer and TOM20 overexpression is associated with increased cell proliferation and invasive migration in colorectal cancer cells (Calais & Bertolin, 2025).

In conclusion, these observations highlight the importance of mitochondrial protein import in disease development.

1.5. Ubiquitin

One major regulator of the MQC is the post-translational modifier ubiquitin (J. W. Harper et al., 2018). This thesis focuses on the one hand on the understanding of the role of ubiquitin in the quality control of mitochondrial protein import. On the other hand, a part of this thesis will focus on the improvement and extension of an ubiquitylation tool. Therefore, the following sections are intended to give a broad understanding of ubiquitin and its cellular roles with a specific focus on mitochondrial quality control.

The post-translational modifier ubiquitin originally called ubiquitous immunopoietic polypeptide was named after its ubiquitous presence in eukaryotic cells (Goldstein et al., 1975). Ubiquitin consists of 76 amino acids that adopt an extremely compact structure based on intramolecular hydrogen bonds (Vijay-Kumar et al., 1987). The secondary structure of ubiquitin consists of one α-helix, one 3_{10}-helix and a five-stranded mixed β-beta sheet **(Fig. 10A)**. Its high cellular abundance can be explained by its direct or indirect involvement in virtually all eukaryotic cellular processes (Dikic & Schulman, 2023). This involvement likely reflects the canonical

degradative function of ubiquitin and its ability to form polymeric chains enabling complex but specific signaling variety (Asimaki et al., 2022). Ubiquitin is attached to proteins via its C-terminal glycine residue. During attachment, an isopeptide bond is formed between this glycine residue and a primary amine of either a lysine or the N-terminal methionine (peptide bond is formed) of the modified protein. Ubiquitin itself contains 7 lysines and an N-terminal methionine allowing the formation of polymeric ubiquitin chains **(Fig. 10B)**. However, recent findings have revealed additional amino acids that can be targeted by ubiquitylation, e.g. serine and threonine via oxyester bonds (Pruneda & Damgaard, 2021). Additionally, lipids and nucleic acids can be targeted by ubiquitylation (Pruneda & Damgaard, 2021; K. Zhu et al., 2024). Furthermore, ubiquitin can also be post-translationally modified, e.g. phosphorylated, methylated and acetylated (Asimaki et al., 2022). The structure of ubiquitin is further characterized by four distinct interaction surfaces, so-called F4, I36, I44 and D58 patches (Hospenthal et al., 2013; Lee et al., 2006; Sloper-Mould et al., 2001). These patches are recognized by ubiquitin binders. While the I44 displays the central hydrophobic binding site, the other patches enable diversified ubiquitin binding **(Fig. 10C)**.

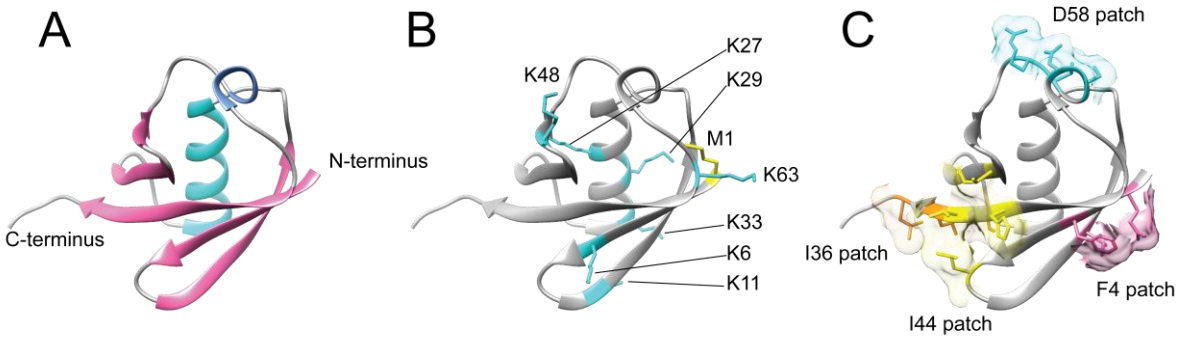

Figure 10 The post-translational modifier ubiquitin. (A) The secondary structure of ubiquitin consists of one α-helix (cyan), one 3_{10}-helix (blue) and a five-stranded mixed β-sheet (magenta). **(B)** Eight residues of ubiquitin carry a primary amine that can be used for ubiquitylation, the seven lysines (cyan) and the N-terminal methionine (yellow). **(C)** Four patches mediate interactions with ubiquitin-binding domains are displayed: the F4 patch (magenta), the I36 patch (orange), the I44 patch (yellow) and the D58 patch (cyan) (PDB: 1UBQ).

1.5.1. The enzymatic cascade

The attachment of ubiquitin is achieved via an enzymatic cascade involving three classes of enzymes **(Fig. 11).** First, ubiquitin is activated by a ubiquitin activating enzyme (E1). Under the consumption of ATP a high-energy thioester bond between ubiquitin and the E1 is formed (Bedford et al., 2011). In human cells two E1s are known, ubiquitin-activating enzyme (UBA) UBA1 and UBA6. While UBA1 is the main E1 in human cells, UBA6 mainly activates ubiquitin-

like modifiers but was also found capable of activating ubiquitin (Bedford et al., 2011). After the activation of ubiquitin, it is handed over from the E1 to one of the ~40 ubiquitin conjugating enzymes (E2s). Afterwards, the interaction between the E2 and a ubiquitin ligase (E3) facilitates the ubiquitylation of the actual substrate. Depending on the type of E3, ubiquitin is either directly transferred from the E2 to the substrate or involves another transfer step (Metzger et al., 2014). Really Interesting New Gene (RING)-type E3s interact with the E2 and the substrate generating target specificity and E2 activity, while the actual transfer happens from the E2 to the substrate. In contrast, Homologous to E6-AP Carboxy Terminus (HECT)-type and RING in between RING (RBR)-type E3s harbor a catalytic cysteine accepting the activated ubiquitin from the E2. Here the HECT or the RBR E3 is facilitating the final ubiquitin transfer step towards the target.

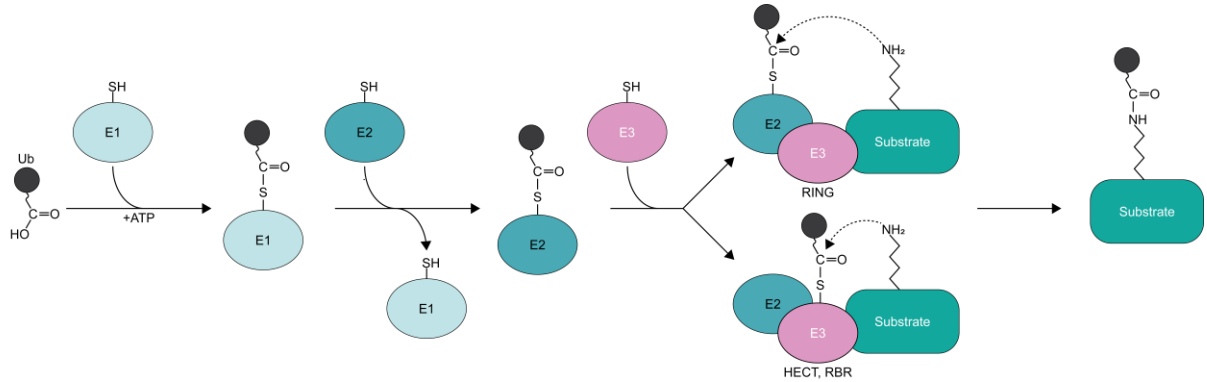

Figure 11 The ubiquitin conjugation cascade. Ubiquitin is first activated by an E1 enzyme in an ATP-dependent step. The high-energy E1-ubiquitin thioester is then transferred to the catalytic cysteine of an E2. Finally, substrate ubiquitylation is mediated by E3s which generate substrate specificity and modulate E2 activity. In the case of RING-type E3s, ubiquitin is transferred directly from the E2 to the substrate, whereas ubiquitylation by HECT- and RBR-type E3s involves an additional transfer from the E2 to the catalytic cysteine of the E3, which then mediates the final ubiquitylation step.

1.5.2. Writers, readers and erasers

Ubiquitin signaling involves 3 processes: writing, reading and erasing of the signal. First, the signal needs to be written. This is performed by so-called writers that establish the ubiquitin signal which is described above **(chapter 1.5.1)**. Every signal requires a recipient that receives the signal and translates it into a response. Therefore, the recipient also needs a module for signal recognition. In the case of ubiquitin, recipients are also called readers. Readers carry ubiquitin binding domains (UBDs) to detect and bind ubiquitin and amplify the cellular response to that particular ubiquitin signal. When the signal is not required anymore, it needs to be removed. This allows regulation of the signal, prevention of overstimulation and maintenance of the free ubiquitin pool (Basar et al., 2021). DUBs fulfill this erasing function by hydrolysis of

the iso-peptide bond formed between substrate and ubiquitin or between two ubiquitin moieties (Komander & Rape, 2012).

1.5.3. Ubiquitin linkages and their cellular role

While the enzymatic interplay between E1, E2 and E3 facilitates the ubiquitylation of a target protein, ubiquitin itself harbors 8 amino acids with a primary amine, suitable for ubiquitylation. Those amino acids, the N-Terminal methionine (M1) and 7 lysines (K6, K11, K27, K29, K33, K48 and K63), serve as the foundation for the formation of ubiquitin chains **(Fig. 10B)**. While lower eukaryotes like *S. cerevisiae* do not have M1 linked ubiquitin chains, in human cells all 8 linkages are detectable (Iwai, 2021; Swatek & Komander, 2016; Wagner et al., 2011). The targeted lysine defines the linkage-type of the ubiquitin chain. Three types of ubiquitylation can be distinguished, monoubiquitylation and multi-monoubiquitylation refers to either the attachment of a single or multiple ubiquitin molecules to lysine of the target protein, while polyubiquitylation refers to the attachment of polyubiquitin chain(s) to the substrate **(Fig. 12)**. Polyubiquitin chains can be further subdivided into homotypic chains with only one specific linkage, heterotypic ubiquitin chains with multiple ubiquitin linkages present in a chain but only a single lysine is targeted per ubiquitin and branched chains where at least 2 lysines are targeted for ubiquitylation within a single ubiquitin molecule. NMR spectroscopy analysis demonstrated that the ubiquitin-linked dimers K6, K11, K29, K33 and K48 can form interfaces thereby adopting a rather compact structure while M1- and K63-linked dimers exhibit a predominantly open confirmation (Akutsu et al., 2016). Those structural differences enable differentiated recognition by ubiquitin readers. In total, a complex combination of ubiquitylation can be achieved which is also called the ubiquitin code and allows the cell to use ubiquitin as key regulator for cellular signaling (Komander & Rape, 2012).

While the canonical ubiquitin linkage K48 usually targets proteins for proteasomal degradation, the role of ubiquitin goes far beyond a simple degradation signal (Komander & Rape, 2012; Suryo Rahmanto et al., 2023; Swatek & Komander, 2016). It was shown that K6 and K63 linked ubiquitin chains were unaffected upon proteasomal inhibition while K11, K27, K29, K33 and K48 linked ubiquitin chains increased, demonstrating their involvement in proteasomal degradation (Wagner et al., 2011). However, recent discoveries highlight the involvement of chain branching in the degradative nature (Akizuki et al., 2024). The following section will give an overview about the cellular role of each linkage.

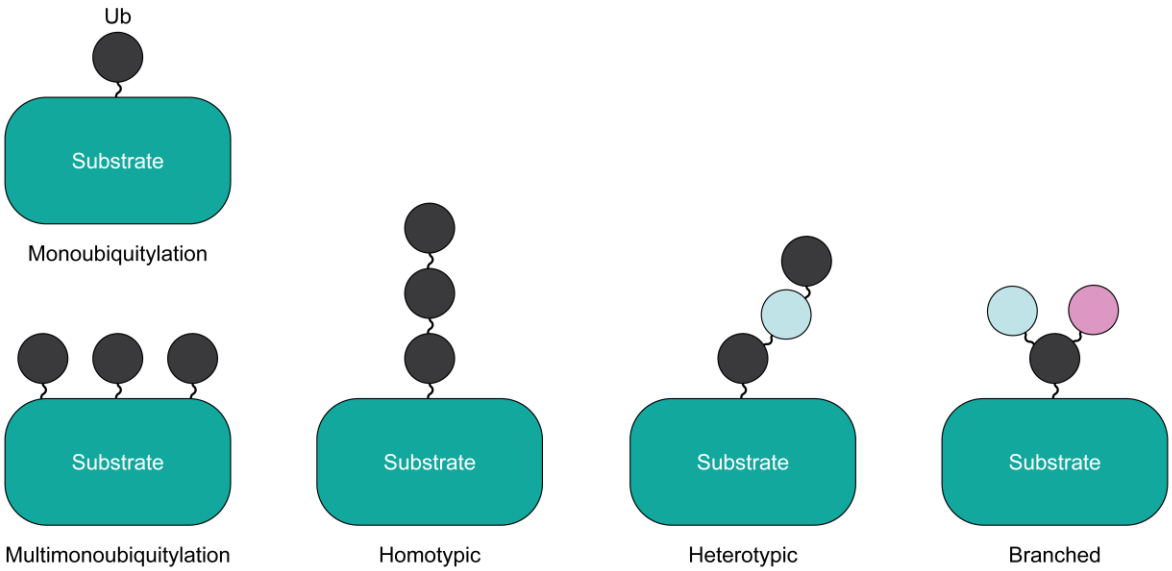

Figure 12 Illustration of the simplified ubiquitin code. Attachment of ubiquitin to a substrate residue leads to the formation of a mono or multimonoubiquitylated substrate, whereas attachment of ubiquitin to another ubiquitin moiety leads to the formation of polyubiquitin chains. Polyubiquitin chains can be homotypic, when the same lysine is used for chain elongation, heterotypic, when different lysines are used within the same chain, or branched, when a single ubiquitin is modified on two lysines at the same time.

1.5.3.1. K6-linked ubiquitin chains

K6-linked ubiquitin chains are low abundant under unstressed conditions (Michel et al., 2017). However, they increase upon UV treatment and mitochondrial damage (Cunningham et al., 2015; Elia et al., 2015). The UV-dependent increase of K6-linked ubiquitin chains is RNF14 mediated and was shown to be involved in the recognition of formed RNA-protein crosslinks (RPCs) and their resolution by VCP (Suryo Rahmanto et al., 2023). Furthermore, K6-linked ubiquitin chains are formed during replication stress and seem to be involved in double-strand-break repair (Tracz & Bialek, 2021). HUWE1 seems to be a major source for K6-linked ubiquitin chains, but other E3s such as RNF14, RNF144A, RNF144B and the mitochondrial E3s PARKIN are also contributing to the formation of this atypical linkage (Michel et al., 2017; Suryo Rahmanto et al., 2023). PARKIN is a central E3 in mitophagy, a process that removes damaged mitochondria **(chapter 1.3.2.3)**. The mitochondrial DUB USP30 preferentially cleaves K6-linked ubiquitin chains, e.g. on TOM20 during mitophagy (Gersch et al., 2017). Additionally, the mitochondrial fusion factor MFN2 was also found to be ubiquitylated with K6-linked ubiquitin and USP8 was found to regulate mitophagy by removal of K6-linked ubiquitin from PARKIN (Durcan et al., 2014; Gersch et al., 2017). Furthermore, it was shown that TRAF6 dependent K6-, K27- and K29-linked ubiquitylation of a Parkinson's disease related mutant of DJ-I drives its aggregation in the cytoplasm (Zucchelli et al., 2010). Altogether this highlights the importance of K6-linked ubiquitin chains in the MQC, but an interplay between K6, K11,

K48 and K63 is suggested (Tracz & Bialek, 2021). Knockdown of USP30 led to an increase of MDVs (König et al., 2021). MDVs are potentially involved in the MIQC and the K6 specificity of USP30 indicates a role of this linkage in the mitochondrial import.

Additionally, K6-linked ubiquitin chains seem to modulate the immune response. A recent publication showed that K6-linked ubiquitylation of IRF3 leads to increased expression of IFNβ and interferon-stimulated genes (Fonseca et al., 2024). Furthermore, the antiviral effector VIPERIN was found to be K6 ubiquitylated (Tracz & Bialek, 2021). It is suggested that potential pathogens can manipulate the ubiquitin code of their host cells, in particular with K6 linked ubiquitin chains. Recently it was discovered that bacterial HECT-like E3s and DUBs have a K6-linked specificity (Franklin et al., 2023b; Warren et al., 2023). LotA, a K6 specific DUB from *L. pneumophila* was shown to inhibit VCP recruitment during infection, while the Enterohemorrhagic *Escherichia coli* (EHEC) type III effector NleL can form K6-linked ubiquitin chains.

1.5.3.2. K11-linked ubiquitin chains

Pioneering work identified K11-linked chains and their importance during mitosis. Cells lacking K11 specific enzymes exhibited strong mitotic defects (Wickliffe, Williamson, et al., 2011). It was shown that K11-linked ubiquitylation by UBE2S, a subunit of the anaphase-promoting complex (APC), leads to the proteasomal degradation of APC substrates (Wu et al., 2010). It was suggested that K11-linked chains are branched with K48-linked chains in order to facilitate their degradative nature (Grice et al., 2015). K11-K48-branched chains formed by UBR4 and UBR5 lead to proteasomal dependent degradation of mitotic regulator (Tracz & Bialek, 2021).

K11-linked chains are also implicated in the innate immune response (van Huizen & Kikkert, 2019). For example, K11-linked ubiquitylation by RNF26 protects STING from degradation (Qin et al., 2014). Furthermore, it is suggested that K11-linked ubiquitylation leads to the degradation of BCL-1, which indirectly inhibits autophagy while promoting RIG-I and MAVS dependent type I IFN response (van Huizen & Kikkert, 2019).

K11-linked ubiquitin chains are also linked to the MQC. Mitophagy was decreased upon overexpression of a ubiquitin variant lacking K11 (Cunningham et al., 2015). Notably, in this study it was further demonstrated that the mitochondrial regulator USP30 exhibits cleavage specificity towards K11. Moreover, also the mitophagy regulator PARKIN facilitates among others K11-linked polyubiquitylation on multiple OMM proteins in order to promote mitophagy (Heo et al., 2015). This shows that like K6, K11-linked polyubiquitylation seems to be involved in the regulation of the MQC.

1.5.3.3. K27-, K29- and K33-linked ubiquitin chains

All three ubiquitin linkages K27, K29 and K33 are low abundant in cells (Agrata & Komander, 2025). The detection of these linkages by MS is technically challenging due to the small peptide size after the tryptic digest.

Interestingly, the ubiquitin residue K27, required for the formation of K27-linked chains is partially buried within the protein and it is not understood how this linkage can be formed (Agrata & Komander, 2025). However, recent work identified that K27-linked ubiquitin chains are involved in the regulation of the innate immune response. This involves the ubiquitylation of factors e.g. NEMO, RIG-I, MAVS and MDA5 (van Huizen & Kikkert, 2019). Furthermore, it was suggested that HACE1-mediated K27-linked ubiquitylation of the epithelial mesenchymal transition regulator YB-1, drives its extra cellular secretion and thereby inhibiting epithelial mesenchymal transition (Palicharla & Maddika, 2015). Moreover, K27-linked chains are involved in the DNA damage response (DDR). It was shown that RNF168 ubiquitylates histones H2A and its variant H2A.X with K27-linked ubiquitin chains (Gatti et al., 2015). Additionally, it was shown that K27-linked chains are predominantly nuclear, involved in proliferation and cell viability and that they drive VCP dependent proteasomal turnover (Shearer et al., 2022).

K29-linked ubiquitin chains are mainly involved in the regulation of proteotoxic stress and are implicated in the cell cycle regulation (Y. Yu et al., 2021). The authors showed that K29-linked ubiquitin chains are enriched in lipid droplets and stress granules upon proteotoxic stress and facilitate VCP-dependent unfolding. It was further shown that K29-linked ubiquitylation of SUV39H1, a writer of H3K9me3 leads to its proteasomal degradation. The K29-linkage mainly depends on TRIP12 and TRABID activity (Arroyo-Gomez et al., 2025). In *S. cerevisiae* K29-linked ubiquitylation is a central component of the ubiquitin fusion degradation (UFD) pathway. Ufd4 decorates UFD substrates with K29-linked ubiquitin chains that are further branched with K48-linked ubiquitin chains by Ufd2 which drives proteasomal degradation (Tong et al., 2025).

K33-linked ubiquitin chains are involved in the immune and antiviral signaling. DNA and RNA virus infection triggers the K33-linked ubiquitylation of TBK1 which results in IRF3 activation (M. Lin et al., 2016). Furthermore, K33-linked ubiquitylation seems to be involved in the regulation of the interferon response by ubiquitylation of type I IFN-induced transcription factor STAT1 (van Huizen & Kikkert, 2019). Additionally, K33-linked ubiquitylation is implicated in T-cell receptor signaling (H. Huang et al., 2010). Further findings suggest that this linkage is involved in autophagy, as autophagy regulators p62 and LC3 colocalize with K33 sensing probes (Nibe et al., 2018). The proapoptotic factor E3 AREL1 was shown to favor K33-linked ubiquitylation over K11 and K48, indicating that K33-linkage might also be involved in apoptotic regulation (Michel et al., 2015).

Introduction

Recently it was shown that human ubiquitin replacement cell lines that only express ubiquitin K27R show enriched mitochondrial ubiquitylation. This points towards a role of K27 or neighboring lysines such as K29 and K33 (Arroyo-Gomez et al., 2025). As described above in addition to K6, also K27- and K29-linked ubiquitin chains on a Parkinson's disease related mutant of DJ-I favor its aggregation in the nucleus (Zucchelli et al., 2010).

1.5.3.4. K48-, K63- and M1-linked ubiquitin chains

Among all ubiquitin linkages, K48-linked chains represent the classical proteasomal degradation signal (Swatek & Komander, 2016). In the year 1989, the lab of Alexander Varshavsky identified the K48-linked ubiquitin chain and its degradative nature (Chau et al., 1989). The ubiquitin residue K48 is essential in *S. cerevisiae* and human cells as a replacement with mutant K48R ubiquitin could not rescue depletion of WT ubiquitin (Arroyo-Gomez et al., 2025; Finley et al., 1994). Furthermore, other atypical linkages can be branched with K48-linked ubiquitin chains to modulate the signaling function. The APC complex utilizes K11-K48-branched ubiquitin chains to mediate rapid substrate degradation (Draczkowski et al., 2025). In *S. cerevisiae* the UFD pathway uses K29-K48-linked for rapid degradation (Tong et al., 2025). While the default function of K48-linked ubiquitin chains seems to be the targeting of substrates for proteasomal degradation, additional non-degradative functions have been reported. In the case of the transcription factor MET4, K48-linked chains block the binding of the transcription machinery and the K48-linked chain must be replaced with a K11-linked chain in order to enable activation of transcription (Y. Li et al., 2019).

In contrast to the degradative nature of K48-linked ubiquitin chains, K63- and M1-linked ubiquitin chains seem to mainly fulfill signaling functions. Among others, K63-linked ubiquitin chains serve as a trafficking signal (Erpapazoglou et al., 2014). It was demonstrated that the formation of K63-linked ubiquitin chains of the EGFR is sufficient to induce internalization via endocytosis (Renz et al., 2024). Furthermore, this signal can further lead to lysosomal degradation (Erpapazoglou et al., 2014). K63-linked ubiquitin chains are also involved the DNA repair. Modification of PCNA with this linkage induces an error-free repair mechanism called template switching in *S. cerevisiae* (Wegmann et al., 2022). Interestingly, also M1-linked ubiquitin chains were sufficient to initiate template switching demonstrating similarities between K63-linked chains and M1-linked chains most likely due to their "linear" and "open" conformation. K63-linked ubiquitin chains are also involved in the regulation of mitophagy. Besides K6-, K11-, K48- also K63-linked ubiquitin chains are regulated by PARKIN and USP30 (Cunningham et al., 2015). Further, important cargo adaptors of autophagy preferentially bind K63-linked chains (Heo et al., 2015).Additionally, K63-linked ubiquitin chains are involve d in the immune response. Here, K63-linked chains regulate among others NF-κB signaling via NEMO (Z. J. Chen, 2005). Antiviral RIG-I/MAVS signaling also underlies K63-linked

ubiquitylation and pathogens such as SARS-CoV-2 modulate the ubiquitin signal during infection (Madiraju et al., 2022).

Like K63-linked ubiquitin chains, M1-linked chains also called linear chains mainly facilitate signaling roles. Linear chains are formed by the linear ubiquitin chain assembly complex consisting of the catalytic subunit HOIP, HOIL-1L and SHARPIN (Oikawa et al., 2020) M1-linked chains have a regulative function in the immune response. They modulate TNF, IL-1 and toll-like receptor pathways (Jahan et al., 2021).

1.5.4. Tools to study mitochondrial import quality control and ubiquitylation

For the analysis of the mitochondrial import quality control and the involvement of ubiquitin, several tools are central to this work. These tools enable (i) controlled, linkage-specific ubiquitylation of a defined substrate, (ii) proximity-based mapping of distinct ubiquitin linkage environments and (iii) induction of acute mitochondrial import stress by a defined model clogger. Each tool will be described in more detail in the following sections.

1.5.4.1. The Ubiquiton: a tool for linkage-specific ubiquitylation

To dissect how specific ubiquitin linkages contribute to the MIQC, a tool capable of substrate targeted, on demand, linkage-specific ubiquitylation would be powerful. Being involved in virtually all cellular processes makes ubiquitin signaling and such a tool, highly relevant for scientific research.

The regulatory versatility of ubiquitin signaling arises from its ability to form a variety of different ubiquitin linkages **(chapter 1.5.3)**. The cell seems to use different ubiquitin linkages to distinguish different cellular compartments and pathways. Therefore, linkage specific E3s have evolved. However, to date we still lack broad knowledge on the role of atypical ubiquitin linkages which is partly explained by the lack of tools that can induce the formation of specific ubiquitin linkages, crucial for their biological analysis. Recently, the laboratory of Helle Ulrich established a tool enabling the polyubiquitylation of the replication factor PCNA with M1, K48 and K63 linkages. For this purpose, tailor-made, linkage specific E3s were developed and directed towards PCNA using a PCNA-interacting peptide (PIP) in *S. cerevisiae* (Wegmann et al., 2022). While proof-of-principle experiments demonstrated that this set of tailor-made E3s allows the analysis of the role of specific linkages on PCNA, a generalized approach would be desired for functional studies of ubiquitin linkages on diverse substrates. Therefore, the laboratory of Helle Ulrich developed a tool based on the established linkage specific PIP-E3s that allows inducible, linkage-specific ubiquitylation of any tag-able protein of interest APC. The so-called Ubiquiton system was validated on cytoplasmic, nuclear and membrane

standing proteins in *S. cerevisiae* and mammalian cells (Renz et al., 2024). The following section will explain the Ubiquiton system in more detail.

The Ubiquiton system was designed to fulfill three main criteria: 1. linkage specificity, 2. inducible substrate recognition and 3. chain initiation ability. The E3s used for the polyubiquitylation of PCNA with M1, K48 and K63 already fulfilled criterion 1 for those linkages (Wegmann et al., 2022). The catalytic domain of the E3 HOIP (amino acids 699-1,072) from the linear ubiquitin chain assembly complex (LUBAC) was utilized for the formation of M1 linked chains. The HOIP domain was fused to two ubiquitin molecules for autoactivation **(Fig. 13A)**. A truncation of the E3 Cue1 (amino acids 24-203) from *S. cerevisiae* containing the interacting domain for the E2 Ubc7 and a ubiquitin binding CUE domain facilitates K48 specificity. K63 polyubiquitylation was achieved by the RING-finger E3 Pib1 (amino acids 91-286) in complex with Ubc13 and Mms2.

In order to overcome the requirement of a substrate-specific recognition motif, a dimerization tool replaced the PIP for the substrate binding. Fusion of the dimerizing domains FK506-binding protein (FKBP) and the FKBP-rapamycin binding protein (FRB) to the E3s and to the substrate enables rapamycin-inducible E3 to substrate recruitment **(Fig. 13B)**. For criterion 3. the chain initiation problem, the most intuitive thought would be the fusion of a monoubiquitin moiety to the substrate. However, fusion of a full monoubiquitin to the substrate would potentially trigger unwanted cellular responses based on endogenous monoubiquitin binders (Asimaki et al., 2022). The fusion of a split-ubiquitin to each dimerizing domain of FRB/FKBP solves this problem. In the absence of rapamycin (Rapa) both split-ubiquitin halves should be prevented from refolding due to separation and thus from recognition by monoubiquitin binders. Upon dimerization of FRB/FKBP upon Rapa induction, both split-ubiquitin halves come in close proximity to each other. This promotes refolding of the split-ubiquitin halves reassembling a full ubiquitin moiety sufficient for chain elongation by the linkage specific E3s (Johnsson & Varshavsky, 1994; Renz et al., 2024). Due to a basal affinity of both, the N-terminal half of ubiquitin (NUb, amino acids 1-37) and the C-terminal half of ubiquitin (CUb, 35-76), a mutation of I13A in NUb (now called NUa) was introduced, which abolishes this basal affinity (Renz et al., 2024). Two interchangeable modules were created that exhibited the best E3 activity towards the split-ubiquitin. The arrangement of NUa-HA-FRB (NUbo) and FKBP-CUb (CUbo) are fused to the substrate, dependent on the desired lysine-target **(Fig 13B)**. At the same time, the other module is fused to the E3 **(Fig 13C + D)**. Importantly, E3(1) activity requires a free N-terminus, and the substrate must be fused to the C-terminus of NUbo.

It is important to note that Rapa treatment can induce mitophagy and leads to the association of p62 and PARKIN to damaged mitochondria which reflects an activation of PINK1/Parkin-dependent MQC (Q. Li et al., 2018). However, Rapa can be replaced by non-

immunosuppressive Rapa analogs called rapalogs. It was previously shown that a rapalog called AP21967 efficiently induces FKBP-FRB heterodimerization without impairment of the mitochondrial integrity (Lazarou et al., 2012).

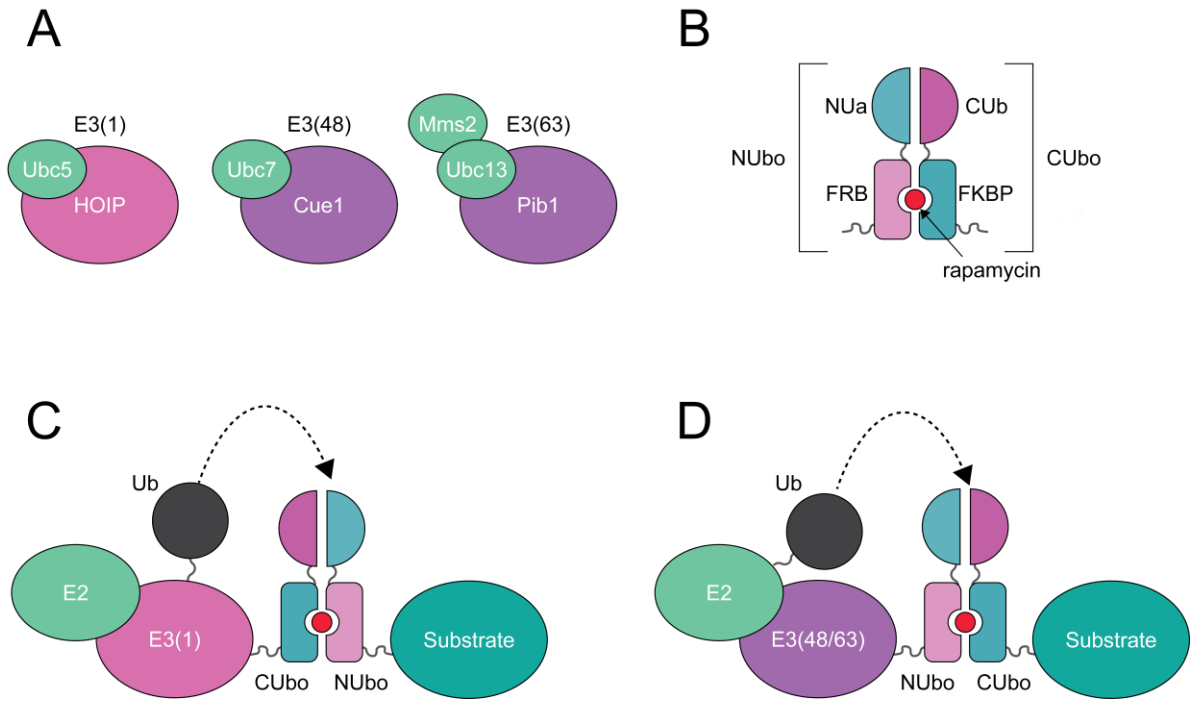

Figure 13 The Ubiquiton. (A) The current Ubiquiton consists of the catalytic domains of the E3s HOIP [E3(1)], Cue1 [E3(48)] and Pib1 [E3(63)] together with the indicated E2 enzymes. **(B)** Substrate-specific chain initiation is achieved via the Ubiquiton modules NUbo and CUbo. The NUbo module consists of an N-terminal split-ubiquitin half carrying the I13A mutation (NUa) fused to an FRB dimerization domain, whereas the CUbo module consists of the C-terminal split-ubiquitin half (CUb) and the FKBP dimerization domain. Rapamycin induced dimerization of FRB and FKBP leads to the refolding of the split-ubiquitin halves. **(C)** + **(D)** Depending on the desired linkage either the NUbo module or the CUbo module is fused to the E3.

1.5.4.2. LinkageID: proximity labeling of ubiquitin linkage environments

Recently, a colleague of mine developed a tool called LinkageID, which enables proximity labeling of proteins associated with defined ubiquitin linkage types (unpublished). The system is based on a split-TurboID approach that catalyzes biotinylation of proteins in its proximity upon refolding of the two split-halves. LinkageID employs a newly engineered split-TurboID variant with enhanced catalytic activity and markedly reduced spontaneous reassembly of the individual halves, thereby minimizing background labeling while preserving high proximal labeling efficiency. (Cho et al., 2020). In the linkageID system, each TurboID half is fused to a ubiquitin variant that contains a single lysine residue, thereby restricting chain formation to one defined linkage type. Reconstitution of split TurboID is thus dependent on ubiquitylation

through that specific lysine. Only proteins in the immediate vicinity of the corresponding ubiquitin linkage are biotinylated and thereby, labeled as linkage-specific interactors. This strategy is supported by a similar approach, namely the fusion of lysine-only ubiquitin variants to split-GFP, which was recently used to visualize K33-linked polyubiquitylation in mammalian cells (Nibe et al., 2018). As these ubiquitins can come into proximity without forming a polyubiquitin chain - for example, in the context of multi-monoubiquitylation or binding to a scaffold with multiple ubiquitin-binding domains - fusion of split TurboID to lysine-less (K0) ubiquitin serves as a crucial control in our experiments. Furthermore, to ensure that N- and C-terminal LinkageID fragments are produced in a 1:1 ratio, both halves were encoded on a single polypeptide. Following translation, endogenous DUBs cleave the fusion C-terminal to the ubiquitin moiety, thereby releasing the two LinkageID components in equimolar amounts (Utsugi et al., 2024). The system has been previously validated on proof-of-concept examples such as accumulation of K48 linkages upon proteasomal inhibition or K63-linked polyubiquitylation of PCNA (data not shown).

1.5.4.3. Studying mitochondrial clogging: The model clogger b2-DHFR

Mitochondrial protein import is essential and deletion of the core import machinery is lethal in *S. cerevisiae* (K. P. Baker & Schatz, 1991). Mitochondrial protein import failure is linked to sever diseases such as neuropathies and myopathies **(chapter 1.4.1)**. This highlights the importance of mitochondrial import studies, and the following section will describe the mitochondrial model clogger b2-DHFR which can be used to study mitochondrial import defects.

Initially, Gottfried Schatz and colleagues fused an MTS to the N-terminus of dihydrofolate reductase (DHFR) (*M. musculus*) in order to analyze the import of this artificial mitochondrial precursor in *S. cerevisiae*. Later on, a similar approach using the fusion of the MTS of b2 to a DHFR moiety demonstrated the inhibition of mitochondrial precursor import (Rassow et al., 1989). Thus, the fusion of an MTS to DHFR served from now on as a model to induce mitochondrial clogging, especially the fusion of b2 to DHFR (Boos et al., 2019).

The mitochondrial clogger b2-DHFR used in this thesis consists of the first 167 N-terminal amino acids of the *S. cerevisiae* L-lactate dehydrogenase b2 encoded by the *CYB2* gene. This part of the clogger will be from now on called b2. b2 is fused to the cytoplasmic DHFR (*M. musculus*) and together both are referenced as b2-DHFR. In *S. cerevisiae*, b2 is encoded in the nucleus, synthesized in the cytoplasm, imported into the mitochondria and sorted into the IMS (Ono et al., 1995). The N-terminal domain of b2 consists of a bipartite sorting signal. This bipartite sorting signal starts with an MTS followed by an HTS sorting signal. Without DHFR, b2 is imported via the stop-transfer pathway into the IMS **(chapter 1.2.5.2)**. Initially, the MTS leads to translocation of b2 through TIM23 into the mitochondrial matrix, whereas the HTS

domain remains arrested in the TIM channel, leading to the lateral release into the IMM **(Fig. 7)** (Edwards et al., 2021). Here, the matrix-facing MTS is cleaved by MPP resulting in the intermediate form of b2. The intermediated form is then processed via a second cleavage event by IMP proteases leading to the release of the mature form of b2 into the IMS (Ono et al., 1995). Furthermore, after the bipartite sorting sequence, b2 contains a heme binding domain (HBD) spanning from amino acids 81-180 (Esaki et al., 1999). The b2 domain that was used for this thesis contains the first 167 N-terminal amino acids ($b2^{167}$) and is typically used for mitochondrial clogging in *S. cerevisiae* and the heme binding domain is not mentioned in most publications using this clogger (Boos et al., 2019; Krämer et al., 2023). It is believed that the HBD cannot perfectly refold due to the lack of 20 amino acids of the HBD in the $b2^{167}$ but it cannot be fully excluded that the HBD could partly refold (Voos et al., 1993). As mentioned before, translocation through the TOM complex requires unfolding of the precursor protein (Matouschek et al., 1997). It was also shown that while clogging, b2-DHFR forms an intermediate upon cleavage of the MTS (Esaki et al., 1999). This intermediate spans the IMS, while DHFR is still arrested in the TOM complex. Additionally, it is also published that the mature form of b2-DHFR can be found bound to the TOM complex, while the actual data is labeled as data not shown in this publication (Esaki et al., 1999). This suggests that the 167 amino acids long N-terminal b2 domain is long enough to reach the matrix through the IMS for cleavage of the precursor into the intermediate and mature form. This is plausible as the shortest distances between OMM and IMM are ~5-6 nm with an average distance of approximately ~10-15 nm and an average length of 0.3-0.4 nm (3-4 Å) per amino acid (Ainavarapu et al., 2007; Barad et al., 2023).

Several publications have used the mitochondrial clogger in *S. cerevisiae* to study mitochondrial clogging. In *S. cerevisiae*, expression of b2-DHFR reduced cell growth and led to the accumulation of mitochondrial precursor proteins in the cytoplasm (Boos et al., 2019). Furthermore, an upregulation of chaperones and components of the proteasome-system along with the suppression of the cytosolic protein synthesis machinery and mitochondrial OXPHOS was detectable. The upregulation of chaperones and the proteasome-system was dependent on Rpn4 and Hsf1, while inactivation of the HAP complex reduced the expression of OXPHOS genes (Boos et al., 2019). Another study showed that mitochondrial precursor proteins accumulating due to the expression of b2-DHFR are redirected towards the ER where they are handled by the unfolded UPR^{ER}.

1.5.4.3.1. Advantages of the b2-DHFR model

Several methods can be used to study mitochondrial clogging. This section will give a quick overview of those tools and will discuss advantages and disadvantages of the mitochondrial clogger b2-DHFR that was used in this thesis.

Introduction

As described above, the mitochondrial clogger b2-DHFR induces clogging by the tight folding of DHFR that is fused to the N-terminal MTS of b2. As an alternative to the mitochondrial model clogger b2-DHFR, chemical compounds or other mitochondrial clogger proteins can be used to analyze mitochondrial import clogging. Protonophores such as CCCP, FCCP or the ionophore Valinomycin neutralize the inner membrane potential Δψm, which is essential for protein translocation into the mitochondria. While these drugs are strong inducers of mitochondrial import clogging, they have also strong side effects such as apoptosis and mitophagy which strongly interfere with mechanistic studies of pure mitochondrial protein import (Berezhnov et al., 2016; Coyne et al., 2023; Lofrumento et al., 2011). Other drugs such as MitoBloCKs or Stendomycin interfere with the TIM complex leading to mitochondrial uncoupling which also interferes with the translocation of precursors through the TOM complex (Filipuzzi et al., 2017; Miyata et al., 2017). While these drugs are inducible like the expression of the mitochondrial clogger b2-DHFR, they either inhibit mitochondrial protein import with tremendous side effects such as mitophagy and apoptosis or inhibit the TIM complex and not the TOM complex. This favors the use of a protein such as b2-DHFR that interferes with the TOM complex directly. Furthermore, in comparison to those mentioned drugs, tagging of b2-DHFR can be highly beneficial to analyze direct modifications of the clogger itself. Under physiological conditions mitochondrial clogging is known to be induced by mutations of precursor proteins leading to defective folding and translocation arrest in the TOM complex (Coyne et al., 2023). On the one hand usage of a protein to induce mitochondrial clogging mimics the physiological conditions of the arrest of a mutant protein. On the other hand, the arrested protein potentially gets modified and removed from the clogged channel. GFP-, BioID- and affinity-tagging allows monitoring of the trafficking, interactome and modification of the clogger which is impossible when using inhibitors. This highly favors the use of a model protein that induces clogging. Beside b2-DHFR other proteins are known to induce mitochondrial clogging such as a mutant version of ADP/ATP translocase 1 (ANT1) and other MTS fusions to DHFR (Coyne et al., 2023; Otera et al., 2007). While the ANT1 mutant would be a more physiological model substrate for mitochondrial import clogging, only the protein expression is inducible, but the clogging “strength” cannot be regulated. In comparison to ANT1, MTS-DHFR fusions arrest in the TOM complex can be enhanced by addition of methotrexate (MTX) (Gruhler et al., 1995). Nevertheless, also the expression of b2-DHFR poses some negative side effects such as overexpression of an artificial recombinant protein, especially containing $DHFR^{mouse}$. This highlights the importance of controls during the analysis of mitochondrial clogging of b2-DHFR. For this thesis, the overexpression of DHFR without b2 served as a negative control.

1.6. Aims of this thesis

This thesis aims to extend our knowledge of mitochondrial import quality control in human cells by combining two essential cellular pathways: ubiquitin signaling and mitochondrial quality control. A mitochondrial model clogger, b2-DHFR, will be established in human cells, followed by in-depth analysis of the cellular response to mitochondrial clogging. Experiments are designed to study the ubiquitylation of the mitochondrial clogger and its surrounding proteome. Furthermore, proximity labeling will be performed to characterize not only the interactome of the clogger but also the interactome of the mitochondrial surface, in particular that of the TOM complex subunit TOM20. Thereby, the aim was to identify not only the writers, readers and erasers of the ubiquitin signaling, but also potential new pathways that have evolved to resolve clogged mitochondrial import.

Lastly, mitochondrial quality control has been linked to atypical ubiquitylation involving PARKIN, MARCH5 and USP30. Therefore, the goal was to extend the established Ubiquiton system, which currently allows inducible ubiquitylation with M1, K48 and K63 to include the atypical linkages K6 and K11. This will enable the induction of defined ubiquitin linkages on any protein of interest (POI), allowing dissection of the sequence of ubiquitin-dependent events and permitting pathway analysis even in the absence of mitochondrial import clogging and under strict prevention of downstream processes such as mitophagy initiation.

2 Material and Methods

2.1. Reagents

2.1.1. Chemical reagents

All chemicals and kits used in this work were purchased from Carl Roth, Sigma-Aldrich or Thermo Fisher Scientific, unless otherwise stated. Chemical purchases from other suppliers are listed below:

AppliChem	DMSO
BioRad	20x Trans-Blot Turbo buffer
BioTrend	IPTG
Enzo Life Science	MG-132
Hycultec	CMPD-39
Invivogen	Hygromycin B Gold
Invivogen	Blasticidin
Life Technologies	SYBR Safe DNA stain
Macherey-Nagel	Nucleo Bond Xtra Midi Plus
MedChemExpress	Bafilomycin A1
Merck KGaA	N-Ethylmaleimide
New England Biolabs	ATP, 10x CutSmart, DNA ladders, dNTPs
Polysciences	Polyethylenimine
Promega	FuGene HD transfection reagent
QIAGEN	Ni-NTA agarose
Roche	cOmplete Protease Inhibitor Cocktail
Takara/Clontech	DNA Ligation Kit, Version 2.1

2.1.2. Proteins

Recombinant proteins ^{NUbo}E3(63), Mms2, Ubc13 were generously provided by and (member and former member of the Ulrich laboratory).

Table 2 Commercial proteins and protein kits used in this work

Protein	Supplier
Bovine serum albumin (BSA)	Sigma-Aldrich
DpnI	CF15 - IMB
FastAP Alkaline Poshpatase	Thermo Fisher Scientific
Gibson assembly mix	CF15 - IMB
Herculase II DNA-polymerase	Agilent
HF DNA-polymerase	CF15 - IMB
PfuUltra DNA-polymerase	Agilent
Prestained protein ladder	CF15 - IMB
Quick blunting kit	New England Biolabs
Restriction endonucleases	New England Biolabs
Sm Nuclease	CF15 - IMB
T4 DNA ligase	CF15 - IMB
T4 Polynucleotide Kinase	New England Biolabs
Taq DNA-polymerase	CF15 - IMB
UBA1	CF15 - IMB
Ubiquitin (bovine erythrocytes)	Sigma-Aldrich

Table 3 Primary antibodies used in this work

ID	Name	Species	Source	Cat. No.	Dilution (WB/IF)
42	FLAG M2	mouse	Sigma	F1804	1:2000
49	GFP	mouse	Roche	11814460001	1:2500
70	His	mouse	Sigma	H1029	1:2500
99	Myc	mouse	CF15-IMB	-	1:2000
261	Ubiquitin VU-1 #1	mouse	tebu-bio	VU101	1:2000
265	Ubiquitin P4D1 #2	mouse	Cell Signaling	3936	1:2000
295	mTOR (human FRB domain)	rabbit	Enzo Life Sciences	ALX-215-065	1:2500
296	FKBP12	rabbit	Enzo Life Sciences	ALX-210-142	1:2500
298	Myc	mouse	Merck	05-724	1:2500 / 1:500
383	HA	mouse	CF15-IMB	-	1:2000
442	Ubiquitin #3	rabbit	Bio-Techne	MAB8595	1:2000
452	LC3B	rabbit	Sigma	L7543	1:2000
454	VSV	rabbit	Thermo Fisher	A00199-40	1:5000
464	Flag	rabbit	Cell Signaling	2368T	1:2000
472	DRP1	rabbit	Cell Signaling	5391	1:2000
482	TOM20	rabbit	Sigma	HPA011562	1:2500 / 1:200
484	PDH	mouse	Abcam	ab110333	1:2500
486	IMMT	rabbit	Proteintech	10179-1-AP	1:2500
487	DHFR	rabbit	Cell Signaling Technology	45710S	4:2500
506	Strepavididin 800CW	-	Licor	926-32230	1:5000
-	p62	mouse	Cell Signaling Technology	88588	1:2000

Table 4 Secondary antibodies used in this work

ID	Name	Species	Source	Cat. No.	Dilution
91	Mouse 680LT	donkey	Licor	926-68022	1:10000
92	Mouse 800CW	donkey	Licor	926-32212	1:10000
154	Rabbit 680LT	donkey	Licor	926-68023	1:10000
155	Rabbit 800CW	goat	Licor	926-32211	1:10000
301	Goat anti-Mouse IgG Alexa Fluor 555	goat	Thermo Fisher	A-21422	1:1000
323	Goat anti-Rabbit IgG Alexa Fluor 647	goat	Invitrogen	A-21244	1:1000
498	Rabbit HRP	goat	Dako	P0448	1:1000
501	Mouse HRP	goat	Dako	P0447	1:1000

2.2. Media and solutions

2.2.1. Media for bacterial cultivation

E. coli strains used for plasmid DNA isolation were grown on Luria Broth (LB) agar plates or in liquid LB medium. For recombinant protein expression, bacteria were either grown in LB or in Terrific Broth (TB) medium. All media and antibiotics were prepared by the IMB media laboratory (CF06-IMB). Antibiotic selection was performed at the following concentrations.

Table 5 Antibiotics used for bacterial selection

Antibiotic	Final concentration [µg/ml]	Supplier
Ampicillin	100	CF06-IMB
Chloramphenicol	34	CF06-IMB
Kanamycin	30	CF06-IMB

2.2.2. Media for cultivation of mammalian cells

HEK293T, HeLa and U2OS cells were cultivated in Dulbecco's Modified Eagle Medium (DMEM) supplemented with 2 mM L-glutamine, 100 U/mL penicillin, 100 U/mL streptomycin and 10% (v/v) fetal bovine serum (FBS). Antibiotic selection for plasmid integration and maintenance was performed using 15 µg/mL Blasticidin (InvivoGen) and 150 µg/mL Hygromycin (InvivoGen).

2.2.3. Buffers and solutions

The following solutions were prepared by the IMB media lab (CF06-IMB): 0.5 M EDTA, 1 M KCl, 2 M $MgCl_2$, 5 M NaCl, 5x PBS, 10x TBE, 1 M Tris-HCl pH 7.5.

Blocking buffer for WB:5% (w/v) skim milk powder in PBST

BPD buffer A: 2M Urea 1% SDS

BPD buffer B: PBS 1% SDS

DPD buffer A: 6M Gua-HCl, 50 mM NaH_2PO_4, 50 mM Na_2HPO_4, 10 mM Tris-HCl pH 8.0, 0.1% Tween 20

DPD buffer B: 8M Gua-HCl, 80 mM NaH_2PO_4, 20 mM Na_2HPO_4, 10 mM Tris-HCl pH 6.3, 0.1% Tween 20

IEX Buffer: 50 mM Tris pH 7.4, 1 M NaCl

IMAC Buffer A: 30 mM Tris-HCl pH 8, 300 mM NaCl, 15 mM imidazole

IMAC Buffer B: 30 mM Tris-HCl pH 8, 300 mM NaCl, 500 mM imidazole

MES buffer: 50 mM MES, 50 mM Tris base pH 7.3, 0.1% (w/v) SDS, 1 mM EDTA

MOPS buffer: 50 mM MOPS, 50 mM Tris base pH 7.7, 0.1% (w/v) SDS, 1 mM EDTA

PBS-T: 0.1% (v/v) Tween20 in PBS

Ponceau S solution: 0.1% (w/v) Ponceau S in 5% (v/v) acetic acid

RIPA buffer: 50 mM Tris-HCl pH 7.5, 150 mM NaCl, 1% IGEPAL CA-630, 0.5% sodium deoxycholate, 0.1% SDS, 2.5 mM $MgCl_2$

SEC Buffer: 20 mM HEPES pH 7.4, 150 mM NaCl, 10% (v/v) glycerol, 1 mM DTT

Simple stain: 67 ml Ethanol (99%), 52 ml phosphoric acid (85%), 115 mg Coomassie Blue G-250, in 1 L H_2O_{dd}

Material and Methods

Trans-Blot Turbo buffer: 1x Trans-Blot Turbo buffer (Bio-Rad), 20% ethanol

Ubi Buffer A: 25 mM Sodium acetate, pH 4.0

Ubi Buffer B: 25 mM Sodium acetate, 1 M NaCl, pH 4.0

Ubiquitylation Buffer: 40 mM HEPES pH 7.4, 8 mM magnesium acetate, 50 mM NaCl

2.3. DNA oligonucleotides

Table 6 DNA oligonucleotides used in this work.

ID	Name	Sequence
6114	GFP_Ub_fwd_GA	TGCTAAGGCTAAGAGGTGTTAGTAAAGGAGAAGAACTTTTCAC
6115	GFP_Ub_rev_GA	CTTTGTTAGCAGCCGGATCCTTATTTGTATAGTTCATCCATGC
6116	FKBPbackbone_UbGFP_rev_GA	AAAAGTTCTTCTCCTTTACTAACACCTCTTAGCCTTAGCA
6117	FKBPbackbone_UbGFP_fwd_GA	TGGATGAACTATACAAATAAGGATCCGGCTGCTAACAAAG
6118	NleL_EcoRI_fwd	CCGGAATTCAGTCAAGGCCGTGCCTGC
6119	NleL_NotI_rev	ATAAGAATGCGGCCGCTCAACGCCACGCAACAGG
6120	Ube2SK100R_EcoRI_fwd	CCGGAATTCAACTCCAACGTGGAGAACCTACCC
6121	Ube2SK100R_NotI_rev	ATAAGAATGCGGCCGCTTATGTCTTCTGCATCTTCAG
6122	UBE3A_MfeI_fwd	GCAACAATTGCTTCAAAAACTGGGTCCGGAT
6124	UBE3A_F849A_NotI_rev	GCAAGCGGCCGCTTACAGCATGCCGGCGCCTTT
6150	HACE1(439-End) EcoRI fwd	CCGGAATTCGCAGATTGTCAGGATGTT
6152	HACE1(439/549-End) NotI rev	ATAAGAAGCGGCCGCTTATGCCATTGTGTAACCAT
6305	short-NleL(aa345-782) EcoRI	TATGAATTCCTATCTGACATACAGGAAAATAT
6306	StopMutUBE2Srev	CTTAGACACCTGCCGTACCTAGGGACCCTCAGCCC
6307	StopMutUBE2Sfwd	GGGCTGAGGGTCCCTAGGTACGGCAGGTGTCTAAG
6389	SDM NleL E705A fwd	CGAGTGATATGTTTGGTACAGCGTATGATTCTCCTGAGATTCTACG

6390	SDM NleL E705A rev.	CGTAGAATCTCAGGAGAATCATACG CTGTACCAAACATATCACTCG
6563	pvHECTE3 EcoRI fwd	ATATAGAATTCATCGAAACCATCAG CAGTCTGTTCG
6564	pvHECT E3 NotI rev	ATATAGCGGCCGCTTAGCGCCAGT GCAGTGGCATAATAC
6897	ATG UBE2S fwd BspEI	ATATTCCGGAATGAACTCCAACGTG GAGAACCTAC
6899	UBE2Sshort rev BamHI	ATATGGATCCCATGGGACCCTCAG CCCCTC
7183	Cub-GFP-his AgeI fwd	ATATATACCGGTGGTATCCCTCCAG ATCAACAAAGATTG
7184	Cub-GFP-his NotI rev	ATATATGCGGCCGCTTAGTGGTGG TGGTGGTGGTGAGAACCTTTG
7311	GA NleLHCO into 5432 ins fwd	GGACTCTAGCGTTTAAACTTAAGCT TACCATGGAACAAAAACTTATTTCT GAAGAAGAC
7312	GA NleLHCO into 5432 ins rev	CACCTGCACTCCCATGGATCCGCT AGCCCTCCAGGCCACGGGGTAG
7313	GA NleLHCO into 5432 bb fwd NheI	CTACCCCGTGGCCTGGAGGGCTAG CGGATCCATGGGAGTGCAGGTG
7314	GA NleLHCO into 5432 bb rev	GTCTTCTTCAGAAATAAGTTTTTGTT CCATGGTAAGCTTAAGTTTAAACGC TAGAGTCC
7350	GA NUa-HA-hFRB(K0) into 6233 ins fwd	GAAGCGGAGGCGCTCTAGAGGGAT CCATGCAGATCTTCGTGAAGACCCT GAC
7351	GA NUa-HA-hFRB(K0) into 6233 ins rev	CTTAGTGGTGGTGGTGGTGGTGAG AACCGCTGATGCGGCGGAACACGT G
7352	GA NUa-HA-hFRB(K0) into 6233 bb fwd	CACGTGTTCCGCCGCATCAGCGGT TCTCACCACCACCACCACCACTAAG
7353	GA NUa-HA-hFRB(K0) into 6233 bb rev	GTCAGGGTCTTCACGAAGATCTGC ATGGATCCCTCTAGAGCGCCTCCG CTTC
7514	Myc_GA_fw	GAGCAGAAGCTGATCAGCGAG
7515	Myc_UltraID_GA_rev	CTCGCTGATCAGCTTCTGCTCCTTC TCCTTGAACTTCTTCAGGTTC
7516	DHFR_GA_rev	GTCTTTCTTCTCGTAGACTTCAAAC
7517	DHFR_UltraID_GA_fw	GAAGTCTACGAGAAGAAAGACTTCA AGAACCTGATCTGGCTG
7694	GA TOM20 into 6354 ins fwd	GGTACCGCTAGCGCCGCCACCATG GTGGGTCGGAACAGCGCC
7695	GA TOM20 into 6354 ins rev	GATGTGCCACCTTCAGATCCGCCA CCTTCAGAACCGCCAGCACCAGAA GCTTCCACATCATCTTCAGCCAAGC TC

7696	GA TOM20 into 6354 bb fwd	GGTGGCGGATCTGAAGGTGGCACA TCTGGCGCTACATTCAAGAACCTGA TCTGGCTGAAGG
7697	GA TOM20 into 6354 bb rev	GGCGCTGTTCCGACCCACCATGGT GGCGGCGCTAGCGGTACC
7698	replace myc with flag fwd	CGACGACAAGTAAGCGGCCGCTCG AGTCTAGAGG
7702	b2 flag rev	TCATCCTTGTAGTCGATGCCGGATC CTTGAAGGGG
7768	GA b2-DHFR-P2-TOM20-UltraID ins fwd	GTTAAAGCAAGCAGGAGACGTGGA AGAAAACCCCGGTCCTATGGTGGG TCGGAACAGCGCCATCG
7769	GA b2-DHFR-P2-TOM20-UltraID ins rev	GTCGTCGTCATCCTTGTAGTCCTTC TCCTTGAACTTCTTCAGG
7770	GA b2-DHFR-P2-TOM20-UltraID bb fwd	CCTGAAGAAGTTCAAGGAGAAGGA CTACAAGGATGACGACGACAAGTA AGCGGCCGCTCGAGTCTAG
7771	GA b2-DHFR-P2A-TOM20-UltraID bb rev	CGTCTCCTGCTTGCTTTAACAGAGA GAAGTTCGTGGCTCCGCTTCCCAG GTCCTCCTCGCTGATCAGCTTCTG
8019	myc-his NotI rev	TCGAGCGGCCGCTTAGTGATGGTG ATGGTGATGGTGATGGTGATGCAG GTCCTCCTCGCTGATCAGCTTC

2.4. Plasmids

Table 7 Plasmids created for this work

ID	Name	Selection	Construction
5409	pET15-His-FKBP-L20-3C-Ub(G76V)-GFP	Amp	GA: Ins: pHU 5333 oHU 6114, 6115 bb: pHU 5232 oHU 6116, 6117
5411	pET-His-TEV-FRB-NleL long	Kan	Restriction cloning:EcoRI and NotI insert: pHU 3603 oHU 6118, 6119 backbone pHU 5240
5412	pET-His-TEV-FRB-UBE2S long (K100R)	Kan	Restriction cloning: EcoRI and NotI insert pHU 3604 oHU 6120, 6121 backbone pHU 5240
5414	pET-His-TEV-FRB-UBE3 (F849A)	Kan	Restriction cloning: MfeI + NotI insert: pHU 4334 oHU 6124, 6123 backbone pHU 5240
5422	pET-His-TEV-FRB-L20-HACE1	Kan	Restriction cloning:EcoRI and NotI insert pHU 2930 oHU 6150, 6152 into backbone pHU 5240
5499	pET15-His-FKBP-L20-3C-Ub(K6R, G76V)-GFP	Amp	Mutagenesis on 5409 with oHU 4365 and 4366
5550	pET-His-TEV-FRB-UBE2S short (K100R)	Kan	Mutagenesis of pHU 5412 with oHU 6306, 6307 to get a stop codon before UBD of UBE2S

5565	pET-His-TEV-FRB-NleL short	Kan	Restriction cloning: EcoRI, NotI insert: 3603 oHU 6305, 6119 backbone oHU 5240.
5607	pET-His-TEV-FRB-NleL long (E705A)	Kan	Mutagenesis of pHU5411 with oHU 6389, 6390
5611	pET-His-TEV-FRB-NleL short (E705A)	Kan	Mutagenesis of pHU5565 with oHU 6389, 6390
5678	pET-His-TEV-FRB-pvHECT	Kan	Restriction cloning using EcoRI and NotI after amplification with insert pHU 5680 oHU 6563 and 6564. backbone: 5420
5870	YIp211-ADH-FKBP-Cub(G76V)-UBE2S long	Amp	GA oHU: 6773, 6774, 6775, 6776 Backbone: 4538 insert: 5412
5871	YIp211-ADH-FKBP-Cub(G76V)-UBE2S short	Amp	GA: oHU: 6773, 6776, 6777, 6778 Backbone: 4538 insert: 5412
5950	YIp211-ADH-NleLYCOlong-FKBP-Cub(G76V)-VSV	Amp	Restriction cloning with BspEI and BamHI. oHU 6901 6902 on G-Block of codon optimized NleL into plasmid 4724.
5954	YIp211-ADH-NleLYCOlong-Cub(G76V)-FKBP-VSV	Amp	Restriction cloning with BspEI and BamHI. oHU 6901, 6902 on G-block of NleL yeast codon optimized into 4725
5955	YIp211-ADH-UBE2Sshort(E139R_E143R)-Cub(G76V)-FKBP-VSV	Amp	Restriction cloning BspEI and BamHI. oHU 6897, 6899 on G-block UBE2Sshort(E139R_143R) into 4725
6233	pcDNA5_FRT_TO-NTOM20-FKBP-CUb-GFP-his	Amp Hyg	PCR Insert: pHU 5964 + oHU 7183 + 7184 Backbone: 6166 Restriction: AgeI, NotI
6354	pcDNA5_FRT_TO_b2-DHFR-UltraID	Amp Hyg	GA backbone: pHU = 6292 oHU =7514, 7516 insert: pHU = UltraID from beli lab oHU =7515, 7517
6377	pcDNA5_FRT_TO_DHFR-UltraID	Amp Hyg	GA: backbone: pHU = 6293 oHU =7514, 7516 insert: pHU = UltraID template (Beli lab) oHU =7515, 7517

6378	pcDNA5_FRT_TO_Su9-DHFR-UltraID	Amp Hyg	GA: backbone: pHU = 6294 oHU =7514, 7516 insert: pHU = UltraID pHU oHU =7515, 7517
6447	pcDNA5_FRT_TO_b2-flag	Amp Hyg	PCR with phosphorylated oHU 7698 and 7702 followed by ligation. Replaces UltraID-Myc with a flag-tag.
6449	pcDNA5_FRT_TO_TOM20-L20-UltraID-flag	Amp Hyg	GA insert: plasmid from ORF collection (media lab) oHU 7694, 7695 backbone: pHU 6354 oHU 7696, 7697
6477	pcDNA5_FRT_TO_b2-DHFR-myc-P2A-TOM20-L20-UltraID-flag	Amp Hyg	GA insert: pHU: 6449 oHU: 7769 + 7768 backbone pHU: 6292 oHU: 7770 +7771
6561	pcDNA5_FRT_TO_b2-DHFR-myc-his	Amp	Restriction cloning: insert pHU 6292 with oHU 4954, 8019 restriction digest with BamHI and NotI into pHU 6292
6562	pcDNA5_FRT_TO_DHFR-myc-his	Amp	Restriction cloning: insert: pHU 6293 with oHU: 4954 and this oHU restriction digest with KpnI and NotI Vector: pHU 6293 with KpnI and NotI cutted
6631	pcDNA5_FRT_TO_DHFR-myc-P2A-TOM20-L20-UltraID-flag	Amp Hyg	GA insert: pHU: 6449 oHU: 7769 + 7768 backbone: pHU: 6293 oHU: 7770 +7771
6710	pcDNA5_FRT_TO-TOM20-NUa-Ub(I13A_K27R_K29R_K33R)-HA-FRB(K0)-his	Amp Hyg	GA: insert oHU 7350 + 7351 on Gblock backbone oHU 7352 + 7353 on 6233
6716	pcDNA5_FRT_TO-Myc-NleL_short_hco-FKBP-CUb(K48_63R_G76V)	Amp Hyg	GA insert Gblock NleLshortHCO oHU 7311 + 7312, bb pHU5432 oHU7313 +7314
6717	pcDNA5_FRT_TO-Myc-NleL_long_hco-FKBP-CUb(K48_63R_G76V)	Amp Hyg	GA insert Gblock NleLlongHCO oHU 7311 + 7312, bb pHU5432 oHU7313 +7314

Table 8 Plasmids that were used in this work but created by others

ID	Name	Selection	From
1809	pOG44	AMP	Boulton Lab
2930	HACE1(ORF)	KAN	Ulrich Lab
2932	pET-3a-Ubi K27R	Amp	Ulrich Lab
3599	pET3a-Ub K11R	Amp	Ulrich Lab
3603	pET15b-His6-FKBP-Cub(G76V)-NleL aa170-782	Amp	Ulrich Lab
3604	pET15b-His6-FKBP-Cub(G76V)-Ube2S K100R-UBD	Amp	Ulrich Lab
3605	pET3a-Ub K6R	Amp	Ulrich Lab
3895	YIp211-ADH-Nua-HA-FRB-E3(48)-VSV	Amp	Ulrich Lab
4334	pTZ12-E6AP ΔN200	Kan	Ulrich Lab
4620	YIp128-CUP1-His6-FKBP-Cub(G76V)-GFP	Amp	Ulrich Lab
4654	YIp211-CUP1-Nua-HA-FRB-E3(63)-VSV	Amp	Ulrich Lab
4701	YIp128-CUP1-Nua-HA-FRB-GFP-His6	Amp	Ulrich Lab
5242	pDEST-His10-hsUbiquitin	Amp	Ulrich Lab
5340	pDEST-His10-hsUbiquitin K48R	Amp	Ulrich Lab
5341	pDEST-His10-hsUbiquitin K63R	Amp	Ulrich Lab
5381	pDEST-His10-hsUbiquitin K0	Amp	Ulrich Lab
5680	pET28a(pOPINB)-His-PvHectE3.dna	Kan	Pruneda Lab
6251	pcDNA5/FRT/TO-LinkageID-HTT-K0	Amp	Ulrich Lab
6252	pcDNA5/FRT/TO-LinkageID-HTT-K6-only	Amp	Ulrich Lab
6253	pcDNA5/FRT/TO-LinkageID-HTT-K11-only	Amp	Ulrich Lab
6254	pcDNA5/FRT/TO-LinkageID-HTT-K27-only	Amp	Ulrich Lab
6255	pcDNA5/FRT/TO-LinkageID-HTT-K29-only	Amp	Ulrich Lab

6256	pcDNA5/FRT/TO-LinkageID-HTT-K33-only	Amp	Ulrich Lab
6257	pcDNA5/FRT/TO-LinkageID-HTT-K48-only	Amp	Ulrich Lab
6258	pcDNA5/FRT/TO-LinkageID-HTT-K63-only	Amp	Ulrich Lab
6292	pcDNA5_FRT_TO_b2-DHFR-myc	Amp	Riemer / Methner Lab
6293	pcDNA5_FRT_TO_DHFR-myc	Amp	Riemer / Methner Lab
6294	pcDNA5_FRT_TO_Su9-DHFR-myc	Amp	Riemer / Methner Lab
-	UltraID	Amp	Beli Lab

2.5. Strains and cell lines

2.5.1. Bacterial strains

Table 9 Bacterial strains used in this work

ID	Strain	Genotype	Source
5	BL21-CodonPlus (DE3)-RIL (Codon+)	B F- ompT hsdSB(rB-mB-) dcm+ Tetr gal l(DE3) endA Hte [argU ileY leuW Camr]	Stratagene
14	Top Ten	F- mcrA Δ(mrr-hsdRMS-mcrBC) φ80lacZΔM15 ΔlacX74 recA1 araD139 Δ(ara-leu)7697 galU galK λ- rpsL(StrR) endA1 nupG	Invitrogen
25	Rosetta 2 (DE3)pLysS	F- ompT hsdSB(rB- mB-) gal dcm (DE3) pLysSRARE2 (CamR)	Novagen

2.5.2. Yeast strains

Table 10 Yeast strains that were used in this work

ID	Strain	int. Plasmid	Mated with	created by
5580	RAPa pdr5	E2/3s targeting Nua	5595	Ulrich Lab
5585	RAPalpha pdr5 His6-CUbo-GFP	4620	5607	Ulrich Lab
5587	RAPalpha pdr5 His6-CUbo-GFP pTDH3-Mms2	4620	5612	Ulrich Lab
5595	RAPalpha pdr5 NUbo-GFP-His6	4701	5580	Ulrich Lab
5607	RAPa pdr5 NUbo-E3(48)-VSV pTDH3-Ubc7	3895	5585	Ulrich Lab
5612	RAPa pdr5 NUbo-E3(63)-VSV pTDH3-Ubc13	4654	5587	Ulrich Lab

2.5.3. Mammalian cell lines

Table 11 Mammalian cell lines that were used in this work

ID	Name	int. plasmid	Source
438	U2OS FlpIn TRex b2-DHFR-myc	6292	This study
439	U2OS FlpIn TRex DHFR-myc	6293	This study
480	HeLa FlpIn TRex b2-DHFR-myc-P2A-TOM20-UID-flag	6477	This study
481	HeLa FlpIn TRex DHFR-myc-P2A-TOM20-UID-flag	6631	This study
453	HeLa FlpIn TRex b2-DHFR-UltraID-myc	6354	This study
455	HeLa FlpIn TRex DHFR-UltraID-myc	6377	This study
157	HEK293T	-	Roukos Lab
169	Flp-In U2OS TREX	-	Penengo Lab
408	Flp-In HeLa TREX	-	Dormann Lab

2.6. Methods

2.6.1. Methods for DNA manipulation

2.6.1.1. Measurement of DNA concentration

DNA concentrations were quantified using the DeNovix DS-11 spectrophotometer.

2.6.1.2. Agarose gel electrophoresis

Agarose gel electrophoresis (AGE) as usually performed with 1% agarose gels (w/v). Therefore, agarose was dissolved in TBE buffer containing an intercalating DNA stain (SYBR™ Safe, 1:1000). DNA was mixed with DNA loading dye and loaded to an agarose gel. For size determination, either a 100 bp or 1 kb (NEB) was used. AGE was performed at 100 V for separation and DNA was visualized using the Fusion FX system (Vilber Lourmat) followed by gel extraction of desired fragments as described.

2.6.1.3. PCR

For the use of molecular cloning experiments, DNA was amplified by polymerase chain reaction (PCR). Therefore, the HF polymerase (CF15-IMB) was used according to the following table **(Table 12)**.

Table 12 PCR reaction mixture

Component	Volume [µl] for 50 µl reaction
10X HF pol. Buffer	5
dNTPs (10 mM)	1
Fwd + rev primer (10 µM)	2.5 (each)
Template (DNA, 1-100 ng)	1
HF pol.	0.75 (2 cU/µl)
DMSO	1
ddH2O	36.25
Total Volume	50

All PCR components were added in a reaction tube and placed in a Professional TRIO cycler (Biometra) according to the following table **(Table 13**Table 1**)**.

Table 13 PCR amplification conditions

Step	Temp. [C°]	Time [s]
1. Initial denaturation	98	30
2. Denaturation	98	10
3. Annealing	T_m (Oligos) -5	30
4. Elongation	72	30 per kbp
5. Final elongation	72	300
30 cycles of step 2-4 before step 5.		

2.6.1.4. Site-directed mutagenesis

Desired point mutations were inserted into plasmid DNA with DNA oligonucleotides containing the respective mutations followed by PCR amplification as described above. The first ten annealing steps were performed at 42°C allowing a better annealing of the mutagenesis DNA oligonucleotides. Afterwards, the remaining 20 annealing cycles were performed at the corresponding melting temperatures of the mutagenesis oligonucleotides. The amplified DNA was subjected to a DpnI (CF15-IMB) digest to remove the plasmid DNA before PCR purification.

2.6.1.5. PCR purification

PCR purification was performed using a PCR purification kit (Thermo Scientific™ GeneJET PCR Purification Kit). PCR amplified DNA was mixed 1:1 with the DNA binding buffer and added to the purification column, followed by full speed centrifugation. DNA wash buffer was added to the column after removal of the flowthrough and another full speed centrifugation step followed. The flowthrough was removed and the purification column was dried at room temperature to remove excessive wash buffer. The DNA was eluted with UP H_2O and DNA concentration was measured as described.

2.6.1.6. Gel extraction

After DNA separation by AGE **(chapter 2.6.1.2)**, DNA was purified using a gel extraction kit (Thermo Scientific™ GeneJET Gel Extraction Kit). Desired DNA fragments were extracted from the agarose gel by mixing with 1:1 extraction buffer according to the weight of the gel pieces. This mix was added to the purification column and processed similar to the PCR purification procedure **(chapter 2.6.1.5)**.

2.6.1.7. Restriction cloning

PCR amplified and plasmid DNA (~2 µg) was digested with restriction enzymes according to the manufacturer's protocol. The restriction digest was usually performed at 37°C in the required restriction buffer (rCutSmart™ buffer, NEBuffer™ r1.1, NEBuffer™ r2.1 and NEBuffer™ r3.1). A DpnI digest was performed on PCR derived purified DNA after the restriction digest as described below to remove remaining methylated plasmid DNA contaminations. Afterwards the reactions were separated by size using AGE and extracted according to **(chapter 2.6.1.6)**. After the extraction, fragments were ligated according to the ligation protocol **(chapter 2.6.1.9)**.

2.6.1.8. DpnI digest of methylated DNA

DpnI is an endonuclease with a high preference for methylated dsDNA with Gm6A/TC sites. DNA purified from *E. coli* is typically methylated at the mentioned sites and the DpnI digest allows removal of undesired template DNA after the PCR. DpnI is compatible with common PCR buffers, however, if required rCutSmart™ buffer was added to the reaction. The restriction digest was performed for 1 h at 37°C followed by PCR purification or heat inactivation at 65°C.

2.6.1.9. DNA ligation

DNA ligation was performed using the T4 DNA ligase (CF15-IMB) or a DNA Ligation Kit (Takara), according to the manufacturers' protocol. Typically, insert and backbone DNA was incubated in a molar ratio of 3:1 with an excess of the insert and a total DNA amount of ~100 µg. The incubation was performed at 16°C for at least 1 h followed by transformation into competent *E. coli* (Top10) as described.

2.6.1.10. Gibson assembly

In addition to restriction cloning, Gibson assembly (GA) was used for scar-free ligation. GA DNA oligonucleotides were designed containing overhangs for the GA. These oligonucleotides were used for PCR amplification as followed by gel extraction as described above. The respective DNA fragments were ligated with a homemade GA mix according to the protocol (CF15-IMB). In brief, DNA fragments were mixed in a ratio of 1:1 followed by addition of an equivalent amount of the GA mix. This mix was incubated at 50°C for 1 h and transformed into competent *E. coli* (Top10).

2.6.1.11. Sequencing

Correct DNA was validated either by Sanger sequencing by the StarSEQ GmbH or Nanopore sequencing by Eurofins Genomics GmbH for whole plasmid sequencing. For the Sanger sequencing, approximately ~700 ng DNA was mixed with an up- or downstream binding DNA oligonucleotide with a final concentration of 10 pM. For whole plasmid sequencing, 3 µg DNA in a volume 20 µl were used.

2.7. Techniques for protein purification and analysis

2.7.1. Purification of ubiquitin

Untagged ubiquitin and ubiquitin variants were purified by acid and heat precipitation. Therefore, cells were lysed in an acidic Ubi Buffer A containing cOmplete™, EDTA-free Protease Inhibitor Cocktail (Roche), followed by sonication (Branson Sonifier 450). The lysate was then incubated at 70°C for 30 minutes, and the precipitate was collected by centrifugation. For ion exchange (IEX), the precipitate was eluted in Ubi Buffer B and the IE was performed using a RESOURCE™ S cation exchange column (Cytiva) **(chapter 2.7.3)**. Afterwards size exclusion chromatography (SEC) was performed as described below **(chapter 2.7.4)**.

2.7.2. IMAC purification of his-tagged proteins

His-tagged proteins were purified by cell lysis in IMAC Buffer A supplemented with cOmplete™, EDTA-free Protease Inhibitor Cocktail (Roche). Cell lysis was performed either by using sonication (Branson Sonifier 450) or a high-pressure cell homogenizer (Constant Systems). When the cell homogenizer was used, the bacterial suspension was supplemented with SM Nuclease (CF15-IMB). The cell lysate was centrifuged at 50,000 x g and 4°C for at least 30 min. Ni-NTA agarose beads (Qiagen) were added to the supernatant and incubated at 4°C for 1 h. The agarose beads were washed with 40 mL IMAC Buffer A followed by elution with 10 mL of IMAC Buffer B. Elution fractions were analyzed by Sodium dodecyl sulfate-polyacrylamide gel electrophoresis (SDS PAGE) and Coomassie-staining.

2.7.3. IEX purification

After determination of the isoelectric point of the POI either cation or anion exchange was chosen. The POI was usually rebuffered to reduce the salt concentration after the initial purification procedure. Afterwards, the POI was loaded on the column and the IEX was performed using an NGC system (Bio-Rad). The column was washed until the UV signal reached the baseline followed by subsequent protein elution using IEX Buffer with 10-20 column volumes (CV). Protein content and purity were determined by SDS PAGE and Coomassie-staining.

2.7.4. SEC of purified proteins

In order to remove impurities and exchange the buffer, an additional SEC step was performed. The SEC was performed using either an NGC system (Bio-Rad) or a Äkta Go system (Cytiva). SEC columns Superdex 75 or Superdex 200 (Cytiva) were equilibrated with 1.5 CV of SEC

Buffer. Afterwards, the desired elution fraction was loaded on the column, followed by a wash step with typically 1 CV. Afterwards the protein was eluted from the column and fractions of 1 mL were analyzed by SDS PAGE and Coomassie-staining. A desired protein concentration was achieved by centrifugation with an Amicon® Ultra Centrifugal Filter (Merck) as described below.

2.7.5. Protein concentration

Amicon® Ultra Centrifugal Filter (Merck) were used to increase protein concentration. A desired molecular weight cut-off (MWCO) typically 0.5x the actual MWCO of the protein was chosen in order to remove excess buffer leading to an increased protein concentration. The protein was loaded onto the filter, followed by centrifugation at 4°C and ~3000-4000 x g.

2.7.6. Protein concentration determination

The DS-11 spectrophotometer (DeNovix) was used to determine concentrations of recombinant proteins. Typically, protein concentration was determined with the molecular weight & extinction coefficient function.

2.7.7. SDS-PAGE analysis

Sodium dodecyl sulfate-polyacrylamide gel electrophoresis SDS-PAGE was used for the separation of proteins according to their size. Therefore, 4x NUPAGE LDS Sample buffer (Thermo Fisher) was added to the protein sample in a ratio of 3:1 and incubated at 95°C for 5 min. Afterwards, samples were loaded on a Bis-Tris precast gel (mPAGE™ 4-12%, Merck or NuPAGE™ 4-12%, Invitrogen) and the respective electrophoresis chambers from the manufacturer were used to apply a voltage of 140V. Samples were either separated in MOPS or MES Buffer according to their size and a homemade protein ladder was used to determine the protein size (CF15-IMB). Afterwards, protein analysis was performed either by Coomassie-staining or by western blotting (WB).

2.7.8. Coomassie-staining

Coomassie-staining was performed to analyze the results of an SDS-PAGE. The gels were incubated in Simple Stain Solution for at least 1 h or overnight at room temperature and excessive stain was removed by the addition of H_2O until the destaining was completed.

2.7.9. Western blotting

Protein specific detection for low abundant proteins was performed by WB. After separation of proteins by SDS-PAGE gels were transferred to a semi-dry wester blotting system called Trans-Blot Turbo Transfer System (Bio-Rad). A nitrocellulose membrane was used as an acceptor of the proteins from the gel and both the nitrocellulose membrane as well as the filter papers were soaked in the supplemented transfer buffer. Two filter papers surrounded the gel and the nitrocellulose membrane and placed into a WB cassette (Bio-Rad). The transfer was performed by applying 20V for 12 min to the cassette. Afterwards, WB Blocking Buffer was added to the membrane for at least 30 min, followed by incubation with primary antibodies in PBS-T for 1 h at RT or overnight at 4°C. Three 5 min washing steps with PBS-T were performed to remove excessive unspecific or unbound primary antibody, before application of secondary antibodies in PBS-T for 1-2 h at RT. Again, three 5 min wash steps with PBS-T were used to remove excessive antibody. The WB was analyzed using either a Fusion FX system (Vilber Lourmat) for HRP-coupled secondary antibodies or by an Odyssey fluorescence scanner (LI-COR) for fluorescently labeled secondary antibodies.

2.7.10. *In vitro* ubiquitylation assay

In vitro substrate ubiquitylation was performed in Ubiquitylation Buffer. The Ubiquitylation Buffer was supplemented with 10 µM ubiquitin (or ubiquitin variants), 50 nM Uba1 (E1, CF15-IMB), 1 µM E2s (UBCH7), 1 µM E3 and an equimolar substrate concentration. Addition of 100 µM ATP were used to activate E1 and thereby the ubiquitylation reaction. The dimerization of FRB and FKBP was initiated by addition of 5 µM Rapa. Reactions were typically carried out at 37°C for 2 h or as indicated.

2.8. Methods for *E. coli*

2.8.1. Bacterial cultivation

For plasmid DNA isolation the TOP10 *E. coli* strain was grown on LB agar plates or in liquid LB medium. For the expression of recombinant proteins, *E. coli* strains were either grown in LB or in TB medium. Bacterial cultivation was performed at 37°C and liquid cultures were incubated at 200 rpm.

2.8.2. Bacterial transformation

For bacterial transformation of plasmid DNA, chemically competent *E. coli* strains were used. Bacteria were thawed on ice for approximately 10 minutes before incubation with ~100 ng of plasmid DNA. After an incubation for 15 min., a heat shock was performed at 42°C for 45 seconds. The bacteria recovered at 37°C for 1 h in LB medium before plating on LB agar plates containing the respective antibiotics for selection.

2.8.3. Plasmid DNA isolation

For the isolation of plasmid DNA, single clones of transformed bacteria were inoculated in liquid LB medium containing the selective antibiotics. Bacteria were harvested during exponential growth. For small scale DNA purification, the GeneJET Plasmid Miniprep Kit (Thermo Fisher Scientific) was used according to the manufacturers' protocol. Large scale DNA purification for transient transfections in mammalian cells was performed using the NucleoBond Xtra Midi kit (MACHEREY-NAGEL) according to the manufacturers' protocol.

2.8.4. Recombinant protein expression

Protein expression was performed in *E. coli* strains BL21-CodonPlus (DE3)-RIL (Codon+) and Rosetta 2 (DE3) pLysS. First the desired expression vector containing the DNA sequence of the desired protein was transformed into the competent *E. coli* strain as described. After antibiotic selection, positive colonies were picked and inoculated with ~50 ml of LB medium. This preculture was grown overnight, if necessary, containing Chloramphenicol. Afterwards, the preculture was diluted to a final OD_{600} of 0.1 in 1 L LB medium. After growth to an OD600 of 0.6, protein expression was induced with 1mM IPTG.

2.9. Methods for *S. cerevisiae*

Experiments were performed according to standard conditions for *S. cerevisiae* (Radford, 1991). In brief, *S. cerevisiae* work was performed under sterile conditions and at 30°C.

2.9.1. Yeast strain construction

Model substrates and E3s for the expansion of the Ubiquiton were integrated into either the *LEU2* or *URA3* locus. Positive clones were confirmed by PCR and WB. Substrates and E3s were paired by mating and diploid yeast cells were used for further investigation.

2.9.2. Ubiquitylation assay in *S. cerevisiae*

Substrate ubiquitylation in *S. cerevisiae* was carried out in synthetic complete medium containing 2% glucose. First, a preculture was grown to saturation overnight followed by dilution to an OD_{600} of 0.2. Supplementation of 100 µM $CuSO_4$ was used to induce the protein expression. Addition of 2 µM Rapa initiated dimerization of FRB and FKBP. Collection was performed after a OD_{600} of 1.0 was reached and approximately ~1-1.5 OD_{600} were harvested and flash-frozen on dry ice. Afterwards cells were lysed as described below and analyzed by SDS PAGE and WB.

2.9.3. TCA cell lysis and respective analysis in *S. cerevisiae*

For the cell lysis and subsequent analysis of the substrate ubiquitylation in *S. cerevisiae* trichloroacetic acid (TCA) precipitation was performed. Therefore, *S. cerevisiae* pellets were resuspended in 1 mL of UP H_2O, followed by addition of 150 µl 1.85 M NaOH and 7.5% (v/v) ß-Mercaptoethanol. The mixture was vortexed and incubated at 4°C for 15 min. Afterwards, 150 µl of 55% cold TCA was added to the mixture, vortexed and incubated at 4°C for 15 min. Centrifugation at 21,000 x g at 4°C was performed to collect the precipitate. After removal of the supernatant, the remaining precipitate was dissolved in 50 µl 2x LDS + 20 mM DTT and boiled at 65°C for 10 min. The eluate was then analyzed by SDS PAGE followed by WB.

2.10. Methods for mammalian cell culture and protein analysis

2.10.1. Cultivation

Mammalian cell culture was performed at 37°C and media were pre-incubated at 37°C unless otherwise indicated. Cells were cultivated in DMEM and maintained at 37°C, 5% CO2 and 85% humidity.

2.10.2. Freezing and thawing

Long-term storage of cells was performed at -150°C in cryovial tubes. Therefore, cells were washed once with prewarmed Dulbecco's Phosphate-Buffered Saline (DPBS) (Gibco) during exponential growth. Afterwards, cells were detached using Trypsin-EDTA-Phenol red (Gibco) and prewarmed complete DMEM was added. Cells were harvested at 300 xg for 3 min. and the cell pellet was resuspended in freezing medium containing 90% complete growth medium with 10% DMSO. Before the final transfer of the cells to -150°C, an initial freezing step was performed at -80°C in a CoolCell Freezing Container.

Material and Methods

For cell thawing, cell-containing cryovial tubes were placed into prewarmed water bath and added into a petri dish containing the respective medium followed by adherence overnight.

2.10.3. Passaging

At ~80-90% confluency cells were passaged in a 1:8 or 1:10 dilution into a new petri dish. Therefore, the cells were washed once with prewarmed DPBS and incubated with 0.05% Trypsin-EDTA for 5-10 min. for detachment. Addition of prewarmed complete growth medium was used to inhibit excessive trypsin activity, before the cells were distributed to a new petri dish containing new complete growth medium.

2.10.4. Counting

The cell number was determined after trypsinization. Therefore, cells were mixed in a ratio of 1:1 with an Erythrosin-B cell staining solution. This mix was added to a cell counting slide and the cell number was counted with a TC20 Automated Cell Counter (BioRad).

2.10.5. Transfection with polyethyleneimine

For the transfection of HEK293T cells with plasmid DNA, polyethyleneimine (PEI) solution was used. A day prior transfection 1-5*10^6 cells were seeded into a 10 cm petri dish. 12 µg of plasmid DNA were mixed with 40 µl of PEI solution and incubated with 2 mL of DMEM media without FBS at RT for 10 min. Afterwards, 6 mL of prewarmed complete DMEM medium were added, and the mix was added to the petri dish. For co-transfection of different plasmid DNAs, the plasmid DNA was premixed in the desired ration resulting in a total DNA amount of 12 µg before the PEI solution was added. For smaller or larger transfection volume each reagent was scaled accordingly.

2.10.6. Transfection with Fugene HD

Fugene HD (Promega) was used for the transient overexpression of plasmid DNA in all cells except HEK293T cells according to manufacturer's protocol. In brief, 3 µg of plasmid DNA was diluted in 500 µl OptiMEM (Gibco) and mixed with 9 µl of FuGENE HD. This mix was incubated for 10 minutes and added to 80% confluent cells in a 10 cm dish. Gene expression was allowed for at least 24 h. For smaller or bigger dish volumes, the reactions were scaled up or down.

2.10.7. Generation of stable cell lines (Flp-In)

For the generation of stable cell lines, the Flp-In™ T-Rex™ system was used. Therefore, 2.7 µg of the Flp-recombinase containing plasmid (pOG44, ID 1809) were mixed with 0.3 µg of the pcDNA5/FRT/TO target plasmid containing the desired DNA insertion. This mix was used to transfect FlpIn TREX cells as described **(chapter 2.10.6)**. After 24 h, the cell medium was replaced with fresh medium and after 48 h the cells the respective antibiotics were added to place the cells under selective pressure for the integration. After ~2 weeks surviving cell colonies were visible and cultivated until confluency. Successful integration was confirmed via WB. Gene expression was induced using a final doxycycline (DOX) concentration of 2 ng/mL.

2.10.8. Harvesting

For the biochemical analysis, cells were washed with DPBS and harvested in 1 mL cold DPBS in a 1.5 mL reaction tube using a cooling centrifuge and 300 xg for 5 min. followed by storage at -80°C.

2.10.9. Preparation of cell lysates

After cell harvesting, the cell pellet was thawed on ice. According to the cell amount an appropriate amount of RIPA buffer containing 1x protease inhibitor cocktail (Roche) and SM nuclease (12 cU/ml, PPCF) was added followed by an incubation for at least 30 min on ice. Cell debris was removed via centrifugation at 21500 xg for 10 min and the supernatant was transferred to a new tube. Protein levels were normalized by BCA assay (Thermo Fisher Scientific) following the manufacturer’s protocol.

2.10.10. Preparation for and analysis by fluorescence microscopy

Microscopy was used to determine protein localization. Therefore, the desired number of cells was seeded on a cover slip. Afterwards, cells were fixed with PBS + 4% formaldehyde for 10 min at RT. Formaldehyde was removed by three washes with PBS and the cells were permeabilized with PBS containing 0.2% Triton X-100 for 15 min at RT. Here, 1:10,000 Hoechst 33342 solution was added to stain the nuclear DNA. Two wash steps were used to remove the permeabilization solution before blocking with PBS + 3% BSA for 1 h at RT. Cells were incubated with diluted primary antibodies in PBS + 3% BSA for 1 h at RT. Excessive primary antibodies were removed by three wash steps with PBS + 0.1% Tween-20. Afterwards, a 1:1,000 dilution of secondary antibodies in PBS + 3% BSA was added for 1 h at RT. Remaining and non-specifically bound secondary antibodies were removed by three wash steps for 5 min with PBS + 0.1% Tween-20.

Material and Methods

Imaging was performed on a Stellaris 8 FALCON laser scanning confocal microscope (Leica) equipped with a white light laser and hybrid detectors. Images were acquired using a 63x/1.40 NA oil-immersion objective (Leica HC PL Apo 63x/1.40 oil CS2) in line-sequential mode. Fluorescence of Hoechst 33342, Alexa Fluor 555 and Alexa Fluor 647 was excited at 405 nm, 579 nm, and 630 nm, respectively. Emission detection bands were set to 430 nm to 510 nm (Hoechst 33342), 585 nm to 630 nm (Alexa Fluor 555), and 640 nm to 750 nm (Alexa Fluor 647). Hoechst 33342 and Alexa Fluor 647 were acquired within the same sequence.

Images were recorded at a format of 1024px * 1024 px with a zoom factor of 2, resulting in a pixel size of 60 nm. Images were acquired with two-times line accumulation. Image processing was performed using Fiji (Fiji Is Just ImageJ).

2.10.11. b2-DHFR expression and MTX

The mitochondrial clogger b2-DHFR constructs and their controls were generally expressed for at least 24 h. Generally, b2-DHFR constructs were either expressed under a DOX-inducible in U2OS or HeLa cells or by transient transfection using PEI in HEK293T cells. Upon PEI transfection the medium was replaced 24 h post transfection, followed by a recovery of 6-8 h. If indicated 100 nM MTX was added to stabilize the clogging. If not indicated otherwise the MTX treatment was performed for 5 h before harvesting.

2.10.12. Denaturing Ni-NTA pull-down

For the enrichment of His-tagged proteins denaturing Ni-NTA pull-downs were performed. Therefore, cell pellets were thawed on ice and resuspended in DPD buffer A supplemented with 10 mM imidazole. Proper cell lysis was obtained using 10 pulses of sonication with a 40% duty cycle and an output of 1 (Branson Ultrasonics sonifier). Afterwards each sample was incubated with 50-100 µl of pre-equilibrated Ni-NTA agarose beads (Qiagen) on a rotation wheel for 1 h at RT. The supernatant was discarded and the beads were washed 3x with 1 mL of DPD buffer A. This was followed by three wash steps with 1 mL DPD buffer B. The his-tagged protein was eluted with 50-100 µl of 1x LDS containing 20 mM DTT and 200 mM Imidazole at 95°C.

2.10.13. Enrichment of biotinylated proteins

For the biotinylation experiments with cells having the UltraID integrated, $1.5*10^6$ cells were seeded into a 10 cm petri dish. After 24 h, the gene expression was induced with 2 ng/mL DOX for 24 hours. The cells were treated with 50 µM biotin at 37°C for 10 min if not otherwise

indicated. The biotin containing medium was replaced with fresh medium for 10 min. Excessive biotin which could potentially compete for binding with the biotinylated proteins was removed by wash steps with PBS. The cells were washed 5x with 2-3 mL of PBS before harvesting with 1 mL of PBS. Cell lysis was performed using 1 mL RIPA buffer followed by normalization with a BCA assay. After normalization the cell lysate was incubated with preequilibrated Pierce™ High Capacity NeutrAvidin™ beads (ThermoFisher Scientific) or Dynabeads™ MyOne™ Streptavidin beads for the HeLa MS (Life Technologies). This mix was incubated for 1 h at RT on a rotating wheel. Afterwards the supernatant was discarded, and the beads were washed once with cold RIPA buffer, once with BPD buffer A and once with BPD buffer B. For the elution 4x LDS with 80 mM DTT was mixed 1:1 with 20 mM biotin leading to an elution buffer of 2x LDS, 40 mM DTT and 10 mM biotin. 50 µl of the elution buffer was added to the beads followed by 15 min boiling at 95°C before analysis via WB.

Cell lysis for the MS experiments was performed in the presence of 10 mM N-Ethylmaleimide (NEM). For the MS experiments with integrated HeLa cell lines, $5*10^6$ cells were seeded into 15 cm petri dishes and washes; harvesting and cell lysis was performed as described above. The biotin treatment was performed for 20 min. Beads were washed with 1 mL RIPA, followed by a single wash step with BPD buffer A and two washes with BPD buffer B. Elution from Streptavidin beads was performed at 95°C for 30 min with 20 mM biotin and 1% SDS.

For the MS experiment in HEK293T cells $5*10^6$ cells were seeded into a 10 cm petri dish. On the next day the cells were PEI transfected with plasmids containing b2-DHFR-UltraID, Su9-DHFR-UltraID and DHFR-UltraID. The biotin treatment was performed for 1 h. Otherwise, the experiment was performed as described above.

2.10.14. LinkageID

For the LinkageID experiments HEK293T cells were transiently transfected with PEI and plasmids encoding the respective LinkageID and b2-DHFR in a ratio of 1:1. Cells were treated with biotin for 3 h to allow sufficient reassembly of the biotin ligase and afterwards washed, lysed and enriched for biotin using Pierce™ High Capacity NeutrAvidin™ beads (Thermo Fisher Scientific) were performed as described above.

2.10.15. b2-flag mitochondrial import assay

In order to monitor mitochondrial protein import, the report b2-flag was co-expressed at a defined 1:1 ratio with the mitochondrial clogger b2-DHFR or the control $DHFR^{only}$. One day prior to transfection, HEK293T cells were seeded to reach ~60% confluency on the day of

transfection. The transfection was performed using PEI solution **(chapter 2.10.5)**. 24 h post-transfection, cells were harvested, lysed and analyzed by WB. If indicated cells were treated with 100 nM MTX. As positive control 50 µM CCCP was used which stops protein import into mitochondria due to uncoupling of the proton gradient which is the driving force mitochondrial protein import (J. Kim et al., 2024). Afterwards the cell pellet was lysed and analyzed by WB.

2.10.16. Clonogenic assay

For the analysis of the lethality of mitochondrial clogger, colony formation assays were performed. The cells with integrated plasmids for the b2-DHFR and the respective controls were used. 500 cells per petri dish were seeded and for statistical analysis 3 petri dishes per condition were used. 2 ng/mL of DOX was added 24 h after the seeding and was replaced every five days with fresh medium containing new DOX due to the short half-life (~48 h). Additionally, 100 nM MTX was added if indicated and was also replaced every five days. After 12-14 days cells were fixed with methanol and incubated for 10 minutes with a crystal violet solution (0.5% in 20% ethanol) and washed with H2O.

2.10.17. Cycloheximide chase assay

For the analysis of the stability of the mitochondrial clogger b2-DHFR a cycloheximide (CHX) chase assay was performed. There for $1.5*10^6$ cells were seeded. On the next day, 2 ng/mL DOX was added to the cells and incubated overnight. Before harvesting, the cells were treated with 100µg*mL^{-1} CHX for 3 h if not otherwise indicated. Protein stability was analyzed via WB.

2.11. Mass spectrometry

Sample processing beyond the biotin enrichment, including initial data processing via MaxQuant in the following sections **(chapters 2.11.1 - 2.11.4)** were performed by the IMB proteomics CF (CF12-IMB).

2.11.1. Enzymatic protein digestion

All samples were processed using the SP3 approach [PMID: 30464214]. Proteins were reduced in 5 mM DTT, alkylated in 15 mM chloroacetamide in the dark and quenched in 5 mM DTT. Enzymatic protein digestion was performed using trypsin at 37°C overnight. Following acidification by formic acid, the peptides were purified by solid phase extraction in a C_{18} StageTip format (Rappsilber et al., 2003).

2.11.2. Liquid chromatography tandem mass spectrometry

Peptides were separated via an in-house packed 45 cm analytical column (inner diameter: 75 µm; ReproSil-Pur 120 C_{18}-AQ 1.9-µm silica particles, Dr. Maisch GmbH) on a Vanquish Neo UHPLC system (Thermo Fisher Scientific). Online reverse phase chromatography was performed through a 70-min non-linear gradient of 1.6-32% acetonitrile with 0.1% formic acid at a nanoflow rate of 300 nl/min. The eluted peptides were sprayed directly by electrospray ionization into an Orbitrap Astral mass spectrometer (Thermo Fisher Scientific). Mass spectrometry was conducted in data-dependent acquisition (DDA) mode using a top50 method with one full scan in the Orbitrap analyser (scan range: 325 to 1,300 m/z; resolution: 120,000, target value: 3×10^6, maximum injection time: 25 ms) followed by 50 fragment scans in the Astral analyser via higher energy collision dissociation (HCD; normalized collision energy: 26%, scan range: 150 to 2,000 m/z, target value: 1×10^4, maximum injection time: 10 ms, isolation window: 1.4 m/z). Precursor ions of unassigned, +1 or higher than +6 charge state were rejected. Additionally, precursor ions already isolated for fragmentation were dynamically excluded for 15 s.

2.11.3. Mass spectrometry data analysis of UBE2S

Mass spectrometry raw files were processed using MaxQuant software (version 2.1.3.0 or 2.6.2.0) (Cox & Mann, 2008). MS/MS mass spectra were searched using Andromeda search engine (Cox et al., 2011) against a target-decoy database containing the forward and reverse protein sequences of the UniProt reference proteome for *E. coli* (release 2022_03 or 2024_04) together with the corresponding recombinant proteins and a default list of common contaminants. Trypsin/P specificity was assigned. Carbamidomethylation of cysteine was set as fixed modification. Methionine oxidation, protein N-terminal acetylation and GlyGly remnant at lysine residue were chosen as variable modifications. The minimum peptide length was set to 7 amino acids. The “second peptide” search function was activated. False discovery rate (FDR) was set to 1% at both peptide and protein levels.

The intensities of peptide evidences associated with each detected GlyGly (K) site were summed and then normalized according to the overall detected peptide intensities in each sample, based on the assumption that the overall peptide intensities were similar across the samples. These normalized summed intensities of GlyGly (K) sites were then used for ubiquitin linkage type analysis.

2.11.4. Mass spectrometry data analysis - UltraID experiments

Mass spectrometry raw data files were processed using MaxQuant software (version 2.6.2.0 or 2.6.6.0) (Cox & Mann, 2008). MS/MS mass spectra were searched using Andromeda search engine (Cox et al., 2011) against a target-decoy database containing the forward and reverse protein sequences of the UniProt reference proteome for *H. sapiens* (104,949 entries, release 2024_04) together with the corresponding transgenic proteins and a default list of common contaminants. Trypsin/P specificity was assigned. Methionine oxidation, protein N-terminal acetylation, carbamidomethylation of cysteine, GlyGly remnant at lysine residue (excluding those at peptide C-terminus) and NEM derivatized cysteine were chosen as variable modifications. The minimum peptide length was set to 7 amino acids. The “second peptide” and the “match between runs” functions were activated. False discovery rate (FDR) was set to 1% at both peptide and protein levels.

For label-free protein quantification, the MaxLFQ algorithm (Cox et al., 2014) was employed without using its default normalization option. Minimum LFQ ratio count was set to one. Both the unique and razor peptides were used for quantification. Differential expression analysis was performed in R statistical environment. Reverse hits, potential contaminants and “only identified by site” protein groups were first filtered out. Normalization of the LFQ protein intensities was performed in two steps, first by median-centring on a logarithmic scale, and second by equalizing the group mean intensities of chick avidin between two groups of samples with or without UltraID in the transgene, or streptavidin between two groups of samples with or without TOM20 in the transgene. Proteins were further filtered to retain only those detected in at least three out of the three or four replicates in either group of each comparison. Following imputation of the missing LFQ intensity values, a linear model was fitted using the limma package in R (Phipson et al., 2016) to assess the difference between the control and treatment groups for each protein, with adjustment for multiple testing using the Benjamini-Hochberg approach (Benjamini & Hochberg, 1995). The log2 fold change and the significance of the difference were displayed on a volcano plot. Only proteins with a minimum log2 fold change of 1 and an FDR-adjusted p value (q value) lower than 0.05 were considered differentially regulated.

Quantification and normalization of the detected GlyGly (K) sites were performed as in the UBE2S experiment. Differential expression analysis at the GlyGly (K) level was conducted in the same manner as the protein level, except for the stringency filtering step. The sites were filtered to retain only those detected in at least two out of three or three out of four replicates in either group of each comparison.

2.11.5. Mitochondrial enrichment factor prediction

In order to validate the MS approaches, a mitochondrial enrichment factor (MEF) was calculated. The MS approach included UltraID constructs that are supposed to localize at the mitochondrial surface. Therefore, the MEF was defined as the ratio between (i) the fraction of mitochondrial proteins among significantly upregulated hits and (ii) the fraction of mitochondrial proteins among all quantified proteins in that dataset. Significantly upregulated mitochondrial hits were collected based on a log2 fold change > 1 and an adjusted p-value (Limma) below 0.05. Further, correct mitochondrial localization was confirmed based on MitoCarta3.0 (Rath et al., 2021). A MEF above 1.0 indicates mitochondrial enrichment.

2.11.6. Median-based mitochondrial protein prediction

As a second validation, a median-based prediction of mitochondrial proteins independent of the mitochondrial enrichment-factor was performed. Quantified proteins were classified as mitochondrial or non-mitochondrial based on MitoCarta3.0 (Rath et al., 2021). Afterwards, proteins were partitioned into mitochondrial and non-mitochondrial groups for each condition. For both groups, the median log2 fold change relative to the respective control was calculated, providing a summary measure that indicates whether mitochondrial proteins were enriched over non-mitochondrial proteins.

2.11.7. Screen for E3s, E3 accessory proteins and DUBs

The MS datasets were screened for ubiquitin related proteins using the following resources: dataset of human E3s (https://esbl.nhlbi.nih.gov/Databases/KSBP2/Targets/Lists/E3-ligases/), dataset of human E3 accessory proteins (https://esbl.nhlbi.nih.gov/Databases/KSBP2/Targets/Lists/E3- ligases/RelatedProteins.html) and dataset of human DUBs (https://esbl.nhlbi.nih.gov/Databases/KSBP2/Targets/Lists/DUBs/). The MS dataset of HEK293T cells (b2- $DHFR^{UID}$, Su9- HFR^{UID} and $DHFR^{UID}$) was screened without further normalization. The dataset of HeLa cells with integrated plasmids was initially screened without further normalization and enriched E3s. E3 accessory proteins and DUBs in the proximity of $TOM20^{UID}$ without mitochondrial clogging from the comparison of DHFR-P2A-$TOM20^{UID}$ vs $DHFR^{only\text{-}UID}$ were also obtained without further analyzation. For the screen of ubiquitin related proteins under mitochondrial clogging the respective comparisons were normalized for the LFQ protein intensities of UltraID and adjusted p-values were calculated using the limma package in R (Phipson et al., 2016).

2.11.8. String database enrichment and GO term analysis

For visualization and clustering of proteins STRING database was used (https://string-db.org/). Therefore, selected groups of proteins were uploaded and clustered using the k-means clustering method using the default cluster setting. Further, STRING database was used for the functional enrichment visualization which was performed using the indicated Gene Ontology enrichment. Terms were grouped by similarity (>= 0.08) and sorted by “Signal”.

2.12. Protein structure prediction and visualization

Proteins structures were either predicted using the AlphaFold3 server or existing structures from PDB were used for examination (https://alphafoldserver.com and https://www.rcsb.org) (Abramson et al., 2024). Visiualization of protein structures were performed using UCSF Chimera (Pettersen et al., 2004).

3 Results

3.1. Analysis of mitochondrial TOM complex clogging

3.1.1. Rationale of the establishment of a mitochondrial clogger in human cells

Mitochondrial protein import and its malfunction were initially analyzed in the model organism *S. cerevisiae*, but in recent years, increasing attention has been directed toward its investigation in human cells but fundamental questions remain unanswered **(chapter 1.3.2)**. In yeast, two major MIQC pathways have been identified: mitoCPR and mitoTAD. MitoCPR involves Msp1-mediated removal of stalled precursors from the TOM complex, with Cis1/TOM70 recruiting Msp1 to clogged import channels. The human orthologue ATAD1 similarly removes stalled precursors from the TOM complex, yet how ATAD1 senses clogged complexes in human cells remains unknown. (J. Kim et al., 2024). MitoTAD, which utilizes Cdc48 and its adaptor Ubx2 to extract ubiquitinated stalled precursors, has been well-characterized in yeast but has not been demonstrated in human cells despite apparent conservation of the machinery (VCP and FAF2) (Borgert et al., 2024). Additionally, MDVs may facilitate removal of clogged membrane sections, but their role and recruitment mechanisms are poorly understood. While ubiquitin appears to play important roles in some of these pathways, its precise functions remain incompletely defined (Borgert et al., 2024).

In summary, clear knowledge gaps exist regarding the human MIQC, particularly concerning the recruitment of quality control factors to clogged import channels and the involvement of ubiquitin. To address these questions, the aim of this work was to establish an inducible mitochondrial clogger model in human cells that would enable on-demand monitoring of the interactome and ubiquitylation status of stalled precursors and allow systematic dissection of factors involved in clogger removal.

3.1.2. The mitochondrial clogger b2-DHFR

To systematically dissect ubiquitin signaling and quality control factor recruitment in human cells, the mitochondrial clogger b2-DHFR, originally established in yeast, was adapted. Utilization of a *bona fide* clogger offers the advantage of targeted protein engineering, enabling detailed dissection of mitochondrial import dynamics and the associated ubiquitin-dependent MQC. In brief, the mitochondrial clogger b2-DHFR construct consists of a MTS fused to a tightly folded DHFR domain, whose folding can be further stabilized by addition of MTX **(Fig. 14A, chapter 1.5.4.3)**. Since mitochondrial protein import requires an unfolded polypeptide state, the tightly folded DHFR domain causes precursor stalling during translocation through

the TOM complex. A DHFR moiety lacking an MTS (DHFR^{only}) served as a cytoplasmic control. A C-terminal myc-tag on both constructs enables detection by western blotting and immunofluorescence (IF) microscopy. AlphaFold3-based modeling illustrates how the folded DHFR domain would appear when stalled in the TOM channel **(Fig. 14B)**.

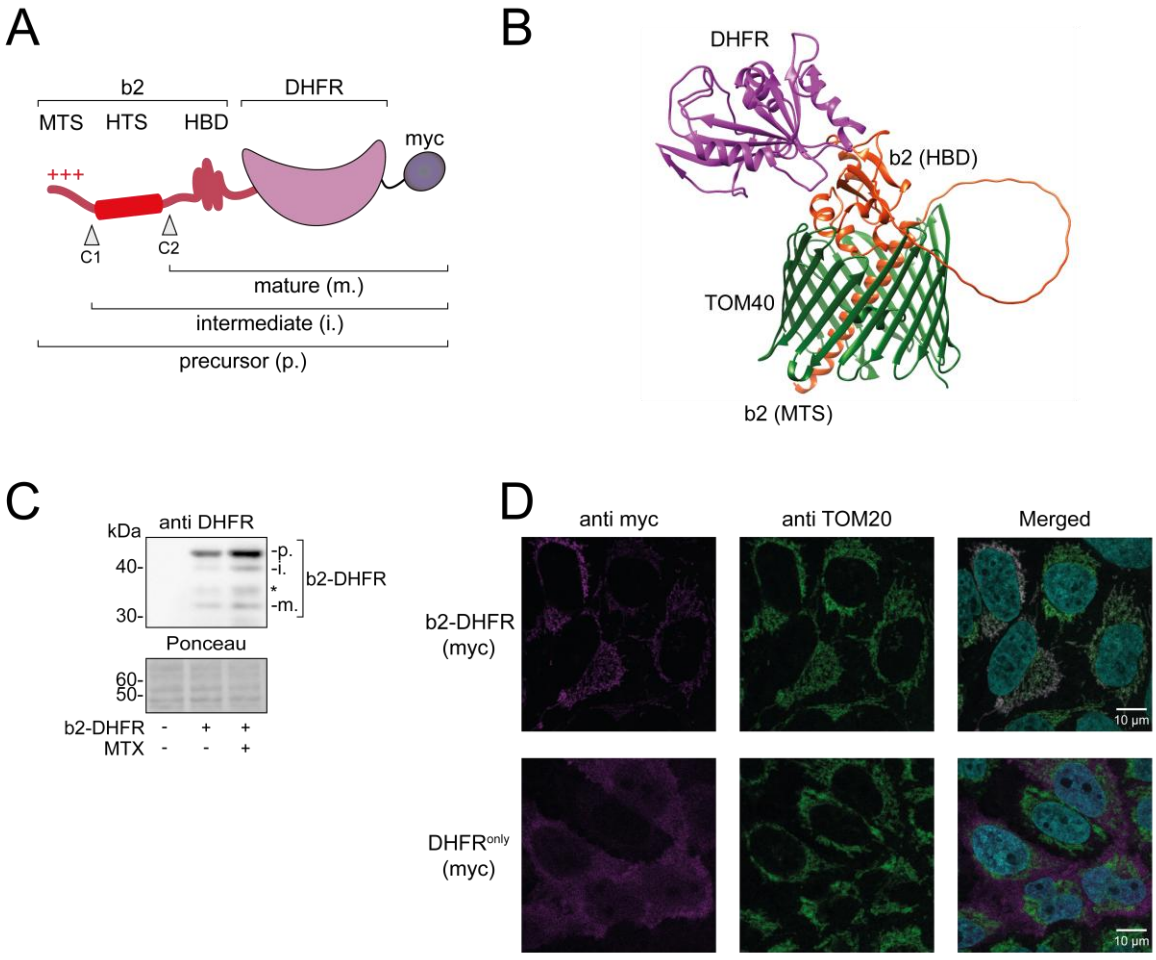

Figure 14 Establishment of the clogger b2-DHFR in human cells. (A) Schematic representation of the b2-DHFR clogger; main processing forms and cleavage sites are indicated. (MTS = mitochondrial targeting sequence, HTS = hydrophobic transmembrane segment, HBD = heme binding domain). **(B)** AlphaFold3 predictions of the pore forming human TOM40 and b2-DHFR-myc; TOM40 displayed in green, b2 domain in orange and DHFR moiety in purple. **(C)** HEK293T cells were transiently transfected with b2-DHFR for 24 h and treated with 100 nM MTX; * indicates an unknown band. **(D)** U2OS cells expressing b2-DHFR-myc or DHFR^{only}-myc for 24 h were analyzed by IF staining; magenta: myc, green: TOM20, Cyan: Hoechst 33342, scale bar: 10 µM.

3.1.3. Validation of the mitochondrial clogger b2-DHFR in human cells

The use of b2-DHFR as a mitochondrial clogger in human cells first required validation of its mitochondrial localization and import clogging activity. The following sections describe the workflow to establish on-demand mitochondrial import clogging in human cells to dissect the mechanistic events triggered by mitochondrial import defects.

3.1.3.1. b2-DHFR is targeted towards mitochondria

First, the expression of b2-DHFR in human cells was investigated. Transient overexpression of b2-DHFR in HEK293T cells resulted in a characteristic three-band pattern, detectable by western blotting (WB), corresponding to precursor, intermediate, and mature forms **(Fig. 14C)**. This is consistent with findings in yeast, where b2-DHFR undergoes two-step proteolytic maturation upon mitochondrial localization (Boos et al., 2019). This suggests correct targeting of b2-DHFR to mitochondria. IF staining of b2-DHFR and the TOM complex subunit TOM20 confirmed their colocalization **(Fig. 14D)**. As expected, $DHFR^{only}$ remained distributed in the cytoplasm. Proximity of b2-DHFR to TOM20 was further validated by proximity labeling followed by WB and MS analysis, described in later chapters **(chapter 3.1.5.1.1 + 3.1.5.2)**.

Together, these data demonstrate that b2-DHFR is expressed and targeted to the TOM complex, fulfilling the prerequisite to study mitochondrial protein import clogging.

3.1.3.2. b2-DHFR expression disturbs mitochondrial protein import

3.1.3.2.1. Design of the mitochondrial import reporter b2-flag

After validation of the correct mitochondrial localization, it was important to confirm that b2-DHFR expression indeed induces mitochondrial import clogging. Established assays to study mitochondrial protein import often involve tedious mitochondrial purification and *in vitro* import reactions, or rely on the analysis of endogenous precursor proteins that are difficult to detect (Murschall et al., 2021). In addition, analysis of mitochondrial clogging by b2-DHFR could be challenging, as the clogger itself might be lost during mitochondrial purification. Thus, a “b2-flag” reporter assay was developed based on the original b2-DHFR construct, retaining the b2 MTS but replacing the DHFR domain with a flag-tag **(Fig. 15A)**. The relatively small flag-tag (8 amino acids) should enable clear discrimination of both b2-conatining constructs during co-expression, without precursor arrest at the TOM complex, caused by larger folded tags such as superfolder GFP (Krakowczyk et al., 2024). Analysis of b2-flag maturation serves as a readout for mitochondrial protein import. Precursor accumulation of b2-flag confirms import clogging, while levels of intermediate and mature forms provide additional insight, though caution is needed due to potential IMS and matrix protease activity.

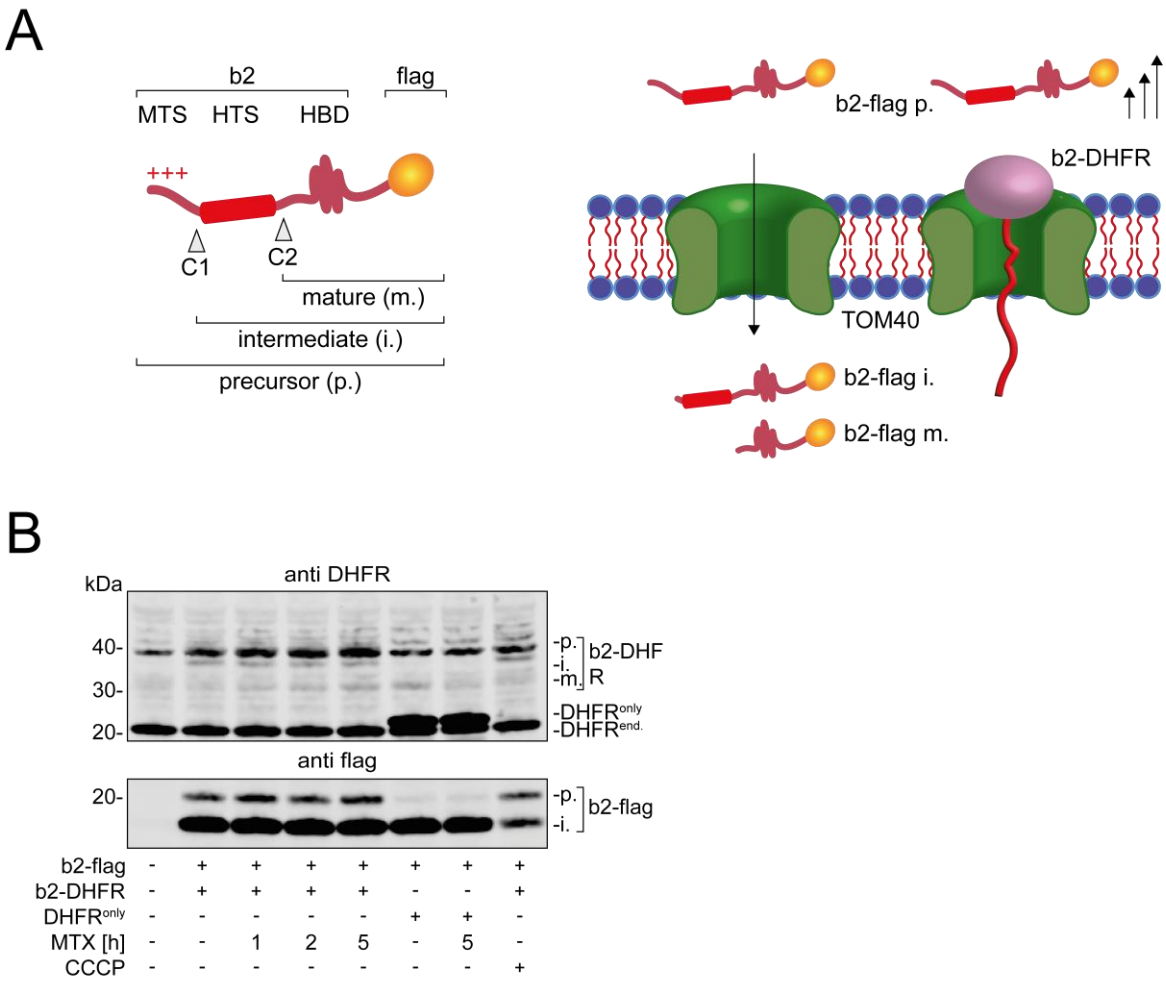

Figure 15 b2-DHFR expression inhibits mitochondrial protein import. (A) Schematic representation of the b2-flag import reporter assay; the b2 MTS serves as a mitochondrial import signal, while a small flag tag allows detection by western blotting. Co-expression of b2-flag with b2-DHFR allows monitoring of the mitochondrial protein import and main processing forms and cleavage sites are indicated (MTS = mitochondrial targeting sequence, HTS = hydrophobic transmembrane segment, HBD = heme binding domain) **(B)** HEK293T cells were co-transfected with b2-flag and either b2-DHFR or DHFR^{only}; 24 h post-transfection, 100 nM MTX was added for the indicated amount of time and 50 µM CCCP was added for 2 h to inhibit mitochondrial protein import (p. = precursor, i. = intermediate, m. = mature).

3.1.3.2.2. b2-flag precursor levels accumulate in the presence of b2-DHFR

In order to confirm that b2-DHFR can block mitochondrial import, b2-flag was co-expressed with b2-DHFR and the DHFR^{only} control in HEK293T cells. Mitochondrial uncoupling by CCCP abolishes the mitochondrial membrane potential ΔΨ which is required for the mitochondrial protein import (Geissler et al., 2000). Therefore, CCCP treatment served as a positive control for impaired mitochondrial import. CCCP treatment resulted in increased accumulation of the b2-flag precursor **(Fig. 15B)**. In contrast, in the presence of DHFR^{only}, the b2-flag precursor was largely undetectable while the intermediate form increased, indicating efficient mitochondrial import under non-stressed conditions. This demonstrates that b2-flag can serve

as a reporter for mitochondrial protein import. Expression of b2-DHFR itself was difficult to monitor due to an overlapping background band. Notably, b2-DHFR expression in the absence or presence of MTX caused significant accumulation of the b2-flag precursor, comparable to CCCP treatment, demonstrating that b2-DHFR induces mitochondrial import clogging. This suggests that the b2-flag assay with transient b2-DHFR overexpression may not be sensitive enough to detect changes induced by MTX-mediated stabilization of the DHFR domain. Further optimization of b2-DHFR and b2-flag expression levels might enable detection of subtle differences in b2-flag precursor accumulation.

In conclusion, b2-DHFR expression results in the accumulation of an artificial mitochondrial precursor, confirming its mitochondrial import clogging activity.

3.1.3.3. Finding optimal clogging conditions by b2-DHFR

After validating functional expression, mitochondrial targeting, and import inhibition by b2-DHFR, optimal MTX clogging conditions were determined to avoid unwanted mitophagy activation. As mitochondrial import requires an unfolded state of the polypeptide chain, the addition of MTX can be used to tighten the clogging **(Fig. 16A)** (Needs et al., 2024). At the same time, addition of MTX could impair mitochondrial function independently of import clogging leading to the induction of mitophagy. Activation of mitophagy would recruit a bulk of protein complexes involved in the clearance of mitochondria and broad ubiquitin signaling through PINK1 and PARKIN (Nguyen et al., 2016). These proteins could create a background which hinders further identification of a clogger-specific quality control. Optimal conditions were tested in a stable HeLa cell line engineered for a subsequent MS proximity labeling screen **(chapter 3.1.5.2).** In brief, this cell line co-expresses b2-DHFR and a TOM20-UltraID (UID, $TOM20^{UID}$) via a P2A site under a doxycycline (DOX-inducible promoter, enabling simultaneous clogging with concurrent proximity labeling at the TOM complex.

First, the stabilization of the b2-DHFR precursor, upon addition of MTX, was analyzed by WB **(Fig 16B)**. The comparison of 1, 2, 5 and 24 h of treatment revealed a time-dependent stabilization of the b2-DHFR precursor. Already after a 2 h MTX treatment the b2-DHFR precursor levels increased. After 5 h a clear stabilization of the b2-DHFR precursor was visible, which slightly increased after 24 h. Precursor stabilization suggests that MTX enhances mitochondrial import clogging, although functional validation is necessary to further support this conclusion.

In summary, precursor stabilization after 5 h of MTX and beyond are optimal to potentially enhance mitochondrial clogging.

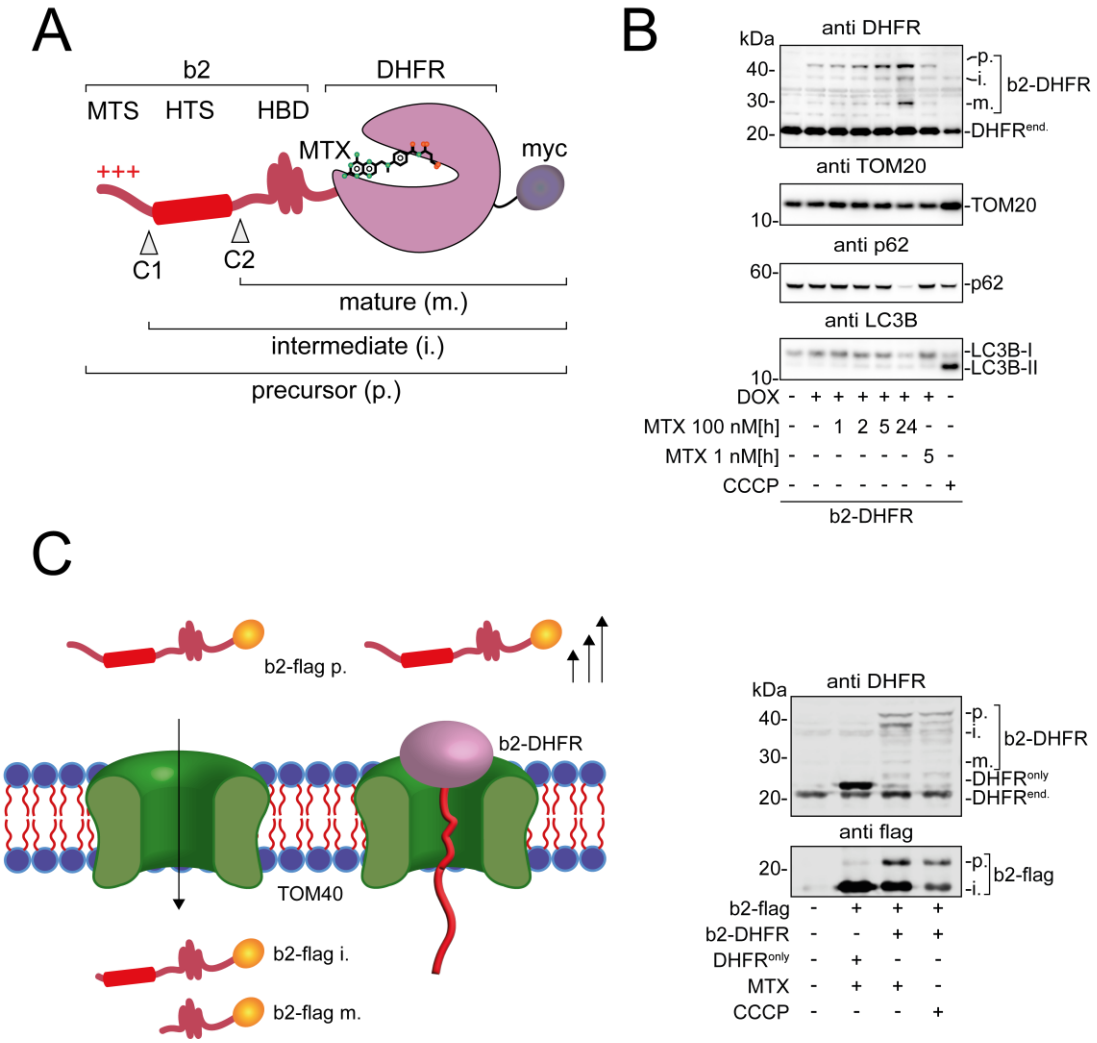

Figure 16 Analysis of optimal mitochondrial clogging conditions. (A) Schematic representation of b2-DHFR clogger bound to its small molecule stabilizer MTX; MTX bound DHFR favors tight folding, (MTS = mitochondrial targeting sequence, HTS = hydrophobic transmembrane segment, HBD = heme binding domain). **(B)** HeLa cells expressing b2-DHFR-P2A-TOM20^{UID} after addition of DOX for 24 h were analyzed for the mitophagy markers p62 and LC3B. After 24 h of expression, cells were treated with 1 and 100 nM MTX for the indicated times; treatment with 50 µM CCCP for 2 h was used to induce mitophagy. **(C)** HEK293T cells were co-transfected with b2-flag and either b2-DHFR or DHFR^{only}; 24 h post-transfection, 100 nM MTX was added for 5 h; treatment with 50 µM CCCP for 2 h was used to inhibit mitochondrial protein import (p. = precursor, i. = intermediate, m. = mature).

3.1.3.4. Optimal clogging conditions do not affect mitophagy markers LC3B and p62

Next, the activation of mitophagy by b2-DHFR was addressed. Two mitophagy markers LC3B and p62 were analyzed in the above describe time-course of the MTX treatment. Cleavage of LC3B-I to LC3B-II and changes in p62 levels indicate induction of mitophagy (I. Kim et al., 2007; A. V. Kumar et al., 2022). Furthermore, changes in mitochondrial protein levels could also indicate mitophagy, thus the OMM marker TOM20 was included in the analysis. The

mitochondrial uncoupler CCCP depletes ΔΨ and is commonly used to induce mitophagy (Mauro-Lizcano et al., 2015). Hence CCCP treatment served as a positive control.

Upon CCCP treatment a clear conversion of LC3B-I to LC3B-II was visible **(Fig. 16B)**. Furthermore, in the presence of CCCP a drop in p62 levels was detectable while a strong increase of the OMM TOM20 was visible. By contrast, a MTX treatment of 1,2 and 5 h did not alter LC3B-I, p62 and TOM20 levels. However, after a 24h MTX treatment, mitophagy markers LC3B, p62 and the mitochondrial marker TOM20 were altered. Surprisingly, p62 levels were stronger decreased compared to the CCCP treatment. The b2-flag assay was repeated with 5 h of MTX and could repeatedly confirm mitochondrial import clogging through the stabilization of the b2-flag precursor, like the CCCP treated condition **(Fig. 16C)**.

In conclusion, a 5 h treatment with 100 nM MTX seemed optimal to further study enhanced mitochondrial clogging without interference with mitophagy.

3.1.4. Analysis of the cellular response to b2-DHFR

3.1.4.1. b2-DHFR-induced mitochondrial clogging impairs clonogenic survival

After the establishment of b2-DHFR as a functional mitochondrial clogger in human cells, the next question was how chronic import stress affects cell proliferation. In *S. cerevisiae*, b2-DHFR expression reduces cell growth after 24 h (Boos et al., 2019). Therefore, clonogenic assays were performed which monitor cell growth and proliferation. Both constructs, b2-DHFR and $DHFR^{only}$ were integrated into U2OS cells under a DOX-inducible promoter using the FlpIn technology. Protein expressions of both constructs were induced by DOX and additionally a MTX treatment was performed. Both treatments were maintained for 12 days, after which colonies were visualized by crystal violet staining to assess long-term proliferative capacity.

DOX treatment of b2-DHFR cells reduced colony numbers and an additional treatment with MTX further decreased clonogenic growth in b2-DHFR-expressing cells **(Fig. 17)**. MTX treatment alone did not significantly affect the cell number. By contrast, the control cell line which expressed $DHFR^{only}$ was only mildly affected by DOX or MTX treatment and combination of both drugs showed no effect.

This suggests that mitochondrial clogging by b2-DHFR, particularly in the presence of MTX, reduces clonogenic survival. Together, these data indicate that sustained mitochondrial import stress compromises the long-term proliferative capacity of human cells.

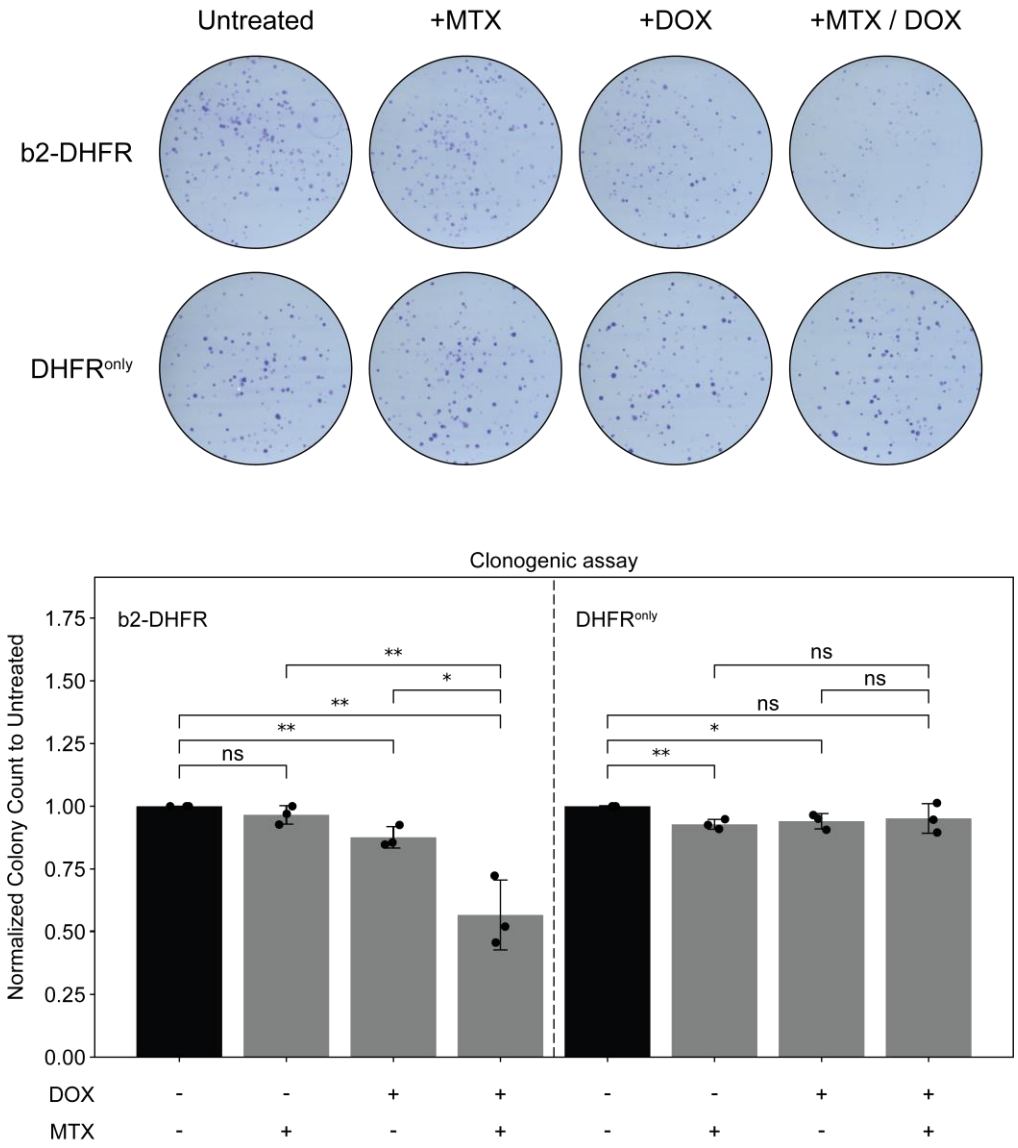

Figure 17 b2-DHFR expression impairs clonogenic survival. Clonogenic survival was monitored in U2OS cells expressing b2-DHFR or DHFR^{only} by addition of DOX for 12 days; 100 nM MTX was added to stabilize folding of the DHFR moiety. Clonogenic survival was counted manually and normalized to the untreated condition, and normalized colony counts were compared between treatment conditions using unpaired two-sided Student's t-test. ($p>0.05$ = ns; $p<0.05$ = *; $p<0.01$ = **) For each condition, three plates (n = 3) were analyzed in three independent biological experiments.

3.1.4.2. The mitochondrial clogger b2-DHFR is rapidly degraded

Several mitochondrial quality control mechanisms that remove arrested precursor proteins at the TOM complex, e.g. mitoTAD and mitoCPR, have been described in *S. cerevisiae* **(chapter 1.3.2)**. It was recently described that ATAD1 removes stalled precursors from the TOM complex analogous to mitoTAD in yeast (Weidberg & Amon, 2018). However, in this publication protein import was inhibited by CCCP and valinomycin and no direct analysis on the stability of a *bona fide* mitochondrial clogger was performed. This raised the question of

how human cells handle the mitochondrial clogger b2-DHFR. Therefore, the degradation dynamics of the clogger b2-DHFR were analyzed in U2OS cells.

To analyze the degradation rate of b2-DHFR, *de novo* protein synthesis was inhibited using cycloheximide (CHX). CHX is a potent inhibitor of the eukaryotic translation that binds to the large ribosomal subunit and blocks the elongation phase of protein biosynthesis (Schneider-Poetsch et al., 2010). After expression of b2-DHFR for 24 h, cells were treated with CHX and b2-DHFR stability was monitored over a period of 5 h. Interestingly, after 2 h of CHX treatment, nearly no b2-DHFR protein was detectable **(Fig. 18)**. Another question was if protein stability would be affected by the addition of MTX which enhances DHFR stability and thereby precursor arrest. Upon MTX treatment the precursor form of b2-DHFR was stabilized and the precursor was detectable after 2 h of CHX chase. After 4 h of CHX treatment, the precursor band was strongly reduced.

This high degradation rate of b2-DHFR may be explained by mitochondrial clearance mechanisms such as mitophagy or apoptosis. Therefore, two mitochondrial marker proteins IMMT, a member of the MICOS complex, TOM20 a TOM complex subunit and endogenous DHFR served as controls. Notably, all these marker proteins were not affected in the short timeframe of the CHX treatment, indicating a clogger-specific degradation mechanism **(Fig. 18)**.

In summary, b2-DHFR displays rapid and selective degradation kinetics that are not accompanied by bulk mitochondrial clearance. Further, MTX treatment affected the degradation of b2-DHFR. However, it cannot be distinguished whether MTX directly decelerates degradation or merely increases precursor abundance, thus rendering it detectable for a longer period. The rapid and selective degradation of b2-DHFR raises the question of whether ubiquitylation contributes to recognition and removal of the clogger.

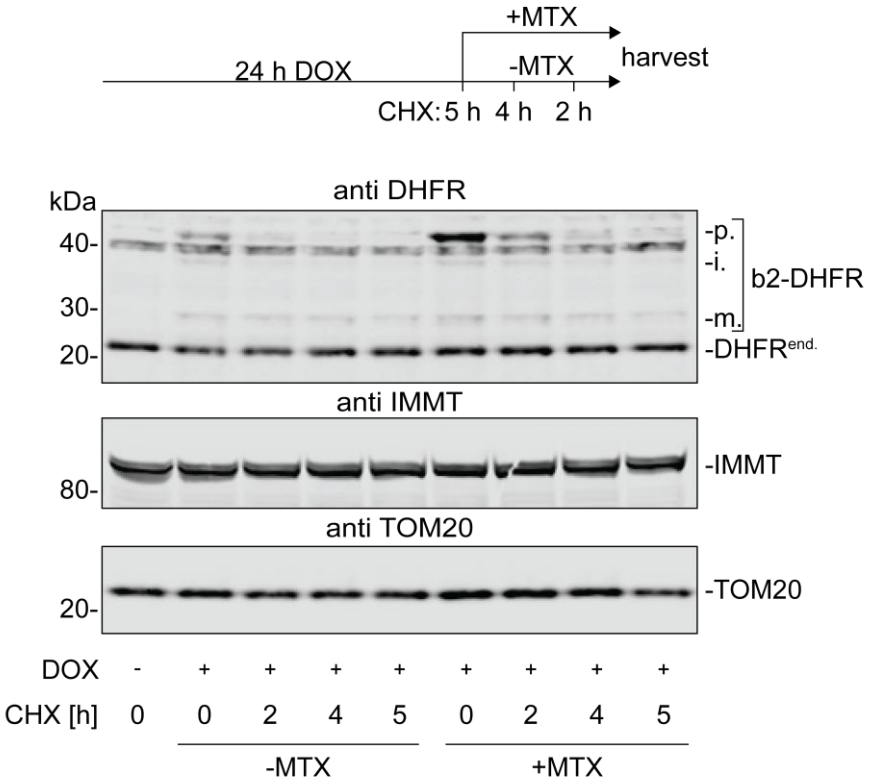

Figure 18 Rapid degradation of clogger b2-DHFR. CHX chase assays were performed to monitor degradation of b2-DHFR; b2-DHFR expression in U2OS cells was induced by addition of DOX, and after 24 h of expression, protein synthesis was inhibited by addition of 100 µg*mL^{-1} CHX for the indicated time with or without addition of 100 nM MTX for 5 h. (p. = precursor, i. = intermediate, m. = mature).

3.1.4.3. Ubiquitylation of b2-DHFR in human cells

The observed rapid turnover of b2-DHFR could be initiated by ubiquitylation of the clogger. Ubiquitylation is a highly conserved post-translational modification that regulates protein stability, typically via proteasomal degradation and contributes to mitochondrial protein import quality control **(chapter 1.3.2 + 1.5.3)**.

3.1.4.3.1. Design of his-tagged b2-DHFR

Finding that b2-DHFR undergoes rapid degradation raised the question of whether ubiquitylation may be involved in the degradative route of b2-DHFR. While K48-linked polyubiquitin chains constitute the predominant signal for proteasome-mediated degradation, other ubiquitin-linkages can induce VCP-dependent or lysosomal degradation (F. Huang et al., 2013; Suryo Rahmanto et al., 2023). In yeast, ubiquitylation recruits Cdc48 and its adaptor Ubx2 (VCP^{hum} and FAF2^{hum}) to stalled precursors, but this pathway has not yet been observed in human cells despite apparent conservation of the machinery (Borgert et al., 2024). Ubiquitylation is challenging to analyze because modification levels are often low and ubiquitin chains can be removed by DUBs or by degradation of the modified protein. A widely used

strategy to overcome these limitations is the overexpression of his-tagged ubiquitin (^{his}Ubi), followed by Ni-NTA enrichment and analysis of the POI in the ubiquitin-enriched fraction (Kirkpatrick et al., 2005; Peng et al., 2003). Therefore, the Ni-NTA enrichment strategy was adapted by tagging the clogger b2-DHFR itself with a his-tag (b2-DHFR^{his}) **(Fig. 19A)**. This enabled direct analysis of the ubiquitylation status of b2-DHFR.

3.1.4.3.2. MTX, VCP and proteasomal inhibition increase ubiquitylation of b2-DHFR

To address the ubiquitylation status of the mitochondrial clogger, b2-DHFR^{his} and its control DHFR$^{only\text{-}his}$ were transiently overexpressed in HEK293T cells, followed by proteasome, lysosome and VCP inhibition. Denaturing pull-downs were performed to ensure that only ubiquitylation of the expressed constructs was detected, eliminating background signals from endogenously ubiquitylated proteins in whole-cell lysates (WCL). Samples were probed with two distinct ubiquitin antibodies to exclude potential detection bias caused by linkage-specific antibody preferences, given the possibility of atypical ubiquitin linkages on the clogger.

Upon addition of MTX, a moderate stabilization of the b2-DHFR precursor was observed in WCL, which was strongly enhanced upon proteasome inhibition **(Fig. 19B)**. With enhanced contrast, a ubiquitylation-like pattern of b2-DHFR species became apparent in WCL upon proteasome Inhibition **(Appendix 1)**. Inhibition of VCP also led to precursor accumulation, albeit to a lesser extent than upon addition of MG132.

Following enrichment, a strong ubiquitylation signal on b2-DHFR^{his} in the presence of MTX was visible which was further enhanced by proteasome inhibition **(Fig. 19C)**. Inhibition of VCP also increased detectable b2-DHFR ubiquitylation in the lower molecular weight range but not as prominent as MG132. Neither USP30 inhibition nor lysosomal inhibition with bafilomycin and chloroquine affected the ubiquitylation of b2-DHFR.

In conclusion, addition of MTX increased the ubiquitylation of b2-DHFR which may reflect the cellular response to potential enhanced clogging by stabilization of the DHFR moiety. While lysosomal inhibition did not affect the ubiquitylation of b2-DHFR, it was increased upon inhibition of VCP. In addition, inhibition of VCP and the proteasome resulted in stabilized b2-DHFR precursor levels, and the latter one resulted in strongly enhanced ubiquitylation of b2-DHFR. This raises the question of which specific ubiquitin linkage-type(s) may be involved in the activity of these pathways.

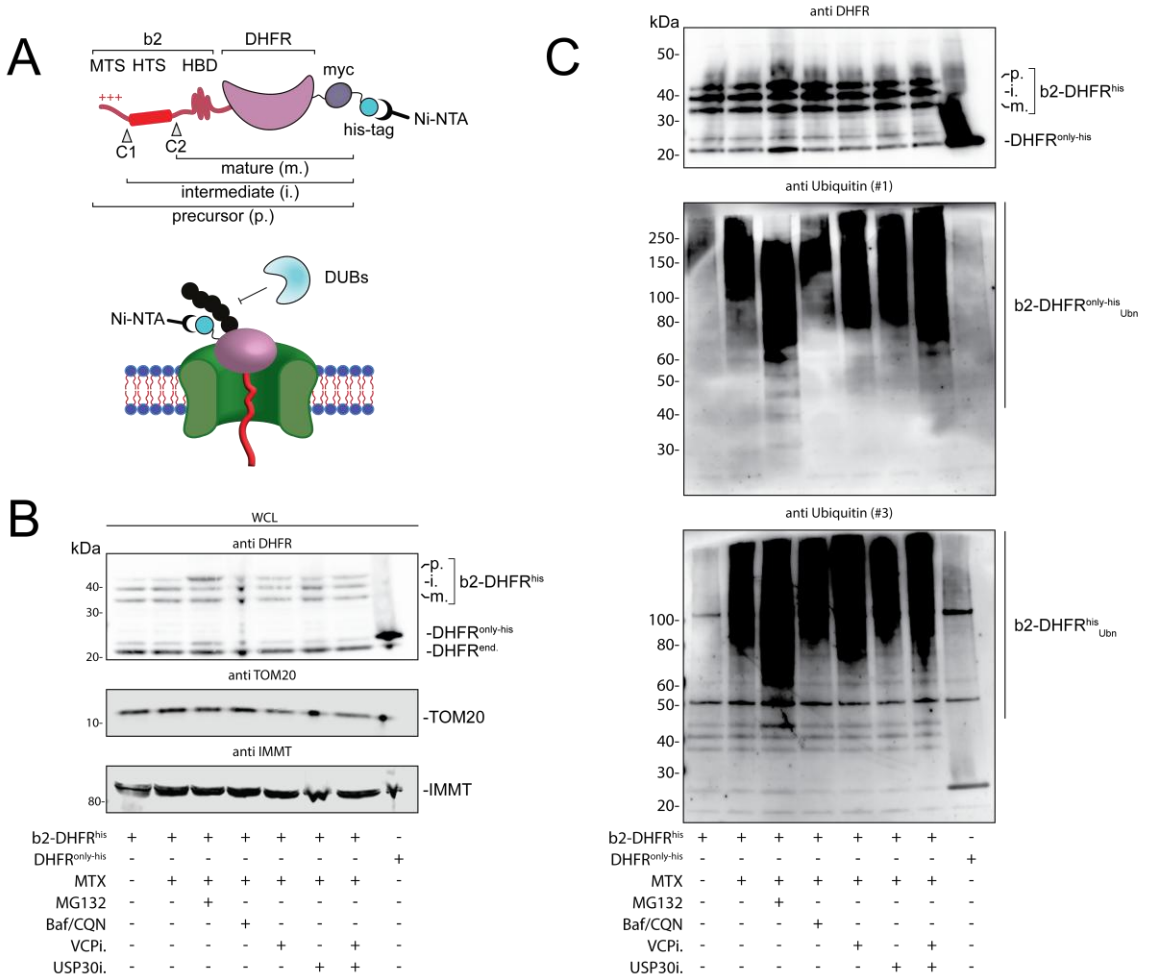

Figure 19 Proteasome inhibition stabilizes b2-DHFR precursor levels. (A) Schematic illustration of the denaturing Ni-NTA pull-down of b2-DHFR. **(B)** Whole-cell lysates of HEK293T cells after transient transfection of b2-DHFR^{his} and DHFR$^{only\text{-}his}$; 24 h post transfection, cells were treated for 5 h with 100 nM MTX followed by 2 h of treatment with the indicated inhibtors (proteasome inhibitor MG132, 30 µM; VCP inhibitor NMS-873, 5 µM; lysosomal inhibitors chloroquine, 10 µM + bafilomycin, 100 nM; USP30 inhibitor CMPD, 200 nM). **(C)** Denaturing Ni-NTA pull-downs were performed in order to analyze the ubiquitylation status of the clogger b2-DHFR; two ubiquitin antibodies were used. (p. = precursor, i. = intermediate, m. = mature).

3.1.4.3.3. Rationale of the his-tagged ubiquitin pull-down

The discovery that b2-DHFR is ubiquitylated upon MTX addition, with ubiquitin levels further stabilized by proteasomal and VCP inhibition, prompted investigation of the ubiquitin linkage type on the clogger. While K48-linked chains are the canonical signal for proteasomal degradation, accumulating evidence shows that atypical ubiquitin linkages can also mediate protein degradation. Recent findings demonstrate that K6-linked ubiquitylation promotes VCP-dependent resolution of RPCs and the known linkage preferences of mitochondrial DUBs and E3s USP30 and MARCH5 beyond K48-linked chains, suggest that b2-DHFR may be modified with atypical ubiquitin chains (Gersch et al., 2017; Shi et al., 2011; Suryo Rahmanto et al., 2023). To investigate b2-DHFR ubiquitylation, a common approach was used that employs

his-tagged ubiquitin (^{his}Ub) enrichment under denaturing conditions to prevent deubiquitylation by DUBs during the purification (Kirkpatrick et al., 2005; Peng et al., 2003).

Lysine-less ubiquitin variants were used that lack K48 ($^{his}Ub^{K48R}$), K63 ($^{his}Ub^{K63R}$) and a ubiquitin variant that lacks all lysines ($^{his}Ub^{K0}$) **(Fig 20A)**. These ubiquitin variants retain a functional C-terminus and can be conjugated to substrates or endogenous ubiquitin, but they cannot be further ubiquitylated at the respective lysine residue that is absent. Especially $^{his}Ub^{K0}$ cannot be further ubiquitylated, thus Ub^{K0} prevents chain elongation. This is in particular interesting, if the ubiquitin chain leads to degradation which would hinder any detection by WB. K48 linked ubiquitin chains for example require a minimum length to initiate proteasomal degradation (Thrower et al., 2000). Capping these chains with $^{his}Ub^{K0}$ would stabilize short chains before they reach a length that leads to degradation.

3.1.4.3.4. b2-DHFR is selectively enriched by $^{his}Ub^{K0}$

Upon enrichment of the ^{his}Ub variants, both the cytoplasmic control $DHFR^{only}$ and b2-DHFR were detected in some ubiquitylated fractions **(Fig. 20B)**. However, neither b2-DHFR nor $DHFR^{only}$ were enriched by $^{his}Ub^{WT}$. This may indicate that ubiquitylation of both proteins triggers degradation or that endogenous DUBs remove the ubiquitin chains prior purification, both would prevent their efficient detection via WB. $DHFR^{only}$ was present in fractions of Ub^{K48R} and Ub^{K0} but not in Ub^{K63R}, which is consistent with K48-linked ubiquitin serving as the canonical proteasomal degradation signal. Only a single band of ubiquitylated $DHFR^{only}$ was observed in $^{his}Ub^{K48R}$ and $^{his}Ub^{K0}$. By contrast, b2-DHFR was neither enriched by $^{his}Ub^{K48R}$ nor by $^{his}Ub^{K63R}$, whereas a clear enrichment was observed with $^{his}Ub^{K0}$. Furthermore, in the $^{his}Ub^{K0}$ condition a ladder-like pattern of the b2-DHFR was detected. This indicates either multi-monoubiquitylation or polyubiquitylation of b2-DHFR by endogenous ubiquitin that is capped by $^{his}Ub^{K0}$. The strong ladder-like ubiquitylation pattern was exclusively visible for b2-DHFR but not for $DHFR^{only}$.

These data suggest that chain elongation and/or linkage composition critically influence the detectability and degradation behavior of b2-DHFR. This is consistent with the observation of the rapid degradation of b2-DHFR. Additionally, $^{his}Ub^{K48R}$ and $^{his}Ub^{K63R}$ did not enrich b2-DHFR, indicating that other atypical linkages (K6, K11, K27, K29, K33) may contribute to its ubiquitylation or that multiple linkages act redundantly. However, initial experiments with ^{his}Ub variants lacking these atypical lysines did not enrich b2-DHFR (data not shown). Therefore, an alternative approach called LinkageID was used to investigate atypical ubiquitylation of b2-DHFR.

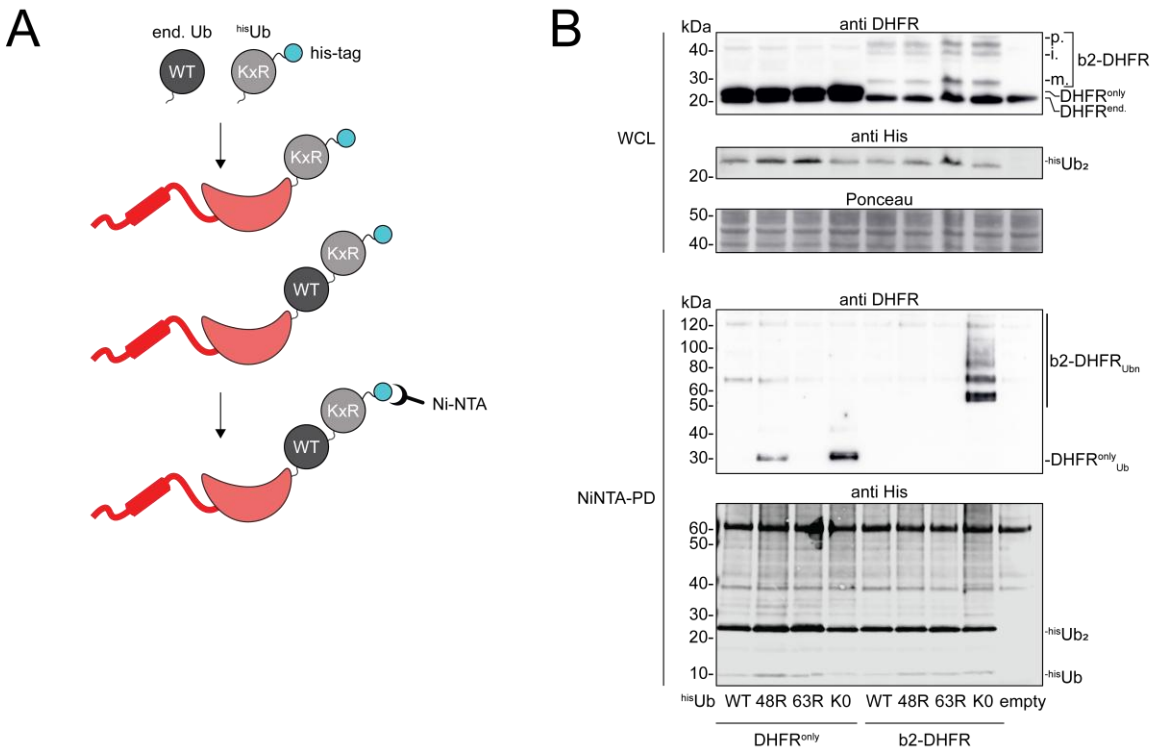

Figure 20 b2-DHFR is selectively enriched by $^{his}Ub^{K0}$. (A) Schematic illustration of the denaturing Ni-NTA pull-down of ^{his}Ub K-to-R replacement variants. ^{his}Ub variants can be attached to *de novo* ubiquitylation sites and to existing ubiquitin chains but cannot further be extended at mutated lysine. **(B)** Whole-cell lysates and denaturing Ni-NTA pull-down samples of HEK293T cells after transient transfection of b2-DHFR and DHFR with the indicated ^{his}Ub variants ($^{his}Ub^{K48R}$ = 48R, $^{his}Ub^{K63R}$ = 63R, $^{his}Ub^{K0}$ = K0). (p. = precursor, i. = intermediate, m. = mature).

3.1.4.4. Understanding the ubiquitylation surrounding b2-DHFR

To overcome the limitations of the ^{his}Ub approach in detecting atypical b2-DHFR ubiquitylation, LinkageID was used, which is a proximity-labeling method that identifies proteins near defined ubiquitin linkages. This is in particular helpful, as it remains unclear whether MQC factors are recruited by ubiquitylation of the clogger itself or by ubiquitin signals formed on neighboring proteins at the TOM complex.

3.1.4.4.1. Rationale for using LinkageID to probe ubiquitylation near the clogger

Recently, a colleague of mine developed a new tool called LinkageID, enabling the labeling of proteins in close proximity to specific ubiquitin linkages **(chapter 1.5.4.2)**. In brief, this tool utilizes a split TurboID fused to lysine-only ubiquitin variants **(Fig. 21A)**. The TurboID parts reassemble only when the specific ubiquitin linkage forms. Upon refolding, all proteins in close proximity of that linkage, such as the ubiquitylated protein, writers, readers and erasers are biotinylated. As a control, split-TurboID fused to lysine-less ubiquitin (K0) accounts for spatial proximity of multiple ubiquitin moieties without linkage formation, such as multi-

monoubiquitylation or binding to proteins with multiple ubiquitin-binding domains. Enrichment of biotinylated proteins enables analysis of protein abundance by WB or MS. Importantly, detection of a protein in a given linkage fraction reflects spatial proximity but does not necessarily mean direct modification with that linkage.

3.1.4.4.2. b2-DHFR and TOM20 are proximal to multiple atypical ubiquitin linkages

To dissect the ubiquitylation in close proximity of a clogged mitochondrial import channel, b2-DHFR was co-expressed with LinkageID constructs in HEK293T cells. After biotin enrichment protein levels of the clogger b2-DHFR itself, IMMT and TOM20 were analyzed **(Fig. 21B+C)**. The clogger b2-DHFR was enriched in the fractions of K6, while K29 and K33 while TOM20 was found enriched in the pool of K27-, K29-, K33- and K63-linked chains **(Fig 21B+C)**. The enrichment of TOM20 was most prominent for the two linkages K33 and K63. IMMT was only enriched in the fraction corresponding to K48-linked chains which is consistent with a recent publication (L. Zhang et al., 2021). These were preliminary experiments and further experiments are required to validate these findings.

Together, these results show that mitochondrial clogging by b2-DHFR is associated with a distinct local ubiquitin landscape of atypical linkages in proximity of b2-DHFR and TOM20.

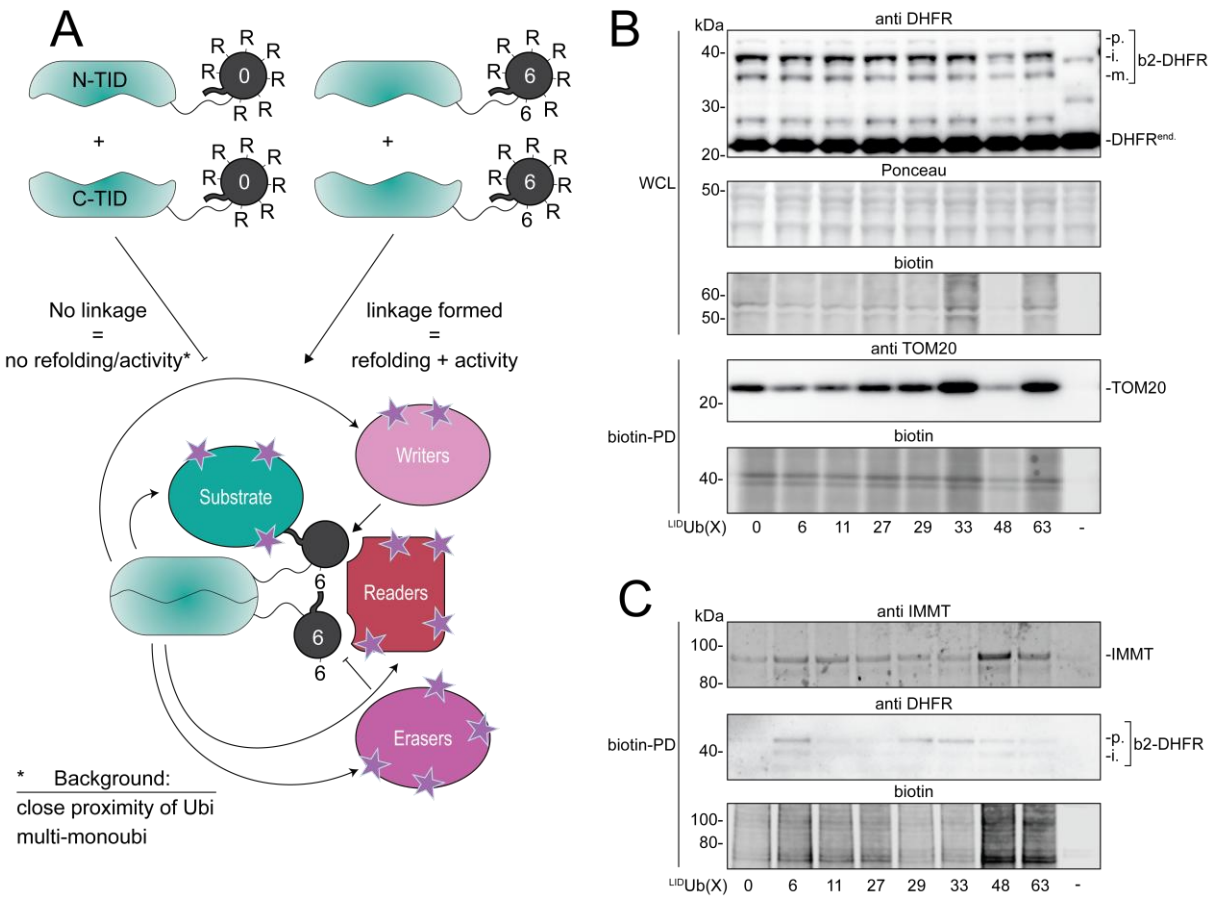

Figure 21 LinkageID reveals atypical ubiquitylation in the proximity of b2-DHFR and TOM20. (A) Schematic illustration of the LinkageID approach. Fusion of split-TurboID fragments to lysine-only ubiquitin variants (^{LID}Ub(X)) allows reassembly of TurboID upon linkage formation and enables biotinylation of proteins in proximity to the respective linkage; lysine-less $^{his}Ub^{K0}$ controls for potential background biotinylation (N-terminal part of TurboID, N-TID; C-terminal part of TurboID, C-TID). **(B)** Whole-cell lysates and biotin pull-down samples of HEK293T cells co-expressing b2-DHFR with LinkageID constructs carrying the indicated lysine. **(C)** Additional experiment investigating the proximity of b2-DHFR to the indicated linkage; experimental set up similar to that in **(B)**. (p. = precursor, i. = intermediate, m. = mature).

3.1.5. Analysis of the interactome of a clogged mitochondrial import channel

Previously, rapid degradation of the clogger b2-DHFR could be demonstrated, and the present data indicate that ubiquitylation contributes to its proteasome-dependent removal. Two independent approaches support the presence of atypical ubiquitin chains either on b2-DHFR itself or in its immediate vicinity at the TOM complex. Such ubiquitin signals may recruit MQC factors that mediate clearance of stalled precursors from the import machinery. On this basis, the subsequent experiments were designed to identify factors that generate the ubiquitin signal

near the clogger and proteins that are recruited to a clogged import channel in response to this modification.

3.1.5.1. Design of b2-DHFR^{UID} to study the interactome of the clogger

Similar to the LinkageID experiments, a proximity-labeling strategy was employed to capture proteins associated with the mitochondrial clogger b2-DHFR. The optimized biotin ligase variant UID was fused directly to the mitochondrial clogger b2-DHFR (b2-DHFR^{UID}) (Kubitz et al., 2022). In addition, UID was also fused to the cytosolic control DHFR^{only} (DHFR$^{only\text{-}UID}$) and to Su9-DHFR (Su9-DHFR^{UID}) **(Fig. 22A)**. Su9 is the N-terminal presequence of subunit 9 of the *Neurospora crassa* F_1F_0-ATP synthase which is a particularly strong MTS, such that Su9-DHFR is generally not expected to induce pronounced import clogging despite the presence of the DHFR moiety (Peker et al., 2023). However, data obtained with Su9-DHFR^{UID} need to be interpreted with caution. The extent to which Su9-DHFR clogs the mitochondrial import channel remains unclear, and the MS analysis therefore focuses mainly on the comparison of b2-DHFR^{UID} vs DHFR$^{only\text{-}UID}$.

The UID-tag was appended C-terminally to b2-DHFR and Su9-DHFR to avoid interference with the MTS. This allows the analysis of the interactome of the mitochondrial clogger b2-DHFR in comparison to a cytosolic control.

3.1.5.1.1. Establishment of b2-DHFR^{UID}

First of all, it was important to confirm that the b2-DHFR^{UID} is functional and capable of labeling OMM proteins such as TOM20. Therefore, b2-DHFR^{UID} and DHFR$^{only\text{-}UID}$ were transiently overexpressed in HEK293T cells. Upon addition of biotin, enhanced UID activity was visible for both constructs **(Fig. 22B)**. Following boitin-enrichment, a clear accumulation of biotinylated proteins was detected, consistent with efficient proximity labeling by the UID fusions. Both constructs displayed clearly distinguishable biotinylation patterns, indicating that they label distinct proximal protein environments. Furthermore, TOM20 was clearly enriched in the b2-DHFR^{UID} condition in comparison to the DHFR$^{only\text{-}UID}$ control **(Fig. 22B)**.

Together, this confirms that b2-DHFR^{UID} is functional and sufficiently targeted towards the TOM complex.

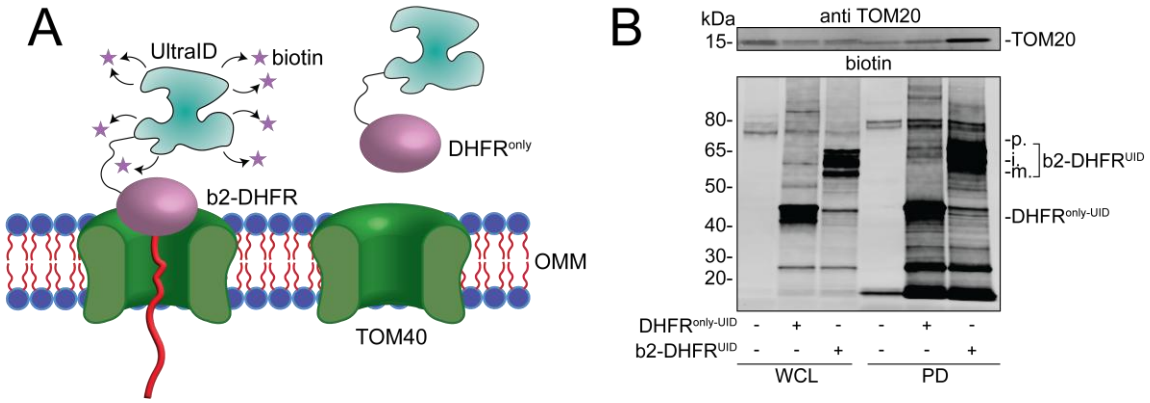

Figure 22 Establishment of b2-DHFR^{UID}. (A) Schematic illustration of the b2-DHFR^{UID} approach; fusion of UID to b2-DHFR allows detection of proteins in the proximity of the mitochondrial clogger b2-DHFR. **(B)** HEK293T cells expressing b2-DHFR^{UID} and DHFR$^{only\text{-}UID}$ for 24 h were treated with 50 µM biotin for 1 h, followed by biotin enrichment (p. = precursor, i. = intermediate, m. = mature).

3.1.5.1.2. Validation of the b2-DHFR^{UID} MS screen

After establishment of the b2-DHFR^{UID} construct, the next aim was to analyze the interactome of the mitochondrial clogger by MS. Experiments were performed in triplicates, comparing b2-DHFR^{UID}, Su9-DHFR^{UID} and DHFR^{UID}. In addition, the USP30 inhibitor CMPD-39 was included. USP30-mediated deubiquitylation of OMM proteins could counteract the b2-DHFR-associated ubiquitin signal and thereby modulate recruitment of mitochondrial quality control factors. First, all samples were analyzed by WB to verify sample quality. Prior to MS analysis, all samples were analyzed by WB to verify sample quality and assess enrichment of selected proteins.

WB analysis confirmed comparable biotinylation signals between input and pull-down samples across all conditions, indicating consistent sample quality **(Fig. 23A+B)**. Additionally, USP30 inhibition did not produce detectable changes by WB. As expected, TOM20 was enriched in proximity to b2-DHFR^{UID}, whereas no comparable enrichment was observed with DHFR$^{only\text{-}UID}$ **(Fig. 23B)**. Together, this justified proceeding with in-depth MS analysis of the samples.

3.1.5.1.3. Mitochondrial proteins are enriched by b2-DHFR^{UID} and Su9-DHFR^{UID}

To further validate the MS approach, a mitochondrial enrichment factor (MEF) was defined. In brief, it compares the ratio of at least 2-fold significantly enriched mitochondrial proteins to all non-mitochondrial hits **(chapter 2.11.5)**.

Both b2-DHFR^{UID} (MEF 7.1) and Su9-DHFR^{UID} (MEF 5.7) showed a robust enrichment of mitochondrial proteins relative to the DHFR$^{only\text{-}UID}$ control, confirming efficient labeling of the mitochondrial proteome in both conditions **(Fig. 23C)**. As an additional control, the median log2 fold change (Log2FC) of mitochondrial proteins was compared with that of non-mitochondrial

proteins, and in both datasets the mitochondrial median exceeded the non-mitochondrial median, indicating a preferential enrichment of mitochondrial proteins **(Fig. 23D)**.

In conclusion, both b2-DHFR^{UID} and Su9-DHFR^{UID} enriched mitochondrial proteins if compared to DHFR^{UID}. This supports efficient and relatively selective labeling of the mitochondrial proteome under the conditions used, providing a suitable basis for downstream analysis.

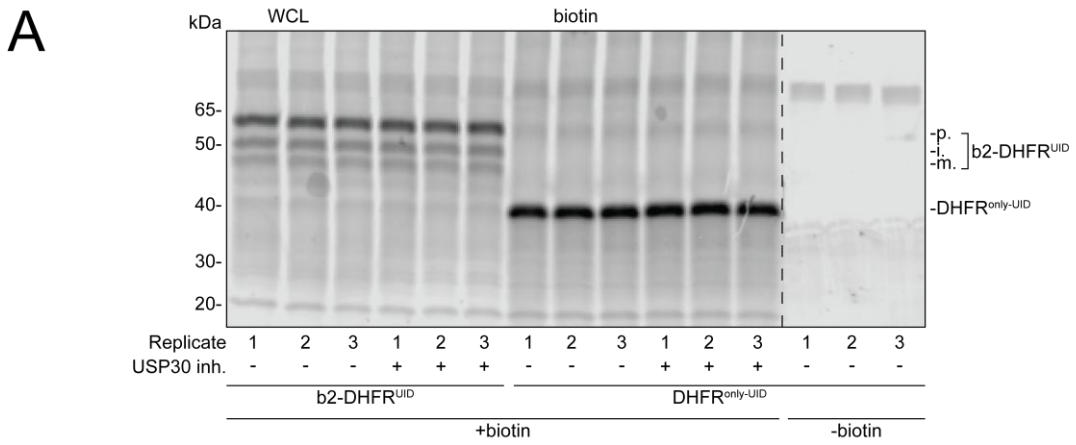
A
kDa
WCL
biotin
65-
50-
40-
30-
20-
-p.
-i.
-m.
b2-DHFR^UID
-DHFR^only-UID
Replicate 1 2 3 1 2 3 1 2 3 1 2 3 1 2 3
USP30 inh. - - - + + + - - - + + + - - -
b2-DHFR^UID
DHFR^only-UID
+biotin
-biotin

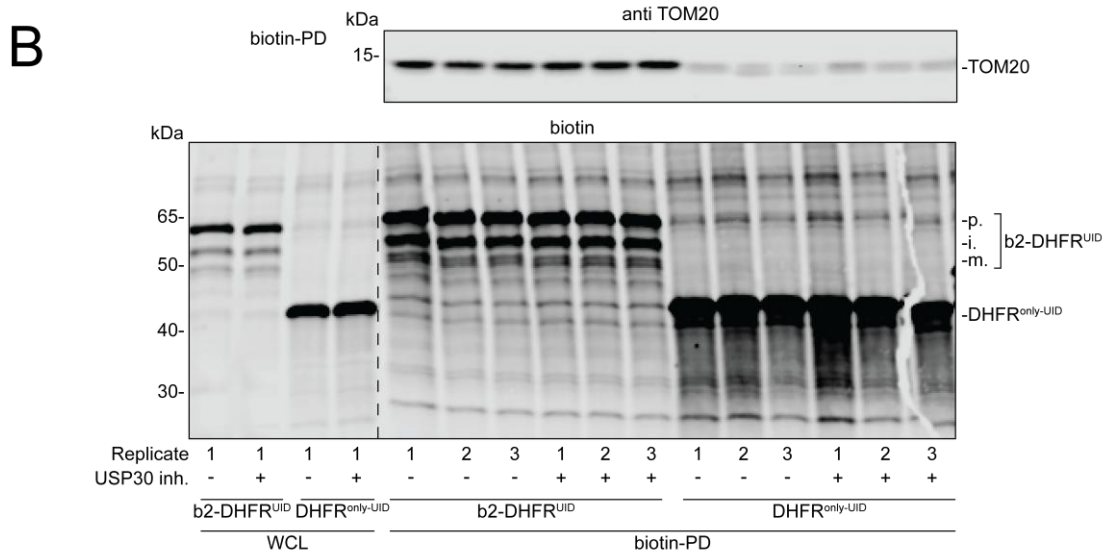
B
kDa
biotin-PD
anti TOM20
15-
-TOM20
kDa
biotin
65-
50-
40-
30-
-p.
-i.
-m.
b2-DHFR^UID
-DHFR^only-UID
Replicate 1 1 1 1 1 2 3 1 2 3 1 2 3 1 2 3
USP30 inh. - + - + - - - + + + - - - + + +
b2-DHFR^UID
DHFR^only-UID
b2-DHFR^UID
DHFR^only-UID
WCL
biotin-PD

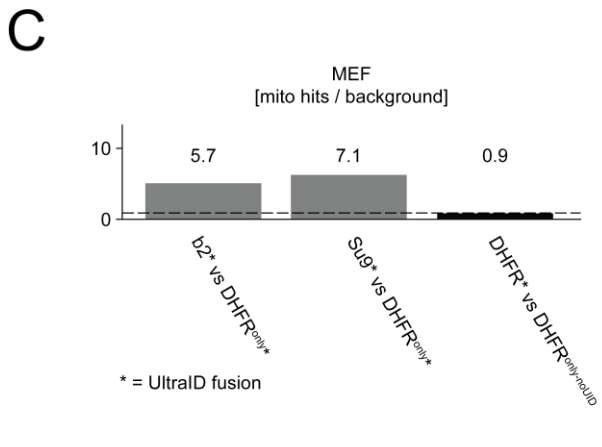
C
MEF
[mito hits / background]
10
0
5.7
7.1
0.9
b2* vs DHFR^only*
Su9* vs DHFR^only*
DHFR* vs DHFR^only-noUID
* = UltraID fusion

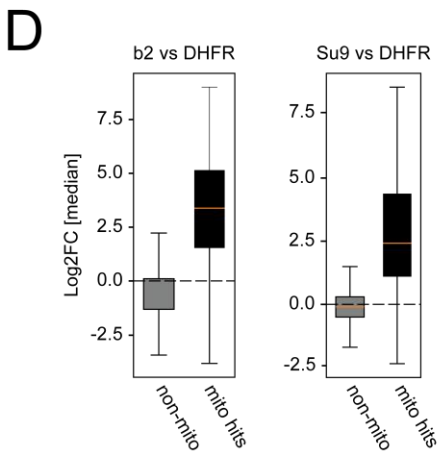
D
b2 vs DHFR
Su9 vs DHFR
Log2FC [median]
7.5
5.0
2.5
0.0
-2.5
non-mito
mito hits

Figure 23 Validation of the b2-DHFR^{UID} MS screen. **(A)** HEK293T cells expressing b2-DHFR^{UID} and DHFR$^{only\text{-}UID}$ for 24 h were either left untreated or treated with 50 µM biotin for 1 h and analyzed for enzymatic activity in whole-cell lysates (p. = precursor, i. = intermediate, m. = mature). **(B)** Biotin enrichment was used to identify proteins in the proximity of b2-DHFR^{UID} and DHFR$^{only\text{-}UID}$. **(C)** The MEF was calculated to probe for mitochondrial enrichment; the MEF describes the ratio between mitochondrial proteins among significantly upregulated hits and the fraction of mitochondrial proteins among all quantified proteins in the dataset (Log2FC > 2, * = UID). **(D)** In addition, mitochondrial enrichment was analyzed with a median-based approach; proteins were classified as mitochondrial or non-mitochondrial based on MitoCarta3.0 and the median Log2FC for both groups was compared.

3.1.5.1.4. The interactome of b2-DHFR^{UID} consists of multiple MQC factors

After validation of the robustness and mitochondrial specificity of the proximity labeling MS dataset, the analysis focused on the interactome of b2-DHFR^{UID} in comparison to the cytoplasmic control. To assess proteins that were specifically enriched or depleted in proximity to the mitochondrial clogger, proteins were visualized in a volcano plot and classified using a threshold of Log2FC > 2 combined with a significance cut-off < 0.05 **(Fig. 24A)**. Multiple proteins related to the MQC such as CLUH, CLPB, USP30, HSPA5, YME1L1, OMA1 and OPA1 were identified. Consistent with an import stress response, GO term analysis revealed significant enrichment of processes potentially related to MIQC, such as “protein targeting to mitochondria”, “protein folding” and “proteolysis” **(Fig. 24B)**. This suggests that a UID based approach enables the detection of potential MIQC factors in proximity to the clogger b2-DHFR.

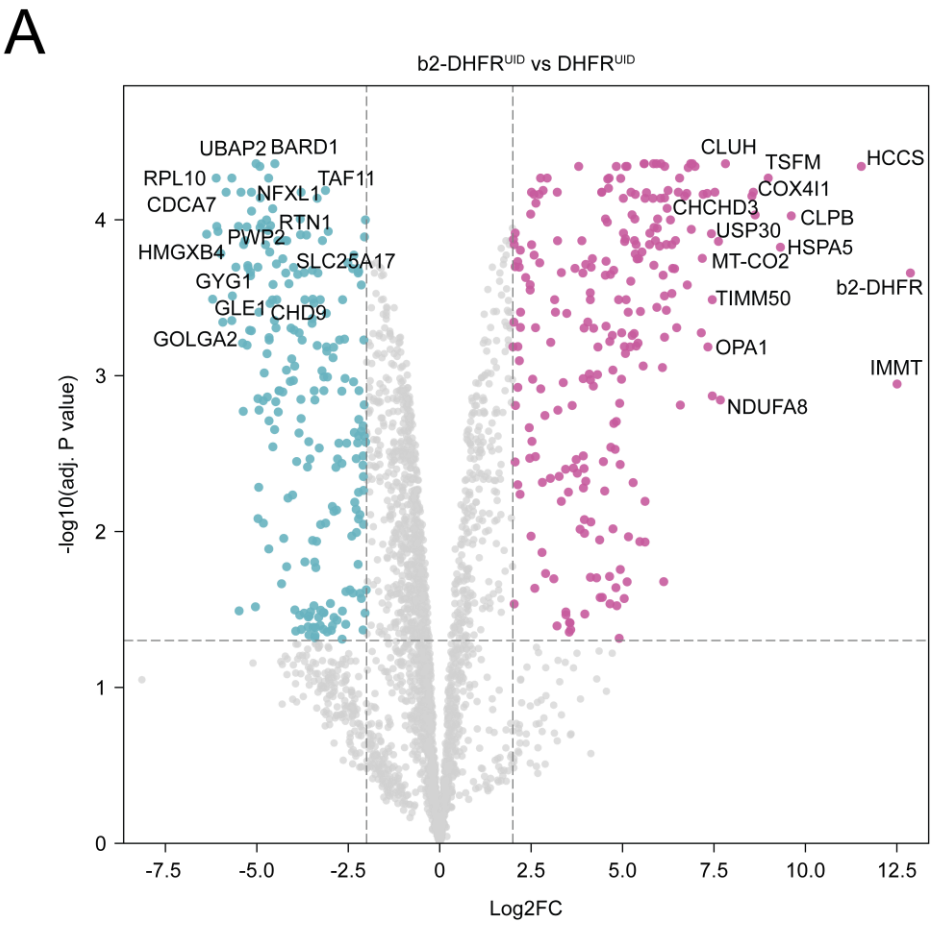
A
b2-DHFR^UID vs DHFR^UID
UBAP2
BARD1
RPL10
TAF11
NFXL1
CDCA7
RTN1
PWP2
HMGXB4
SLC25A17
GYG1
GLE1
CHD9
GOLGA2
CLUH
TSFM
HCCS
COX4I1
CHCHD3
CLPB
USP30
HSPA5
MT-CO2
b2-DHFR
TIMM50
OPA1
IMMT
NDUFA8
-log10(adj. P value)
Log2FC
0
1
2
3
4
-7.5
-5.0
-2.5
0
2.5
5.0
7.5
10.0
12.5

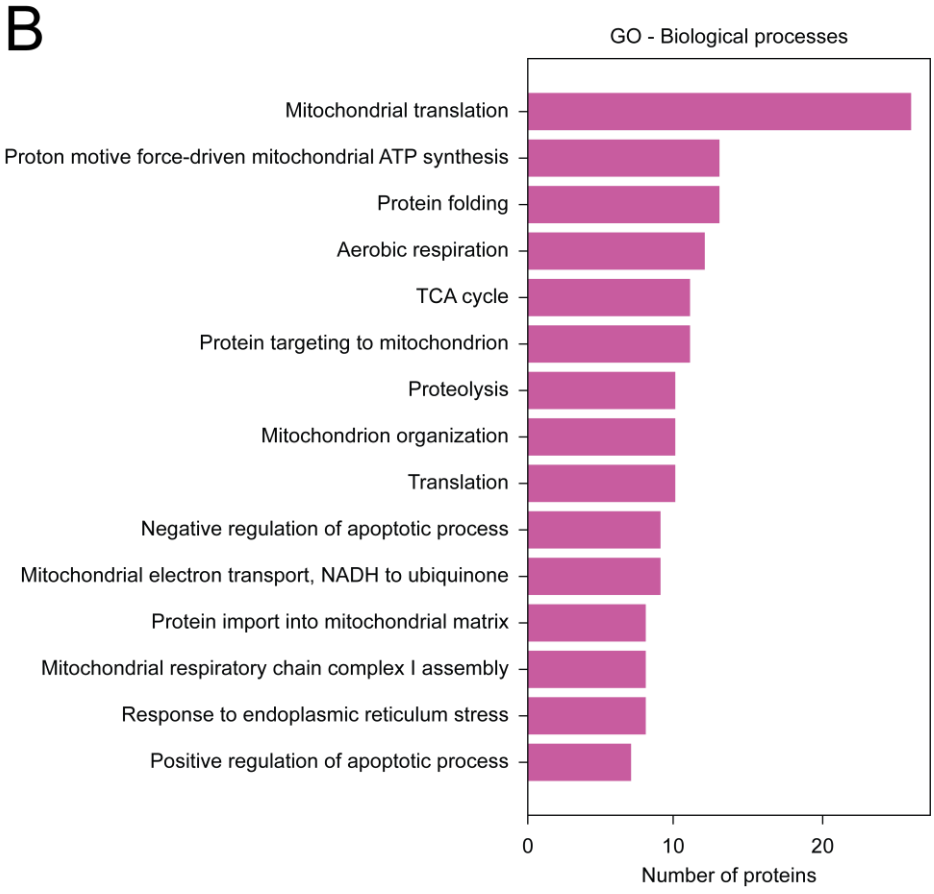
B
GO - Biological processes
Mitochondrial translation
Proton motive force-driven mitochondrial ATP synthesis
Protein folding
Aerobic respiration
TCA cycle
Protein targeting to mitochondrion
Proteolysis
Mitochondrion organization
Translation
Negative regulation of apoptotic process
Mitochondrial electron transport, NADH to ubiquinone
Protein import into mitochondrial matrix
Mitochondrial respiratory chain complex I assembly
Response to endoplasmic reticulum stress
Positive regulation of apoptotic process
0
10
20
Number of proteins

Figure 24 The interactome of b2-DHFR^{UID} consists of multiple MQC factors. **(A)** Vulcano blot representing upregulated (magenta) and downregulated (blue) proteins in the comparison of b2-DHFR^{UID} vs DHFR$^{only\text{-}UID}$ (cut-offs: Log2FC > 2 and limma-based p.value < 0.05). **(B)** GO term enrichment analysis of biological processes for the upregulated proteins identified in **(A)**.

3.1.5.1.5. Atypical linkage-specific ubiquitin peptide remnants can be detected under mitochondrial import stress

Given that b2-DHFR is potentially ubiquitylated with an atypical linkage, the MS datasets of b2-DHFR^{UID}, Su9-DHFR^{UID} and DHFR$^{only\text{-}UID}$ were screened for linkage-specific diGly-peptide remnants. Detection of linkage-specific diGly-peptide remnants does not demonstrate that b2-DHFR or Su9-DHFR themselves carry that particular ubiquitin linkage; rather, it indicates that the enriched pool of biotinylated proteins is co-enriched for ubiquitin chains of that linkage type.

K6-, K11-, K48-, and K63-linked ubiquitin remnants were detected in both comparisons b2-DHFR^{UID} vs. DHFR$^{only\text{-}UID}$ and Su9-DHFR^{UID} vs. DHFR$^{only\text{-}UID}$ **(Fig. 25A)**. All ubiquitin linkages increased in b2-DHFR^{UID} and Su9-DHFR^{UID} compared to DHFR$^{only\text{-}UID}$. Notably, these linkages were more abundant in b2-DHFR^{UID} than in Su9-DHFR^{UID}. The combined ubiquitin signal was significantly enriched in both b2-DHFR^{UID} vs. DHFR$^{only\text{-}UID}$ (~2.5 Log2FC) and b2-DHFR^{UID} vs. Su9-DHFR^{UID} (~1.9 Log2FC). This might indicate that more pronounced import clogging in the b2-DHFR^{UID} condition compared to Su9-DHFR^{UID} enhances ubiquitylation, but further experiments are required to validate this idea.

In summary, MS analysis revealed enrichment of K6-, K11-, K48-, and K63-linked ubiquitin remnants in the b2-DHFR^{UID} dataset. This is consistent with previous findings that b2-DHFR is in proximity of atypical ubiquitin linkages particularly K6, while TOM20 is found in proximity to K63-linked chains during import clogging **(chapter 3.1.4.4)**.

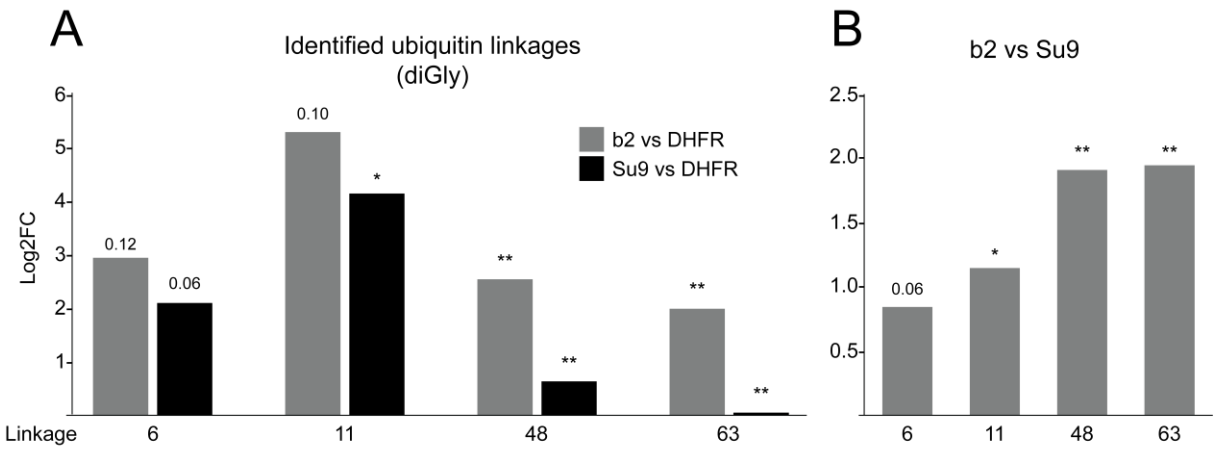

Figure 25 diGly remnants of ubiquitin linkages in the proximity of b2-DHFR^{UID}. (A) Quantification of diGly remnants from different ubiquitin linkages identified in the comparisons b2-DHFR^{UID} and Su9-DHFR^{UID} vs DHFR$^{only\text{-}UID}$. **(B)** Analysis of diGly remnants of ubiquitin linkage in the comparison b2-DHFR^{UID} vs Su9-DHFR^{UID}. For the quantification in **(A)** and **(B)** log2-transformed intensities from three biological replicates per condition were calculated and log2-fold changes were analyzed; p-values were calculated using an unpaired, two-sided Welch's t-test (assuming unequal variances) to assess differences between conditions and are indicated above each bar (* < 0.05, ** < 0.01).

3.1.5.1.6. The b2-DHFR^{UID}/DHFR^{UID} proximity labeling setup might exhibit a mitochondrial localization bias

Inspection of enriched GO-terms further highlighted mitochondrial compartments and processes, including "mitochondrial translation", "TCA-cycle", "protein import into the mitochondrial matrix", in the b2-DHFR^{UID} vs DHFR$^{only\text{-}UID}$ comparison **(Fig. 24B)**. Therefore, it was reasoned that the initial proximity labeling setup captured mitochondrial proteins per se. A possible explanation would be a localization bias in this proximity labeling strategy: b2-DHFR^{UID} accumulates at the clogged TOM complex and biotinylates proteins in its immediate vicinity, whereas DHFR$^{only\text{-}UID}$ is largely cytosolic and cannot access the outer membrane to the same extent. As a result, mitochondrial proteins are enriched partly due to the bait localization itself, making it difficult to distinguish constitutively proximal mitochondrial proteins and import clogging related MIQC factors

To minimize this bias, a solution would be a fusion of the UID to an OMM protein, e.g. a subunit of the TOM complex. This would allow independent expression of b2-DHFR and DHFR^{only} while the UID is constitutively anchored at the mitochondrial surface.

3.1.5.2. Optimized proximity labeling strategy: Mitochondrial surveillance with TOM20^{UID}

3.1.5.2.1. Rationale of an optimized TOM20-based proximity labeling approach

To overcome the mitochondrial localization bias underlying the comparison to a cytoplasmic DHFR^{UID}, the proximity labeling set up was redesigned to employ a mitochondria-anchored surface control. Mitochondrial clogging occurs at the TOM complex on the OMM, and it was speculated that factors mediating removal of the clogger are likely to be recruited to its cytoplasmic side. Subunits of the TOM complex would be perfect candidates for the UID tagging, as they would be in proximity of the TOM complex. As direct UID-tagging of the pore forming subunit TOM40 could interfere with the channel function, other TOM subunits were considered as potential candidates. TOM receptors TOM20, TOM22 and TOM70 could be suitable, as their structure and orientation in the TOM complex are known (Akram et al., 2025; Su et al., 2022). While TOM22 constitutively associates with the TOM complex, TOM20 and TOM70 interact in a dynamic manner (Bhagawati et al., 2021). This means that tagging of TOM22 with UID would enable close monitoring of the TOM channel, while TOM20 UID-tagging might additionally detect changes more distal from the TOM complex during import clogging. Since TOM20 has been validated for biotin-proximity labeling in several studies, a TOM20-UID fusion (TOM20^{UID}) was used to capture these more distant changes in the interactome of a clogged mitochondrial channel **(Fig. 26A)** (Meurant et al., 2023).

3.1.5.2.2. Design of the optimized TOM20-based proximity labeling approach

As above described using TOM20^{UID} could be a suitable solution to overcome the mitochondrial localization bias of the above-described proximity labeling approach. To validate the mitochondrial localization of TOM20^{UID} the initial DHFR^{UID} was included for further experiments **(Fig. 26A)**. Additionally, b2-DHFR^{UID} was included which allows comparison of changes proximal to TOM20 and directly in the vicinity of the clogger itself.

To ensure equal expression levels of b2-DHFR and TOM20^{UID} plasmids were designed in a way that supports expression of both b2-DHFR and TOM20^{UID} from the same transcript. The P2A sequence between b2-DHFR/DHFR and TOM20^{UID} results in ribosomal skipping, releasing both peptides into the cytoplasm (Rao et al., 2025). This allows simultaneous expression of b2-DHFR or DHFR and TOM20^{UID} from the same plasmid **(Fig 26B)**.

The comparison of TOM20^{UID} in the absence and presence of b2-DHFR is thought to monitor the mitochondrial surface proteome under basal conditions and during mitochondrial import stress. While a comparison of b2-DHFR^{UID} and DHFR^{only} + TOM20^{UID} should give insight into the proximity of the mitochondrial clogger without an underlying mitochondrial localization bias.

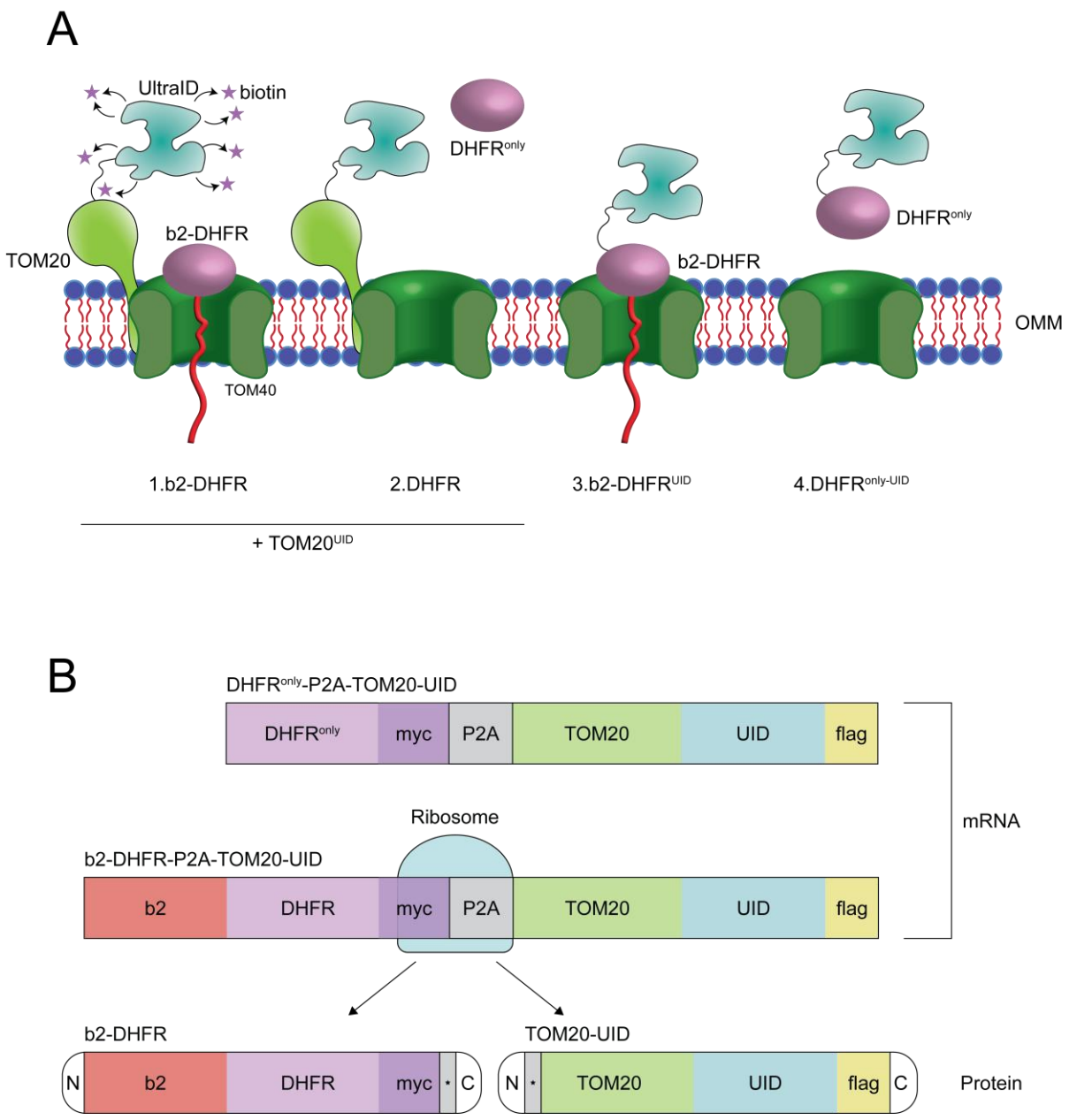

Figure 26 The optimized TOM20-based proximity labeling approach. (A) Schematic illustration of UID fusion constructs used for an optimized proximity labeling approach during mitochondrial clogging; UID was fused to TOM20 (TOM20^{UID}), b2-DHFR (b2-DHFR^{UID}) and DHFR^{only} (DHFR$^{only\text{-}UID}$). **(B)** Schematic representation of the P2A construct b2-DHFR-P2A-TOM20^{UID}; the P2A sequence results in ribosomal skipping and the release of the two independent polypeptide chains encoding b2-DHFR and TOM20^{UID} (* = P2A remnant from the ribosomal skipping event).

3.1.5.2.3. Establishment of the P2A-TOM20^{UID} constructs

Initially, expression and enzymatic activity of each P2A-TOM20^{UID} fusion construct were tested by transient overexpression in HEK293T cells. Both constructs, b2-DHFR-P2A-TOM20^{UID} and DHFR-P2A-TOM20^{UID} were expressed and showed the expected molecular weights, indicating successful ribosomal skipping by the P2A sequence to generate two independent polypeptides

(Fig 27A). Next, it was important to confirm that both TOM20^{UID} fusion proteins show enzymatic activity. A biotin enrichment of the above-described samples showed that in both TOM20^{UID} conditions upon addition of biotin a strong increase of biotinylated proteins occurred **(Fig. 27A)**. This suggests a proper enzymatic function of UID domain fused to TOM20. The biotinylation pattern of TOM20^{UID} was altered in the presence of b2-DHFR compared to DHFR^{only}. This indicates a change in the proximity proteome of TOM20 during mitochondrial import stress.

3.1.5.2.4. b2-DHFR is in the proximity of TOM20^{UID}

To investigate whether b2-DHFR localizes near TOM20^{UID} the biotinylated fraction from HEK293T cells overexpressing b2-DHFR-P2A-TOM20^{UID} was analyzed. Previously, b2-DHFR^{UID} fractions showed an enrichment of TOM20 compared to DHFR$^{only\text{-}UID}$ fractions **(Fig. 22B + Fig. 23B)**. An enrichment of b2-DHFR (but not DHFR^{only}) in the TOM20^{UID} provides further validation of this approach. Despite much lower b2-DHFR precursor levels compared to DHFR^{only}, biotin enrichment of TOM20^{UID} yielded significantly more b2-DHFR than DHFR^{only} **(Fig. 27B)**. The biotinylation of b2-DHFR by TOM20^{UID} was already visible in WCL when probed for biotin. Furthermore, MTX treatment increased b2-DHFR levels in the pull-down samples but did not affect DHFR^{only} levels. This suggests that b2-DHFR remains longer in the proximity of TOM20^{UID} and could be compatible with enhanced clogging in the presence of MTX. In addition, expression of TOM20^{UID} did not affect PDH levels, an abundant MM protein, suggesting that it does not alter overall mitochondrial protein abundance or organelle integrity **(Fig. 27B)**. Additionally, it was tested whether USP30 inhibition affects b2-DHFR levels or its enrichment by TOM20^{UID}. There was no visible change in b2-DHFR levels in WCL and after biotin enrichment upon USP30 inhibition **(Fig. 27B)**. Notably, TOM20^{UID} levels decreased upon b2-DHFR expression in the presence of the USP30 inhibitor. Thus, similar b2-DHFR levels after enrichment need to be interpreted with caution. However, it is important to note that TOM20^{UID} did not decrease upon inhibition of USP30 in the presence of DHFR^{only}. This may indicate that cells already experiencing mitochondrial import stress are less able to cope with additional mitochondrial challenges imposed by USP30 inhibition.

In conclusion, the P2A-TOM20^{UID} constructs are functional upon transient expression in HEK293T cells. Furthermore, TOM20^{UID} localizes in close proximity to b2-DHFR, and MTX treatment appears to prolong the time that both remain in proximity to each other.

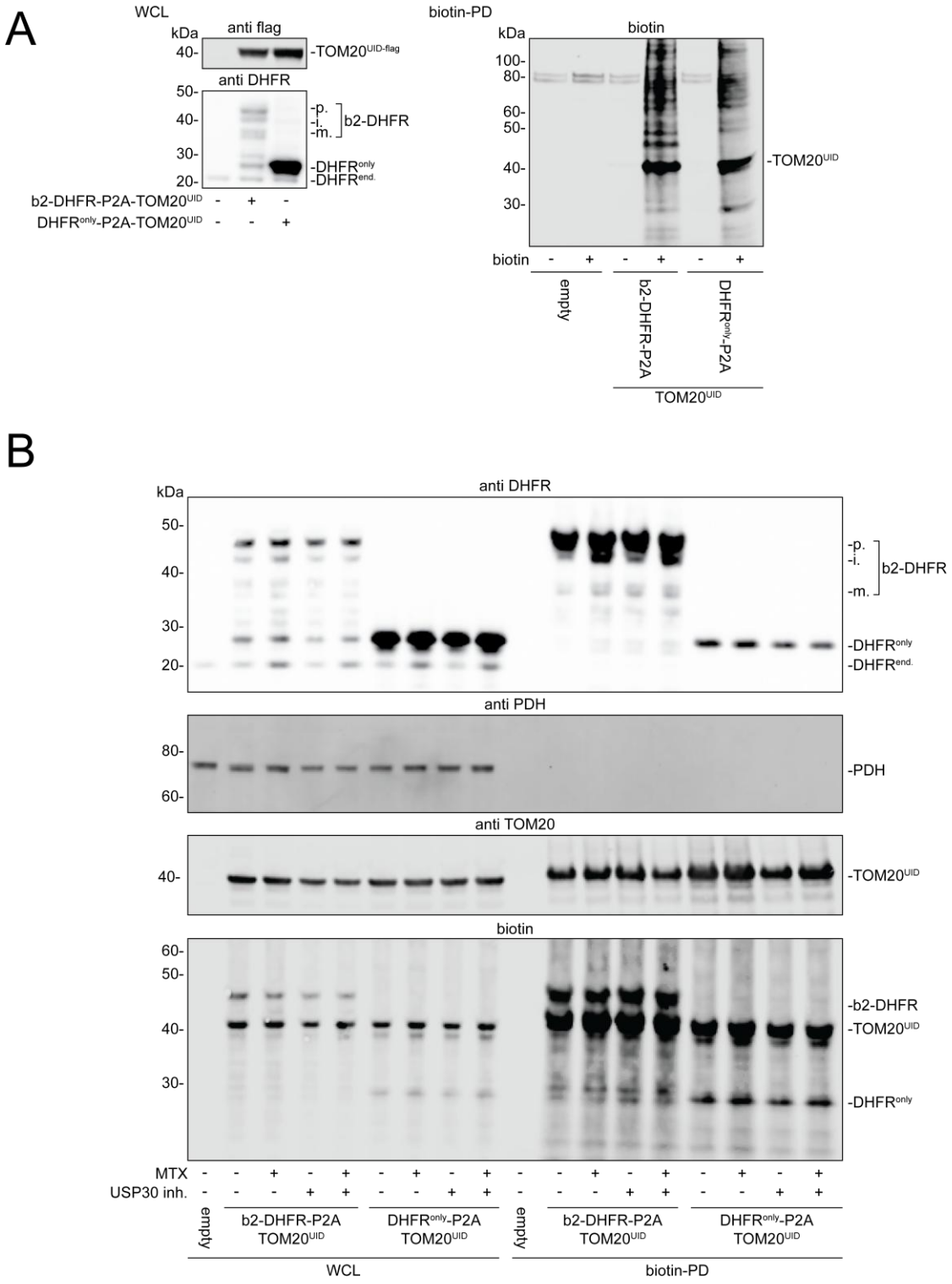

Figure 27 TOM20^{UID} enriches the mitochondrial clogger b2-DHFR. (A) HEK293T cells expressing b2-DHFR-P2A-TOM20^{UID} and DHFR^{only}-P2A-TOM20^{UID}; TOM20^{UID} was detected via the C-terminal flag-tag. Enzymatic activity of TOM20^{UID} was validated by addition of 50 µM biotin for 20 min, followed by enrichment of biotinylated proteins. **(B)** Both constructs from **(A)** were expressed in HEK293T cells and treated with 100 nM MTX for 5 h and 200 nM USP30 inhibitor CMPD for 2 h; thereafter 50 µM biotin was added for 20 min and biotinylated proteins were enriched (p. = precursor, i. = intermediate, m. = mature).

3.1.5.2.5. Integration of b2-DHFR-P2A-TOM20^{UID} into HeLa cells

After the initial validation of the P2A-TOM20^{UID} constructs by transient overexpression in HEK293T cells the next step was to proceed with the identification of interactors of TOM20^{UID} during mitochondrial clogging. Therefore, each construct was integrated into HeLa cells, a common human model cell line (Adey et al., 2013). In contrast to HEK293T cells, HeLa cells have little to no endogenous PARKIN expression, which is beneficial for excluding PARKIN-mediated mitophagy during the analysis (Lechado-Terradas et al., 2022). Therefore, both P2A-TOM20^{UID} constructs were stably integrated into HeLa FlpIn cells via FRT recombination. This allows inducible and isogenic expression by a defined single-copy integration that is suggested to avoid overexpression artefacts (Sokhi et al., 2023). Successful integration and protein expression were confirmed by WB **(Fig. 28A)**. Analysis of mitophagy markers LC3B and p62 showed no alteration under the established expression conditions of b2-DHFR-P2A-TOM20^{UID} with an MTX treatment for 5 h **(Fig. 16B)**.

3.1.5.2.6. Setup and validation of the optimized TOM20^{UID}-based MS experiment

Next, the interactome of the TOM20^{UID} and the mitochondrial clogger b2-DHFR^{UID} were analyzed. In this optimized MS approach, both P2A-TOM20^{UID} constructs and the previously described b2-DHFR^{UID} and DHFR$^{only\text{-}UID}$ constructs from the initial MS approach were included **(Fig. 26A+B)**. All constructs were expressed in HeLa cells by DOX addition, with or without additional MTX treatment for 5 h. For statistical validation, each condition was performed in quadruplicates. After addition of biotin, all biotinylated proteins were enriched and analyzed by MS.

To validate the optimized MS data set as described for the initial b2-DHFR^{UID} vs DHFR^{UID} approach. The UID constructs, b2-DHFR^{UID} and b2-DHFR-P2A-TOM20^{UID} (referenced as b2-DHFR + TOM20^{UID}), that should be targeted to the mitochondria, were compared with the cytoplasmic control DHFR$^{only\text{-}UID}$. First, for both constructs the MEF was calculated which compares the ratio of at least 2-fold significantly enriched mitochondrial proteins to all non-mitochondrial hits **(chapter 2.11.5)**. Both conditions, b2-DHFR^{UID} and b2-DHFR-P2A-TOM20^{UID} showed an MEF above 1 in the absence and presence of MTX suggesting a mitochondrial enrichment **(Fig. 28B)**.

To complement this analysis, a median-based assessment of mitochondrial enrichment independent of the MEF was applied. Mitochondrial proteins were grouped as mitochondrial and non-mitochondrial based on MitoCarta3.0 and the median Log2FC of both groups were compared. Mitochondrial UIDs showed an increased median Log2FC for mitochondrial proteins, whereas non-mitochondrial proteins were decreased **(Fig. 28C)**. Together both the MEF and the median-based analysis suggest that the b2-DHFR^{UID} and TOM20^{UID} are correctly targeted to mitochondria.

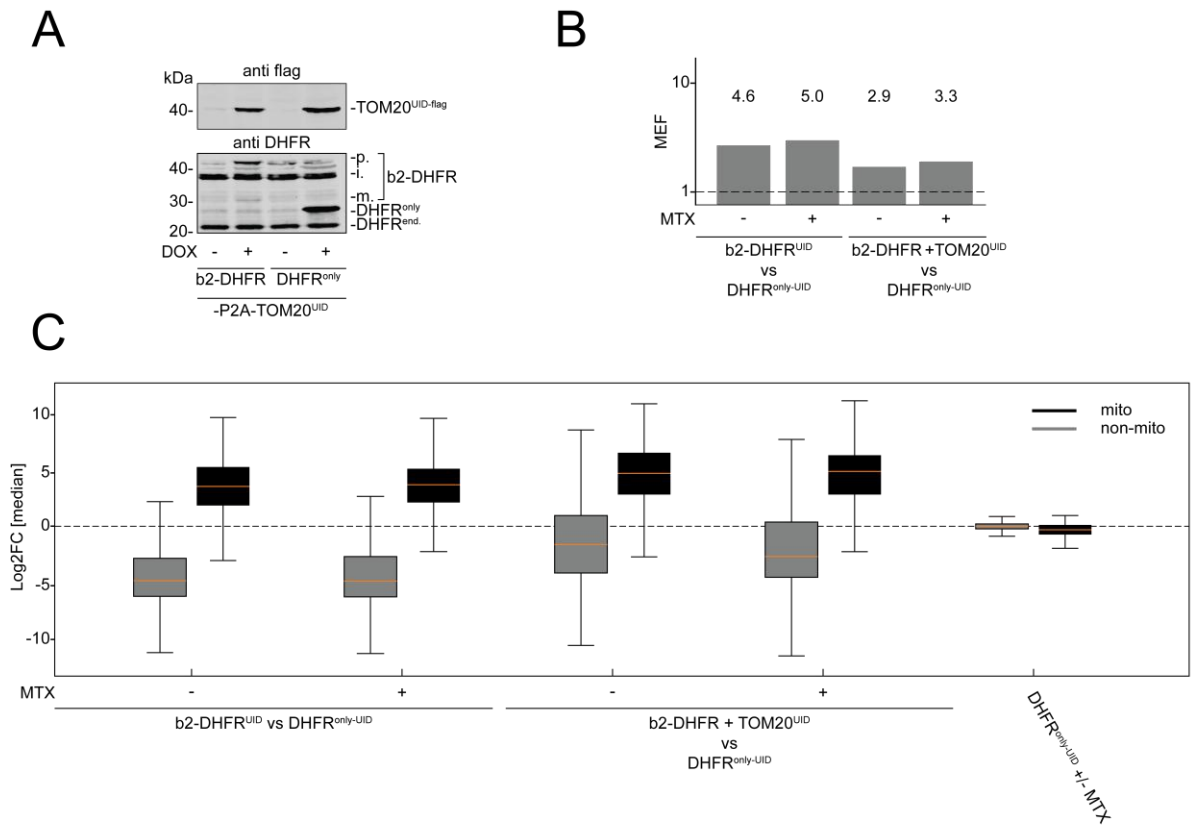

Figure 28 Validation of the optimized MS approach with TOM20^{UID}. (A) Both constructs, b2-DHFR-P2A-TOM20^{UID} and DHFR^{only}-P2A-TOM20^{UID}, were stably integrated into HeLa cells under a DOX-inducible promotor. **(B)** The MEF was calculated by comparing the mitochondrial UID fuisions b2-DHFR^{UID} and TOM20^{UID} (+b2-DHFR) with the cytoplasmic control DHFR$^{only-UID}$ in the absence and presence of MTX; the MEF defines the ratio of significantly upregulated mitochondrial proteins to all mitochondrial proteins among all quantified proteins in the dataset (Log2FC > 2). **(C)** A median-based approach was further used to validate the enrichment of mitochondrial proteins in the comparisons in **(B)**; proteins were classified as mitochondrial or non-mitochondrial based on MitoCarta3.0 followed by comparison of the median Log2FC of both groups.

Another step of validation was to confirm that TOM20^{UID} enriches b2-DHFR, which would indicate that both proteins are in proximity during mitochondrial clogging. Previously, proximity labeling of the b2-DHFR^{UID} enriched endogenous TOM20. Now in the optimized approach, b2-DHFR was consistently the top hit of the enriched proteins by TOM20^{UID} in the absence and presence of MTX **(Fig. 29A+B)**. Furthermore, MTX treatment appeared to further increase the enrichment of b2-DHFR as suggested by an elevated Log2FC of b2-DHFR.

Together these findings suggest that both b2-DHFR^{UID} and TOM20^{UID} are correctly targeted to mitochondria and that TOM20^{UID} is in proximity to b2-DHFR, a prerequisite for monitoring mitochondrial clogging.

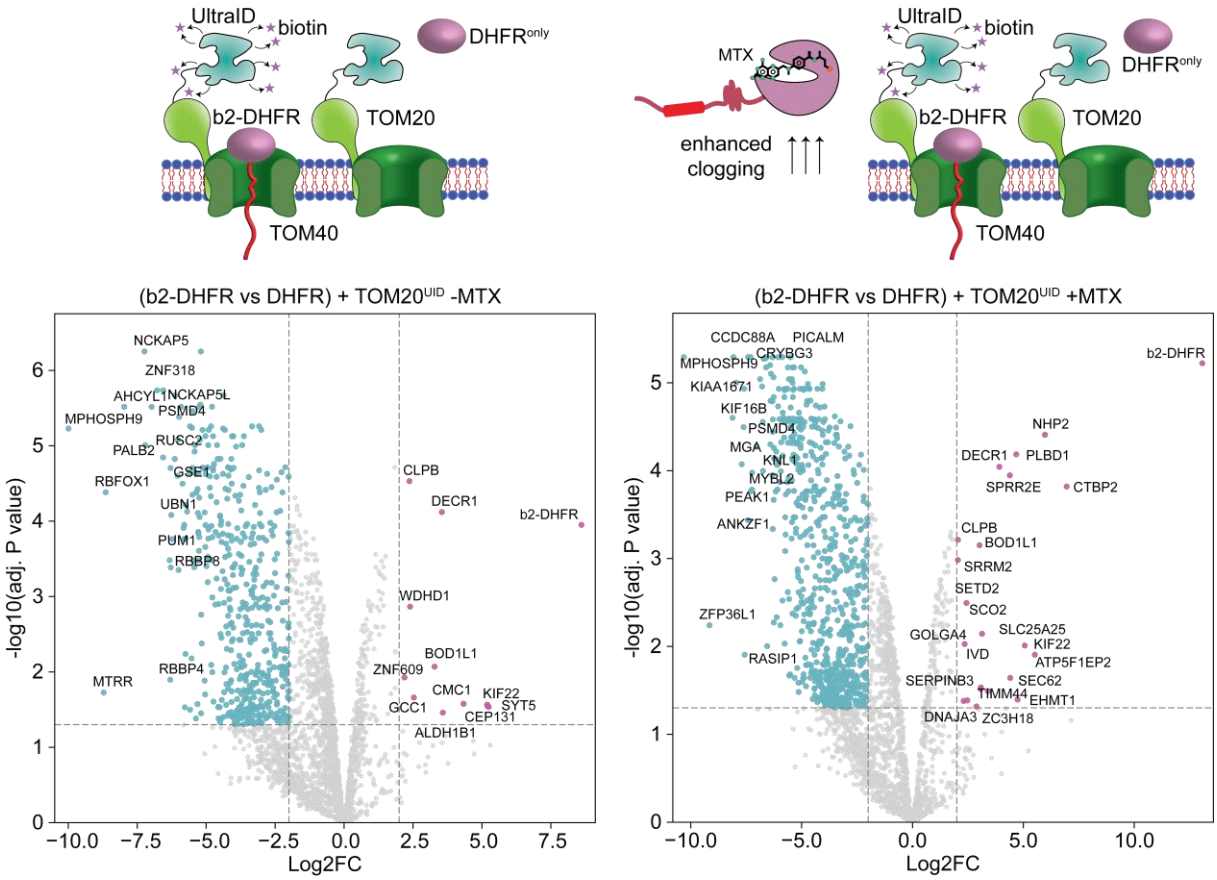

Figure 29 b2-DHFR is the top hit enriched by TOM20^{UID}. Vulcano blots showing upregulated (magenta) and downregulated (blue) proteins from the comparison b2-DHFR + TOM20^{UID} and DHFR^{only} + TOM20^{UID} in the absence and presence of the of MTX (cut-offs: Log2FC > 2 and limma-based p.value < 0.05).

3.1.5.2.7. Comparison of the initial and the optimized MS approach

The next question was whether the optimized approach using TOM20^{UID} could reduce the mitochondrial localization bias that arose from comparing the mitochondrially targeted b2-DHFR^{UID} with the cytoplasmic DHFR$^{only\text{-}UID}$ control. Therefore, upregulated proteins from the comparison b2-DHFR^{UID} vs DHFR^{UID} were compared with those from the new condition b2-DHFR^{UID} vs DHFR^{only} + TOM20^{UID}, in the presence of MTX. In total, both conditions identified 411 significantly upregulated proteins (Log2FC > 1) **(Fig. 30A)**. While 128 proteins were found in both comparisons, 264 proteins did not overlap. GO-term analysis of the cellular component of the overlapping fraction showed many mitochondria-related GO-terms such as “IMM”, and “Mitochondrial envelope” **(Fig. 30B)**. Proteins only detected by b2-DHFR^{UID} vs DHFR$^{only\text{-}UID}$ are related to GO-terms of the ribosome and mitochondria, in particular mitochondrial matrix **(Fig. 30C)**. Of these 264 proteins, 147 are mitochondrial and 79 are mitochondrial matrix proteins. This indicates that using TOM20^{UID} as a control removed many mitochondrial proteins from the enrichment list; however, it remains difficult to confirm whether these proteins were enriched

solely due to mitochondrial localization bias. Furthermore, the optimized comparison with TOM20^{UID} enabled detection of 19 additional upregulated proteins, 9 of which are annotated as involved in ubiquitin-like conjugation **(Appendix 2)**.

In summary, the optimized TOM20^{UID} approach might reduce the mitochondrial localization bias, by removing 264 proteins of which ~55% are annotated as mitochondrial.

A

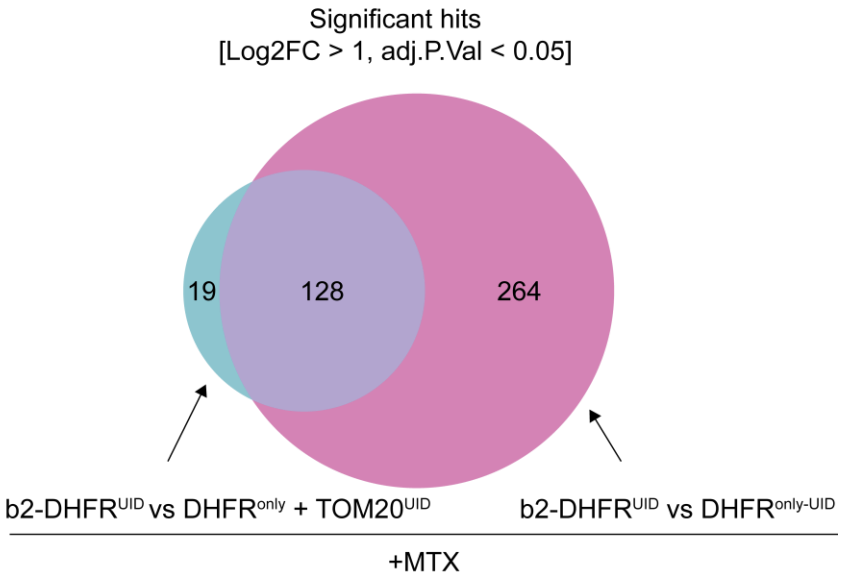
Significant hits
[Log2FC > 1, adj.P.Val < 0.05]
19
128
264
b2-DHFR^UID vs DHFR^only + TOM20^UID
b2-DHFR^UID vs DHFR^only-UID
+MTX

B

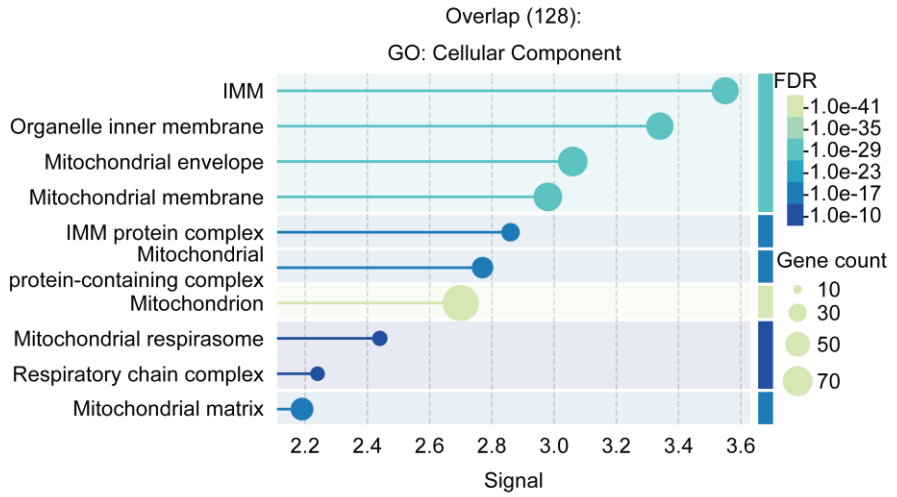
Overlap (128):
GO: Cellular Component
IMM
Organelle inner membrane
Mitochondrial envelope
Mitochondrial membrane
IMM protein complex
Mitochondrial protein-containing complex
Mitochondrion
Mitochondrial respirasome
Respiratory chain complex
Mitochondrial matrix
2.2
2.4
2.6
2.8
3.0
3.2
3.4
3.6
Signal
FDR
-1.0e-41
-1.0e-35
-1.0e-29
-1.0e-23
-1.0e-17
-1.0e-10
Gene count
10
30
50
70

C

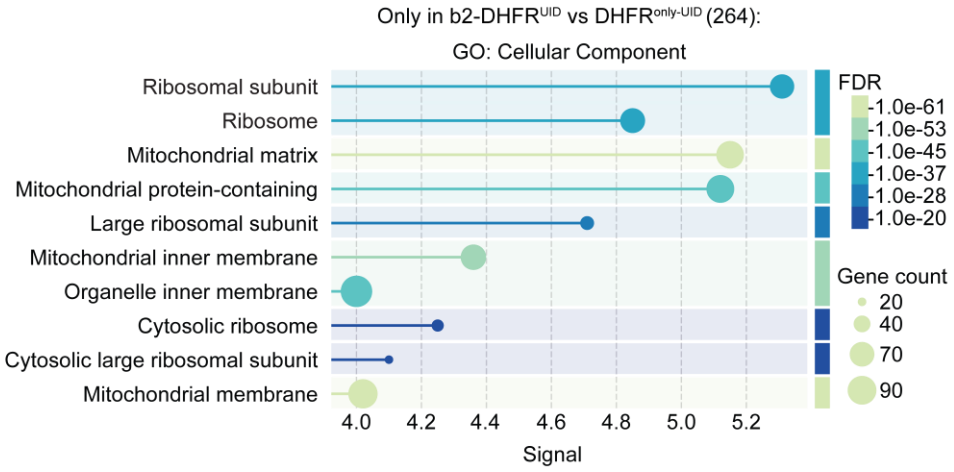
Only in b2-DHFR^UID vs DHFR^only-UID (264):
GO: Cellular Component
Ribosomal subunit
Ribosome
Mitochondrial matrix
Mitochondrial protein-containing
Large ribosomal subunit
Mitochondrial inner membrane
Organelle inner membrane
Cytosolic ribosome
Cytosolic large ribosomal subunit
Mitochondrial membrane
4.0
4.2
4.4
4.6
4.8
5.0
5.2
Signal
FDR
-1.0e-61
-1.0e-53
-1.0e-45
-1.0e-37
-1.0e-28
-1.0e-20
Gene count
20
40
70
90

Figure 30 Comparison of the initial and the optimized MS approach with TOM20^{UID}. (A) Venn diagram comparing significant upregulated proteins (Log2FC > 1) from b2-DHFR^{UID} vs DHFR^{only} + TOM20^{UID} with b2-DHFR^{UID} vs DHFR$^{only\text{-}UID}$ in the presence of MTX. **(B)** GO term enrichment analysis (cellular component) of upregulated proteins identified in both comparisons in **(A)**. **(C)** GO term enrichment analysis (cellular component) of upregulated proteins identified only in the comparison b2-DHFR^{UID} vs DHFR$^{only\text{-}UID}$ that might reflect a mitochondrial localization bias. GO-term enrichment analysis in **(B)** and **(C)** were performed using STRING database; signal is a combined score that balances enrichment strength and statistical confidence by integrating Log10(observed / expected) and -log(FDR).

3.1.5.2.8. b2-DHFR^{UID} enriches central mitochondrial proteins

Next the interactome of a clogged mitochondrial import channel was investigated. Therefore, the interactome of the clogger b2-DHFR^{UID} was compared with that of DHFR^{only}-P2A-TOM20^{UID} (referenced as DHFR^{only} + TOM20^{UID}) and clustered all significant enriched proteins (log2FC > 1, adj. P. Val. < 0.05, -MTX) with STRING database. Two big clusters were visible **(Fig. 31A)**. Cluster one was enriched in highly important mitochondrial proteins such as proteins required for OXPHOS, the essential desulfurase NFS1 which is the central enzyme of the NIA machinery required for all Fe-S clusters and subunits of the MICOS complex involved in the mitochondrial organization and cristae formation **(Fig. 31A+B)**. On the other hand, a second cluster consisting of proteins involved in the mitochondrial translation termination and gene expression regulation was increased. Notably, very similar protein clusters were also identified in the presence of MTX (data not shown). Strikingly none of the enriched proteins were found to be encoded by the mitochondrial genome, which means that all the identified proteins rely on the cytoplasmic import. This might indicate that those identified proteins are likely to represent the mitochondrial response to clogged import by upregulation of essential mitochondrial proteins. Interestingly, the most consistently identified protein in the MS screens was CLPB. This protein together with TIM44, DNAJA3 and NDUA6 seem to connect the two above mentioned protein clusters. Furthermore, KEGG based GO-term enrichment analysis revealed that many of the upregulated hits are linked to severe disease such as Huntington disease, Alzheimer's disease, Parkinson's disease and Prion disease **(Fig. 31C)**.

Together, the analysis of b2-DHFR^{UID} revealed that many highly important and disease-associated proteins, involved in central mitochondrial functions including OXPHOS and Fe-S cluster biogenesis, were increased in the proximity of b2-DHFR^{UID}.

A

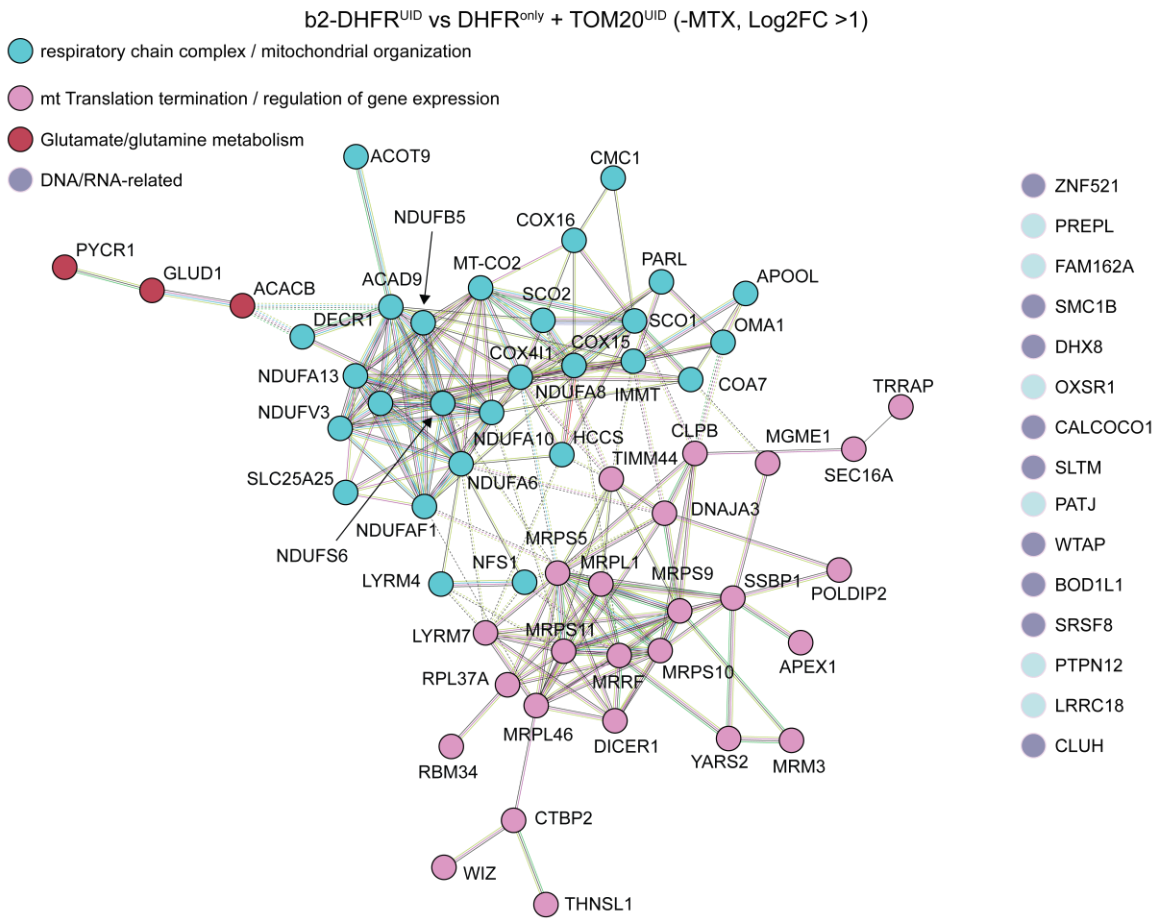
b2-DHFR^UID vs DHFR^only + TOM20^UID (-MTX, Log2FC >1)
respiratory chain complex / mitochondrial organization
mt Translation termination / regulation of gene expression
Glutamate/glutamine metabolism
DNA/RNA-related
ACOT9
CMC1
NDUFB5
COX16
PYCR1
GLUD1
ACACB
ACAD9
MT-CO2
PARL
APOOL
SCO2
DECR1
SCO1
OMA1
COX4I1
COX15
NDUFA13
NDUFA8
IMMT
COA7
TRRAP
NDUFV3
NDUFA10
HCCS
CLPB
MGME1
TIMM44
SEC16A
SLC25A25
NDUFA6
DNAJA3
NDUFAF1
NDUFS6
MRPS5
NFS1
MRPL1
MRPS9
SSBP1
POLDIP2
LYRM4
LYRM7
MRPS11
APEX1
RPL37A
MRRF
MRPS10
MRPL46
DICER1
YARS2
MRM3
RBM34
CTBP2
WIZ
THNSL1
ZNF521
PREPL
FAM162A
SMC1B
DHX8
OXSR1
CALCOCO1
SLTM
PATJ
WTAP
BOD1L1
SRSF8
PTPN12
LRRC18
CLUH

B

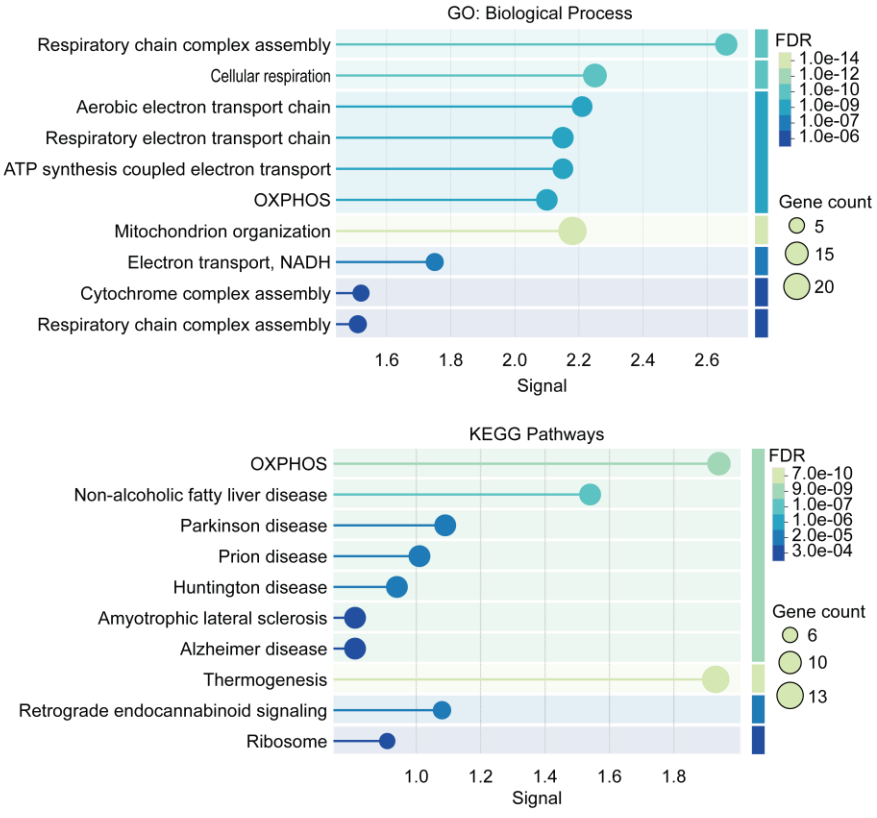
GO: Biological Process
Respiratory chain complex assembly
Cellular respiration
Aerobic electron transport chain
Respiratory electron transport chain
ATP synthesis coupled electron transport
OXPHOS
Mitochondrion organization
Electron transport, NADH
Cytochrome complex assembly
Respiratory chain complex assembly
1.6
1.8
2.0
2.2
2.4
2.6
Signal
FDR
1.0e-14
1.0e-12
1.0e-10
1.0e-09
1.0e-07
1.0e-06
Gene count
5
15
20
KEGG Pathways
OXPHOS
Non-alcoholic fatty liver disease
Parkinson disease
Prion disease
Huntington disease
Amyotrophic lateral sclerosis
Alzheimer disease
Thermogenesis
Retrograde endocannabinoid signaling
Ribosome
1.0
1.2
1.4
1.6
1.8
Signal
FDR
7.0e-10
9.0e-09
1.0e-07
1.0e-06
2.0e-05
3.0e-04
Gene count
6
10
13

Figure 31 b2-DHFR^{UID} enriches central mitochondrial proteins. (A) Significantly upregulated proteins in the proximity of b2-DHFR^{UID} compared to TOM20^{UID} (+DHFR^{only}) were clustered using STRING database and k-means clustering (-MTX; Log2FC > 1). **(B)** Additional GO term enrichment analysis of the k-means clustering were performed using STRING and are displayed according to their signal strength, a combined score that balances enrichment strength and statistical confidence by integrating log10(observed / expected) and -log(FDR).

3.1.5.2.9. TOM20^{UID} enriches RNA binding proteins during mitochondrial clogging

The improved MS approach did not only enable to analyze the interactome of the mitochondrial clogger b2-DHFR^{UID} in comparison to TOM20^{UID}, but also the interactome of the TOM complex subunit TOM20 during mitochondrial clogging. In order to understand proximal changes of this TOM receptor, the upregulated interactome of b2-DHFR + TOM20^{UID} in comparison to DHFR^{only} + TOM20^{UID} was analyzed upon addition of MTX. Intriguingly, the interactome of TOM20 during mitochondrial clogging was highly enriched with RNA processing factors involved in splicing **(Fig. 32A+B)**. Multiple of these RNA processing factors were also enriched in the proximity of b2-DHFR^{UID} in the presence of MTX (data not shown). This is surprising, as those proteins reside mainly in the nuclear speckle inside of the nucleus and TOM20 is a membrane-bound OMM protein. Furthermore, two clusters of proteins surrounded the RNA-related cluster. One cluster centered around ribosomal subunits, and the second cluster was enriched in proteins involved in the fatty acid chain synthesis and metabolic processes, which were also represented GO-term analysis of the biological processes **(Fig. 32B)**. Again, CLPB, TIM44, DNAJA3 and NDU6 connect all three clusters, suggesting a central role for these proteins during mitochondrial clogging.

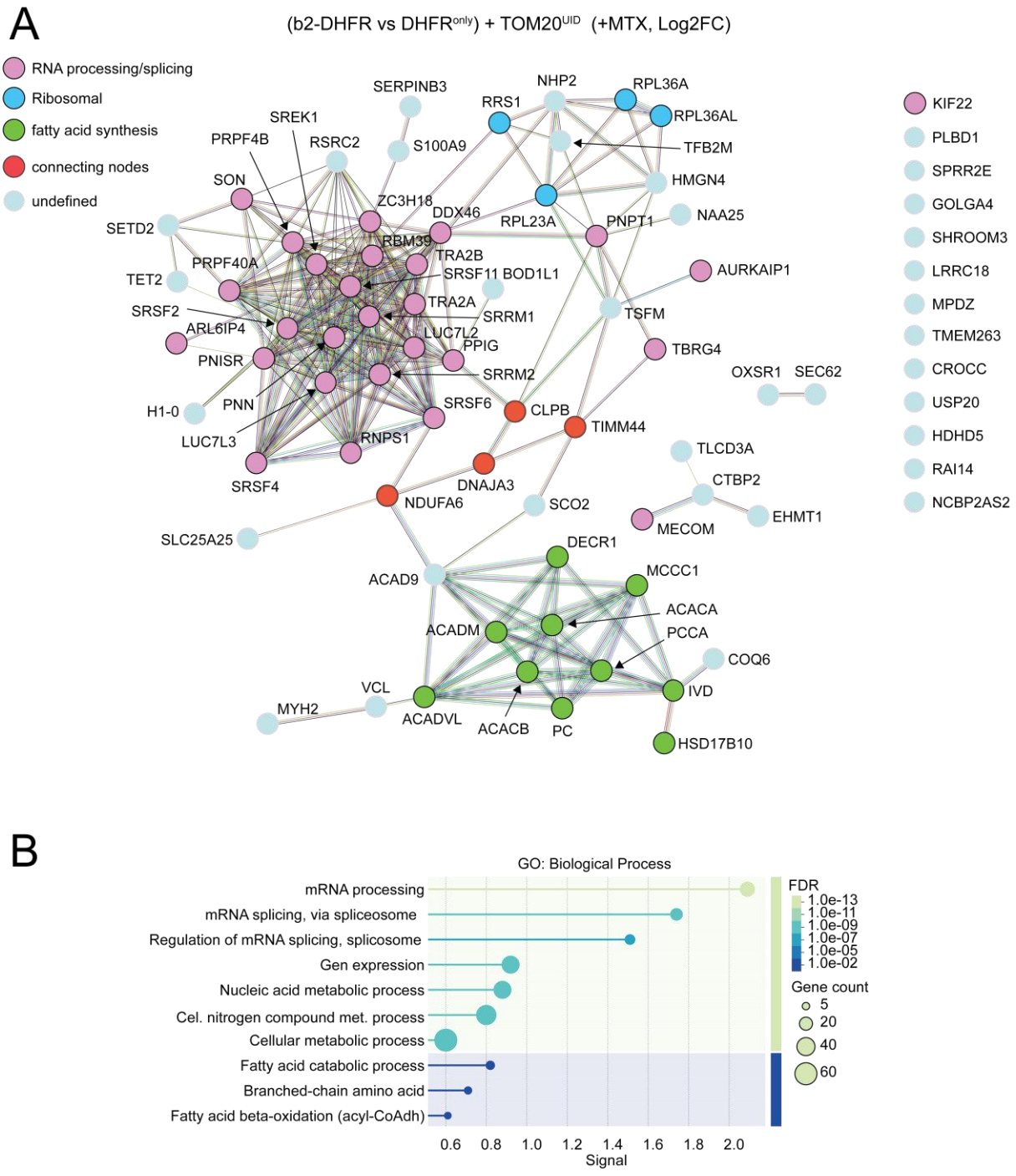

Figure 32 TOM20^{UID} enriches RNA binding proteins during mitochondrial clogging. (A) Significantly upregulated proteins in the proximity of TOM20^{UID} during mitochondrial clogging (comparison b2-DHFR-P2A-TOM20^{UID} vs DHFRonly-P2A-TOM20^{UID}) were clustered based on k-means clustering using STRING database (+MTX; Log2FC > 2). **(B)** GO term enrichment analysis were performed using STRING and are displayed according to their signal strength, a combined score that balances enrichment strength and statistical confidence by integrating log10(observed / expected) and -log(FDR). Original cluster names were simplified and the cluster name “connecting nodes” was added manually.

3.1.5.2.10. Clogging reduces the TOM20^{UID} proximity to a BRCA1-associated protein cluster

The next question was whether there is a common pattern in the downregulated fraction of the TOM20^{UID} interactome during mitochondrial clogging, with and without MTX. Therefore, highly downregulated proteins (log2FC < -5 [~32x FC]) were investigated by a similar cluster analysis using STRING DB. Strikingly, downregulated proteins in the condition without MTX clustered around the tumor suppressor and DNA damage repair factor BRCA1 **(Fig 33A+B)**. The addition of MTX led to an even higher number of proteins clustering around BRCA1 (data not shown). Among proteins of this cluster there was PABL2 which is a component of the BRCA complex (Sy et al., 2009). In addition, ubiquitin-related and BRCA1-associated proteins such as the histone modifying E3 RNF168, DDB1 and UIMC1 were also found in the BRCA1-centered cluster (Krais et al., 2021; Lv et al., 2010; Sobhian et al., 2007).

In summary, mitochondrial clogging was associated with a reduced proximity of BRCA1 and several BRCA1-associated factors to TOM20^{UID}. Notably, this pattern is consistent with previous reports showing that BRCA1 can localize to mitochondria and that mitochondrial BRCA1 is subject to stress-dependent regulation (Coene et al., 2005; Miyahara et al., 2021).

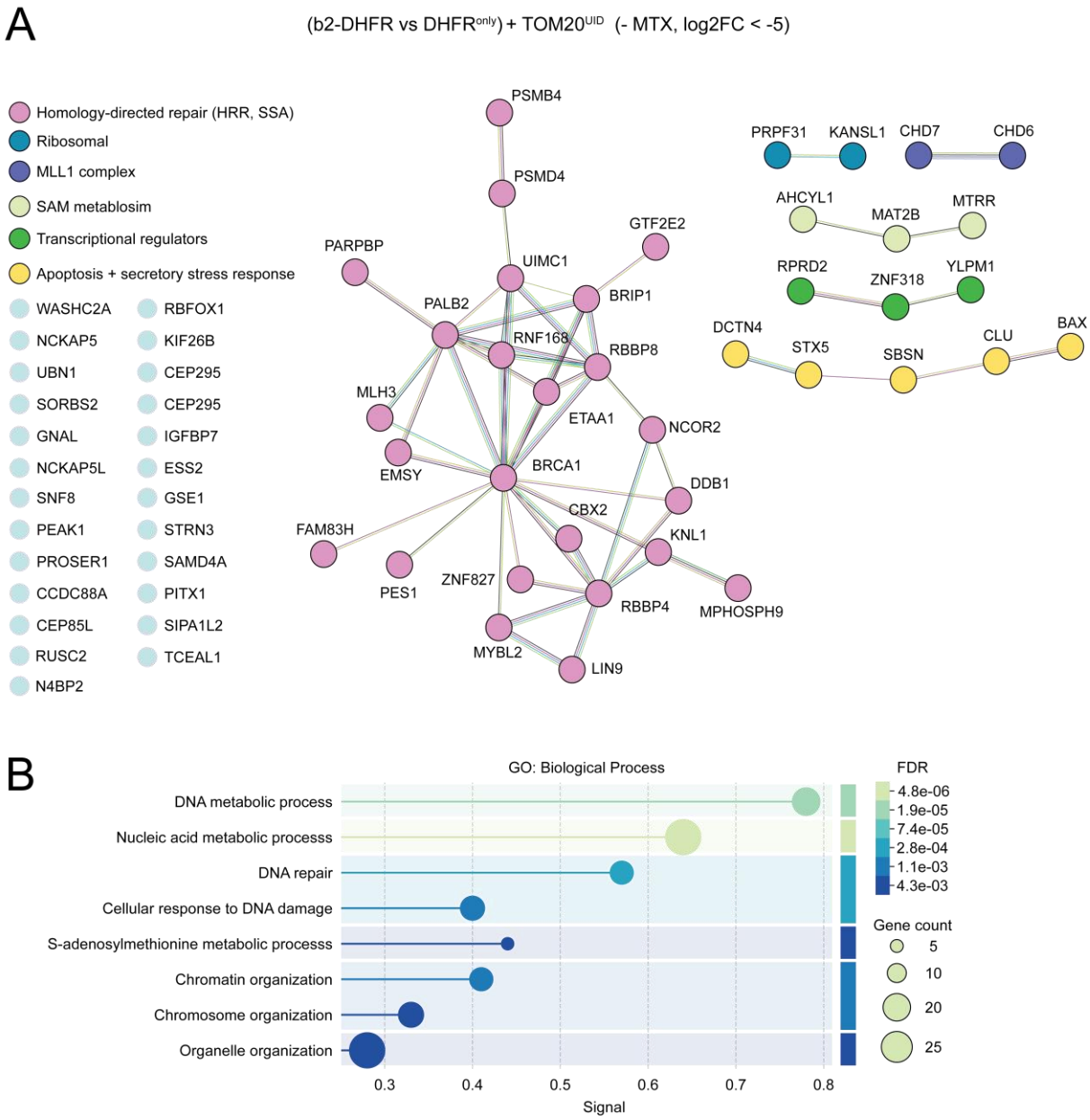

Figure 33 Clogging reduces the TOM20^{UID} proximity to a BRCA1-associated protein cluster. (A) Significantly downregulated proteins in the proximity of TOM20^{UID} during mitochondrial clogging (comparison b2-DHFR-P2A-TOM20^{UID} vs DHFRonly-P2A-TOM20^{UID}) were clustered based on k-means clustering using STRING database (-MTX; Log2FC < -5). (B) GO term enrichment analysis were performed using STRING database and are displayed according to their signal strength, a combined score that balances enrichment strength and statistical confidence by integrating log10(observed / expected) and -log(FDR).

3.1.5.3. Identification of ubiquitin-related proteins during mitochondrial clogging

After identifying several clusters that were differentially enriched in the proximity of TOM20^{UID} during mitochondrial clogging, the next question was whether ubiquitin-related proteins, such as E3s or DUBs, accumulate near the mitochondrial clogger b2-DHFR or TOM20. Building on previous findings that b2-DHFR is ubiquitylated and resides in proximity to atypical ubiquitin

chains, ubiquitin-associated factors were then systematically assessed in these proximity-labeling datasets.

3.1.5.3.1. Identification of E3s and DUBs in the vicinity of TOM20 independent of import stress

First, the question was whether $TOM20^{UID}$ proximity labeling in the absence of mitochondrial clogging could capture E3s and DUBs near TOM20. As TOM20 serves as a receptor of the TOM complex, such an analysis could reveal previously unrecognized mitochondrial ubiquitin "writers" and "erasers" and thereby improve understanding of mitochondrial regulation. To this end, the condition $DHFR^{only}$ + $TOM20^{UID}$ was compared with the cytosolic control $DHFR^{only\text{-}UID}$, which provides an appropriate non-mitochondrial control. Proteins enriched in this comparison were screened for annotated human E3s, E3-accessory proteins (non-catalytic complex subunits), and DUBs.

Multiple writers and erasers were identified in the proximity of $TOM20^{UID}$ **(Appendix 3 + Table 14)**, with the mitochondrial E3s MUL1 and MARCH5 and the mitochondrial DUB USP30 among the top hits. This indicates that this strategy robustly identifies mitochondrial interactors and that multiple of the discovered E3s and DUBs may represent novel regulators of mitochondrial ubiquitin signaling.

Table 14 E3s and DUBs identified in the proximity of TOM20UID. Enriched proteins from the comparison DHFRonly + TOM20UID vs DHFRonly-UID. Functional descriptions are based on UniProt entries unless otherwise stated ($p < 0.5$, *; $p < 0.01$ = **; $p < 0.001$ = ***).

Protein	Log2FC	p-val.	Functional description
MUL1	8.0	***	Control of mitochondrial morphology by promoting mitochondrial fragmentation, and influences mitochondrial localization
MGRN1	7.3	***	Plays a role in the regulation of endosome-to-lysosome trafficking
TRIM4	6.6	***	Mediates K63-linked polyubiquitylation of the innate immune receptor RIGI
PEX12	6.6	***	Required for peroxisome organization by mediating export of the PEX5 receptor from peroxisomes, the retro translocation channel is composed of PEX2, PEX10 and PEX12
RBX1	6.0	***	RBX1-mediated ubiquitination of SESN2 promotes cell death upon prolonged mitochondrial damage (A. Kumar & Shaha, 2018)
ZFPL1	5.7	***	Required for cis-Golgi integrity and efficient ER to Golgi transport
RNF187	5.1	***	Acts as a coactivator of JUN-mediated gene activation in response to growth factor signaling via the MAP3K1 pathway
TRIM58	4.8	***	Induced during late erythropoiesis, directly binds and ubiquitylates the intermediate chain of the microtubule motor dynein

MARCH F5	4.0	*	Mitochondrial E3 plays a crucial role in the control of mitochondrial morphology as a positive regulator of mitochondrial fission
OBI1	3.6	***	Essential for DNA replication origin activation during S phase
CNOT4	3.0	*	Plays role in QC of translation of OMM-localized mRNA, involved in activation of the JAK/STAT pathway
MECOM	2.9	*	Most likely wrong annotated functions as transcriptional regulator, overexpression modulated genes from cellular energy-related pathways, including glycolysis, the TCA cycle, and oxidative phosphorylation (Fenouille et al., 2017)
PEX10	2.7	*	Required for peroxisome organization by mediating export of the PEX5 receptor from peroxisomes, the retro translocation channel is composed of PEX2, PEX10 and PEX12
TRIM23	1.9	***	Plays essential role in autophagy activation during viral infection
RNF10	1.8	***	Ubiquitylation of 40S ribosomal proteins RPS2/us5 and RPS3/us3 in response to ribosome stalling
STUB1	1.4	***	Plays a role in the maintenance of mitochondrial morphology and promotes mitophagic removal of dysfunctional mitochondria, targets misfolded chaperone substrates towards proteasomal degradation
BRCA1	0.7	*	Specifically mediates formation of K6-linked ubiquitin chains, plays a central role in DNA repair
ITCH	0.6	*	Ubiquitylates MAVS through 'Lys-48'-linked conjugation resulting in MAVS proteasomal degradation
USP30	9.6	***	Tethered to the OMM, acts as a key inhibitor of mitophagy
USP33	8.3	***	Antagonizes PARKIN's role in mitophagy (Niu et al., 2020)
USP54	6.5	***	Mediates deubiquitylation of PLK4, specifically mediates K63-linked deubiquitylation
USP53	5.1	***	K63-linked deubiquitylation of tight junction proteins, such as MARVELD2 and LSR
USP32	4.8	***	Target proteins such as RAB7A and LAMTOR1; acts as a positive regulator of the mTORC1 signaling
USP42	3.0	*	Important role during spermatogenesis
COPS5	1.7	***	Part of CSN complex, essential regulator mediating the deneddylation of the cullin subunits of the SCF-type E3 complexes
USP14	1.3	***	Proteasome-associated, releases ubiquitin from the proteasome targeted ubiquitinated proteins
EIF3H	0.9	**	Interaction with mutant Huntingtin (Sap et al., 2021)
USP20	0.8	*	Regulation of mitophagy through PINK1 stabilization (Park et al., 2025)
USP7	0.5	*	KO leads to disordered mitochondrial biogenesis and dynamics and early neonatal lethality in mice (Yan et al., 2024)

3.1.5.3.2. Identification of E3s and DUBs during mitochondrial import clogging

Next, the analysis addressed whether ubiquitin-related proteins are enriched in the vicinity of the mitochondrial clogger b2-DHFR or in the proximity of TOM20 during mitochondrial clogging. First, the initial proximity-labeling dataset comparing b2-DHFR^{UID} and DHFR$^{only\text{-}UID}$ in HEK293T cells was screened for human E3s and DUBs. Again, the mitochondrial DUB USP30 emerged as one of the top hits, and PJA2 and PJA1 were the most enriched E3s in this dataset **(Table 15)**. Both PJA1 and PJA2 were also significantly upregulated in the b2-DHFR^{UID} vs Su9-DHFR^{UID} comparison (suggested as mild/non-clogging control), indicating that their enrichment is not solely attributable to the mitochondrial localization bias caused by the comparison with DHFR$^{only\text{-}UID}$. PJA1 was recently discovered to ubiquitylate the mitochondrial protein PGAM5 (S.-Y. Huang et al., 2024). PJA2 was shown to promote atypical ubiquitin linkages, including K6-linked chains that were detected near b2-DHFR (Faust et al., 2017; Schiefer & Hale, 2024). Among the identified DUBs, USP11 was reported to have a linkage-preference for K6- , K33- and K63-linked ubiquitin chains (S. Harper et al., 2014), all of which were enriched near b2-DHFR or TOM20 during mitochondrial clogging **(chapter 3.1.4.4.2)**.

Table 15 E3s and DUBs upregulated in the proximity of b2-DHFR^{UID}. Enriched in the initial HEK293T screen from the comparison b2-DHFRUID vs DHFRonly-UID. Proteins also identified as upregulated in the comparison b2-DHFRUID vs Su9-DHFRUID are marked with an asterisk. Functional descriptions are based on UniProt entries unless otherwise stated ($p < 0.5$, *; $p < 0.01$ = **; $p < 0.001$ = ***).

Protein	Log2FC	p-val.	Functional description
PJA2*	1.70	***	Targeting for proteasomal degradation, essential for PKA-mediated long-term memory processes
PJA1*	1.01	**	Ubiquitinates and degrades the mitochondrial outer membrane protein PGAM5 which affects DRP1 phosphorylation, mitochondrial morphology, Δψm, mitochondrial ROS and ATP production (S.-Y. Huang et al., 2024); may be involved in protein sorting
RBX1	0.78	*	Cullin-RING-based E3, mediates proteasomal degradation
RNF135	0.77	*	Regulates RIG-I signaling related to mitochondrial MAVS (Oshiumi et al., 2009)
OBI1*	0.73	**	Essential for DNA replication origin activation during S phase
STUB1	0.54	*	Plays a role in the maintenance of mitochondrial morphology; may regulate myosin assembly with UBE4B and VCP
USP30*	8.63	***	Tethered to the mitochondrial outer membrane, acts as a key inhibitor of mitophagy
USP11*	2.06	**	Role in the regulation of pathways leading to NF-kappa-B activation
USP14*	1.20	**	Inhibition promotes mitophagy and corrects mitochondrial dysfunction (Chakraborty et al., 2018)

USP19*	0.75	*	Attenuates mitochondrial damage and ferroptosis and KD alters expression of Mfn1, Mfn2 and Drp1 (W. Yu et al., 2024)
USP1*	0.67	*	Modulates mitochondrial fission (Bian et al., 2024)

The initial proximity-labeling screen may have been biased towards mitochondrial E3s and DUBs due to the localization bias underlying the comparison with a cytosolic $DHFR^{only\text{-}UID}$ control, complicating identification of truly clogging-related candidates. To address this limitation, the optimized MS dataset with $TOM20^{UID}$ was analyzed. Interestingly, an initial screening approach could only identify ZNF521 as a potential clogging-related E3. However, this protein lacks confirmed ubiquitination activity, and its annotation in the human E3 dataset likely stems from predictions based on its multiple zinc finger domains resembling RING-like motif. To detect more subtle changes, the dataset was normalized to total UID levels, which did not alter the enrichment or downregulation of the previously described clusters, as these clusters described highly enriched or downregulated proteins and the UID construct was underrepresented in conditions of mitochondrial clogging. The normalized data were then screened for human E3s, ligase-accessory proteins, and DUBs in the following comparisons: b2-$DHFR^{UID}$ vs $DHFR^{only}$ + $TOM20^{UID}$ and b2-DHFR + $TOM20^{UID}$ vs $DHFR^{only}$ + $TOM20^{UID}$ (both minus and plus MTX). This enables identification of ubiquitin-related factors in the proximity of the mitochondrial clogger and of the OMM during clogging.

Three E3s RNF216, RBBP6 and PEX10, were identified in the proximity of b2-DHFR, together with the above-described transcription cofactor ZNF521 **(Fig. 34 + Table 16)**. RBBP6 and PEX10 were also detected in the vicinity of TOM20 during mitochondrial clogging, with PEX10 being enriched both in the absence and presence of MTX **(Fig. 35)**. Moreover, PEX12 was identified alongside PEX10 in the TOM20 proximity under clogging conditions; both are involved in peroxisome organization (Okumoto et al., 2014). This pattern may indicate that mitochondrial clogging affects contact between mitochondria and peroxisomes. In addition, MUL1 and RBX1 were enriched in the proximity of TOM20. MUL1 is a well-established OMM protein that contributes to the MQC by regulating mitophagy, mitochondrial fusion/fission and maintaining ER-mitochondrial contact sites (Puri et al., 2020). Besides the cullin-RING E3 RBX1, several cullin scaffold subunits, CUL4A, CUL4B and CUL2, were identified in the proximity of TOM20. A role for RBX1 in mitochondrial damage and ER-mitochondria crosstalk has previously been described (A. Kumar & Shaha, 2018; Song et al., 2025).

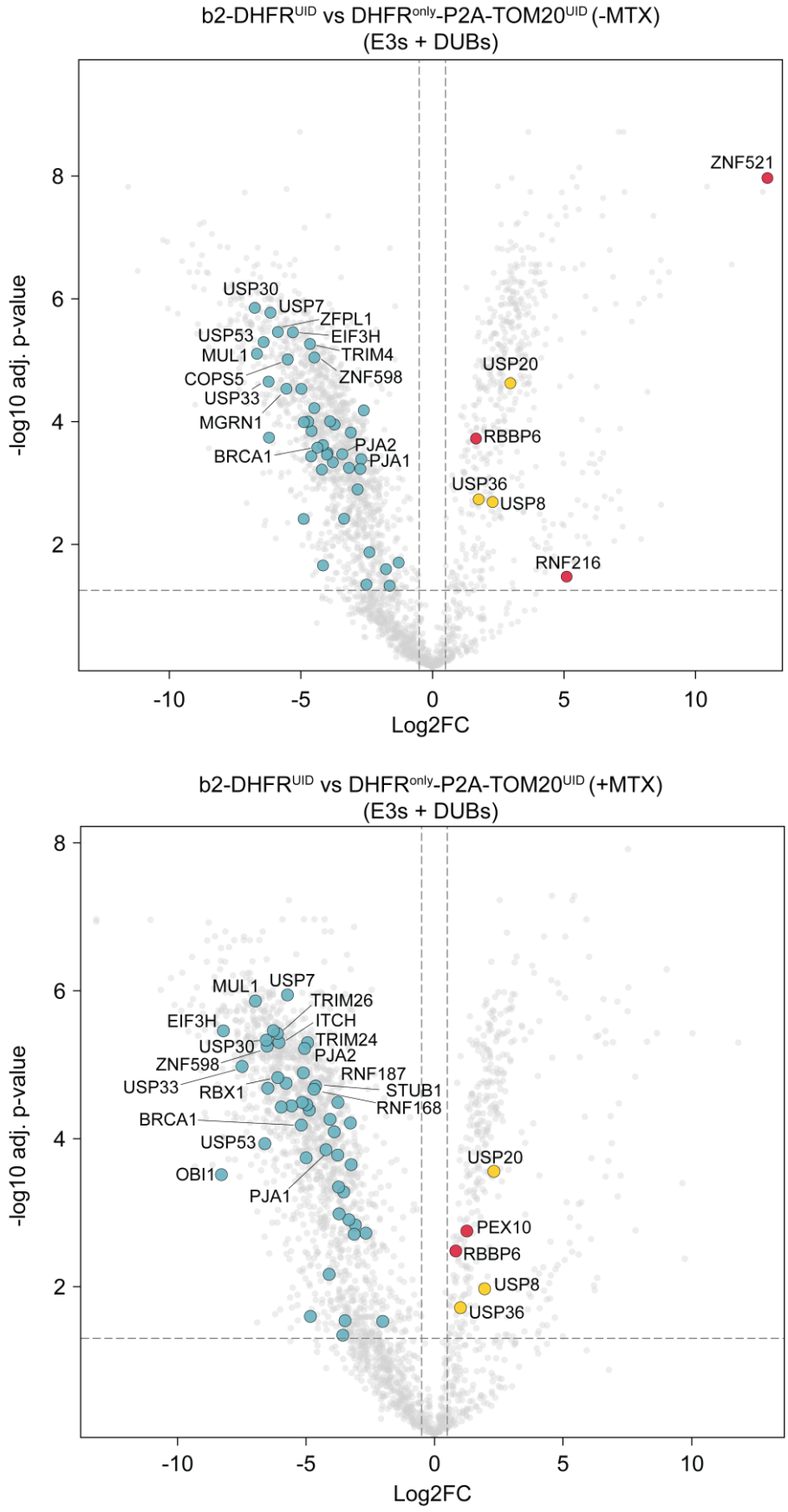

Figure 34 Ubiquitin related proteins in proximity of b2-DHFR. The MS dataset was normalized for UID intensities and screened for E3s (red) and DUBs (yellow) in the absence and presence of MTX (cut-offs: Log2FC > 0.5 and limma-based p.value < 0.05).

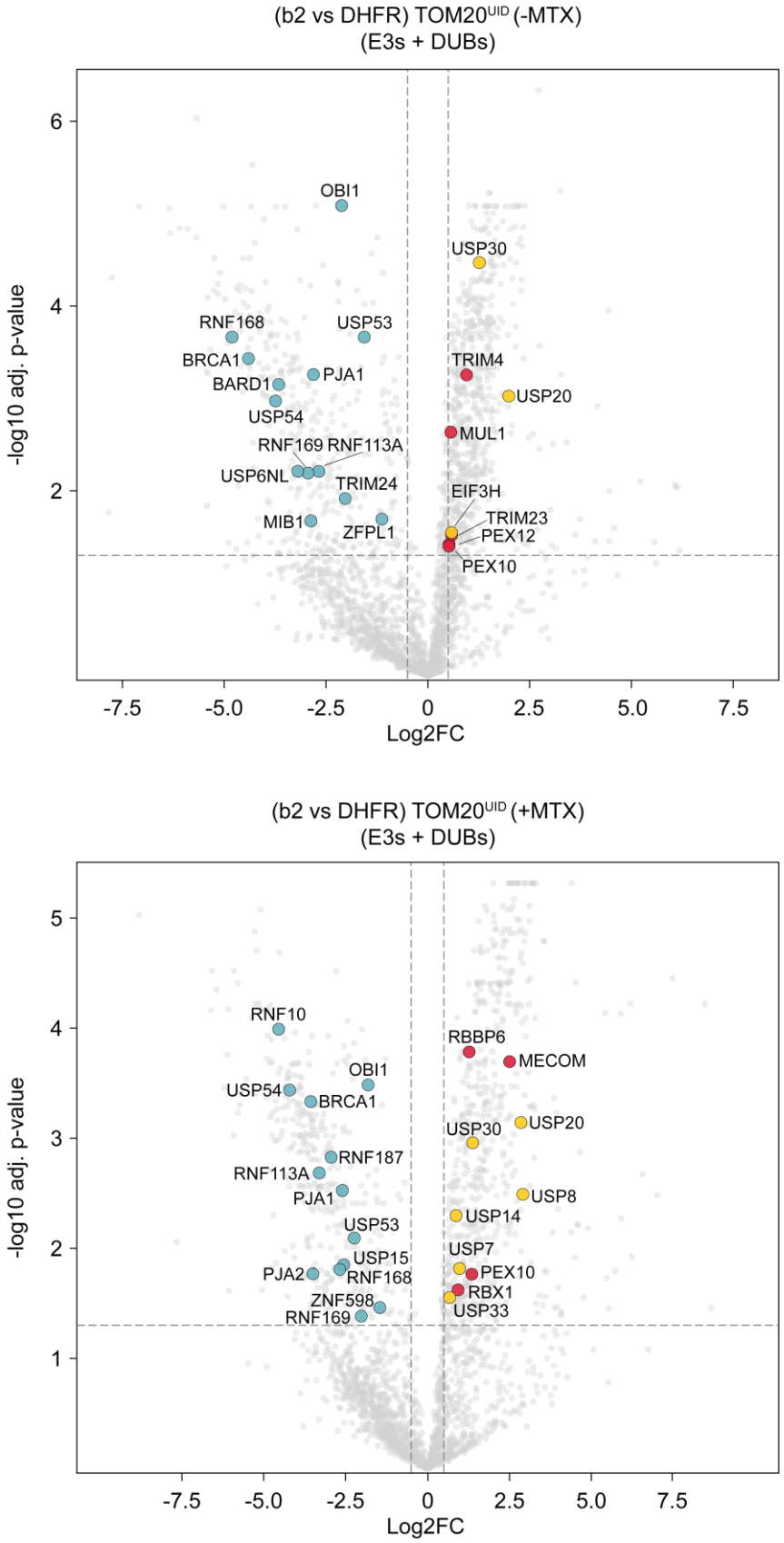

Figure 35 Ubiquitin related proteins in proximity of TOM20 during mitochondrial clogging. The MS datasets b2-DHFR-P2A-TOM20^{UID} vs DHFR^{only}-P2A-TOM20^{UID} in the absence and presence of MTX were normalized for UID intensities and screened for E3s (red) and DUBs (yellow). (cut-offs: Log2FC > 0.5 and limma-based p.value < 0.05).

Results

Table 16 E3s identified in the TOM20-based proximity labeling approach. Enriched E3s based on Fig. 34. Condition 1: b2-DHFR^{UID} vs DHFR + TOM20^{UID} without MTX; 2: b2-DHFR^{UID} vs DHFR + TOM20^{UID} with MTX; b2-DHFR + TOM20^{UID} vs DHFR + TOM20^{UID} without MTX; b2-DHFR + TOM20^{UID} vs DHFR + TOM20^{UID} with MTX. Functional descriptions are based on UniProt entries unless otherwise stated ($p < 0.5$, *; $p < 0.01$ = **; $p < 0.001$ = ***).

Protein	Log2FC	p-val.	Condition	Functional description
ZNF521	12.73	***	1	most likely wrongly annotated, functions as transcription factor that can both act as an activator or a repressor depending on the context
RNF216	5.10	*	1	regulation of antiviral responses by promoting the degradation of TRAF3, TLR4 and TLR9, required for the microtubule-dependent transport of neuronal RNA
MECOM	2.51	***	4	most likely wrongly annotated functions as transcriptional regulator, overexpression modulated genes from cellular energy-related pathways, including glycolysis, the TCA cycle, and oxidative phosphorylation (Fenouille et al., 2017)
RBBP6	1.66	***	1, 2, 4	promotes ubiquitylation of YBX1, leading to its degradation by the proteasome, regulates DNA-replication and the stability of chromosomal common fragile sites
PEX10	1.35	*	2, 3, 4	required for peroxisome organization by mediating export of the PEX5 receptor from peroxisomes, the retro translocation channel is composed of PEX2, PEX10 and PEX12
TRIM4	0.95	***	3	mitochondrial interacting RING E3 sensitizes cells to H2O2 (Tomar et al., 2015), RIG-I signaling (Okamoto et al., 2017)
RBX1	0.93	*	4	RBX1-mediated ubiquitination of SESN2 promotes cell death upon prolonged mitochondrial damage (A. Kumar & Shaha, 2018)
TRIM23	0.58	*	3	Plays an essential role in autophagy activation during viral infection
MUL1	0.57	**	3	control of mitochondrial morphology by promoting mitochondrial fragmentation, and influences mitochondrial localization
PEX12	0.52	*	3	required for peroxisome organization by mediating export of the PEX5 receptor from peroxisomes, the retro translocation channel is composed of PEX2, PEX10 and PEX12

Several DUBs were identified in the proximity of b2-DHFR and TOM20 during clogging. Among these, the mitochondrial DUB USP30 was detected exclusively in the TOM20-proximal sample **(Table 17)**. By contrast, USP20 emerged as the strongest upregulated DUB in the proximity of both b2-DHFR and TOM20 during clogging. Besides USP20, USP8 was also identified in the proximity of b2-DHFR and TOM20. USP8 and USP20 have recently been implicated as

regulators of mitophagy by removal of polyubiquitin chains from PINK1 (Durcan et al., 2014; Park et al., 2025). This suggests that both DUBs may also contribute to the MIQC in the clogging context. In particular, USP8 was shown to preferentially cleave K6-linked chains which aligns with the identification of K6-linked chains in the proximity of b2-DHFR.

Table 17 DUBs identified in the TOM20-based proximity labeling approach. Enriched E3s based on Fig. 34. Condition 1: b2-DHFR^{UID} vs DHFR + TOM20^{UID} without MTX; 2: b2-DHFR^{UID} vs DHFR + TOM20^{UID} with MTX; b2-DHFR + TOM20^{UID} vs DHFR + TOM20^{UID} without MTX; b2-DHFR + TOM20^{UID} vs DHFR + TOM20^{UID} with MTX. Functional descriptions are based on UniProt entries unless otherwise stated ($p < 0.5$, *; $p < 0.01$ = **; $p < 0.001$ = ***).

Protein	Log2FC	p-val.	Condition	Functional description
USP20	2.96	****	1, 2, 3, 4	regulation of mitophagy through PINK1 stabilization (Park et al., 2025)
USP8	2.91	**	1, 2, 4	regulation of mitophagy in osteoclasts through the stabilization of Parkin (Chaugule et al., 2026)
USP36	1.76	**	1, 2	regulates stability of mitochondrial superoxide dismutase SOD2 (M.-S. Kim et al., 2011)
USP30	1.38	**	3, 4	Tethered to the mitochondrial outer membrane, acts as a key inhibitor of mitophagy
USP7	0.98	*	4	KO leads to disordered mitochondrial biogenesis and dynamics and early neonatal lethality in mice (Yan et al., 2024)
USP14	0.88	**	4	inhibits mitophagy and promotes tumorigenesis (Z. Wang et al., 2025), degradation of alpha synuclein (Srinivasan et al., 2025)
USP33	0.68	*	4	antagonizes PARKIN during mitophagy (Niu et al., 2020)
EIF3H	0.58	*	3	interaction with mutant Huntingtin (Sap et al., 2021)

3.1.5.3.3. Identification of the VCP adaptor UBXN4 in the proximity of TOM20 during import clogging

After identifying ubiquitin writers and readers that accumulate near b2-DHFR and TOM20 during import stress, the next question was whether any VCP adaptors could be detected in the proximity of b2-DHFR or TOM20. Previous experiments showed that VCP inhibition resulted in increased ubiquitylation of b2-DHFR, consistent with yeast, where Cdc48 (VCP^{hum}) is recruited to stalled mitochondrial precursors in a ubiquitin- and Ubx2 (FAF2^{hum})-dependent manner. Therefore, the above-described datasets were screened for VCP adaptors. While no VCP adaptor was enriched in the proximity of b2-DHFR, UBXN4 was enriched near TOM20 under mitochondrial clogging conditions both in the absence and presence of MTX (normalized dataset). UBXN4 has recently been reported to cooperate with the VCP adaptor FAF2 and with the mitochondrial AAA-ATPase ATAD1, a MIQC factor involved in the removal of mistargeted or arrested mitochondrial precursors (Aweida & Cohen, 2022; Wolf et al., 2021).

Results

In summary, several E3s and DUBs were identified in the proximity of the clogger and of TOM20 during mitochondrial import clogging. Among these, MQC-factors MUL1, USP8, USP20 and USP30 were prominently enriched. This suggests that they may also contribute to the MIQC. In addition, the VCP adaptor UBXN4 was detected in the vicinity of TOM20 under clogging conditions, pointing to a potential role in recruiting VCP and/or ATAD1 to arrested mitochondrial precursors.

3.2. Expansion of the Ubiquiton tool to study ubiquitylation in mitochondrial clogging

3.2.1. Rationale of expanding the Ubiquiton towards atypical ubiquitin linkages

Multiple lines of evidence pointed towards a role for ubiquitylation, in particular of atypical chain types, during mitochondrial import clogging. First, b2-DHFR is ubiquitylated, and this modification is further enhanced upon proteasome inhibition **(chapter 3.1.4.3.2)**. Second, both b2-DHFR and TOM20 reside in the proximity of atypical ubiquitin linkages **(chapter 3.1.4.4)**. Third, diGly remnants corresponding to atypical linkages (K6, K11, K63) as well as K48 were more abundant in the enriched fraction of the initial MS screen comparing b2-DHFR$^{\mathbf{UID}}$ with DHFR$^{\mathbf{only\text{-}UID}}$ **(chapter 3.1.5.1.5)**.

Therefore, the aim was to develop an experimental approach that would permit a detailed dissection of atypical ubiquitin linkages in the context of mitochondrial clogging. Recently, the Ulrich lab has developed the so-called Ubiquiton, a molecular toolbox for the induction of linkage-specific ubiquitylation **(chapter 1.5.4)**. It consists of optimized linkage-specific E3s that are recruited to the POI via an FRB-FKBP dimerization system and uses a split-ubiquitin strategy to initiate chain formation while reducing cellular off-targets. So far, three of the eight ubiquitin linkages (M1, K48, K63) can be generated by the Ubiquiton system. The present work focused on the expansion of the Ubiquiton towards additional atypical linkages, with the goal of eventually analyzing the ubiquitylation signaling underlying MIQC.

3.2.2. Identification of new Ubiquiton candidates

To identify new candidates for the Ubiquiton, the literature was screened for enzymes with reported linkage specificity, and five promising hits were selected. Two HECT-like bacterial E3s, NleL and pvHECT, were chosen as candidates for promoting K6-linked chains (Franklin et al., 2023b; D. Y. Lin et al., 2011) **(Fig. 36A)**. Several studies have demonstrated that the E2 UBE2S possesses an E3-independent ubiquitylation activity with a preference for K11-linked chains (Liess et al., 2019; Wickliffe, Lorenz, et al., 2011; Wu et al., 2010). Furthermore, the

F849A mutant of the HECT E3 UBE3A has been reported to preferentially assemble K11-linked chains (Ries et al., 2019). In addition, HACE1 was described to ubiquitylate its substrate YB-1 with K27-linked chains.(Palicharla & Maddika, 2015).

3.2.3. Design of an initial *in vitro* screen for linkage-specificity of the new candidates

After identifying five new Ubiquiton candidates, their linkage preference was tested in an *in vitro* Ubiquiton-like setup on the model substrate GFP, because the tight FRB-FKBP dimerization system and a generalized substrate may influence the linkage-specificity. Furthermore, fusion of split-ubiquitin halves can negatively affect recombinant protein expression and solubility in *E. coli* (data not shown). Therefore, a simplified version of the Ubiquiton was designed that retains FRB-FKBP-mediated recruitment but replaces the split-ubiquitin with a full-length wild-type (WT) ubiquitin fused to GFP as a model substrate. The E3 (or E2 in case of UBE2S) was fused to an FRB moiety, while GFP carried an FKBP fusion resulting in FKBP-Ub-GFP **(Fig. 36B)**. Linkage-specificity was then monitored by addition of K to R ubiquitin mutants (Ub^{KxR}), lacking a specific lysine that is required for the respective ubiquitin-linkage formation. Further, Rapa was used to induce FRB-FKBP dimerization. A reduction in GFP ubiquitylation in the presence of a particular K to R mutant suggests linkage-specificity of the Ubiquiton candidate. To control that this effect is specific for the respective lysine, a ubiquitin mutant of the canonical K48 residue (Ub^{K48R}) was included as a control.

3.2.4. Initial *in vitro* screen for linkage-specificity of the new candidates

For solubility and expression reasons, HECT and HECT-like E3s were N-terminally truncated retaining an extended C-terminal HECT domain, which is required for the ubiquitylation activity (Kamadurai et al., 2013). The following truncations were expressed: NleL (aa 170-782, $NleL^{long}$), pvHECT (aa 276-746), HACE1 (aa 446-924), and UBE3A (aa 226-889). Furthermore, the F849A mutant of UBE3A was used, as this variant has been reported to exhibit a preference for K11-linked chains (Ries et al., 2019). Moreover, the C-terminal lysine-rich tail of UBE2S was replaced with the ZnF-UBP UBD of USP5 ($UBE2S^{long}$). The lysine-rich tail is prone to autoubiquitylation, which can promote UBE2S turnover, whereas the ZnF-UBP domain was shown to enhance UBE2S processivity on free ubiquitin chains (Bremm et al., 2010). In addition, the autoubiquitylation site K100 was replaced by arginine, as autoubiquitylation of this residue inhibits UBE2S activity (Liess et al., 2019).

First, the truncations of all five new Ubiquiton candidates were tested in the simplified Ubiquiton setup. All five proteins exhibited enzymatic activity **(Fig 36C1-5)**. NleL did not display any K6

specificity in the initial screen, and the K48R ubiquitin variant also did not affect NleL activity **(Fig. 36C1**). Notably, the GFP substrate was ubiquitylated by NleL even in the absence of Rapa. This might indicate an affinity of NleL towards the substrate independent of FRB/FKBP dimerization, potentially via the ubiquitin moiety of the substrate. Similarly, the second potential K6 specific candidate pvHECT also did not show strong K6 specificity in simplified Ubiquiton setup **(Fig. 36C2)**. In contrast to the first two candidates, UBE2S showed a strong decrease in ubiquitylation when K11 was no longer available **(Fig. 36C3)**. The ubiquitylation of GFP was reduced to a similar extent as with a ubiquitin K0 variant that lacks all lysine residues. The activity of the second K11-Ubiquiton candidate, UBE3A, was also reduced in the presence of Ub^{K11R} **(Fig. 36C4)**. However, this reduction was less pronounced than for UBE2S, and the absence of K48 had an even stronger impact on the GFP ubiquitylation. Furthermore, the potential K27-linkage candidate HACE1 did not display specificity towards either K27 or K48 in this assay **(Fig. 36C5)**.

Summarizing, these experiments reveal linkage specificity of UBE2S and UBE3A towards K11, which was particularly pronounced for UBE2S, whereas the other new candidates were not affected by removal of the lysine corresponding to their proposed linkage.

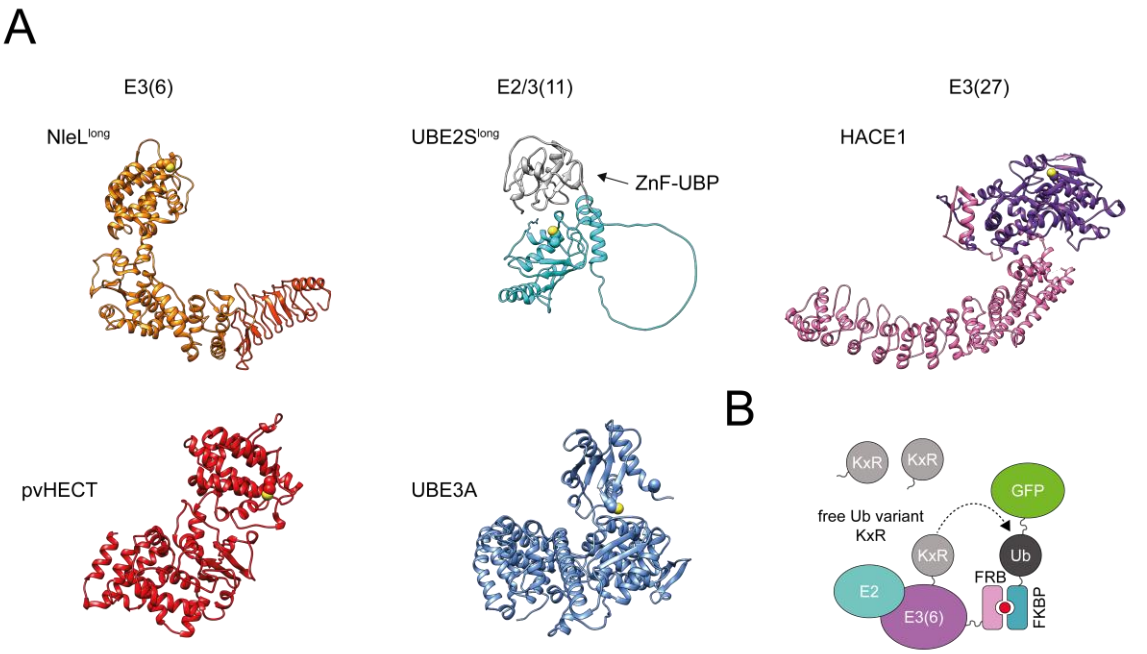
A
E3(6)
E2/3(11)
E3(27)
NleL^long
UBE2S^long
ZnF-UBP
HACE1
pvHECT
UBE3A
B
KxR
KxR
GFP
free Ub variant
KxR
KxR
Ub
FRB
E2
E3(6)
FKBP

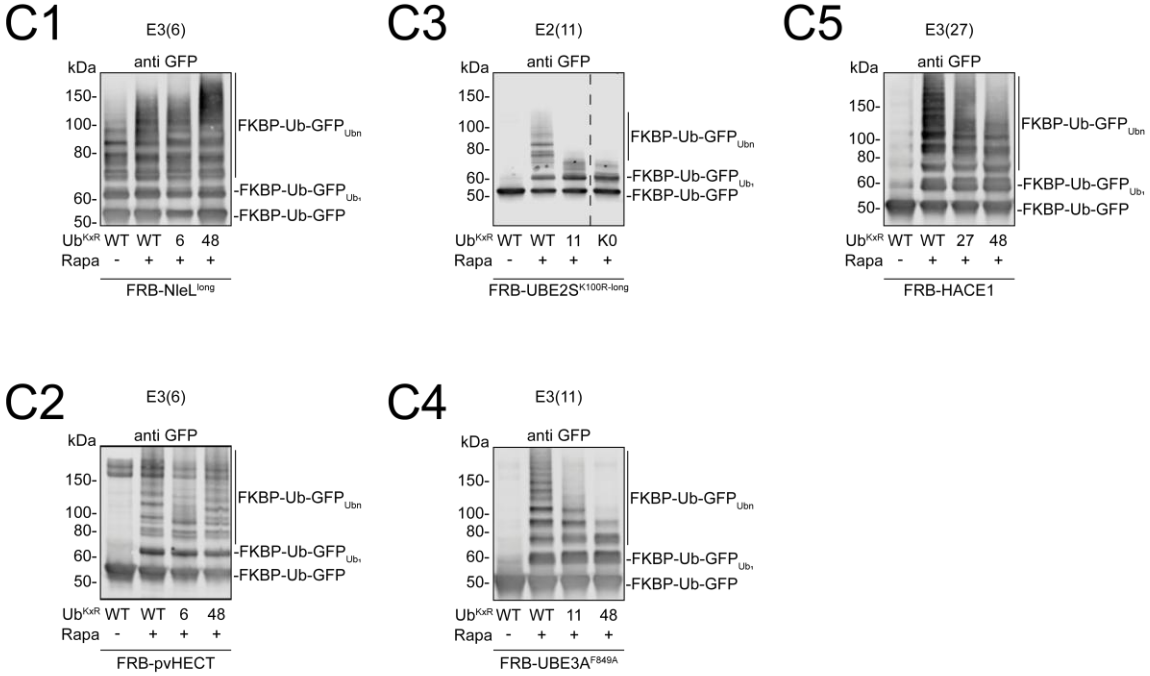
C1
E3(6)
kDa
anti GFP
150-
100-
80-
60-
50-
FKBP-Ub-GFP_Ubn
FKBP-Ub-GFP_Ub1
FKBP-Ub-GFP
Ub^KxR WT WT 6 48
Rapa - + + +
FRB-NleL^long
C3
E2(11)
kDa
anti GFP
150-
100-
80-
60-
50-
FKBP-Ub-GFP_Ubn
FKBP-Ub-GFP_Ub1
FKBP-Ub-GFP
Ub^KxR WT WT 11 K0
Rapa - + + +
FRB-UBE2S^K100R-long
C5
E3(27)
kDa
anti GFP
150-
100-
80-
60-
50-
FKBP-Ub-GFP_Ubn
FKBP-Ub-GFP_Ub1
FKBP-Ub-GFP
Ub^KxR WT WT 27 48
Rapa - + + +
FRB-HACE1
C2
E3(6)
kDa
anti GFP
150-
100-
80-
60-
50-
FKBP-Ub-GFP_Ubn
FKBP-Ub-GFP_Ub1
FKBP-Ub-GFP
Ub^KxR WT WT 6 48
Rapa - + + +
FRB-pvHECT
C4
E3(11)
kDa
anti GFP
150-
100-
80-
60-
50-
FKBP-Ub-GFP_Ubn
FKBP-Ub-GFP_Ub1
FKBP-Ub-GFP
Ub^KxR WT WT 11 48
Rapa - + + +
FRB-UBE3A^F849A

Figure 36 *In vitro* screen for linkage specificity of new Ubiquiton candidates. (A) Protein structures of the new Ubiquiton candidates were either taken from existing structures or predicted with AlphaFold3 (NleL, PDB: 3NB2; residues 170-782, orange; truncated part used in later experiments, residues 343-782, dark orange; UBE2S, cyan, fused to the ZnF-UBP UBD of USP5, grey, AF3; HACE1, PDB: 8H8X, full length magenta; truncated construct residues 446-924, purple; pvHECT, residues 276-746, AF3; UBE3A, residues 226-889). **(B)** Illustration of the simplified Ubiquiton setup used to screen for linkage specificity of the Ubiquiton candidates in **(A)**; Ubiquiton candidates were fused to FRB and FKBP-L20-Ub(WT)-GFP served as a substrate during linkage specificity monitoring with ubiquitin K-to-R mutants. **(C1-5)** E3s (1 µM) were incubated with equimolar amounts of UBCH7 (except for UBE2S) and FKBP-Ub^{WT}-GFP, 100 µM ATP, 50 nM UBA1 and 10 µM WT ubiquitin or indicated variants (Ub K-to-R mutants or lysine-less UbK0), and FRB-FKBP dimerization was induced with 5 µM rapamycin; E3 reactions were incubated at 37°C and UBE2S at 30°C for 2 h.

3.2.5. *In vitro* optimization of the K6- and K11-Ubiquiton candidates NleL and UBE2S

During the mitochondrial investigations b2-DHFR, a mitochondrial import clogger, was found in proximity to K6-linked ubiquitin chains. Furthermore, an initial mass spectrometry screen comparing b2-$DHFR^{UID}$ and $DHFR^{only\text{-}UID}$ revealed an enrichment of diGly remnants corresponding to K6-, K11-, K48- and K63-linked ubiquitin chains in the mitochondrial clogger fraction. A role for K6- and K11-linked ubiquitylation is further supported by the linkage preference of a key mitochondrial DUB, USP30, which has some linkage preference for K6- and K11-linked chains (Cunningham et al., 2015). The Ubiquiton is already established for K48- and K63-linked chains, hence the focus of this work was on establishing K6- and K11-Ubiquiton candidates.

3.2.5.1. *In vitro* Optimization of NleL

3.2.5.1.1. The K6-Ubiquiton candidate NleL changes its ubiquitylation pattern in the presence of Ub^{K6R}

K6-linked chains might participate in mitochondrial import quality control, as suggested by the proximity of the clogger b2-DHFR to this linkage and the increased abundance of K6-linkage remnants in the initial MS screen. These findings prompted me to reinvestigate the Ubiquiton candidate NleL.

Removal of K6 through the Ub^{K6R} variant in the initial linkage-preference screen did not affect the ligase activity of NleL **(Fig. 36C1)**. However, it remains possible that NleL prefers K6-linkages under normal conditions but switches to an alternative linkage type(s) when K6 is not available. Previous work demonstrated that NleL predominantly assembles K6-linked ubiquitin chains, but can also form K48-linked chains to a lesser extent (Hospenthal et al., 2013). Interestingly, analysis of free ubiquitin chains formed by NleL revealed a clear change of the pattern of those free chains in the presence of Ub^{K6R} **(Fig. 37)**. A change in the ubiquitylation

pattern suggests that another ubiquitin linkage is formed and supports the idea that NleL might preferably form K6-linked chains while switching to an alternative linkage(s) in the absence of K6.

In summary, blocking K6-linked ubiquitylation revealed that NleL changes its ubiquitylation pattern on free ubiquitin chains, indicating a K6-preference with considerable flexibility in its linkage usage. Because the ultimate goal was to apply NleL to substrates in human cells, where endogenous WT ubiquitin still allows K6-linked chain formation but also permits alternative linkages, the next aim was to optimize NleL to increase its linkage preference.

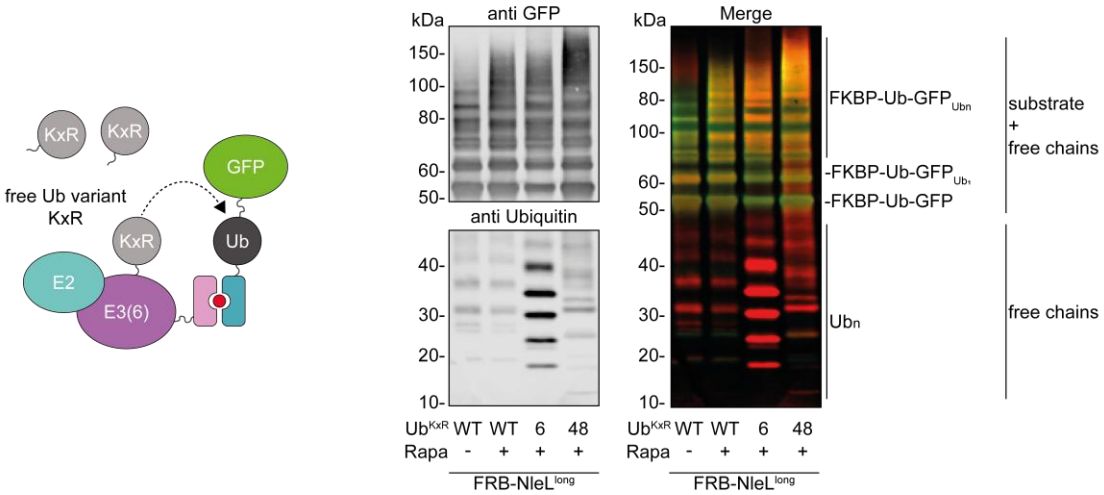

Figure 37 NleL changes its ubiquitylation pattern in the presence of Ub^{K6R}. Western blot from Figure 36C1 additionally probed for ubiquitin; 1 µM FRB-NleL was incubated with equimolar amounts of UBCH7 and FKBP-Ub^{WT}-GFP, 100 µM ATP, 50 nM UBA1 and 10 µM WT ubiquitin or the indicated variants (Ub K-to-R mutants or lysine-less UbK0), and FRB-FKBP dimerization was induced with 5 µM rapamycin; reactions were incubated at 37°C for 2 h.

3.2.5.1.2. Rationale for the mutant NleL^{E705A}

A recent study reported that mutation of the NleL residue E705 to alanine (NleL^{E705A}) enhances its preference for assembling K6-linked chains on free ubiquitin (Franklin et al., 2023a). Because purification of the initial NleL construct (aa 170-782) was limited by poor solubility, the mutation was instead introduced into a more N-terminally truncated NleL variant (NleL^{short}, aa 343-782). Initial tests showed that the WT form of the shortened construct was enzymatically active and yielded higher protein amounts during purification (data not shown).

3.2.5.1.3. Mutant NleL^{E705A} exhibits enhanced substrate-directed ubiquitylation

To test whether NleL^{E705A} displays enhanced linkage specificity towards K6-linked chains, its activity was tested in the simplified Ubiquiton set up with a FKBP-Ub^{K6R}-GFP substrate. Both

Results

NleL^{WT} and NleL^{E705A} showed decreased substrate ubiquitylation in the presence of Ub^{K6R} **(Fig. 38A)**. Mutant NleL^{E705A} exhibited an increased enzymatic activity compared to the WT. Notably, mutant NleL^{E705A} produced clearly fewer free ubiquitin chains than NleL^{WT}, and an accumulation of monomeric ubiquitin was observed in the Ub^{K6R} and Ub^{K48R} condition. To further confirm the reduction of free chains, the activity of NleL^{WT} and NleL^{E705A} in the absence of the GFP model substrate was analyzed. A clear reduction in low molecular weight ubiquitin chains was visible in the mutant condition **(Fig. 38B)**. Again, the presence of Ub^{K6R} altered the ubiquitylation pattern of both NleL^{WT} and NleL^{E705A}.

So far, the linkage specificity of NleL^{E705A} was tested with a substrate carrying a K6R ubiquitin. To analyze whether a substrate fused to a lysine free Ub^{K0} would reduce NleL^{E705A} activity, a GFP fusion to the C-terminal half of a split ubiquitin (CUb) that lacks all lysine residues (FKBP-CUb^{K0R}-GFP) was used. When Ub^{K6R} was present in the reaction, a decrease in GFP ubiquitylation by NleL^{E705A} was observed, although the signal was still far from being completely depleted **(Fig. 38C)**. Interestingly, even when only Ub^{K0} was available and the substrate ubiquitin was lysine-free, NleL^{E705A} still displayed detectable ubiquitylation activity. This observation suggests that NleL may initiate ubiquitylation directly on lysine residues of the substrate protein. Repeatedly, an increase in free monoubiquitin in the probe with GFP-CUb^{K0} was observable compared to the GPF carrying a Ub^{WT}-fusion **(Fig. 38C)**. This accumulation was visible in the presence of free Ub^{WT} and was more pronounced with Ub^{K6R}, Ub^{K48R} and Ub^{K0}.

Together, these findings suggest that the E705A mutation in NleL enhances substrate-specific ubiquitylation while reducing the formation of free ubiquitin chains. Both features represent favorable improvements for the *in vivo* application of NleL.

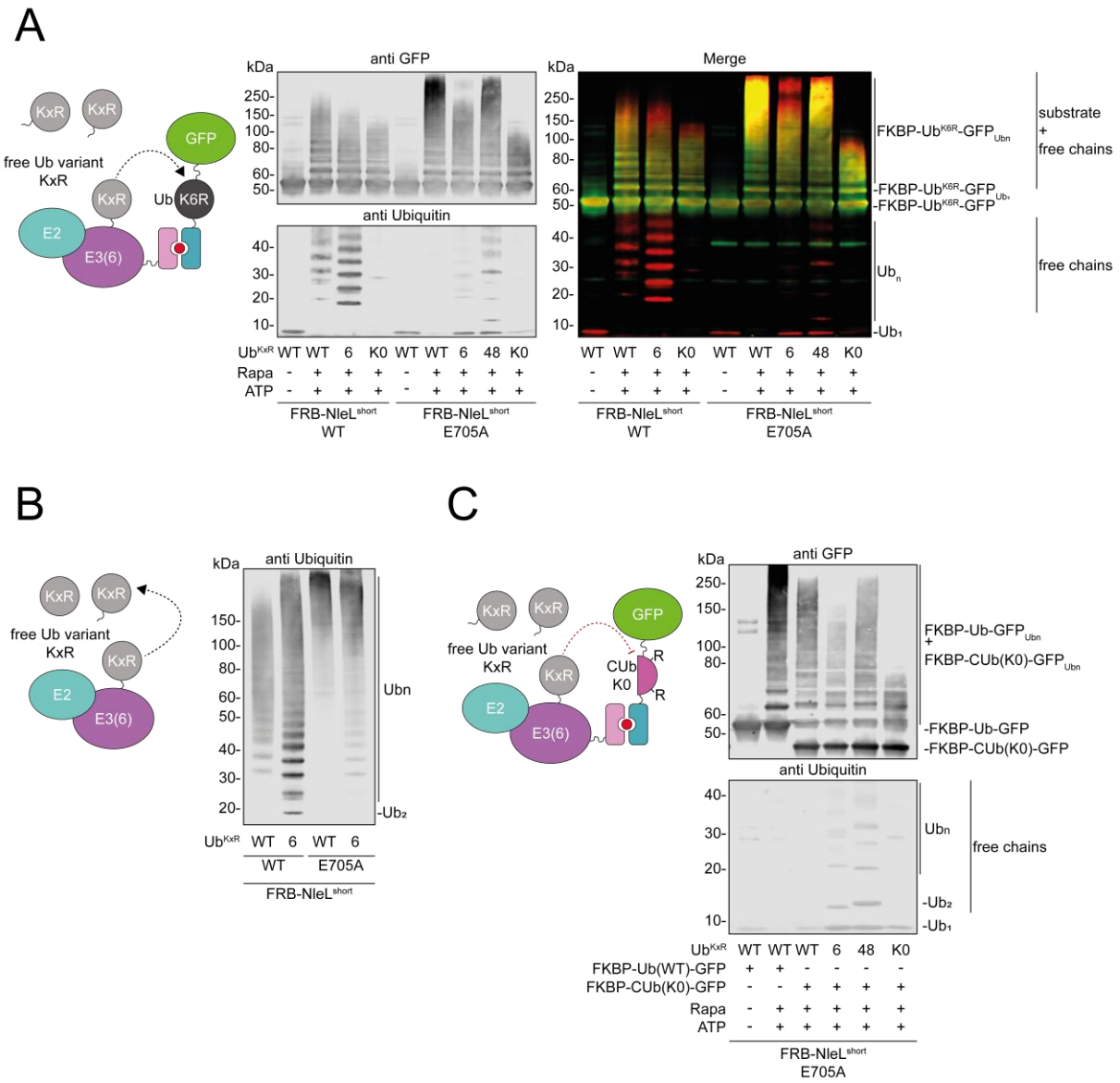

Figure 38 NleL^{E705A} enhances substrate-directed ubiquitylation. (A) 1 µM WT FRB-NleL^{short} (aa 343-782) or FRB-NleL$^{E705A\text{-}short}$ were incubated with equimolar amounts of UBCH7 and FKBP-Ub^{K6R}-GFP, 100 µM ATP, 50 nM UBA1 and 10 µM WT ubiquitin or indicated variants (Ub K-to-R mutants or lysine-less UbK0), and FRB-FKBP dimerization was induced with 5 µM rapamycin; reactions were incubated at 37°C for 2 h. **(B)** To test formation of free chains by the NleL variants, reactions similar to those in **(A)** were performed but lacking the GFP substrate. **(C)** To test a lysine-less substrate, FKBP-CUb^{K0}-GFP was used; reaction conditions were similar to those in **(A)** with incubation at 30°C for 1 h.

3.2.5.2. *In vitro* Optimization of UBE2S

3.2.5.2.1. Comparison of UBE2S to the established E3(63)

After the *in vitro* optimization of the K6-Ubiquiton candidate NleL, attention was turned to the K11-Ubiquiton candidate UBE2S. In the initial screen using the simplified Ubiquiton setup, UBE2S displayed clear specificity for assembling K11-linked ubiquitin chains **(Fig. 36C3)**. In this screen, the presence of Ub^{K11R} restricted UBE2S activity to the formation of a ubiquitin

dimer, as K11 of the substrate-attached ubiquitin was still available. However, UBE2S appeared to retain minimal activity beyond the formation of a ubiquitin-dimer on the GFP-Ub^{WT} substrate in the presence of Ub^{K11R} substrate and was therefore compared to the already established Ubiquiton candidate E3(63) in the simplified Ubiquiton setup. The comparison of $UBE2S^{long}$ and E3(63) revealed a similar restriction of both enzymes with the respective ubiquitin variants Ub^{K11R} and Ub^{K63R} **(Fig. 39A)**. This suggests that UBE2S is a promising candidate for the K11-Ubiquiton.

3.2.5.2.2. Analysis of the ZnF-UBP fusion to UBE2S

For the initial screen a ZnF-UBP domain of USP5 was fused to UBE2S, which was shown to enhance K11-linkage specificity on free chains (Bremm et al., 2010). However, such a UBD could complicate *in vivo* use, as it may increase off target ubiquitylation by recruiting UBE2S to endogenous ubiquitylation sites and perturbing the cellular pool of free ubiquitin. It would be interesting whether removal of this ZnF-UBP domain would affect linkage specificity and processivity of UBE2S. In order to address this question, a UBE2S construct lacking the ZnF-UBP domain ($UBE2S^{short}$) was generated and compared to $UBE2S^{long}$ in the simplified Ubiquiton setup.

In this assay, $UBE2S^{short}$ and $UBE2S^{long}$ showed comparable processivity **(Fig. 39B)**. The ubiquitylation activity of both enzymes, was reduced to a similar extent in the presence of Ub^{K11R}. This may be explained by the FRB-FKBP dimerization module, which enforces proximity between enzyme and substrate so that ZnF-UBP-mediated recruitment and positioning might become largely dispensable under these conditions.

3.2.5.2.3. Analysis of UBE2S on a substrate carrying a lysine-less ubiquitin

In this screen, UBE2S was first tested on a GFP substrate carrying a Ub^{WT} fusion. To determine whether the residual lysine 'off-target' activity could be eliminated, a lysine-less FKBP-CUb^{K0R}-GFP substrate was used. Surprisingly, removal of all lysines on CUb did not prevent the formation of a ubiquitin dimer on GFP-CUb^{K0} **(Fig. 39C)**. This might reflect that UBE2S targets another lysine on the substrate under the tight interaction due to the dimerization by FRB-FKBP.

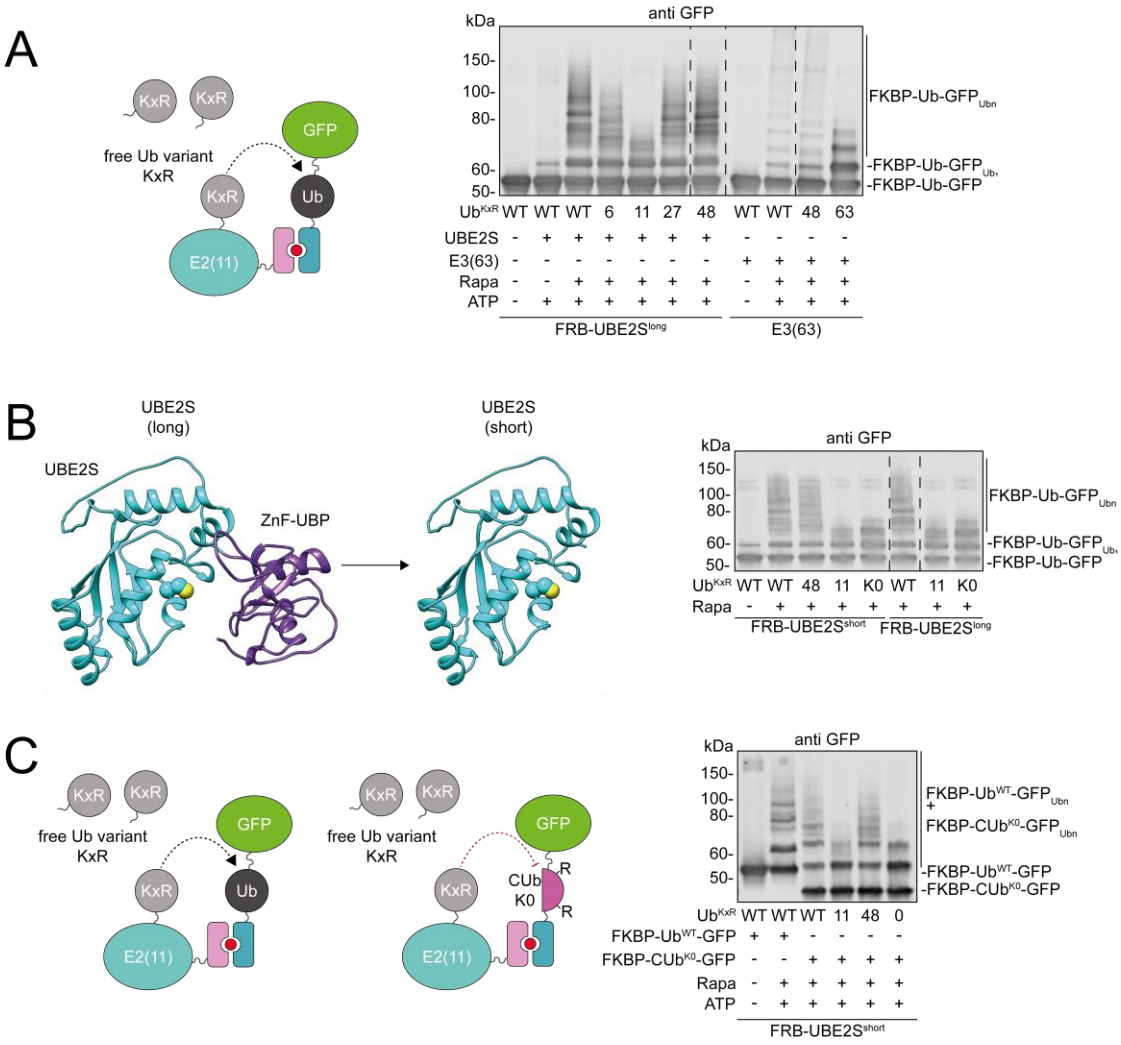

Figure 39 UBE2S^{short} and UBE2S^{long} exhibit similar specificity and processivity. (A) For comparison of UBE2S and the established E3(63), 1 µM FRB-E3(63) was incubated with equimolar amounts of Mms2/Ubc13; reactions of FRB-UBE2S^{long} and FRB-E3(63) contained FKBP-Ub^{K6R}-GFP, 100 µM ATP, 50 nM UBA1 and 10 µM WT ubiquitin or indicated variants (Ub K-to-R mutants or lysine-less Ub^{K0}), and FRB-FKBP dimerization was induced with 5 µM rapamycin; reactions were incubated at 37°C for 2 h. **(B)** Comparison of UBE2S lacking the ZnF-UBP domain (UBE2S^{short}) with UBE2S^{long} **(A)**. **(C)** Test of a lysine-less substrate FKBP-CUb^{K0}-GFP with FRB-UBE2S^{short}; reaction conditions of **(B)** and **(C)** were similar to those in **(A)** but **(C)** was incubated at 30°C for 1 h.

3.2.5.2.4. Mutant UBE2S$^{E139/143R}$ shows enhanced ubiquitylation activity

In vivo usage of a Ubiquiton candidate requires strong enzymatic activity as cellular DUBs and limitations of the ubiquitin pool might interfere with the ubiquitylation activity. A recent study demonstrated that charge-swapping UBE2S residues E139 and E143 to arginine increases the ubiquitylation activity of UBE2S on free ubiquitin dimer formation (Welsh et al., 2022) **(Fig. 40)**. Thus, this mutation was implemented in the long UBE2S construct (UBE2S$^{E139/143R\text{-}long}$) and analyzed the behavior of this mutant in the simplified Ubiquiton setup. While the K11-

linkage specificity of UBE2SE$^{139/143R\text{-}long}$ remained unchanged, the double mutant displayed an enhanced ubiquitylation activity compared to the UBE2S$^{WT\text{-}long}$ **(Fig. 40)**. This enhanced activity of UBE2S$^{E139/143R\text{-}long}$ indicates that this variant is particularly well suited for *in vivo* applications.

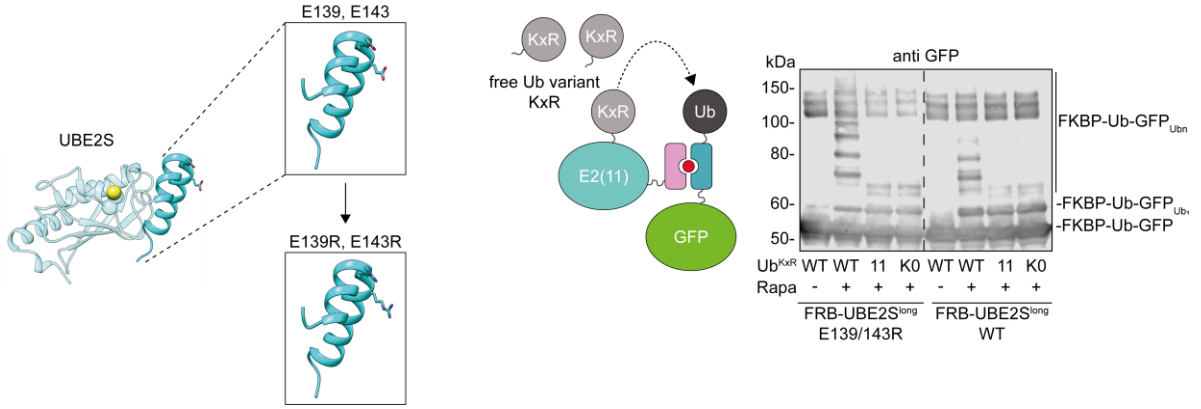

Figure 40 Mutant UBE2S$^{E139/143R}$ shows enhanced ubiquitylation activity. FRB-UBE2S^{long} and mutant FRB-UBE2S$^{E139/143R\text{-}long}$ were incubated with FKBP-Ub-GFP, 100 µM ATP, 50 nM UBA1 and 10 µM WT ubiquitin or indicated variants (K-to-R Ub mutants or lysine-less Ub^{K0}), and FRB-FKBP dimerization was induced with 5 µM rapamycin; reactions were incubated at 37°C for 2 h.

3.2.5.2.5. Analysis of the linkage specificity of UBE2S variants via MS

While UBE2S showed clear K11-linkage specificity in the simplified Ubiquiton setup, it was investigated whether the optimizations affected this linkage preference. Therefore, ubiquitylation reactions of UBE2S^{short}, UBE2S^{long} and UBE2S$^{E139/43R\text{-}long}$ in the simplified Ubiquiton setup containing $^{FKBP\text{-}Ub}$GFP as a substrate were analyzed by MS. Interestingly, UBE2S^{short} exhibited a decreased K11-linkage specificity as compared to UBE2S^{long} (~52% and ~62%) **(Fig. 41)**. Both UBE2S variants also formed K48- and K63-linked chains (~15% and ~30%) The double mutant UBE2S$^{E139/143R\text{-}long}$ showed increased K11-linkage specificity (~74%). Notably, this experiment was not performed in triplicates and requires further repetition, but it suggests that introduction of the double mutant enhanced the K11-linkage specificity of UBE2S.

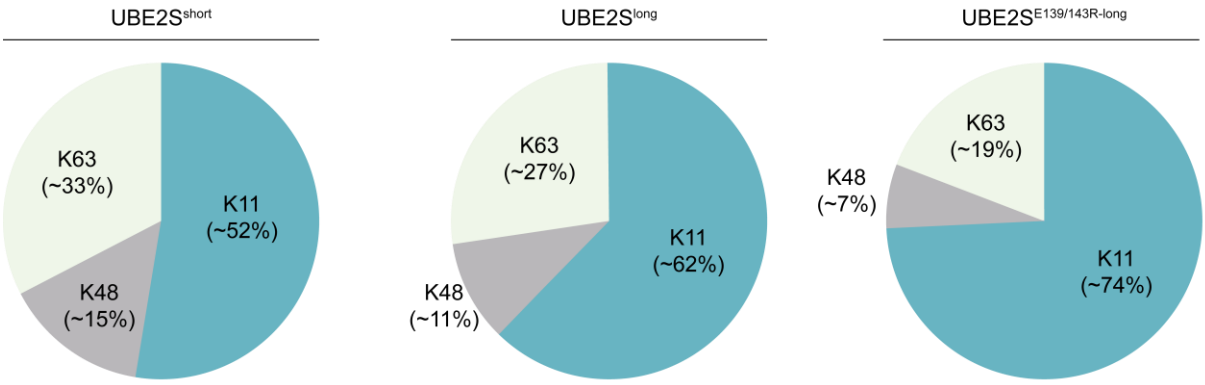

Figure 41 Analysis of the linkage specificity of UBE2S variants by MS. The indicated FRB-UBE2S variants (1 µM) were incubated with equimolar amounts of $^{FKBP\text{-}Ub}$GFP, 100 µM ATP, 50 nM UBA1 and 10 µM WT ubiquitin, and FRB-FKBP dimerization was induced with 5 µM rapamycin; reactions were incubated at 37°C for 10 min followed by analysis via MS (n=1).

3.2.6. *In vivo* application of NleL and UBE2S

3.2.6.1. Analysis of UBE2S ubiquitylation activity on a model GFP substrate in yeast

After the initial characterization and optimization of the new Ubiquiton candidates NleL and UBE2S in the simplified Ubiquiton setup, the aim was to implement them *in vivo*. Therefore, both enzymes were tested on a model substrate GFP in the “full” Ubiquiton setup. A fusion of the Ubiquiton module NUbo to GFP (^{NUbo}GFP) served as a substrate, while the CUbo module was fused to UBE2S. Both the Ubiquiton substrate and the corresponding Ubiquiton candidate were stably integrated into the genome of *S. cerevisiae* under an ADH1 promoter.

First, the activity of UBE2S^{short} and UBE2S^{long} was compared with the already established E3(63). For both UBE2S constructs, addition of Rapa resulted in substrate ubiquitylation with a single linkage **(Fig. 42A)**. However, when compared to E3(63) the activity was limited. Therefore, the mutant UBE2S$^{E139/143R\text{-}short}$ was tested for enhanced activity as suggested by previous findings *in vitro* **(Fig. 40)**. Again, an additional GFP band upon expression of UBE2S$^{E139/143R}$ in the presence of Rapa was visible **(Fig. 42B)**. Nevertheless, the double mutant did not introduce any new additional band. Finally, the detection of longer K11-linked chains seemed not to be prevented by proteasomal degradation, as no additional GFP bands appeared after proteasome inhibition with MG132 **(Fig. 42B)**.

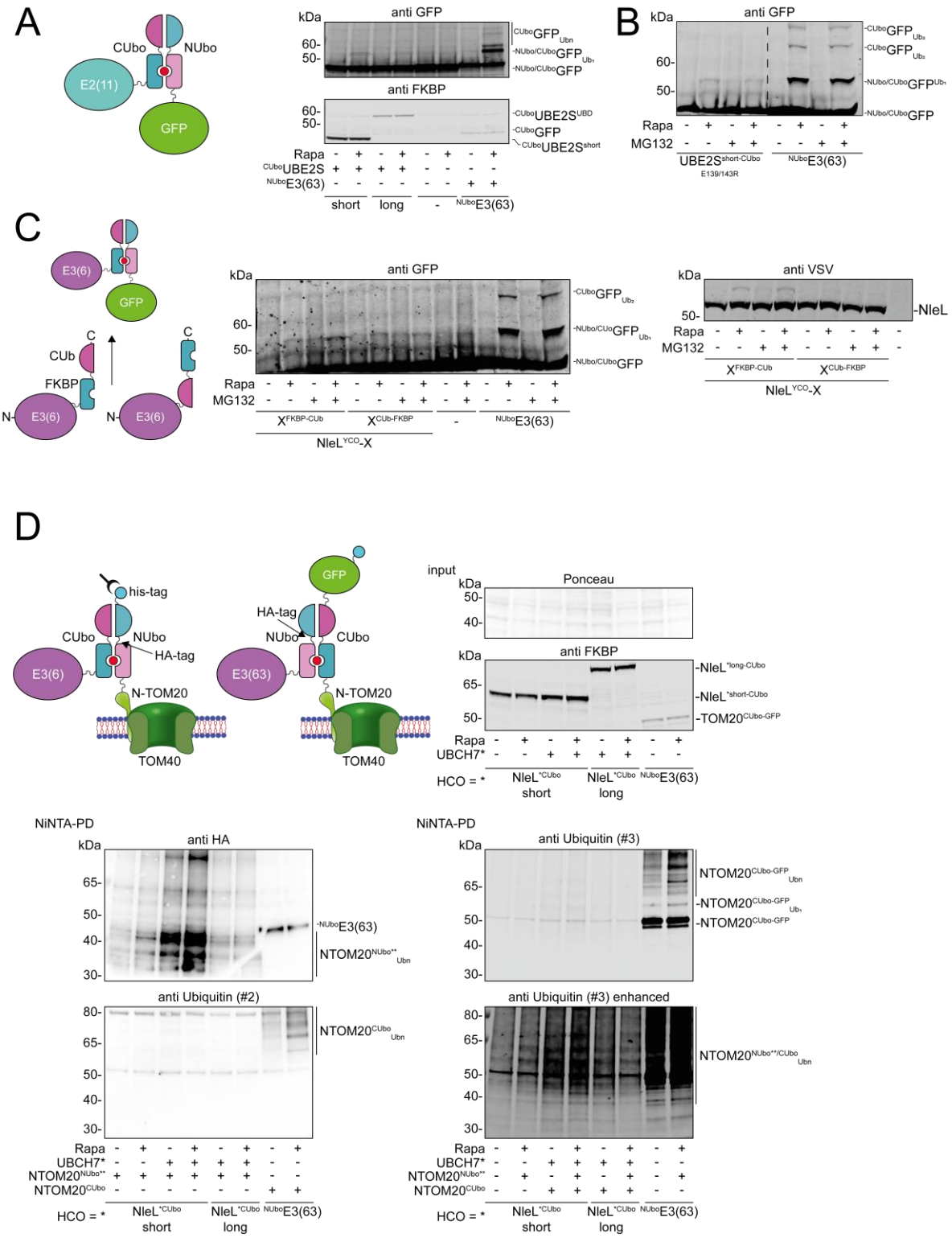
A
CUbo
NUbo
E2(11)
GFP
kDa
anti GFP
anti FKBP
Rapa
short
long
B
anti GFP
Rapa
MG132
C
E3(6)
GFP
CUb
FKBP
anti GFP
anti VSV
NIeL
Rapa
MG132
D
his-tag
HA-tag
N-TOM20
TOM40
E3(63)
input
Ponceau
anti FKBP
NiNTA-PD
anti HA
anti Ubiquitin (#2)
anti Ubiquitin (#3)
anti Ubiquitin (#3) enhanced
UBCH7*
HCO = *

Figure 42 *In vivo* application of NleL and UBE2S. (A) Diploid yeast cells expressing combinations of ^{NUbo}GFP and ^{CUbo}UBE2S^{short} and ^{CUbo}UBE2S^{long}; for E3(63) diploid yeast cells expressing ^{CUbo}GFP, ^{NUbo}E3(63) and Ubc13 were used. Addition of 2.5 µM rapamycin for 90 min was used for ligase recruitment to GFP substrates. **(B)** Diploid yeast cells expressing combinations of ^{NUbo}GFP and UBE2S$^{E139/143R\text{-}short\text{-}CUbo}$; with E3(63) setup and ligase recruitment as in **(A)**. **(C)** Diploid yeast cells co-expressing NleL$^{long\text{-}YCO\text{-}FKBP\text{-}CUb}$ and NleL$^{long\text{-}YCO\text{-}CUb\text{-}FKBP}$ and NUbo^{GFP}; the E3(63) setup and rapamycin induction were as in **(A)**. **(D)** HEK293T cells transiently transfected with NleL$^{short\text{-}HCO\text{-}CUbo}$, NleL$^{long\text{-}HCO\text{-}CUbo}$ and NTOM20$^{NUboK29/33R}$ and if indicated with UBCH7^{HCO}; ^{NUbo}E3(63) was co-transfected with NTOM20$^{CUbo\text{-}GFP}$ and Mms2/Ubc13; the NUbo-module fused to E3(63) and GFP contains an HA-tag for detection, and 1 µM rapamycin was added for 2 h. NTOM20 substrates were his-tagged and denaturing Ni-NTA pull-downs were performed for substrate enrichment; human codon-optimized = *, optimized NUbo module with human codon-optimized FRB^{K0} and NUa$^{K27/29/33R}$ indicated with **.

3.2.6.2. Analysis of NleL ubiquitylation activity on a GFP model substrate in yeast

The next aim was to test NleL in the “full” Ubiquiton arrangement in yeast. Initial tests did not show any activity of NleL in this model organism, potentially arising from problems to detect the protein expression of NleL (data not shown). Because NleL is of bacterial origin, its expression in *S. cerevisiae* may be limited by suboptimal codon usage. To address this potential limitation, the NleL coding sequence was codon-optimized for *S. cerevisiae*, resulting in a robustly expressed codon-optimized NleL (NleL^{YCO}) **(Fig. 42C)**. A C-terminal fusion of the CUbo module to NleL was chosen because the catalytic cysteine of NleL resides close to the C terminus. In addition, an alternative CUbo architecture was tested in which the relative order of the C-terminal CUb and FKBP modules was swapped. This might increase activity due to closer proximity of the refolded split-ubiquitin to the catalytic cysteine.

In both fusion orientations, NleL displayed detectable ligase activity **(Fig. 42C)**. However, this activity remained noticeably weaker when compared to E3(63). Notably, an additional form of NleL itself was detected upon addition of Rapa in the NleL$^{FKBP\text{-}CUb}$ arrangement which was obsolete in NleL$^{CUb\text{-}FKBP}$ construct. It may reflect autoubiquitylation of the ligase following the refolding of the split ubiquitin. Such autoubiquitylation could inhibit E3 activity as it is known for E2s and promote degradation (Bie & Ciechanover, 2011; Scaglione et al., 2007)

In conclusion, both NleL and UBE2S exhibited activity towards ^{NUbo}GFP. Nevertheless, if compared to the established E3(63) both enzymes exhibited relatively low activity and further optimization would be beneficial for *in vivo* usage.

3.2.6.3. Application of NleL on a mitochondrial model substrate in human cells

The activity of NleL^{YCO} on the model substrate ^{NUbo}GFP was promising. Therefore, it was next tested whether NleL can ubiquitylate a mitochondrial model substrate. The established E3(63) was included as well, as previous experiments suggested a role K6- and K63-linked ubiquitylation in the MIQC **(chapter 3.1.4.4 + 3.1.5.1.5)**. A C-terminally truncated version of TOM20 (NTOM20) that retains the membrane anchor and is efficiently targeted to the mitochondria was used as a mitochondrial model substrate (data not shown). The NUbo module was optimized, the FRB domain was human codon-optimized and all lysines on FRB and lysines K27, K29 and K33 on the NUa half were replaced by arginine in order to prevent endogenous ubiquitylation. This optimized NUbo module was fused to the C-terminus of NTOM20 (NTOM20^{NUbo}) to preserve the native N-terminal membrane anchor, resulting in a mitochondrial model substrate for the K6 candidate NleL **(Fig. 42D)**. Furthermore, integration of the CUbo module into a NTOM20-GFP construct (NTOM20$^{CUbo\text{-}GFP}$) served as the model substrate for ^{NUbo}E3(63). Both substrates were also equipped with a C-terminal his-tag to perform denaturing PDs. Human codon-optimized NleL (NleL^{HCO}) was extended by the CUbo module (NleL$^{HCO\text{-}CUbo}$) and both the long and short version of NleL were tested. Each substrate was co-expressed with its respective E3 in mammalian cells followed by denaturing PDs. Upon expression of ^{NUbo}E3(63) and NTOM20$^{CUbo\text{-}GFP}$ a basal ubiquitylation signal on NTOM20$^{CUbo\text{-}GFP}$ was already visible in the absence of Rapa **(Fig. 42D)**. This might reflect endogenous ubiquitylation triggered by the artificial recruitment of the tightly folded GFP moiety to the OMM. In comparison, NTOM20^{NUbo} expression did not trigger a comparable ubiquitylation. Addition of Rapa in the E3(63) condition enhanced this signal, demonstrating that ^{NUbo}E3(63) is functional in the context of ubiquitylation of a mitochondrial model substrate. Furthermore, upon addition of NleL$^{short\text{-}HCO}$ in the presence of Rapa a ubiquitylation pattern emerged on NTOM20^{NUbo}. To further boost NleL activity UBCH7 was additionally overexpressed, as co-expression of the E2 UBCH7 was previously shown to enhance the activity of the Ubiquiton candidate E3(48) (Renz et al., 2024). Upon addition of Rapa enhanced ubiquitylation of NTOM20^{NUbo} by NleL$^{short\text{-}HCO}$ was visible **(Fig. 42D)**. Initially, the ubiquitylation of NTOM20^{NUbo} by NleL$^{short\text{-}HCO}$ was not detected when probed for ubiquitin. Therefore, a second ubiquitin antibody was tested, as ubiquitin antibodies may have linkage preferences. The second ubiquitin antibody could detect the ubiquitin signal introduced by NleL with enhanced contrast. Interestingly, the additional expression of UBCH7 in the absence of Rapa again seemed to trigger a basal endogenous ubiquitylaton of NTOM20^{NUbo} **(Fig. 31B)**. This might be explained by mitochondrial interactors such as PARK2 and MUL1 of UBCH7 according to BioGRID database.

In conclusion, the ubiquitylation of the mitochondrial model substrate NTOM20 by NleL$^{short\text{-}HCO}$ and ^{NUbo}E3(63) was demonstrated in an initial experiment. However, further experiments are

required to analyze the specific linkage-type that is formed by NleL on NTOM20 and to improve the enzymatic activity of NleL.

4 Discussion

Mitochondrial protein import is fundamental for eukaryotic cell viability, and its failure is linked to diverse pathologies, including neurodegenerative diseases, neuropathies and cancer. As ~99% of mitochondrial proteins are imported via the TOM complex, stalled precursors at the translocase pose a substantial threat to mitochondrial integrity.

In yeast, several MIQC pathways are known to deal with stalled mitochondrial precursors including mitoTAD and mitoCPR (Ravanelli et al., 2020). In the mitoTAD pathway, Cdc48 (VCP^{hum}) extracts stalled precursors leading to their proteasomal degradation. Cdc48 recruitment is facilitated via Ubx2 ($FAF2^{hum}$) which recognizes ubiquitylated precursors (Schuberth et al., 2004). In the mitoCPR response, Msp1 ($ATAD1^{hum}$) is recruited to stalled mitochondrial precursors in a Cis1-dependent manner (Weidberg & Amon, 2018).

Recent work has begun to uncover analogous MIQC mechanisms in human cells and mechanisms have been discovered that deal with arrested mitochondrial precursors. Similar to yeast mitoCPR, mammalian ATAD1 was shown to extract stalled precursors from the TOM complex (J. Kim et al., 2024). However, Cis1 is not conserved in mammals, and the precise mechanism how ATAD1 is recruited to clogged TOM complex remains unclear. By contrast, a direct VCP-dependent mitoTAD-like pathway at TOM has not been conclusively demonstrated in human cells (Borgert et al., 2024). It was recently shown that MARCH5 and USP30 participate in the regulation of mitochondrial protein import through (de)ubiquitylation (Phu et al., 2020). This raises the question of which downstream factors are recruited through the ubiquitylation at the TOM complex, particularly if MIQC factors such as VCP or ATAD1 are targeted to ubiquitylated precursors during mitochondrial import stress. Although several studies have analyzed the interactome of TOM complex subunits, the TOM-proximal interactome during mitochondrial import stress has not yet been systematically characterized (Akram et al., 2024; Meurant et al., 2023). Moreover, the preference of USP30 for non-canonical K6-linked chains suggests that atypical ubiquitin linkages may participate in regulating mitochondrial protein import, but the linkage landscape at clogged TOM complexes remains largely unexplored.

To address these questions, this thesis pursued three main aims. First, the establishment of a mitochondrial model clogger, b2-DHFR, in human cells to analyze ubiquitylation events during mitochondrial import clogging. Second, a TOM20-based proximity-labeling approach to define the interactome of a clogged mitochondrial import channel. Third, the extension of the linkage-specific ubiquitylation tool Ubiquiton towards atypical ubiquitin linkages enabling detailed dissection of the ubiquitylation landscape at b2-DHFR and TOM20 under clogging conditions.

4.1. Establishment and characterization of b2-DHFR in human cells

The first aim of this study was to establish a mitochondrial model clogger in human cells. While several treatments such as CCCP or MitoBloCKs are commonly used to perturb mitochondrial import in mammalian systems, these approaches act indirectly by collapsing Δψm or interfering with precursor import machinery globally (Krakowczyk et al., 2024; Schäfer et al., 2022). Such a collapse of Δψm also triggers mitophagy, which in turn leads to global mitochondrial ubiquitylation (Antico et al., 2021). Such a global ubiquitin response complicates both the detection of clogging-specific ubiquitylation events and the analysis of factors that act directly at stalled import channels. In contrast, a *bona fide* import clogger allows direct and specific induction of translocation arrest on a defined substrate, thereby enabling the analysis of ubiquitylation events and recruitment of quality control factors directly to the stalled precursor. Although physiological cloggers such as a mutant form of the mitochondrial carrier ANT1 have been described (Coyne et al., 2023), the model clogger b2-DHFR offers a key advantage: the extent of import arrest can be fine-tuned through addition of MTX, which stabilizes the DHFR fold (Boos et al., 2019). The b2-DHFR construct has already been established in *S. cerevisiae*, and the present work aimed to establish and validate this model in human cells.

First, it was demonstrated that b2-DHFR is functionally expressed and targeted to mitochondria. Expression of b2-DHFR resulted in the expected mitochondrial precursor processing into intermediate and mature forms, consistent with previous observations in yeast (Boos et al., 2019). The predominant species was the precursor form, which became further stabilized upon addition of MTX indicating that enhanced folding of the DHFR domain causes pronounced stalling at the TOM complex. Interestingly, the detection of both intermediate and mature species raises the possibility that b2-DHFR-induced clogging may be partially permissive, allowing limited translocation, or that mitochondrial processing to the mature form can proceed while the precursor is stalled at the TOM complex. Mitochondrial processing of b2-DHFR requires translocation of the b2 presequence into the matrix **(chapter 1.2.5.2)** (Edwards et al., 2021). The distance between the OMM and IMM averages around 10-15 nm, with the shortest regions measuring approximately 5-6 nm. Considering that the b2 domain consists of 167 amino acids, and each amino acid contributes about 0.33-0.38 nm in length, the b2 domain could theoretically span the IMS and reach the matrix even while being arrested at the TOM complex. This interpretation is supported by observations reporting that the mature form of b2-DHFR can still associate with the TOM complex, although the corresponding data were labeled as “not shown” in that publication (Esaki et al., 1999). Collectively, these considerations make it plausible that b2-DHFR could physically bridge the outer and inner membranes, allowing partial translocation and processing while remaining arrested at the TOM channel.

4.1.1. Validation of effective mitochondrial clogging in human cells using b2-DHFR

The requirement of MTX to enhance mitochondrial clogging is, among other factors, based on the idea that detection of the mature form of b2-DHFR reflects a partially permissive form of clogging (Eilers & Schatz, 1986). Stabilization of the folded b2-DHFR precursor by MTX was therefore expected to increase the extent of mitochondrial import stalling. In line with the above-described hypothesis that b2-DHFR may be processed while remaining arrested at the TOM complex, a mitochondrial import assay in the presence and absence of MTX could clarify whether MTX enhances mitochondrial clogging. Initial import assays using purified mitochondria, however, did not yield evidence of import arrest by b2-DHFR. This led to the consideration that b2-DHFR might be released or lost during the mitochondrial isolation procedure, thereby diminishing the detectable clogging effect. To address this potential limitation, a new mitochondrial import reporter assay was developed, consisting of the MTS of b2 fused to a small flag-tag, which is unlikely to interfere with mitochondrial import.

As anticipated, the precursor form of b2-flag was almost absent under basal conditions, whereas expression of b2-DHFR led to a robust accumulation of the precursor, comparable to the effect observed after treatment with the mitochondrial uncoupler CCCP. Surprisingly, MTX addition did not further enhance precursor accumulation. This observation raises the question of whether MTX truly augments mitochondrial clogging or whether its impact remains below the detection threshold of the assay. One possibility is that the established reporter system lacks the sensitivity to resolve incremental differences upon MTX stabilization. However, an alternative and perhaps more compelling interpretation is that expression of b2-DHFR alone already causes near-complete clogging of the import machinery, a level comparable to that observed upon collapse of the membrane potential. This would align with the idea that b2-DHFR can be processed into its mature form even while remaining arrested at the TOM complex, as previously discussed.

4.1.2. b2-DHFR allows specific induction of mitochondrial import clogging without interference with mitophagy

As described above, the use of a *bona fide* mitochondrial clogger such as b2-DHFR eliminates the need to use mitochondrial uncouplers such as CCCP, which also induce mitophagy by collapsing Δψm (Xiao et al., 2017). Induction of mitophagy would lead to recruitment of autophagy factors and global mitochondrial ubiquitylation, thereby complicating the analysis of clogging-specific downstream events (Antico et al., 2021). To determine whether expression of the clogger b2-DHFR also triggers mitophagy, the established mitophagy markers p62 and

LC3B were analyzed. This analysis was additionally aimed at identifying the optimal conditions for inducing mitochondrial import clogging without concomitant activation of mitophagy. Treatment with 100 nM MTX for 5 h successfully stabilized precursor levels of b2-DHFR while leaving p62, LC3B, and TOM20 levels unchanged. p62 and LC3B represent markers downstream of PINK1 stabilization, as they are recruited to ubiquitinated mitochondria, for autophagosome membrane formation (S. Wang et al., 2023). Analysis of earlier mitophagy markers such as PINK1 stabilization or increased detection of phosphorylated ubiquitin (Ser65) would further clarify if b2-DHFR expression induces mitophagy. Notably, basal levels of mitophagy occur under unchallenged conditions which is important to clear malfunctioning mitochondria (Doblado et al., 2021). Hence, it could be possible that a certain amount of "pre-damaged" mitochondria could undergo mitophagy in the presence of b2-DHFR.

4.2. Analysis of the cellular response to the mitochondrial clogger b2-DHFR

Following the initial validation of the b2-DHFR clogger system and identification of optimal induction conditions that avoid mitophagy activation, the next objective was to investigate the cellular mechanisms responsible for recognizing and eliminating the stalled mitochondrial import clogger b2-DHFR.

4.2.1. Rapid degradation of the mitochondrial import clogger b2-DHFR

To first assess the turnover rate of the mitochondrial clogger, CHX chase experiments were performed to monitor b2-DHFR stability over time. Rapid degradation of the clogger b2-DHFR was visible in U2OS cells. Already 2 h after inhibition of the protein synthesis nearly no b2-DHFR was detectable by WB. In U2OS cells only 5% of all proteins exhibit a half-life below 8 h, while in non-dividing cells it was shown that mitochondrial proteins seem to be more stable than proteins belonging to other cell compartments (J. Li et al., 2021; Mathieson et al., 2018). This indicates that cells try to avoid mitochondrial clogging by rapid degradation of b2-DHFR. In the presence of MTX which enhances folding of the DHFR domain, b2-DHFR precursor levels were more stable during the CHX chase which may indicate that cells have more trouble to remove the stabilized form of the mitochondrial clogger. However, MTX increased b2-DHFR precursor abundance already prior to protein synthesis inhibition, which could simply reflect greater detectability during the CHX chase rather than impaired clearance of the stabilized clogger. Therefore, additional experiments would be required to determine whether cells encounter greater difficulty extracting the MTX-stabilized precursor or whether the observed persistence merely results from the elevated starting levels of the precursor species.

4.2.2. Proteasomal inhibition stabilizes ubiquitylation of b2-DHFR

Given the rapid turnover of the mitochondrial clogger b2-DHFR, the next experiments investigated the underlying cellular mechanisms responsible for this efficient clearance. Since ubiquitylation plays a central role in targeting proteins for proteasomal degradation, the involvement of ubiquitin signaling in b2-DHFR recognition and extraction was specifically examined **(chapter 1.5.3)**. Two complementary assays demonstrated robust ubiquitylation of the mitochondrial clogger b2-DHFR. Enrichment of b2-DHFR under denaturing conditions revealed strong ubiquitylation of the clogger specifically upon MTX-induced stabilization of the DHFR domain. Furthermore, VCP inhibition partially stabilized the b2-DHFR precursor levels and an increased ubiquitylation of the clogger was visible. By contrast, neither lysosomal inhibition with chloroquine and bafilomycin nor inhibition of the mitochondrial DUB USP30 increased the ubiquitin signal on b2-DHFR. VCP is a hexameric AAA+ ATPase that is involved among others in the removal of ubiquitinated proteins from membranes, protein complexes, chromatin and ribosomes (Kilgas & Ramadan, 2023; Suryo Rahmanto et al., 2023). Recently, it was shown that OMA1 removes stalled mitochondrial precursors and it was suggested that their degradation partially depends on VCP (Krakowczyk et al., 2024). In yeast, Cdc48 is recruited to stalled mitochondrial precursors by Ubx2 binding to ubiquitin (Mårtensson et al., 2019). This supports the idea that ubiquitylation of the clogger could similarly promote VCP-dependent proteasomal degradation in human cells and thereby account for the rapid b2-DHFR turnover observed in the CHX chase assay. While FAF2, the human orthologue of yeast Ubx2 was not enriched in the MS datasets, UBXN4 was enriched in the proximity of TOM20 during mitochondrial clogging. UBXN4 may be involved a potential recruitment of VCP to a clogged mitochondrial import channel **(Fig. 43)**. Several atypical ubiquitin linkages are linked to VCP-dependent extraction (Meyer & Rape, 2014; Shearer et al., 2022; Suryo Rahmanto et al., 2023), hence a potential modification of b2-DHFR and TOM20 with atypical ubiquitin linkages could be involved in a VCP and proteasome-dependent removal of the clogger, which will be discussed in the following section.

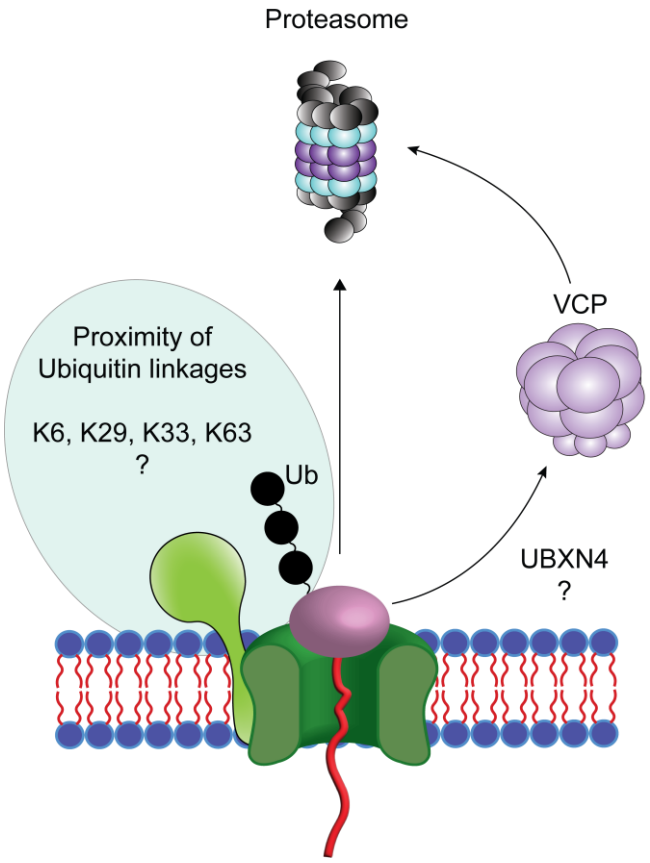

Figure 43 Hypothetical model for ubiquitin- and VCP-dependent extraction of b2-DHFR. While multiple atypical ubiquitin linkages were enriched in the proximity of the mitochondrial clogger, b2-DHFR ubiquitylation was stabilized upon VCP and proteasome inhibition. In addition, the VCP adaptor UBXN4 was enriched in the proximity of TOM20 during mitochondrial import clogging. Given that VCP-dependent extraction of mitochondrial precursors is already known in yeast and some of the identified atypical ubiquitin linkages, e.g. K6 and K29 are linked to VCP-dependent processes, this may indicate an interplay of atypical ubiquitin linkages leading to mitochondrial translocase clearance in a VCP-proteasome-dependent manner in human cells (Suryo Rahmanto et al., 2023; Y. Yu et al., 2021).

4.2.3. Atypical ubiquitylation during mitochondrial import stress

In order to analyze the ubiquitylation of the clogger b2-DHFR, a pull-down approach with K-to-R and lysine-less ^{his}Ub variants were performed. These ubiquitin variants can be attached to endogenous ubiquitylation sites and to endogenous ubiquitin and endogenous WT ubiquitin is still available for ubiquitylation. In addition, attachment of the ^{his}Ub variants cannot be further extended at the site of the replaced lysine(s). In particular, the $^{his}Ub^{K0}$ variant prevents further chain elongation of any lysine-based linkage, which might prevent build-up of degradative chains on b2-DHFR, resulting in their stabilization and hence leading to their detection via WB. While b2-DHFR was not enriched in the presence of $^{his}Ub^{K48R}$ or $hisUb^{K63R}$, expression of $^{his}Ub^{K0}$ showed ubiquitylation of b2-DHFR with multiple ubiquitin moieties. This was surprising because $^{his}Ub^{K0}$ cannot be further extended to a polyubiquitin chain on b2-DHFR. This suggests either multi-monoubiquitylation of b2-DHFR with $^{his}Ub^{K0}$ or the formation of an

endogenous ubiquitin chain which initially has no degradative nature and requires a certain length or further chain branching to become degradative. For instance, it was shown that K29- and K63-linked chains require chain-branching by K48-linked chains and thereby initiate proteasome-dependent degradation (Liu et al., 2017; Ohtake et al., 2018). Thus, capping of endogenous chains on the clogger with $^{his}Ub^{K0}$ could block the buildup of a degradative signal allowing its detection via WB. Notably, b2-DHFR was found neither in fractions of $^{his}Ub^{K48}$ nor $^{his}Ub^{K63}$, which suggests the formation of atypical ubiquitin chains beyond K48 or K63. However, it is still possible that a mix of these linkages can be present on the clogger.

In order to analyze the linkage specific ubiquitylation of the clogger b2-DHFR an alternative approach was used. Recently, my colleague Kirill Petriukov developed LinkageID, a method capable of detecting proteins in proximity to specific ubiquitin linkages. Notably, this technique only shows the close proximity to a specific linkage but cannot distinguish if a protein is ubiquitylated with that linkage. Initial experiments showed that the clogger b2-DHFR is detected in the linkages K6, K29 and K33. Both, K6- and K29-linked chains have been implicated in VCP-dependent processes such as RPC resolution and proteotoxic stress (Suryo Rahmanto et al., 2023; Y. Yu et al., 2021). This would match the idea of the VCP-dependent proteasomal degradation of the clogger **(Fig. 43)**.

Additionally, ubiquitin-based signaling as a sensor for mitochondrial clogging may also be established on proteins surrounding the arrested mitochondrial precursor such as subunits of the TOM complex. Therefore, ubiquitin linkages in the proximity of the TOM complex receptor TOM20 were investigated during mitochondrial clogging. In an initial experiment, TOM20 was predominantly enriched in the linkages K33 and K63, while also slightly increased in the K29 linkage. The overlap of the linkages K29 and K33 from both the clogger and the TOM receptor TOM20 may indicate that either TOM20 or b2-DHFR (or both) are ubiquitylated with those linkages and due to the close proximity at the TOM complex, both proteins are enriched in these fractions. Both K33- and K63-linked chains are known for their degradation independent function in signaling and protein trafficking (H. Huang et al., 2010; Liao et al., 2022). Finding that trafficking related linkages were enriched in the proximity of TOM20 could indicate an alternative hypothesis. These linkages could induce the formation of MDVs, an alternative MQC mechanism. A regulatory role of K6-linked chains in the context of MDVs would also be plausible since the mitochondrial DUB USP30 has a linkage preference for K6-linked ubiquitin chains and its activity seems to counteract MDV formation (König et al., 2021).

Furthermore, diGly motives of the linkages K6, K11; K48 and K63 were also enriched upon clogging in the initial HEK293T MS approach, which supports a role of K6- and K63-linked chains during mitochondrial import stress. Absence of K29- and K33-linked chains might be explained by their short diGly motives which makes them difficult to detect via MS. In

conclusion, this provides an insight into the cellular ubiquitylation upon mitochondrial import stress and suggests a role of atypical ubiquitin linkages in proximity of b2-DHFR and TOM20. Further experiments are required to elucidate which specific ubiquitin linkages are formed on b2-DHFR or whether and how TOM20 might be ubiquitylated. The pull-down of his-tagged b2-DHFR or TOM20 could be combined with a tool called UbiCRest assays that utilizes linkage specific DUBs to analyze the abundance of particular linkage (Hospenthal et al., 2015). K6-linked chains could be specifically tackled using the K6-specific DUB LotA (Warren et al., 2023). Additionally, MS-based analysis would enable comprehensive and quantitative linkage identification. The combination of both, quantitative MS with UbiCRest would not only provide insight into the quantity of each linkage but would also reveal potential branching architectures of these ubiquitin chains. In order to understand the underlying cellular signaling of these linkages one could use a Ubiquiton-based approach to induce the linkage formation on b2-DHFR. One could analyze which factors are recruited to the established linkage and investigate whether this affects removal of b2-DHFR from the TOM complex.

4.3. From Ubiquiton to MIQC: Tool development for inducible K6/K11 polyubiquitylation

As described above, the involvement of several atypical ubiquitin linkages in the MIQC is suggested. A broad palette of techniques is available to study atypical ubiquitylation. Most of these tools allow analysis of the linkage type but do not allow *de novo* synthesis of a specific ubiquitin linkage on a POI **(chapter 1.5.4)**. Recently the lab of Helle Ulrich has developed the Ubiquiton, a tool that enables inducible and linkage-specific ubiquitylation of virtually any tag-able POI in cells. So far, the Ubiquiton is limited to three ubiquitin linkages namely M1, K48 and K63. Therefore, the goal was to expand the Ubiquiton towards the atypical linkages K6 and K11, which were both enriched in one of the MS datasets upon mitochondrial clogging. While the K11-Ubiquiton candidate UBE2S showed a high linkage selectivity, the K6-candidate NleL showed activity in the presence of Ub^{K6R} and built free chains in the presence of the model substrate GFP. Interestingly, in the presence of the variant Ub^{K6R}, a change in the ubiquitylation pattern of NleL was visible which suggests formation of an alternative linkage-type. A possible explanation for the remaining ubiquitylation activity of NleL in the presence of Ub^{K6R} could be that NleL preferentially builds K6-linked chains but can alternatively also form other linkage-types. This is supported by findings that NleL prefers to form K6-linked chains which seem to be branched with K48-linked chains (Hospenthal et al., 2013; Valkevich et al., 2014). The tight dimerization system FRB-FKBP “glues” NleL to the substrate and thereby positions multiple lysines in close proximity to the catalytic center of NleL (Y.-C. Lin et al., 2013). An alternative reversible dimerization system with a higher off rate may be beneficial for a higher linkage

specificity of NleL. For instance, one could test a dimerization system based on the ligand rCD1 or a nanobody-based GFP directed system. Both are suggested to have a higher off-rate and/or reversibility compared to the Rapa based system (Farrants et al., 2020; Schifferer et al., 2017). Furthermore, several mutations and organism-specific codon optimizations were introduced into the protein encoding DNA sequences to enhance selectivity, processivity and expression. *In vitro*, mutant UBE2S$^{E139/143R}$ shows enhanced activity over the WT like mutant NleL^{E705A} which additionally exhibits decreased formation of free chains. Initial testing *in vivo* revealed activity of both enzymes in *S. cerevisiae* and both, the K6 candidate NleL and the previously established E3(63) were able to ubiquitylate a C-terminal truncation of TOM20 in human cells. Surprisingly, two ubiquitin antibodies had problems to detect the ubiquitin chains formed by NleL. It is well known, that some ubiquitin antibodies exhibit linkage-specific preferences (Emmerich & Cohen, 2015). Especially the K6 linkage seems to adopt a tight structure involving an interface of the patches I36 and I44, which are common binding motives and could explain the detection problems (Agrata & Komander, 2025). This is an important finding highlighting the importance of antibodies and techniques suitable for the detection of K6-linked chains regarding further analysis of the atypical linkages for the purpose of mitochondrial clogging.

Based on the literature, several ubiquitin linkages may be involved in the regulation of the MQC **(chapter 1.5.3)**. The ability to induce specific ubiquitin linkages would allow us to dissect the role of each linkage in more detail, especially in the absence of the actual stressor, e.g. mitochondrial import stress. This would enable an analysis without interference of multiple QC mechanisms at the same time.

4.4. Analysis of the interactome of the mitochondrial clogger and TOM20

Next, the focus of this work shifted to the cellular response to mitochondrial import clogging. Therefore, a proximity labeling system was designed that targets the interactome of both the mitochondrial import clogger itself and the OMM protein TOM20, a core subunit of the TOM complex. This represents the first analysis of the interactome of a mitochondrial import clogger and of the OMM under defined mitochondrial import stress. One recent study used a BioID fusion to nuclear excluded Hsp104 during mitochondrial import stress in *S. cerevisiae* but neither the clogging protein nor the OMM was tagged with the BioID (Kohler et al., 2024). In mammalian cells, several studies have characterized the OMM interactome by fusing biotin ligases to TOM20 or TOM70, yet these approaches were applied under unchallenged conditions and not during import stress (Akram et al., 2025; Cho et al., 2020; Meurant et al., 2023). Furthermore, it was demonstrated that the expression of a TOM20 fusion with APEX2 did not affect the overall mitochondrial function (Akram et al., 2025). Of important note for the

following sections is that enriched proteins represent the proximity of TOM20^{UID} or b2-DHFR^{UID}, but it cannot be concluded from the data if the expression of these proteins is altered during mitochondrial clogging. Furthermore, important identified proteins should be confirmed by WB to control false positive hits. In addition, mitochondria are known to form contact sites with other cell organelles such as the ER and the nucleus (Rieusset, 2018; Zervopoulos et al., 2022) and mitochondrial membrane sections can be removed from the mitochondria via MDVs during mitochondrial stress (Soubannier, Rippstein, et al., 2012). All this can contribute to the relocation of TOM20 under mitochondrial import stress and thus can alter its proximity.

4.4.1. Identification of new potential mitochondrial E3s and DUBs independently of mitochondrial import stress

To validate the mitochondrial interactome the dataset was first screened for known mitochondrial E3s and DUBs such as MARCH5, MUL1, and USP30. First the comparison of DHFR^{only}-P2A-TOM20^{UID} vs DHFR$^{only-UID}$ was performed. This comparison reflects the proximity of TOM20 without mitochondrial import clogging. All three known mitochondrial E3s/DUBs were highly enriched in the TOM20^{UID} fraction when compared to the cytoplasmic DHFR^{UID}. Surprisingly, multiple additional E3s and DUBs were enriched in the proximity of TOM20, among others the E3s MGRN1, TRIM4, PEX10/PEX12 and RBX1 and DUBs USP33, USP54, USP53, USP32, USP20. This shows that the MS dataset may be used not only to study ubiquitin-related proteins in the proximity of TOM20 as a marker for the OMM but also during unchallenged conditions.

4.4.2. Proximity labeling of b2-DHFR^{UID} and TOM20^{UID} reveals potential ubiquitin writers and erasers during mitochondrial clogging

4.4.2.1. Identification of ubiquitin writers in the initial MS approach in HEK293T cells

Several findings suggest a role of ubiquitylation, in particular with atypical ubiquitin linkages, during mitochondrial clogging. To investigate which ubiquitin writers and erasers may be involved in the establishment of this ubiquitin signal, the MS datasets were screened for E3s and DUBs during mitochondrial import stress. In the initial MS approach comparing b2-DHFR^{UID} and DHFR$^{only-UID}$ in HEK293T cells, the E3s PJA1, PJA2, RBX1, RNF135, OBI1 and STUB1 were upregulated. PJA1, PJA2 and OBI1 were both increased in b2-DHFR^{UID} when compared to the potential “weaker” mitochondrial clogger Su9-DHFR^{UID}.

PJA1 was recently shown to be linked to several neurodegenerative diseases such as Alzheimer's, Parkinson's and Huntington disease and further involved in synaptic integrity and vesicle trafficking (C. Li et al., 2025), which suggests a potential role of PJA1 in the MQC as these diseases and the synaptic integrity partially relies on mitochondrial function. Furthermore, there is direct evidence that PJA1 facilitates the degradation of the mitochondrial protein PGAM5 (S.-Y. Huang et al., 2024) This study also demonstrated interaction of PJA1 and PGAM5 with the mitochondrial fission factor DRP1. Additionally, it was shown that DRP1 phosphorylation, which regulates mitochondrial fission, was dependent on PJA1 and a knock down of PJA1 resulted in lower ATP levels, and increased production of mROS (S.-Y. Huang et al., 2024). It was shown that DRP1 activity is involved in the biogenesis of MDVs, which are thought to be involved in the MQC by recycling of mitochondrial membrane sections (König et al., 2021).

Mitochondrial evidence for PJA2 is limited to its expression in neuronal cells and its link to Alzheimer's disease (Gong et al., 2020; Lignitto et al., 2011). However, PJA2 was shown to form the atypical ubiquitin linkages K27, K29 and K33 on the HIV-1 protein Tat (Faust et al., 2017), which would match the linkages K29 and K33 that are in close proximity to the clogger b2-DHFR and TOM20 under mitochondrial import stress. Enrichment of PJA2 in the interactome of the mitochondrial clogger might indicate an involvement of PJA2 in the formation of these linkages.

Notably, PJA1 and PJA2 were in the downregulated fraction of the clogging-related comparisons in the optimized $TOM20^{UID}$-based approach in HeLa cells. This questions the function of both E3s in the MIQC. It could be that these inconsistencies rely on the different experimental setup. In the initial MS approach HEK293T cells were transiently transfected, which resulted in higher protein levels compared to the Flp-In integrated setup in HeLa cells. Different cell lines or expression levels of the mitochondrial clogger may lead to the usage of different cellular mechanisms. To clarify this discrepancy and the role of these two E3s in the MIQC further experiments are necessary. For example, the denaturing pull-down of b2-DHFR could be performed in the absence of PJA1 or PJA2 while monitoring the ubiquitylation status of the clogger. Furthermore, microscopy could be used to analyze if PJA1 or PJA2 are recruited to the mitochondrial membrane during import stress. For example, a proximity ligation assay could be suitable to analyze the recruitment of both E3s to the TOM complex or to the mitochondrial clogger. Furthermore, TOM20 dissociates from the TOM complex upon precursor delivery and thus might not be in the proximity of the clogged pore during the ubiquitylation process (Bhagawati et al., 2021). It was shown that TOM22 stably associates with the TOM complex and would be a suitable replacement for TOM20 in order to identify the ubiquitylation machinery of a clogged mitochondrial channel (Dekker et al., 1998).

4.4.2.2. Identification of ubiquitin writers and erasers in the optimized TOM20^{UID}-based MS approach in HeLa cells

While multiple E3s could be detected in the proximity of b2-DHFR in the initial MS approach in HEK293T cells, there was a discrepancy compared to the optimized approach with TOM20^{UID} in HeLa cells. For instance, in the optimized MS approach using the TOM20^{UID}-based proximity labeling approach in HeLa cells, PJA1 and PJA2 were decreased in the proximity of b2-DHFR^{UID} or TOM20^{UID} during mitochondrial clogging. However, additional E3s were identified in the optimized approach such as RBBP6, RNF216, TRIM4, MUL1, PEX10 and PEX12, MECOM and RBX1. The RING-type E3 RBBP6 was enriched in the proximity of b2-DHFR^{UID} in the absence and presence of MTX as well as in the proximity of TOM20^{UID} in the presence of MTX. RBBP6 mediates proteasomal degradation of YB-1, which is among other involved in translational repression and mRNA splicing (Chibi et al., 2008; Xie et al., 2025). So far, evidence of a mitochondrial role of RBBP6 is very limited and requires further investigation. In addition to RBBP6, peroxisomal E3s PEX10 and PEX12 were enriched in clogging-related fractions. Enrichment of these two peroxisomal E3s may indicate an alteration of the mitochondrial-peroxisomal crosstalk during mitochondrial clogging.

Furthermore, multiple DUBs were enriched in the proximity of b2-DHFR^{UID} or TOM20^{UID} during mitochondrial clogging, such as USP7, USP8, USP14, USP20, USP30, USP33 and USP36. Notably, the mitochondrial DUB USP30 was only enriched in the proximity of TOM20 during mitochondrial clogging but was strongly decreased in the comparison of b2-DHFR^{UID} with TOM20^{UID}. This may indicate an exclusive role of USP30 in the vicinity of TOM20 during import stress. However, it is also possible that USP30, a key DUB of the OMM is already highly abundant in the proximity of TOM20 which complicates a direct comparison with the mitochondrial clogger b2-DHFR.

By contrast, the DUB USP20 was enriched in several clogging-related conditions, especially in conditions comparing the clogger b2-DHFR^{UID} with the OMM marker TOM20^{UID}. Recently a link between the MQC and USP20 was demonstrated (Park et al., 2025). USP20 can interact with PARKIN1, stabilizes PARKIN1 protein levels and thus is involved in the regulation of mitophagy. Hence, it could be possible that USP20 might be involved in MQC mechanisms beyond mitophagy such as TOM complex clearance upon precursor arrest.

In conclusion, the MS dataset includes several potential candidates that mediate and regulate the ubiquitylation of the clogger b2-DHFR and its close vicinity. Further experiments are required to clarify their involvement in the MIQC. First, mitochondrial localization and the interaction of these proteins with b2-DHFR or TOM20 (during mitochondrial import stress), should be validated by microscopy and WB. Furthermore, the involvement of these candidates in the ubiquitylation of b2-DHFR or other OMM proteins during mitochondrial clogging should

be addressed. For instance, the ubiquitylation status of b2-DHFR or OMM proteins could be analyzed either using the denaturing pull-downs or LinkageID in the absence of these candidates.

4.4.2.3. Key mitochondrial proteins are enriched in the proximity of b2-DHFR

After the analysis of ubiquitin writers and erasers, the focus shifted to overall changes of proteins in the proximity of b2-DHFR^{UID} or TOM20^{UID}. GO-term enrichment analysis and STRING clustering of enriched proteins in the proximity of the mitochondrial clogger in comparison to TOM20^{UID} could reveal two major groups. Group one is enriched for proteins with key mitochondrial functions such as OXPHOS, mitochondrial organization glutamate metabolism and Fe-S cluster biogenesis while the second group of proteins are involved in the regulation of mitochondrial translation.

Enrichment of these key mitochondrial proteins in group one is consistent with a previous findings showing that mitochondrial stress in *C. elegans* leads to the upregulation of nuclear encoded OXPHOS genes, Fe-S cluster biogenesis factors that are essential for the maturation of OXPHOS complexes and enzymes of the glutamate metabolism (Braymer & Lill, 2017; Nargund et al., 2015). Mitochondrial import stress in *S. cerevisiae* also leads to an upregulation of factors of the TCA cycle, iron homeostasis and glutamate metabolism (Mishra et al., 2025). Those findings align with cluster one. Furthermore, MICOS subunits APOOL and IMMT were also upregulated in the proximity of the mitochondrial clogger. In a recent publication MICOS subunit MIC19 was found to be enriched in the pull-down fraction of a mitochondrial clogger in human cells (Krakowczyk et al., 2024). While MICOS is required for the cristae formation, MICOS is also involved in the regulation of OXPHOS and has a role in the mitochondrial protein import by interacting with the TOM complex (Horvath et al., 2015; Kondadi, Anand, Hänsch, et al., 2020; Kondadi, Anand, & Reichert, 2020). Additionally, glutamate is a anaplerotic substrate for the TCA cycle via conversion to α-ketoglutarate (D. Zhang et al., 2024). A recent publication also found that FXN a core component of the NIA machinery is upregulated in the cytoplasm of mouse cells upon expression of mitochondrial clogger mutant of Ant1 (Coyne et al., 2023). In the same publication it was shown that the mitochondrial glutamate dehydrogenase DHE3 and OAT which is required for the formation of L-glutamate are also upregulated upon mitochondrial clogging in human cells, which would be consistent with the glutamate metabolism-related cluster that was enriched in the proximity of b2-DHFR.

Notably, most of the proteins from group one localize in the IMS or in the mitochondrial matrix. This points towards the question of whether a subpopulation of b2-DHFR is successfully translocated through the TOM complex leading to the proximity and enrichment of proteins belonging to group one. Alternatively, as group one represents proteins highly demanded for key mitochondrial functions their import could be essential to ensure these functions during

mitochondrial import stress leading to their accumulation in the proximity of a clogged mitochondrial channel. Notably, not a single mitochondrially encoded protein was detected by b2-DHFR^{UID} despite the high sensitivity of our Orbitrap Astral mass spectrometer. Further experiments are necessary to confirm any increased abundance of proteins belonging to group one at the site of a clogged mitochondrial import channel. For instance, a proximity labeling approach based on TOM22, which does not dissociate from the TOM complex, in the presence of b2-DHFR would be suitable to investigate an enrichment of these key mitochondrial proteins.

The second detected cluster of proteins regulates mitochondrial translation. This cluster participates in the translation of mitochondrial encoded OXPHOS genes (Kremer & Rehling, 2024). Mitochondrial-encoded proteins form the catalytic cores of OXPHOS complexes, and their tight translational regulation is critical to coordinate complex assembly with nuclear-encoded OXPHOS subunits (Nargund et al., 2015). An enrichment of factors involved in regulating mitochondrial translation would be plausible, as mitochondrial import clogging prevents nuclear-encoded subunits from arriving inside the mitochondria for the complex assembly.

4.4.2.4. Analysis of the TOM20 interactome during mitochondrial import stress

While b2-DHFR^{UID} is suitable to detect proteins in the proximity of the mitochondrial clogger, the optimized approach based on TOM20^{UID} allows the analysis of changes in proximity of the TOM complex. Additionally, due to the ability of TOM20^{UID} to dissociate from the TOM complex, it enables enrichment of proteins at the OMM more distant from the site of clogging.

Analysis of proteins enriched in the proximity of TOM20^{UID} during mitochondrial import clogging showed an enrichment of NDUFA6, an OXPHOS subunit (Complex I) and OXPHOS-related proteins. For instance, ACAD9 is an assembly factor for the respiratory chain complex I (Schiff et al., 2015) and other proteins involved in the fatty acid metabolism were enriched. The fatty acid metabolism provides electron donors for OXPHOS and its deficiency negatively affects OXPHOS and *vice versa* (Nsiah-Sefaa & McKenzie, 2016). The enrichment of factors involved in the fatty acid metabolism are consistent with findings that expression of the clogger mutant of ANT1 resulted in the cytoplasmic upregulation of fatty acid-related factors THIM and THIL that facilitate fatty acid β-oxidation (Coyne et al., 2023). It was shown that cells compensate mild OXPHOS deficiency by fatty acid metabolism (Timper et al., 2018). This suggests that proteins in the proximity of TOM20 during mitochondrial clogging may reflect a compensation for mitochondrial OXPHOS deprivation which is in line with proteins enriched in the proximity of b2-DHFR^{UID}. Additionally, upon expression of b2-DHFR, a strong enrichment for RNA binding proteins (RBPs) found in the nuclear speckle is visible in the proximity of TOM20^{UID}. Notably, some RBPs were detected in TOM20^{UID} with and without mitochondrial clogging which is in common with a previous study showing an enrichment of RBPs in the proximity of TOM20

under unchallenged conditions (Akram et al., 2024; Meurant et al., 2023). However, upon expression of b2-DHFR, a strong shift towards RNA splicing factors enriched in the nuclear speckle was visible. Master regulators and scaffolds of the nuclear speckle such as SON, SRRM2 were present (Ilik et al., 2020). It was previously shown that ribotoxicity leads to a reorganization of the nuclear speckle and recruitment of splicing factors (Sung et al., 2023). Publications in *S. cerevisiae* and *C. elegans* report splicing as a regulator of stress (Parenteau et al., 2025; Xia et al., 2022). In particular it was shown that mitochondrial stress leads to splicing-dependent activation of the mitochondrial UPR in *C. elegans* (Xia et al., 2022). Together this may suggest a regulatory role of these RBPs in proximity of TOM20 upon expression of b2-DHFR to overcome the induced mitochondrial import stress.

In conclusion, enriched proteins in the proximity of TOM20 under mitochondrial import stress seem to define a mitochondrial-nuclear stress module. Several proteins involved in mitochondrial metabolism, especially in OXPHOS and fatty acid metabolism are represented. Furthermore, a group of splicing related nuclear speckle proteins is enriched which may suggest re-wiring of transcription and RNA processing upon mitochondrial import stress **(Fig. 44)**.

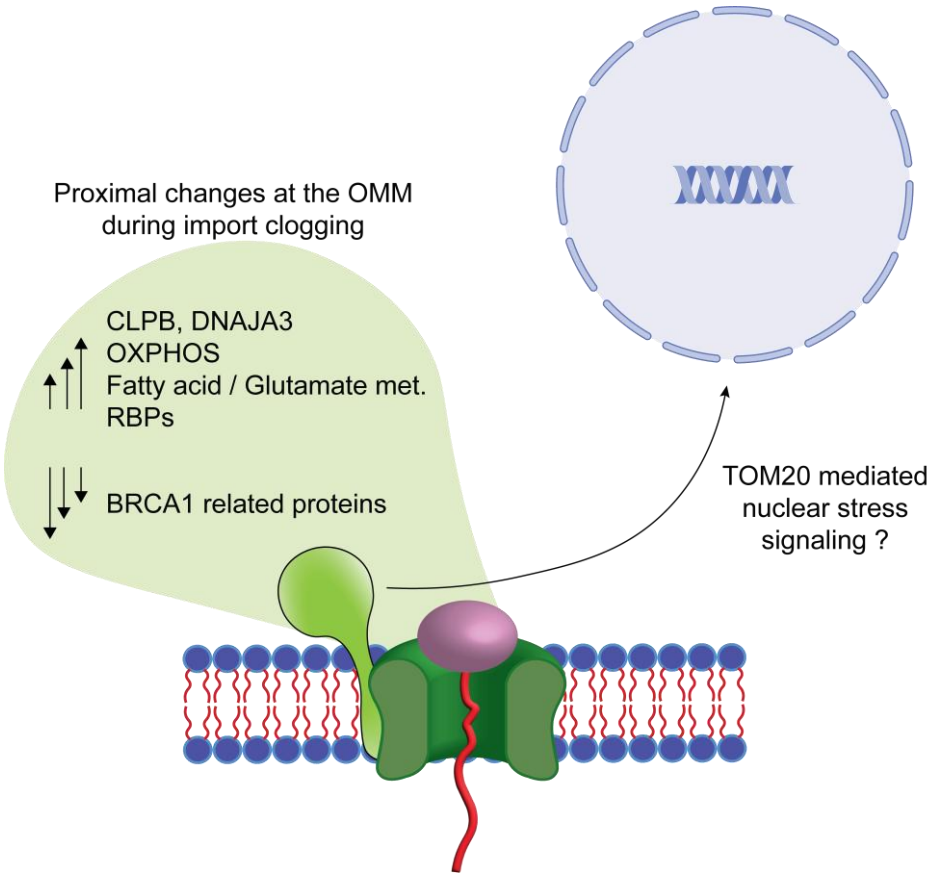

Figure 44 Alterations in the proximity of a clogged mitochondrial import channel. Key mitochondrial proteins involved in OXPHOS, fatty acid and glutamate metabolism were enriched in proximity to the OMM, potentially reflecting the cellular demand for these central mitochondrial processes. Additionally, a cluster of nuclear speckle RBPs was enriched and a BRCA1-centered cluster of proteins was depleted in the proximity of TOM20 which may reflect mito-nuclear stress signaling mediated by TOM20. Proteins CLPB and DNAJA3 act as connecting nodes between the metabolic and RBP-related clusters potentially highlighting their role in the mitochondrial homeostasis during import clogging.

4.4.2.5. CLPB, DNAJA3, NDUFA6 and TIM44 as central nodes linking mitochondrial import stress to OXPHOS and MQC

Interestingly, four proteins, CLPB, DNAJA3, NDUA6 and TIM44 seem to connect the identified protein clusters in proximity to b2-DHFR and TOM20 during mitochondrial clogging.

NDUA6, a critical subunit of the respiratory chain complex aligns well with the observed increase of OXPOHS-related proteins during mitochondrial clogging (Angerer et al., 2014). Interestingly, NDUA6 was among a small group of OXPHOS subunits that were selectively affected by reduced mitochondrial fatty acid synthesis, which may be explained by its interaction with acetylated ACP, whose modification state depends on faffy acid availability (Nowinski et al., 2020). Thus, NDUFA6 could represent a “bridging factor” between the two clusters of OXPHOS- and fatty acid metabolism-related proteins. Notably, in the STRING network NDUFA6 also emerged as a connecting node to a cluster of RBPs via the splicing factor SRSF6.

By contrast, CLPB, DNAJA3 and TIM44 can directly be linked to MQC and mitochondrial protein import defects. TIM44 is a core scaffold and regulator for the recruitment of the TIM23-associated import motor, and inhibition of TIM44 causes mitochondrial import defects (Hutu et al., 2008). Most nuclear-encoded OXPHOS subunits rely on $TIM23^{PAM}$-dependent import into mitochondria (Tang et al., 2020). Furthermore, OXPHOS is the main driver of the proton motive force that is required for the establishment of Δψm (Zorova et al., 2018). Thus, increased proximity of TIM44 to a clogged mitochondrial import channel could reflect an adaptive cellular response to overcome mitochondrial import defects at the OMM to maintain OXPHOS and Δψm.

DNAJA3 is a mitochondrial HSP40-family co-chaperone, required for maintenance of mitochondrial protein homeostasis, folding and translocation across mitochondrial membranes and is linked to cell survival, proliferation and regulation of apoptosis (Felipe Perez et al., 2024; Sayson et al., 2024). Genetic loss of DNAJA3 in mice leads to mitochondrial dysfunctions including impaired Δψm and reduced OXPHOS complex levels (Sayson et al., 2024). Furthermore, DNAJA3 is involved in the DRP1-dependent mitochondrial fragmentation (Elwi

et al., 2012). Together with these functions, an increased abundance of DNAJA3 in the proximity of clogged mitochondrial import channels may represent an elevated demand for this MQC factor during mitochondrial import clogging.

The mitochondrial disaggregase CLPB was the most consistently upregulated hit in the optimized TOM20-based UID approach. It was upregulated in all clogging-related conditions (-/+ MTX) and was also identified as upregulated in the initial MS approach in HEK293T cells. CLPB is linked to several mitochondria-related diseases, including congenital neutropenia, developmental delay/intellectual disability and progressive brain atrophy, and CLPB activity led to increased solubility of Parkinson's diseases-related α-synuclein (Cupo & Shorter, 2020; Heath et al., 2026). Loss of CLPB in human cells resulted in decreased solubility of multiple mitochondrial proteins including OXPHOS components (Cupo & Shorter, 2020). Although a direct role of CLPB in the mitochondrial protein import has not been demonstrated, a potential function has been suggested based on its close evolutionary relationship to yeast Hsp78 which is linked to mitochondrial protein import (Cupo & Shorter, 2020). Given that CLPB was consistently upregulated in proximity to b2-DHFR and TOM20 during mitochondrial import stress, it would be important to further investigate its role in mitochondrial protein import.

Together, NDUA6, CLPB, DNAJA3 and TIM44 were identified as central nodes that connect b2-DHFR/TOM20-proximal protein clusters related to OXPHOS, fatty acid metabolism and mitochondrial quality control during import clogging. NDUA6 may function as a metabolic "bridge" between OXPHOS, fatty acid metabolism and RBPs, whereas TIM44, DNAJA3 and CLPB point to an adaptive MQC response that aims to sustain mitochondrial protein import, respiratory chain function and Δψm under mitochondrial import stress.

So far, these proteins have been identified in proximity of b2-DHFR and TOM20 during mitochondrial import stress and further analysis is required to dissect their specific function during import stress. Initial experiments could investigate if the expression of these proteins is also upregulated during mitochondrial import stress. Therefore, one could analyze transcriptional changes by RT-qPCR and total protein levels via WB and MS. As a follow-up one could investigate if loss of these factors would contribute to the severity of mitochondrial import defects in human cells.

4.4.2.6. BRCA1 is decreased in proximity to TOM20 during mitochondrial import stress

A large portion of proteins decreased in the proximity of $TOM20^{UID}$ during mitochondrial import stress can be grouped in a cluster associated with DNA repair. Many of these proteins were clustered around BRCA1. BRCA1 is a well-established nuclear tumor suppressor renowned for homologous recombination-mediated DNA repair, yet multiple studies also demonstrate its

localization to mitochondria. (Coene et al., 2005; Maniccia et al., 2009). BRCA1 seems to be involved in the regulation of mitochondrial fusion/fission and mitophagy (Q. Chen et al., 2020), and it was previously shown that mitochondrial damage leads to PINK1-dependent degradation of BRCA1 (Miyahara et al., 2021). Here it was shown that PINK1 can localize inside the nucleus, suggesting nuclear degradation of BRCA1. In unchallenged conditions, PINK1 is translocated through the TOM complex into the mitochondria (Matsuda et al., 2010), and nuclear PINK1 accumulation was enhanced upon mitochondrial uncoupling induced by CCCP (Miyahara et al., 2021). Mitochondrial uncoupling collapses ΔΨm and thereby stalls mitochondrial protein import (Bogorodskiy et al., 2021). A hypothesis to explain the decreased abundance of BRCA1 in proximity of TOM20 would be that mitochondrial import clogging prevents the translocation of PINK1 into the mitochondria. This could lead to accumulation of PINK1 in the cytoplasm and nucleus leading to the degradation of BRCA1 and reduced proximity labeling by $TOM20^{UID}$. However, further experiments are required to validate this idea. Total BRCA1 levels during mitochondrial import stress could be analyzed by WB. Investigations of PINK1 accumulation in the cytoplasm and nucleus during expression of b2-DHFR by microscopy and proximity of PINK1 to BRCA1 could be analyzed by proximity labeling strategies.

In summary a remodeling of proteins in the proximity of TOM20 during mitochondrial import stress that describes the downregulation of DNA maintenance factors that align around the tumor suppressor BRCA1. Previous studies have described regulatory roles of BRCA1 in mitochondrial dynamics and quality control which may suggest that the decrease in BRCA1 in proximity of the OMM marker TOM20 could reflect the involvement of BRCA1 in a stress response to mitochondrial import clogging.

4.4.3. Potential re-localization of TOM20 during mitochondrial import stress

Surprisingly, many nuclear proteins were enriched by $TOM20^{UID}$ with and without mitochondrial import stress. Upon mitochondrial clogging, a cluster of splicing-related nuclear speckle proteins was enriched in the proximity of TOM20. This suggests either that these nuclear speckle proteins enrich at the OMM or that TOM20 relocates to the nucleus or its periphery. Previously it was shown that several mitochondrial proteins, e.g. TCA cycle factors can localize to the nucleus and roles in the DNA repair and epigenetic regulation are suggested (W. Li et al., 2022; Tang, 2015; Wang et al., 2017). In addition, it was shown that the nucleus serves as a compartment for the degradation of non-imported mitochondrial precursor proteins (Shakya et al., 2021). Recent publications demonstrated Tom70 mediated mitochondrial-nuclear contact sites in *S. cerevisiae* (Eisenberg-Bord et al., 2021; Ruediger et al., 2025). Further, in-depth analysis of mitochondrial complexes in *S. cerevisiae* shows that the nuclear transcription

factor Gis1 forms a complex with Tom20, Tom22, Tom40 and Hsp60 (Schulte et al., 2023). In combination with the data of enriched nuclear speckle proteins with these findings, one could hypothesize a role of TOM20 either in mitochondrial-nuclear contact sites or inside the nucleus. TOM20 as one of the major mitochondrial import receptors could function as a nuclear sensor for mitochondrial import stress **(Fig. 44)**. Nevertheless, these ideas need further careful validation. For example, one could investigate the localization of TOM20 during mitochondrial import stress by microscopy. As a potential nuclear localization of TOM20 might be a rather rare event, one could perform subcellular fractionation and investigate the presence of TOM20 in the nuclear fraction by WB. This could be analyzed in the absence and presence of b2-DHFR which would give an insight into whether mitochondrial import stress alters the localization of TOM20.

4.5. Future perspectives

4.5.1. Linkage specific ubiquitylation of b2-DHFR

The observation that the mitochondrial clogger b2-DHFR is ubiquitylated, together with evidence for atypical ubiquitin linkages in the vicinity of b2-DHFR and TOM20, raises several central questions: (i) which ubiquitin writer(s) establish the ubiquitin signal on b2-DHFR, (ii) which linkage type(s) are formed on b2-DHFR, and (iii) which ubiquitin readers decode this signal and mediate MIQC.

To address the first question, the E3s identified in proximity to b2-DHFR or TOM20 during mitochondrial clogging represent promising candidates and could be investigated. Analysis of the ubiquitylation status of b2-DHFR in the absence of these E3s would clarify whether they contribute to establishing the ubiquitin signal on the clogger. However, because TOM20 can dissociate from the TOM complex, TOM20-based proximity labeling may not be optimal to capture E3s acting at a clogged TOM channel. UID tagging of TOM22, which constitutively associates with the TOM complex, could provide a more stable detection of E3s that target b2-DHFR at the TOM complex.

To define the linkage architecture on b2-DHFR, denaturing pull-downs of b2-DHFR under conditions of proteasome and/or VCP inhibition could be subjected to a UbiCRest assay in combination with MS analysis (Hospenthal et al., 2015). A combination of both methods would give insight into the quantity of a given linkages while simultaneously resolving heterotypic chain architectures.

Once the linkage type(s) on b2-DHFR are clarified, one could continue to identify readers of that linkage. A repeat of the LinkageID approach using the relevant linkage(s) in the presence and absence of b2-DHFR, followed by MS, could reveal proteins that preferentially bind these

chains. If the identified linkage(s) can be induced by the Ubiquiton system, combining the Ubiquiton with a UID-based proximity labeling strategy would be particularly useful. This would enable the controlled establishment of the respective linkage on b2-DHFR, followed by an unbiased identification of proteins that accumulate in the proximity polyubiquitylated b2-DHFR.

4.5.2. The role of VCP in the removal of stalled mitochondrial precursors

So far inhibition of VCP and the proteasome led to increased ubiquitylation of b2-DHFR and stabilized precursor levels, supporting a model in which VCP extracts stalled precursors from the TOM complex for proteasomal degradation. To directly probe the involvement of VCP at the mitochondrial surface, VCP recruitment to mitochondria during import stress could be assessed using PLA and IF co-staining for VCP with b2-DHFR and/or TOM20. Such experiments would reveal whether VCP physically engages clogged TOM complexes. In addition it would be important to clarify whether VCP would act broadly on other mitochondrial cloggers, for instance a physiologically relevant mutant form of the mitochondrial carrier ANT1 could be tested (Coyne et al., 2023). Given that the VCP adaptor UBXN4 was already detected near TOM20 under mitochondrial import stress, it will also be important to test whether UBXN4 depletion stabilizes b2-DHFR, thus functionally linking UBXN4 to a VCP-dependent extraction.

4.5.3. Validation of TOM20^{UID}-based proximity labeling

The TOM20^{UID}-based proximity labeling experiments revealed enrichment of several functional protein groups, including factors involved in OXPHOS, fatty acid metabolism, and glutamate metabolism, whereas a BRCA1-centered protein cluster was depleted in proximity of TOM20 during mitochondrial import clogging. However, proximity labeling alone cannot distinguish between changes in total protein abundance and changes in spatial redistribution toward or away from the TOM complex or the OMM. To address this limitation, it will be important to quantify total protein levels of selected candidates during mitochondrial import stress. It will be informative to determine whether BRCA1 levels decrease specifically in the proximity of TOM20 during mitochondrial clogging, or whether global BRCA1 abundance is also affected. BRCA1 is a key tumor suppressor implicated in the development of breast and ovarian cancers, and evidence that mitochondrial import stress perturbs global BRCA1 levels would therefore be of considerable medical relevance (Stefansson & Esteller, 2012).

Furthermore, it would be interesting to investigate the function of the node-connecting proteins CLPB, DNAJA3, NDU6 and TIM44 during mitochondrial import clogging **(chapter 4.4.2.5**). In particular it would be interesting to investigate the proposed role of the consistently identified hit CLPB during mitochondrial protein import. (Cupo & Shorter, 2020).

4.5.4. Localization of TOM20 during mitochondrial clogging

A surprising outcome of the TOM20^{UID} experiments was the enrichment of nuclear speckle proteins in the vicinity of TOM20 during mitochondrial import stress. This raises the question of where these proteins encounter TOM20. One possibility is that nuclear speckle proteins become enriched at the OMM; alternatively, mitochondrial import stress may enhance contacts at the mito-nuclear interface, or a fraction of TOM20 may even re-localize to the nucleus. To monitor the spatial fate of TOM20 and its proximal environment over time, cells expressing the b2-DHFR-P2A-TOM20^{UID} construct could be pulse-labeled with biotin, followed by imaging of the biotin signal. After removal of biotin, the redistribution of labeled TOM20 and labeled proteins in its proximity could be tracked to determine whether a biotin signal appears in the nucleus. At the same time, subcellular fractionation followed by immunoblotting for TOM20 in nuclear and mitochondrial fractions would provide a biochemical readout of a potential nuclear re-localization of TOM20. Comparing TOM20 distribution in the presence and absence of b2-DHFR would reveal whether mitochondrial import stress actively drives TOM20 into nuclear compartments, potentially linking TOM20 dynamics to mito-nuclear communication and stress signaling.

5 Appendix

5.1. Abbreviations

µm	Micrometer
µM	Micromolar
Å	Ångström
aa	Amino acid
adj. P. Val.	Adjusted P-Values (Limma)
ADP	Adenosine diphosphate
AGE	Agarose gel electrophoresis
ANT1	ADP/ATP translocase 1
APC	Anaphase-promoting complex
ATAD1	ATPase family AAA domain-containing protein 1
ATF	Activating transcription factor
ATP	Adenosine triphosphate
b2	MTS of cytochrome b2
b2-DHFR	Mitochondrial model clogger, Fusion of b2 with DHFR
BAK	Bcl-2 homologous antagonist/Killer
BAX	Bcl-2-associated X
BCL1	B-cell lymphoma 1
BNIP3	Bcl1-Interacting Protein 3
BRCA1	Breast Cancer Type 1 Susceptibility Protein
C°	Degrees Celsius
Ca	Calcium
CCCP	Carbonyl Cyanide M-Chlorophenyl Hydrazone
Cdc48	Cell Division Control Protein 48
CF	Core Facility
cGAS	Cyclic GMP-AMP Synthase
CHCHD	Coiled-Coil-Helix-Coiled-Coil-Helix Domain-containing protein
CHOP	C/Ebp homologous protein
CHX	Cycloheximide
CLPB	Caseinolytic peptidase B

Appendix

CoA	Coenzyme A
C-terminus	Carboxy terminus
CUb	C-terminal half of ubiquitin
CUbo	FKBP-Cub
CUE	Coupling of ubiquitin conjugation to ER degradation
Cue1	Cue-domain-containing Protein 1
CV	Column Volumes
DDA	Data-dependent acquisition
DDR	DNA damage response
DELE1	Dap3-Binding cell death enhancer 1
DFCP1	Double Fyve-domain-containing protein 1
DHFR	Dihydrofolate reductase
DJ-I	Parkinsonism-associated deglycase
DMEM	Dulbecco'S Modified Eagle Medium
DMSO	Dimethyl sulfoxide
DNA	Deoxyribonucleic acid
DnaJ	Prototypical J-Domain Protein
DNM1L	Dynamin-1-like protein 1
Doa10	Ubiquitin ligase Doa10
DOX	Doxycycline
DPBS	Dulbecco's Phosphate-Buffered Saline
Dsk2	Ubiquitin domain-containing protein Dsk2
DTT	Dithiothreitol
DUB	Deubiquitylating enzyme
E1	Ubiquitin activating enzyme
E2	Ubiquitin conjugating enzymes
E3	Ubiquitin ligase
E3(1)	Ubiquiton E3 specific for M1-linked chains
E3(48)	Ubiquiton E3 specific for K48-linked chains
E3(63)	Ubiquiton E3 specific for K63-linked chains
EGFR	Epidermal growth factor receptor
EHEC	Enterohemorrhagic Escherichia Coli
eIF2α	Eukaryotic translation initiation factor 2

EMT	Epithelial mesenchymal transition
ER	Endoplasmic Reticulum
Erv1	ER-vacuole protein 1
FAD	Flavin adenine dinucleotide
FAF2	Fas-associated factor family member 2
FAO	Fatty acid oxidation
FBS	Fetal bovine serum
FCCP	Carbonyl cyanide-P-trifluoromethoxy phenylhydrazone
FDR	False discovery rate
Fe-S	Iron Sulfur
FKBP	FK506-binding protein
flag	Flag epitope tag
FRB	FKBP-Rapamycin binding protein
FUNDC1	Fun14 domain-containing protein
GA	Gibson assembly
GFP	Green fluorescent protein
GO	Gene ontology
h	Hour
H3K9me3	Trimethylation of lysine 9 on histone H3
HACE1	Hect domain and ankyrin repeat containing E3
HBD	Heme binding domain
HCD	Higher energy collision dissociation
HCl	Hydrochloric dcid
HECT	Homologous to E6-Ap carboxy terminus
his	Polyhistidine tag
HOIL-1L	Haem-oxidized Irp2 E3 1-like
HOIP	Hoil-1-interacting protein
HRI	Heme-regulated Eif2A kinase
Hsf1	Heat shock factor 1
HSP	Heat shock protein
HTRA2	High-temperature requirement protein A2
HTS	Hydrophobic transmembrane segment
HUWE1	HECT, UBA and WWE domain containing E3 1

Appendix

Icp55	Intermediate cleaving peptidase 55
IEX	Ion exchange
IF	Immunofluorescence
IFNβ	Interferon beta
IMM	Inner mitochondrial membrane
IMMP2L	IMM peptidase subunit 2-like
Imp	IMM peptidase
IMS	Mitochondrial intermembrane space
IRF3	Interferon regulatory factor 3
J-proteins	Dnaj-related cochaperones
K	Lysine
KO	Knockout
LB	Luria broth
LC3	Microtubule associated protein 1 light chain 3
LFQ	Label-free protein quantification
Log2FC	log2 fold change
LotA	Legionella outer membrane protein A
LUBAC	Linear ubiquitin chain assembly complex
M	Molar
M1	Met1-linked
MARCH5	Membrane associated ring-CH-type finger 5
MAVS	Mitochondrial antiviral-signaling protein
MCU	IMM Calcium uniporter complex
MDA5	Melanoma differentiation-associated protein 5
MDCs	Mitochondrial-derived compartments
MDVs	Mitochondrial-derived vesicles
MEF	Mitochondrial enrichment factor
MET4	Met4 transcription factor
MFF	Mitochondrial fission factor
MFN	Mitofusin
Mge1	Mitochondrial Grpe protein 1
MIA	Mitochondrial intermembrane space Assembly
MICOS	Mitochondrial contact site and cristae organizing system

MIM	IMS import machinery
min	Minute
MIP	Mitochondrial intermediate peptidases
MIQC	Mitochondrial import quality control
MIRO	Mitochondrial Rho GTPase
mitoCPR	Mitochondrial compromised protein import response
mitoNUC	Nuclear-associated mitoprotein degradation
mitoTAD	Mitochondrial protein translocation-associated degradation
mM	Millimolar
MPP	Mitochondrial processing peptidase
MQC	Mitochondrial quality control
mRNA	Messenger RNA
MS	Mass spectrometry
Msp1	Protein-degrading AAA Family ATPase Msp1
mtDNA	Mitochondrial DNA
MTS	Mitochondrial targeting sequences
mtUPR	Mitochondrial unfolded protein response
MTX	Methotrexate
MWCO	Molecular weight cut-off
myc	Myc epitope tag
NAD+	Nicotinamide adenine dinucleotide
NBR1	Neighbor of BRCA1 gene 1
NDP52	Nuclear dot protein 52 kDa
NEM	N-Ethylmaleimide
NEMO	NF-κB Essential Modulator
NF-κB	Nuclear factor kappa-light-chain-Enhancer of activated B-cells
NIX	Nip-3-like protein X
nm	Nanometer
NMR	Nuclear magnetic resonance
Npl4	Nuclear protein localization protein 4
N-terminus	Amino terminus
NUa	NUb^{I13A}
NUb	N-terminal half of ubiquitin

Appendix

NUbo	NUa-HA-FRB
Oct1	Metalloendopeptidase
OD	Optical density
OMA1	Oma1 zinc metallopeptidase
OMM	Outer mitochondrial membrane
OPTN	Optineurin
OXPHOS	Oxidative phosphorylation
p62	Sequestosome 1
PAM	Presequence translocase-associated motor
PARKIN	Parkin RBR E3
PARL	Presenilin-associated rhomboid-like protease
PBS	Phosphate-buffered saline
PCNA	Proliferating cell nuclear antigen
PCR	Polymerase chain reaction
PEI	Polyethyleneimine
pH	Power of hydrogen
PHB2	Prohibitin 2
PINK1	Pten Induced Kinase 1
PIP	PCNA-Interacting peptide
POI	Protein of interest
Pth2	Parathyroid hormone 2
R	Arginine
RAF	Rapidly accelerated fibrosarcoma kinase
Rapa	Rapamycin
RAS	Rat sarcoma family small GTPase
RBP	RNA-binding protein
RBR	RING in between RING
RIG-I	RNA sensor RIG-I
RING	Really Interesting New Gene
RNA	Ribonucleic acid
RNF	Ring finger protein
ROS	Reactive oxygen species
RPC	RNA-protein crosslinks

Rpn4	Stress-regulated transcription factor Rpn4
rRNA	Ribosomal RNA
Rsp5	NEDD4 family E3
RT	Room temperature
RT-qPCR	Reverse transcription quantitative polymerase chain reaction
SAM	Sorting and assembly machinery
SARS-CoV-2	Severe acute respiratory syndrome coronavirus 2
SDS-PAGE	Sodium dodecyl sulfate-polyacrylamide gel electrophoresis
SEC	Size exclusion chromatography
SLC	Solute carrier
SPOTs	Structures positive for OMM
SRSF6	Serine- and arginine-rich splicing factor 6
Sti1	Chaperone activator Sti1
STING	Stimulator of interferon genes
TB	Terrific broth
TBE	Tris-Borate-EDTA buffer
TBK1	TANK binding kinase 1
TCA	Tricarboxylic acid
TCA	Trichloroacetic acid
TIM	Translocase of the IMM
TLR	Toll-Like receptor
TMD	Transmembrane domain
TNF	Tumor necrosis factor
TOM	Translocase of the OMM
TRAF6	TNF receptor associated factor 6
TRIP12	Thyroid hormone receptor interactor 12
tRNA	Transfer RNA
Ub	Ubiquitin
UBA	Ubiquitin-activating enzyme
Ubc	Ubiquitin-conjugating enzyme
UBD	Ubiquitin-binding domain
Ubl	Ubiquitin-like
UBR	UBR-box E3

UBX	Ubiquitin regulatory X domain
Ubx2	UBX domain-containing protein 2
UFD	Ubiquitin fusion degradation
UID	UltraID
UIM	Ubiquitin-interacting motif
ULK1	Unc-51-like kinase 1
UPR	Unfolded protein response
UPS	Ubiquitin-proteasome system
USP	Ubiquitin-specific protease
UV	Ultraviolet
VCP	Valosin-containing protein
VDAC	Voltage-dependent anion channel
VIPERIN	Virus inhibitory protein
WB	Western blot(ting)
WCL	Whole-cell lysates
WIPI1	WD repeat domain phosphoinositide-interacting protein 1
WT	Wild-type
YME1L1	Yeast mitochondrial escape 1-like 1
Δψm	Mitochondrial membrane potential

5.2. Supplementary data

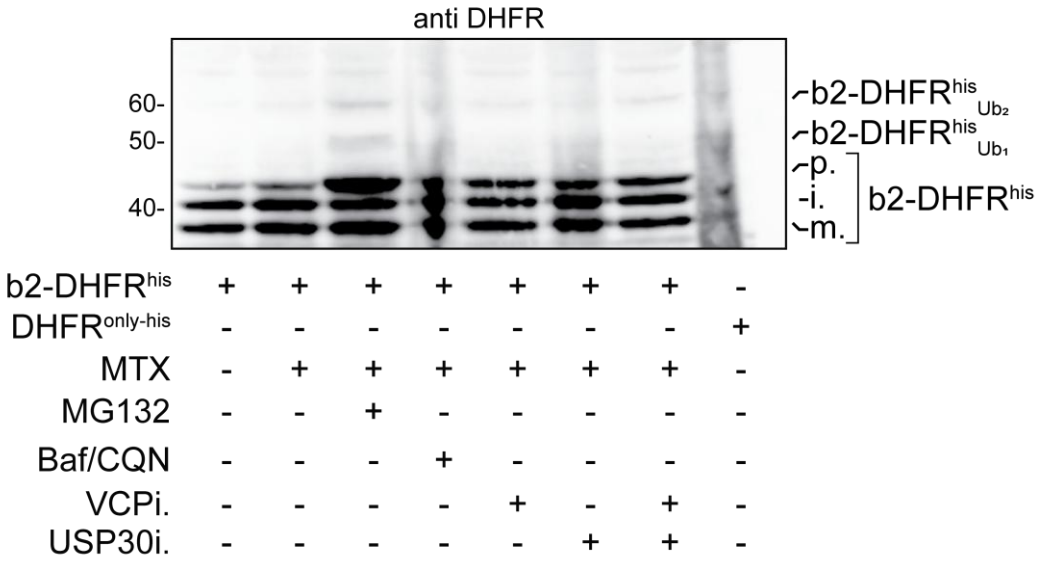

Appendix 1 Enhanced exposure of whole-cell lysates from Fig. 19. HEK293T cells after transient transfection of b2-DHFR^{his} and DHFR$^{only-his}$; 24 h post transfection, cells were treated for 5 h with 100 nM MTX followed by 2 h of treatment with the indicated inhibitors (proteasome inhibitor MG132, 30 µM; VCP inhibitor NMS-873, 5 µM; lysosomal inhibitors chloroquine, 10 µM + bafilomycin, 100 nM; USP30 inhibitor CMPD, 200 nM).

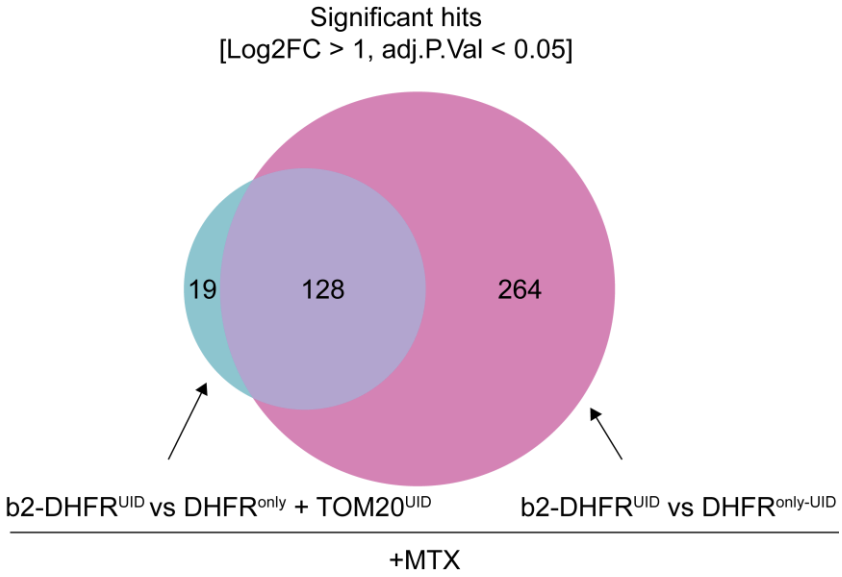

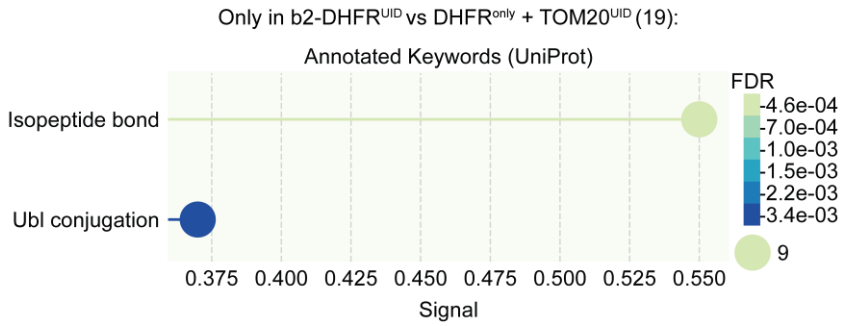

Appendix 2 GO term analysis of proteins exclusively upregulated in b2-DHFR^{UID} vs DHFR^{only}-P2A-TOM20^{UID}. Venn diagram related to **Fig. 30** comparing significant upregulated proteins (Log2FC > 1); GO-term enrichment analysis of annotated keywords was performed using STRING database; signal is a combined score that balances enrichment strength and statistical confidence by integrating Log10(observed / expected) and -log(FDR).

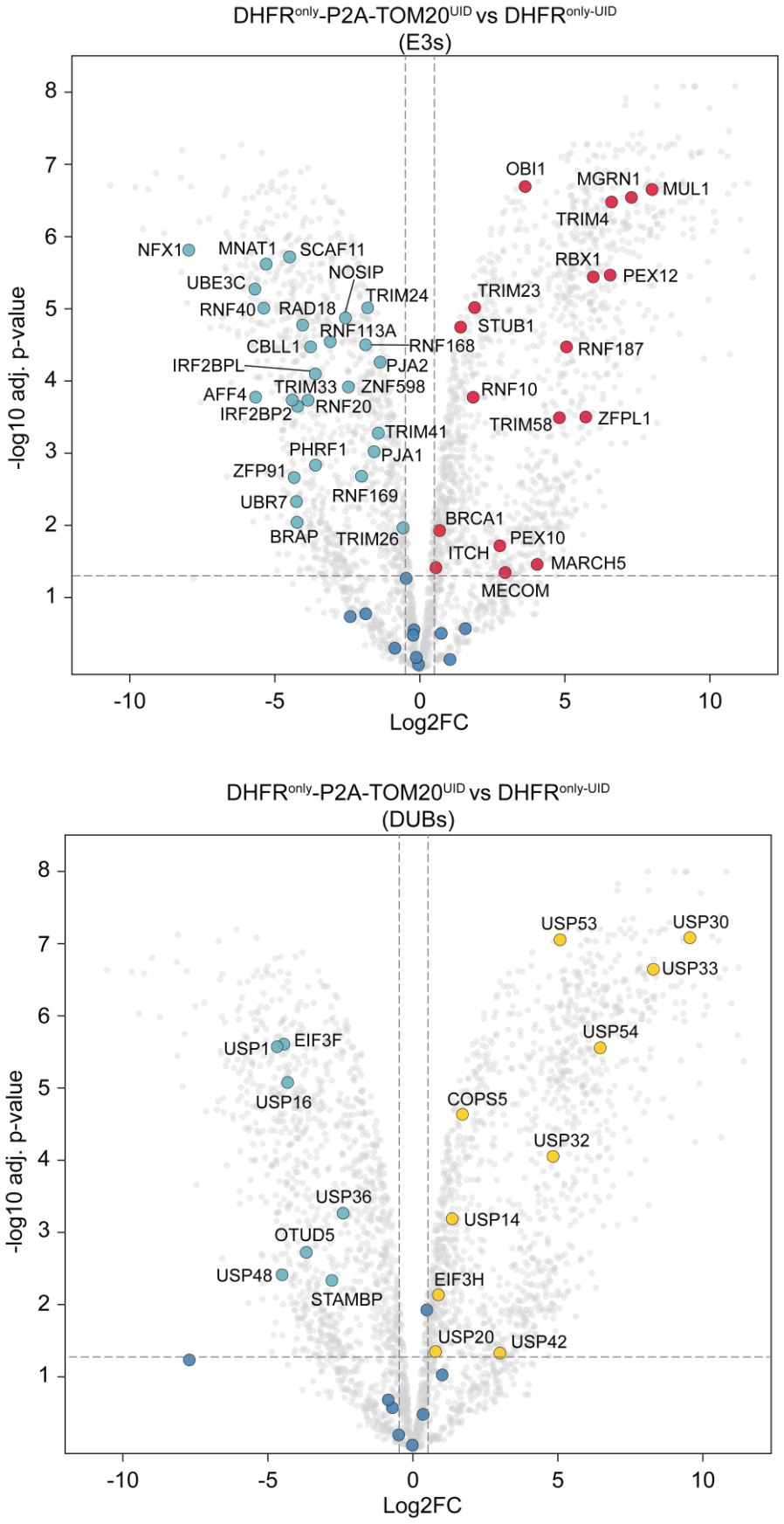

Appendix 3 Ubiquitin related proteins in proximity of TOM20 under unchallenged conditions. The MS dataset DHFR^{only}-P2A-TOM20^{UID} vs DHFR$^{only-UID}$ was screened for E3s (red) and DUBs (yellow). (cut-offs: Log2FC > 0.5 and limma-based p.value < 0.05).

5.3. Publications

Weisert, N., Majewski, V., Hartleb, L., Luko, K., Lototska, L., **Krapoth, N. C.**, ... & Butter, F. (2024). TelAP2 links TelAP1 to the telomere complex in Trypanosoma brucei. *Scientific Reports*, *14*(1), 30493.

Steinhilper, R., Boß, L., Freibert, S. A., Schulz, V., **Krapoth, N.**, Kaltwasser, S., ... & Murphy, B. J. (2024). Two-stage binding of mitochondrial ferredoxin-2 to the core iron-sulfur cluster assembly complex. *Nature Communications*, *15*(1), 10559.

Werner, A. D., **Krapoth, N.**, Norris, M. J., Heine, A., Klebe, G., Saphire, E. O., & Becker, S. (2024). Development of a crystallographic screening to identify Sudan virus VP40 ligands. *ACS omega*, *9*(30), 33193-33203.

Schulz, V., Steinhilper, R., Oltmanns, J., Freibert, S. A., **Krapoth, N.**, Linne, U., ... & Lill, R. (2024). Mechanism and structural dynamics of sulfur transfer during de novo [2Fe-2S] cluster assembly on ISCU2. *Nature Communications*, *15*(1), 3269.

Renz, C., Asimaki, E., Meister, C., Albanèse, V., Petriukov, K., **Krapoth, N. C.**, ... & Ulrich, H. D. (2024). Ubiquiton—an inducible, linkage-specific polyubiquitylation tool. *Molecular cell*, *84*(2), 386-400.

Rahmanto, A. S., Blum, C. J., Scalera, C., Heidelberger, J. B., Mesitov, M., Horn-Ghetko, D., Gräf JF, Mikicic I, Hobrecht R, Orekhova A, Ostermaier M, Ebersberger S, Möckel MM, **Krapoth N**, Da Silva Fernandes N, Mizi A, Zhu Y, Chen JX, Choudhary C, Papantonis A, Ulrich HD, Schulman BA, König J, Beli, P. (2023). K6-linked ubiquitylation marks formaldehyde-induced RNA-protein crosslinks for resolution. *Molecular Cell*, *83*(23), 4272-4289.

Freibert, S. A., Boniecki, M. T., Stümpfig, C., Schulz, V., **Krapoth, N.**, Winge, D. R., Mühlenhoff U, Stehling O, Cygler M, Lill R. (2021). N-terminal tyrosine of ISCU2 triggers [2Fe-2S] cluster synthesis by ISCU2 dimerization. *Nature Communications*, *12*(1), 6902.

Appendix

5.4. Bibliography

Abramson, J.; Adler, J.; Dunger, J.; Evans, R.; Green, T.; Pritzel, A.; Ronneberger, O.; Willmore, L.; Ballard, A. J.; Bambrick, J.; Bodenstein, S. W.; Evans, D. A.; Hung, C.-C.; O'Neill, M.; Reiman, D.; Tunyasuvunakool, K.; Wu, Z.; Žemgulytė, A.; Arvaniti, E., . . . Jumper, J. M. (2024). Accurate structure prediction of biomolecular interactions with AlphaFold 3. *Nature*, *630*(8016), 493–500. https://doi.org/10.1038/s41586-024-07487-w

Adey, A.; Burton, J. N.; Kitzman, J. O.; Hiatt, J. B.; Lewis, A. P.; Martin, B. K.; Qiu, R.; Lee, C., & Shendure, J. (2013). The haplotype-resolved genome and epigenome of the aneuploid HeLa cancer cell line. *Nature*, *500*(7461), 207–211. https://doi.org/10.1038/nature12064

Agrata, R., & Komander, D. (2025). Ubiquitin-A structural perspective. *Molecular Cell*, *85*(2), 323–346. https://doi.org/10.1016/j.molcel.2024.12.015

Ahting, U.; Thun, C.; Hegerl, R.; Typke, D.; Nargang, F. E.; Neupert, W., & Nussberger, S. (1999). The TOM core complex: The general protein import pore of the outer membrane of mitochondria. *The Journal of Cell Biology*, *147*(5), 959–968. https://doi.org/10.1083/jcb.147.5.959

Ainavarapu, S. R. K.; Brujic, J.; Huang, H. H.; Wiita, A. P.; Lu, H.; Li, L [Lewyn]; Walther, K. A.; Carrion-Vazquez, M.; Li, H [Hongbin], & Fernandez, J. M. (2007). Contour length and refolding rate of a small protein controlled by engineered disulfide bonds. *Biophysical Journal*, *92*(1), 225–233. https://doi.org/10.1529/biophysj.106.091561

Akizuki, Y.; Kaypee, S.; Ohtake, F., & Ikeda, F. (2024). The emerging roles of non-canonical ubiquitination in proteostasis and beyond. *The Journal of Cell Biology*, *223*(5). https://doi.org/10.1083/jcb.202311171

Akram, S.; Zittlau, K. I.; Maček, B., & Jansen, R.-P. (2024). *Proximity labeling reveals differential interaction partners of the human mitochondrial import receptor proteins TOMM20 and TOMM70.* https://doi.org/10.1101/2024.10.25.620316

Akram, S.; Zittlau, K. I.; Sharma, K.; Fitzgerald, J. C.; Rafiq, N.; Maček, B., & Jansen, R.-P. (2025). Proximity Labeling Reveals RNA-Binding Proteins Associating with the Human Mitochondrial Import Receptor TOMM20. *Journal of Proteome Research.* Advance online publication. https://doi.org/10.1021/acs.jproteome.5c00905

Akutsu, M.; Dikic, I., & Bremm, A. (2016). Ubiquitin chain diversity at a glance. *Journal of Cell Science*, *129*(5), 875–880. https://doi.org/10.1242/jcs.183954

Alberts, B.; Johnson, A., & Lewis, J. (2002). *Molecular biology of the cell* (4th ed.). Garland Science. https://www.ncbi.nlm.nih.gov/bookshelf/br.fcgi?book=mboc4

Appendix

Anderson, A. J.; Jackson, T. D.; Stroud, D. A., & Stojanovski, D. (2019). Mitochondria-hubs for regulating cellular biochemistry: Emerging concepts and networks. *Open Biology*, *9*(8), 190126. https://doi.org/10.1098/rsob.190126

Anderson, S.; Bankier, A. T.; Barrell, B. G.; Bruijn, M. H. de; Coulson, A. R.; Drouin, J.; Eperon, I. C.; Nierlich, D. P.; Roe, B. A.; Sanger, F.; Schreier, P. H.; Smith, A. J.; Staden, R., & Young, I. G. (1981). Sequence and organization of the human mitochondrial genome. *Nature*, *290*(5806), 457–465. https://doi.org/10.1038/290457a0

Angerer, H.; Radermacher, M.; Mańkowska, M.; Steger, M.; Zwicker, K.; Heide, H.; Wittig, I.; Brandt, U., & Zickermann, V. (2014). The LYR protein subunit NB4M/NDUFA6 of mitochondrial complex I anchors an acyl carrier protein and is essential for catalytic activity. *Proceedings of the National Academy of Sciences*, *111*(14), 5207–5212. https://doi.org/10.1073/pnas.1322438111

Antico, O.; Ordureau, A.; Stevens, M.; Singh, F.; Nirujogi, R. S.; Gierlinski, M.; Barini, E.; Rickwood, M. L.; Prescott, A.; Toth, R.; Ganley, I. G.; Harper, J. W., & Muqit, M. M. K. (2021). Global ubiquitylation analysis of mitochondria in primary neurons identifies endogenous Parkin targets following activation of PINK1. *Science Advances*, *7*(46), eabj0722. https://doi.org/10.1126/sciadv.abj0722

Araiso, Y.; Imai, K., & Endo, T [Toshiya] (2022). Role of the TOM Complex in Protein Import into Mitochondria: Structural Views. *Annual Review of Biochemistry*, *91*, 679–703. https://doi.org/10.1146/annurev-biochem-032620-104527

Arroyo-Gomez, J.; Murray, M. J.; Guérillon, C.; Wang, J [Juanjuan]; Isaakova, E.; Reverón-Gómez, N.; Koutrouli, M.; Suryo Rahmanto, A.; Mitrofanov, K.; Ingham, A.; Schovsbo, S.; Weischenfeldt, K.; Coscia, F.; Typas, D.; Völker-Albert, M.; Solis, V.; Jensen, L. J.; Groth, A.; Mund, A., . . Mailand, N. (2025). Functional landscape of ubiquitin linkages couples K29-linked ubiquitylation to epigenome integrity. *The EMBO Journal*, *44*(23), 6944–6978. https://doi.org/10.1038/s44318-025-00599-7

Asimaki, E.; Petriukov, K.; Renz, C.; Meister, C., & Ulrich, H. D. (2022). Fast friends - Ubiquitin-like modifiers as engineered fusion partners. *Seminars in Cell & Developmental Biology*, *132*, 132–145. https://doi.org/10.1016/j.semcdb.2021.11.013

Aweida, D., & Cohen, S. (2022). The AAA-ATPase ATAD1 and its partners promote degradation of desmin intermediate filaments in muscle. *EMBO Reports*, *23*(12), e55175. https://doi.org/10.15252/embr.202255175

Badrie, S.; Draken, J. A., & Mokranjac, D. (2024). In vitro import of mitochondrial precursor proteins into yeast mitochondria. *Methods in Enzymology*, *706*, 347–363. https://doi.org/10.1016/bs.mie.2024.07.016

Baker, K. P., & Schatz, G. (1991). Mitochondrial proteins essential for viability mediate protein import into yeast mitochondria. *Nature*, *349*(6306), 205–208. https://doi.org/10.1038/349205a0

Baker, M. J.; Blau, K. U.; Anderson, A. J.; Palmer, C. S.; Fielden, L. F.; Crameri, J. J.; Milenkovic, D.; Thorburn, D. R.; Frazier, A. E.; Langer, T., & Stojanovski, D. (2024). Clpb disaggregase dysfunction impacts the functional integrity of the proteolytic SPY complex. *The Journal of Cell Biology*, *223*(3). https://doi.org/10.1083/jcb.202305087

Baker, M. J.; Yek, K. Q., & Stojanovski, D. (2025). Quality control at the powerhouse: Mitochondrial proteostasis dysfunction and disease. *Biochemical Society Transactions*, *53*(4), 1–13. https://doi.org/10.1042/BST20253044

Barad, B. A.; Medina, M.; Fuentes, D.; Wiseman, R. L., & Grotjahn, D. A. (2023). Quantifying organellar ultrastructure in cryo-electron tomography using a surface morphometrics pipeline. *The Journal of Cell Biology*, *222*(4). https://doi.org/10.1083/jcb.202204093

Basar, M. A.; Beck, D. B., & Werner, A. (2021). Deubiquitylases in developmental ubiquitin signaling and congenital diseases. *Cell Death and Differentiation*, *28*(2), 538–556. https://doi.org/10.1038/s41418-020-00697-5

Becker, T.; Song, J [Jiyao], & Pfanner, N [Nikolaus] (2019). Versatility of Preprotein Transfer from the Cytosol to Mitochondria. *Trends in Cell Biology*, *29*(7), 534–548. https://doi.org/10.1016/j.tcb.2019.03.007

Bedford, L.; Lowe, J.; Dick, L. R.; Mayer, R. J., & Brownell, J. E. (2011). Ubiquitin-like protein conjugation and the ubiquitin-proteasome system as drug targets. *Nature Reviews. Drug Discovery*, *10*(1), 29–46. https://doi.org/10.1038/nrd3321

Benda, C. (1898). Ueber die Spermatogenese der Vertebraten und hoherer Evertebraten.: I. Theil. Ueber die vegetativen Geschlechtszellen. *Verhandlungen Der Physiologischen Gesellschaft Zu Berlin in Archiv Für Physiologie*, 385–392. https://eurekamag.com/research/024/054/024054539.php

Benjamini, Y., & Hochberg, Y. (1995). Controlling the False Discovery Rate: A Practical and Powerful Approach to Multiple Testing. *Journal of the Royal Statistical Society Series B: Statistical Methodology*, *57*(1), 289–300. https://doi.org/10.1111/j.2517-6161.1995.tb02031.x

Berezhnov, A. V.; Soutar, M. P. M.; Fedotova, E. I.; Frolova, M. S.; Plun-Favreau, H.; Zinchenko, V. P., & Abramov, A. Y. (2016). Intracellular pH Modulates Autophagy and Mitophagy. *The Journal of Biological Chemistry*, *291*(16), 8701–8708. https://doi.org/10.1074/jbc.M115.691774

Beverly, K. N.; Sawaya, M. R.; Schmid, E., & Koehler, C. M. (2008). The Tim8-Tim13 complex has multiple substrate binding sites and binds cooperatively to Tim23.

Journal of Molecular Biology, *382*(5), 1144–1156. https://doi.org/10.1016/j.jmb.2008.07.069

Bhagawati, M.; Arroum, T.; Webeling, N.; Montoro, A. G.; Mootz, H. D., & Busch, K. B. (2021). The receptor subunit Tom20 is dynamically associated with the TOM complex in mitochondria of human cells. *Molecular Biology of the Cell*, *32*(20), br1. https://doi.org/10.1091/mbc.E21-01-0042

Bian, S.; Ni, W.; Zhou, L [Linlin]; Tong, Y.; Dai, C.; Zhao, X [Xuying]; Qiang, Y.; Gao, J [Jie]; Xiao, Y [Yifu]; Liu, W [Wei]; Chen, C.; Lin, S [Shengli]; Gong, J.; Zhao, S.; Chen, Y [Yinqi]; Lin, Z.; Liu, D [Dong]; Zhao, H [Hui], & Zheng, W. (2024). Ubiquitin-specific protease 1 facilitates hepatocellular carcinoma progression by modulating mitochondrial fission and metabolic reprogramming via cyclin-dependent kinase 5 stabilization. *Cell Death and Differentiation*, *31*(9), 1202–1218. https://doi.org/10.1038/s41418-024-01342-1

Bie, P. de, & Ciechanover, A. (2011). Ubiquitination of E3 ligases: Self-regulation of the ubiquitin system via proteolytic and non-proteolytic mechanisms. *Cell Death and Differentiation*, *18*(9), 1393–1402. https://doi.org/10.1038/cdd.2011.16

Bogorodskiy, A.; Okhrimenko, I.; Maslov, I.; Maliar, N.; Burkatovskii, D.; Ameln, F. von; Schulga, A.; Jakobs, P.; Altschmied, J.; Haendeler, J.; Katranidis, A.; Sorokin, I.; Mishin, A.; Gordeliy, V.; Büldt, G.; Voos, W [Wolfgang]; Gensch, T., & Borshchevskiy, V. (2021). Accessing Mitochondrial Protein Import in Living Cells by Protein Microinjection. *Frontiers in Cell and Developmental Biology*, *9*, 698658. https://doi.org/10.3389/fcell.2021.698658

Boob, A. G.; Tan, S.-I.; Zaidi, A.; Singh, N.; Xue, X.; Zhou, S.; Martin, T. A.; Chen, L.-Q., & Zhao, H [Huimin] (2025). Design of diverse, functional mitochondrial targeting sequences across eukaryotic organisms using variational autoencoder. *Nature Communications*, *16*(1), 4151. https://doi.org/10.1038/s41467-025-59499-3

Boos, F.; Krämer, L.; Groh, C.; Jung, F.; Haberkant, P.; Stein, F [Frank]; Wollweber, F.; Gackstatter, A.; Zöller, E.; van der Laan, M.; Savitski, M. M.; Benes, V., & Herrmann, J. M. (2019). Mitochondrial protein-induced stress triggers a global adaptive transcriptional programme. *Nature Cell Biology*, *21*(4), 442–451. https://doi.org/10.1038/s41556-019-0294-5

Borgert, L.; Becker, T., & Brave, F. den (2024). Conserved quality control mechanisms of mitochondrial protein import. *Journal of Inherited Metabolic Disease*, *47*(5), 903–916. https://doi.org/10.1002/jimd.12756

Braymer, J. J., & Lill, R. (2017). Iron-sulfur cluster biogenesis and trafficking in mitochondria. *The Journal of Biological Chemistry*, *292*(31), 12754–12763. https://doi.org/10.1074/jbc.R117.787101

Bremm, A.; Freund, S. M. V., & Komander, D. (2010). Lys11-linked ubiquitin chains adopt compact conformations and are preferentially hydrolyzed by the deubiquitinase Cezanne. *Nature Structural & Molecular Biology*, *17*(8), 939–947. https://doi.org/10.1038/nsmb.1873

Bykov, Y. S.; Rapaport, D.; Herrmann, J. M., & Schuldiner, M. (2020). Cytosolic Events in the Biogenesis of Mitochondrial Proteins. *Trends in Biochemical Sciences*, *45*(8), 650–667. https://doi.org/10.1016/j.tibs.2020.04.001

C Mereschkowsky (1905). Über Natur und Ursprung der Chromatophoren im Pflanzenreiche. *Biol Centralbl*, *25*, 593. https://cir.nii.ac.jp/crid/1370004237548072452

Cadenas, E., & Davies, K. J. (2000). Mitochondrial free radical generation, oxidative stress, and aging. *Free Radical Biology & Medicine*, *29*(3-4), 222–230. https://doi.org/10.1016/s0891-5849(00)00317-8

Calais, H., & Bertolin, G. (2025). Stress at the gates: Mitochondrial import dysfunctions, response pathways, and therapeutic potential. *Mitochondrion*, *87*, 102107. https://doi.org/10.1016/j.mito.2025.102107

Callegari, S.; Cruz-Zaragoza, L. D., & Rehling, P. (2020). From TOM to the TIM23 complex - handing over of a precursor. *Biological Chemistry*, *401*(6-7), 709–721. https://doi.org/10.1515/hsz-2020-0101

Chacinska, A.; Koehler, C. M.; Milenkovic, D.; Lithgow, T., & Pfanner, N [Nikolaus] (2009). Importing mitochondrial proteins: Machineries and mechanisms. *Cell*, *138*(4), 628–644. https://doi.org/10.1016/j.cell.2009.08.005

Chacinska, A.; Lind, M.; Frazier, A. E.; Dudek, J.; Meisinger, C [Chris]; Geissler, A [Andreas]; Sickmann, A [Albert]; Meyer, H. E [Helmut E.]; Truscott, K. N [Kaye N.]; Guiard, B [Bernard]; Pfanner, N [Nikolaus], & Rehling, P. (2005). Mitochondrial presequence translocase: Switching between TOM tethering and motor recruitment involves Tim21 and Tim17. *Cell*, *120*(6), 817–829. https://doi.org/10.1016/j.cell.2005.01.011

Chakraborty, J.; Stockum, S. von; Marchesan, E.; Caicci, F.; Ferrari, V.; Rakovic, A.; Klein, C.; Antonini, A.; Bubacco, L., & Ziviani, E. (2018). Usp14 inhibition corrects an in vivo model of impaired mitophagy. *EMBO Molecular Medicine*, *10*(11). https://doi.org/10.15252/emmm.201809014

Chau, V.; Tobias, J. W.; Bachmair, A.; Marriott, D.; Ecker, D. J.; Gonda, D. K., & Varshavsky, A. (1989). A multiubiquitin chain is confined to specific lysine in a targeted short-lived protein. *Science (New York, N.Y.)*, *243*(4898), 1576–1583. https://doi.org/10.1126/science.2538923

Chaugule, S.; Yang, Y.-S.; Sato, T.; Mayer, E., & Shim, J.-H. (2026). Usp8-mediated mitochondrial regulation in osteoclasts is essential for skeletal development. *Cellular*

and Molecular Life Sciences : CMLS, *83*(1), 72. https://doi.org/10.1007/s00018-025-06012-0

Chen, K.-H.; Dasgupta, A.; Ding, J.; Indig, F. E.; Ghosh, P., & Longo, D. L. (2014). Role of mitofusin 2 (Mfn2) in controlling cellular proliferation. *FASEB Journal : Official Publication of the Federation of American Societies for Experimental Biology*, *28*(1), 382–394. https://doi.org/10.1096/fj.13-230037

Chen, Q.; Lei, J. H.; Bao, J.; Wang, H [Haitao]; Hao, W.; Li, L [Licen]; Peng, C.; Masuda, T.; Miao, K.; Xu, J [Jun]; Xu, X [Xiaoling], & Deng, C.-X. (2020). Brca1 Deficiency Impairs Mitophagy and Promotes Inflammasome Activation and Mammary Tumor Metastasis. *Advanced Science (Weinheim, Baden-Wurttemberg, Germany)*, *7*(6), 1903616. https://doi.org/10.1002/advs.201903616

Chen, Z. J. (2005). Ubiquitin signalling in the NF-kappaB pathway. *Nature Cell Biology*, *7*(8), 758–765. https://doi.org/10.1038/ncb0805-758

Chibi, M.; Meyer, M.; Skepu, A.; G Rees, D. J.; Moolman-Smook, J. C., & Pugh, D. J. R. (2008). Rbbp6 interacts with multifunctional protein YB-1 through its RING finger domain, leading to ubiquitination and proteosomal degradation of YB-1. *Journal of Molecular Biology*, *384*(4), 908–916. https://doi.org/10.1016/j.jmb.2008.09.060

Cho, K. F.; Branon, T. C.; Rajeev, S.; Svinkina, T.; Udeshi, N. D.; Thoudam, T.; Kwak, C.; Rhee, H.-W.; Lee, I.-K.; Carr, S. A., & Ting, A. Y. (2020). Split-TurboID enables contact-dependent proximity labeling in cells. *Proceedings of the National Academy of Sciences*, *117*(22), 12143–12154. https://doi.org/10.1073/pnas.1919528117

Coene, E. D.; Hollinshead, M. S.; Waeytens, A. A. T.; Schelfhout, V. R. J.; Eechaute, W. P.; Shaw, M. K.; van Oostveldt, P. M. V., & Vaux, D. J. (2005). Phosphorylated BRCA1 is predominantly located in the nucleus and mitochondria. *Molecular Biology of the Cell*, *16*(2), 997–1010. https://doi.org/10.1091/mbc.e04-10-0895

Colina-Tenorio, L.; Horten, P.; Pfanner, N [N.], & Rampelt, H [H.] (2020). Shaping the mitochondrial inner membrane in health and disease. *Journal of Internal Medicine*, *287*(6), 645–664. https://doi.org/10.1111/joim.13031

Cox, J.; Hein, M. Y.; Luber, C. A.; Paron, I.; Nagaraj, N., & Mann, M. (2014). Accurate proteome-wide label-free quantification by delayed normalization and maximal peptide ratio extraction, termed MaxLFQ. *Molecular & Cellular Proteomics : MCP*, *13*(9), 2513–2526. https://doi.org/10.1074/mcp.M113.031591

Cox, J., & Mann, M. (2008). Maxquant enables high peptide identification rates, individualized p.P.B.-range mass accuracies and proteome-wide protein quantification. *Nature Biotechnology*, *26*(12), 1367–1372. https://doi.org/10.1038/nbt.1511

Cox, J.; Neuhauser, N.; Michalski, A.; Scheltema, R. A.; Olsen, J. V., & Mann, M. (2011). Andromeda: A peptide search engine integrated into the MaxQuant environment. *Journal of Proteome Research*, *10*(4), 1794–1805. https://doi.org/10.1021/pr101065j

Coyne, L. P.; Wang, X [Xiaowen]; Song, J [Jiyao]; Jong, E. de; Schneider, K.; Massa, P. T.; Middleton, F. A.; Becker, T., & Chen, X. J. (2023). Mitochondrial protein import clogging as a mechanism of disease. *ELife*, *12.* https://doi.org/10.7554/eLife.84330

Cunningham, C. N.; Baughman, J. M.; Phu, L.; Tea, J. S.; Yu, C [Christine]; Coons, M.; Kirkpatrick, D. S.; Bingol, B., & Corn, J. E. (2015). Usp30 and parkin homeostatically regulate atypical ubiquitin chains on mitochondria. *Nature Cell Biology*, *17*(2), 160–169. https://doi.org/10.1038/ncb3097

Cupo, R. R., & Shorter, J. (2020). Skd3 (human ClpB) is a potent mitochondrial protein disaggregase that is inactivated by 3-methylglutaconic aciduria-linked mutations. *ELife*, *9.* https://doi.org/10.7554/eLife.55279

Dan Dunn, J.; Alvarez, L. A.; Zhang, X [Xuezhi], & Soldati, T. (2015). Reactive oxygen species and mitochondria: A nexus of cellular homeostasis. *Redox Biology*, *6*, 472–485. https://doi.org/10.1016/j.redox.2015.09.005

Dekker, P. J.; Ryan, M. T.; Brix, J.; Müller, H.; Hönlinger, A., & Pfanner, N [N.] (1998). Preprotein translocase of the outer mitochondrial membrane: Molecular dissection and assembly of the general import pore complex. *Molecular and Cellular Biology*, *18*(11), 6515–6524. https://doi.org/10.1128/MCB.18.11.6515

Demishtein-Zohary, K., & Azem, A [Abdussalam] (2017). The TIM23 mitochondrial protein import complex: Function and dysfunction. *Cell and Tissue Research*, *367*(1), 33–41. https://doi.org/10.1007/s00441-016-2486-7

Devi, L.; Prabhu, B. M.; Galati, D. F.; Avadhani, N. G., & Anandatheerthavarada, H. K. (2006). Accumulation of amyloid precursor protein in the mitochondrial import channels of human Alzheimer's disease brain is associated with mitochondrial dysfunction. *The Journal of Neuroscience : The Official Journal of the Society for Neuroscience*, *26*(35), 9057–9068. https://doi.org/10.1523/JNEUROSCI.1469-06.2006

Dietmeier, K.; Hönlinger, A.; Bömer, U.; Dekker, P. J.; Eckerskorn, C.; Lottspeich, F.; Kübrich, M., & Pfanner, N [N.] (1997). Tom5 functionally links mitochondrial preprotein receptors to the general import pore. *Nature*, *388*(6638), 195–200. https://doi.org/10.1038/40663

Dikic, I., & Schulman, B. A. (2023). An expanded lexicon for the ubiquitin code. *Nature Reviews. Molecular Cell Biology*, *24*(4), 273–287. https://doi.org/10.1038/s41580-022-00543-1

Appendix

Dizdaroglu, M., & Jaruga, P. (2012). Mechanisms of free radical-induced damage to DNA. *Free Radical Research*, *46*(4), 382–419. https://doi.org/10.3109/10715762.2011.653969

Doan, K. N.; Grevel, A.; Mårtensson, C. U.; Ellenrieder, L.; Thornton, N.; Wenz, L.-S.; Opaliński, Ł.; Guiard, B [Bernard]; Pfanner, N [Nikolaus], & Becker, T. (2020). The Mitochondrial Import Complex MIM Functions as Main Translocase for α-Helical Outer Membrane Proteins. *Cell Reports*, *31*(4), 107567. https://doi.org/10.1016/j.celrep.2020.107567

Doblado, L.; Lueck, C.; Rey, C.; Samhan-Arias, A. K.; Prieto, I.; Stacchiotti, A., & Monsalve, M. (2021). Mitophagy in Human Diseases. *International Journal of Molecular Sciences*, *22*(8). https://doi.org/10.3390/ijms22083903

Dolezal, P.; Likic, V.; Tachezy, J., & Lithgow, T. (2006). Evolution of the molecular machines for protein import into mitochondria. *Science (New York, N.Y.)*, *313*(5785), 314–318. https://doi.org/10.1126/science.1127895

Draczkowski, P.; Chen, S.-N.; Chen, T.; Wang, Y.-S.; Shih, H.-A.; Huang, J. Y. C.; Tsai, M.-C.; Lin, S.-Y.; Lin, S [Steven]; Viner, R.; Chang, Y.-C.; Wu, K.-P., & Hsu, S.-T. D. (2025). Structural basis of K11/K48-branched ubiquitin chain recognition by the human 26S proteasome. *Nature Communications*, *16*(1), 9094. https://doi.org/10.1038/s41467-025-64719-x

Durcan, T. M.; Tang, M. Y.; Pérusse, J. R.; Dashti, E. A.; Aguileta, M. A.; McLelland, G.-L.; Gros, P.; Shaler, T. A.; Faubert, D.; Coulombe, B., & Fon, E. A. (2014). Usp8 regulates mitophagy by removing K6-linked ubiquitin conjugates from parkin. *The EMBO Journal*, *33*(21), 2473–2491. https://doi.org/10.15252/embj.201489729

Eaglesfield, R., & Tokatlidis, K. (2021). Targeting and Insertion of Membrane Proteins in Mitochondria. *Frontiers in Cell and Developmental Biology*, *9*, 803205. https://doi.org/10.3389/fcell.2021.803205

Edwards, R.; Eaglesfield, R., & Tokatlidis, K. (2021). The mitochondrial intermembrane space: The most constricted mitochondrial sub-compartment with the largest variety of protein import pathways. *Open Biology*, *11*(3), 210002. https://doi.org/10.1098/rsob.210002

Eilers, M., & Schatz, G. (1986). Binding of a specific ligand inhibits import of a purified precursor protein into mitochondria. *Nature*, *322*(6076), 228–232. https://doi.org/10.1038/322228a0

Elia, A. E. H.; Boardman, A. P.; Wang, D. C.; Huttlin, E. L.; Everley, R. A.; Dephoure, N.; Zhou, C.; Koren, I.; Gygi, S. P., & Elledge, S. J. (2015). Quantitative Proteomic Atlas of Ubiquitination and Acetylation in the DNA Damage Response. *Molecular Cell*, *59*(5), 867–881. https://doi.org/10.1016/j.molcel.2015.05.006

Elwi, A. N.; Lee, B.; Meijndert, H. C.; Braun, J. E. A., & Kim, S.-W. (2012). Mitochondrial chaperone DnaJA3 induces Drp1-dependent mitochondrial fragmentation. *The International Journal of Biochemistry & Cell Biology*, *44*(8), 1366–1376. https://doi.org/10.1016/j.biocel.2012.05.004

Emmerich, C. H., & Cohen, P. (2015). Optimising methods for the preservation, capture and identification of ubiquitin chains and ubiquitylated proteins by immunoblotting. *Biochemical and Biophysical Research Communications*, *466*(1), 1–14. https://doi.org/10.1016/j.bbrc.2015.08.109

Endo, T [Toshiya], & Wiedemann, N [Nils] (2025). Molecular machineries and pathways of mitochondrial protein transport. *Nature Reviews. Molecular Cell Biology*, *26*(11), 848–867. https://doi.org/10.1038/s41580-025-00865-w

Erpapazoglou, Z.; Walker, O., & Haguenauer-Tsapis, R. (2014). Versatile roles of k63-linked ubiquitin chains in trafficking. *Cells*, *3*(4), 1027–1088. https://doi.org/10.3390/cells3041027

Esaki, M [M.]; Kanamori, T.; Nishikawa, S. i., & Endo, T [T.] (1999). Two distinct mechanisms drive protein translocation across the mitochondrial outer membrane in the late step of the cytochrome b(2) import pathway. *Proceedings of the National Academy of Sciences of the United States of America*, *96*(21), 11770–11775. https://doi.org/10.1073/pnas.96.21.11770

Farrants, H.; Tarnawski, M.; Müller, T. G.; Otsuka, S.; Hiblot, J.; Koch, B.; Kueblbeck, M.; Kräusslich, H.-G.; Ellenberg, J., & Johnsson, K. (2020). Chemogenetic Control of Nanobodies. *Nature Methods*, *17*(3), 279–282. https://doi.org/10.1038/s41592-020-0746-7

Faust, T. B.; Li, Y [Yang]; Jang, G. M.; Johnson, J. R.; Yang, S.; Weiss, A.; Krogan, N. J., & Frankel, A. D. (2017). Pja2 ubiquitinates the HIV-1 Tat protein with atypical chain linkages to activate viral transcription. *Scientific Reports*, *7*, 45394. https://doi.org/10.1038/srep45394

Felipe Perez, R.; Mochi, G.; Khan, A., & Woodford, M. (2024). Mitochondrial Chaperone Code: Just warming up. *Cell Stress & Chaperones*, *29*(3), 483–496. https://doi.org/10.1016/j.cstres.2024.05.002

Fenouille, N.; Bassil, C. F.; Ben-Sahra, I.; Benajiba, L.; Alexe, G.; Ramos, A.; Pikman, Y.; Conway, A. S.; Burgess, M. R.; Li, Q [Qing]; Luciano, F.; Auberger, P.; Galinsky, I.; DeAngelo, D. J.; Stone, R. M.; Zhang, Y [Yi]; Perkins, A. S.; Shannon, K.; Hemann, M. T., . . . Stegmaier, K. (2017). The creatine kinase pathway is a metabolic vulnerability in EVI1-positive acute myeloid leukemia. *Nature Medicine*, *23*(3), 301–313. https://doi.org/10.1038/nm.4283

Appendix

Filipuzzi, I.; Steffen, J.; Germain, M.; Goepfert, L.; Conti, M. A.; Potting, C.; Cerino, R.; Pfeifer, M.; Krastel, P.; Hoepfner, D.; Bastien, J.; Koehler, C. M., & Helliwell, S. B. (2017). Stendomycin selectively inhibits TIM23-dependent mitochondrial protein import. *Nature Chemical Biology*, *13*(12), 1239–1244. https://doi.org/10.1038/nchembio.2493

Fillingame, R. H.; Angevine, C. M., & Dmitriev, O. Y. (2003). Mechanics of coupling proton movements to c-ring rotation in ATP synthase. *FEBS Letters*, *555*(1), 29–34. https://doi.org/10.1016/s0014-5793(03)01101-3

Finkel, T., & Holbrook, N. J. (2000). Oxidants, oxidative stress and the biology of ageing. *Nature*, *408*(6809), 239–247. https://doi.org/10.1038/35041687

Finley, D [D.]; Sadis, S.; Monia, B. P.; Boucher, P.; Ecker, D. J.; Crooke, S. T., & Chau, V. (1994). Inhibition of proteolysis and cell cycle progression in a multiubiquitination-deficient yeast mutant. *Molecular and Cellular Biology*, *14*(8), 5501–5509. https://doi.org/10.1128/mcb.14.8.5501-5509.1994

Fonseca, D.; Pisanelli, G.; Seoane, R.; Miorin, L., & García-Sastre, A. (2024). Trim65 regulates innate immune signaling by enhancing K6-linked ubiquitination of IRF3 and its chromatin recruitment. *Cell Reports*, *43*(12), 114960. https://doi.org/10.1016/j.celrep.2024.114960

Franklin, T. G.; Brzovic, P. S., & Pruneda, J. N. (2023a). Bacterial ligases reveal fundamental principles of polyubiquitin specificity. *Molecular Cell*, *83*(24), 4538-4554.e4. https://doi.org/10.1016/j.molcel.2023.11.017

Franklin, T. G.; Brzovic, P. S., & Pruneda, J. N. (2023b). Bacterial mimicry of eukaryotic HECT ubiquitin ligation. *BioRxiv : The Preprint Server for Biology.* Advance online publication. https://doi.org/10.1101/2023.06.05.543783

Freibert, S.-A.; Boniecki, M. T.; Stümpfig, C.; Schulz, V.; Krapoth, N.; Winge, D. R.; Mühlenhoff, U.; Stehling, O.; Cygler, M., & Lill, R. (2021). N-terminal tyrosine of ISCU2 triggers 2Fe-2S cluster synthesis by ISCU2 dimerization. *Nature Communications*, *12*(1), 6902. https://doi.org/10.1038/s41467-021-27122-w

Frezza, C. (2017). Mitochondrial metabolites: Undercover signalling molecules. *Interface Focus*, *7*(2), 20160100. https://doi.org/10.1098/rsfs.2016.0100

Gatti, M.; Pinato, S.; Maiolica, A.; Rocchio, F.; Prato, M. G.; Aebersold, R., & Penengo, L. (2015). Rnf168 promotes noncanonical K27 ubiquitination to signal DNA damage. *Cell Reports*, *10*(2), 226–238. https://doi.org/10.1016/j.celrep.2014.12.021

Geissler, A [A.]; Krimmer, T.; Bömer, U.; Guiard, B [B.]; Rassow, J., & Pfanner, N [N.] (2000). Membrane potential-driven protein import into mitochondria. The sorting sequence of cytochrome b(2) modulates the deltapsi-dependence of translocation of the matrix-

targeting sequence. *Molecular Biology of the Cell*, *11*(11), 3977–3991. https://doi.org/10.1091/mbc.11.11.3977

Gersch, M.; Gladkova, C.; Schubert, A. F.; Michel, M. A.; Maslen, S., & Komander, D. (2017). Mechanism and regulation of the Lys6-selective deubiquitinase USP30. *Nature Structural & Molecular Biology*, *24*(11), 920–930. https://doi.org/10.1038/nsmb.3475

Giacomello, M.; Pyakurel, A.; Glytsou, C., & Scorrano, L. (2020). The cell biology of mitochondrial membrane dynamics. *Nature Reviews. Molecular Cell Biology*, *21*(4), 204–224. https://doi.org/10.1038/s41580-020-0210-7

Giorgi, C.; Marchi, S., & Pinton, P. (2018). The machineries, regulation and cellular functions of mitochondrial calcium. *Nature Reviews. Molecular Cell Biology*, *19*(11), 713–730. https://doi.org/10.1038/s41580-018-0052-8

Gold, V. A. M.; Ieva, R.; Walter, A.; Pfanner, N [Nikolaus]; van der Laan, M., & Kühlbrandt, W. (2014). Visualizing active membrane protein complexes by electron cryotomography. *Nature Communications*, *5*, 4129. https://doi.org/10.1038/ncomms5129

Goldstein, G.; Scheid, M.; Hammerling, U.; Schlesinger, D. H.; Niall, H. D., & Boyse, E. A. (1975). Isolation of a polypeptide that has lymphocyte-differentiating properties and is probably represented universally in living cells. *Proceedings of the National Academy of Sciences of the United States of America*, *72*(1), 11–15. https://doi.org/10.1073/pnas.72.1.11

Gong, M.; Ye, S.; Li, W.-X.; Zhang, J [Jian]; Liu, Y [Yanjun]; Zhu, J [Jie]; Lv, W.; Zhang, H [Hui]; Wang, J [Jing]; Lu, A., & He, K. (2020). Regulatory function of praja ring finger ubiquitin ligase 2 mediated by the P2rx3/P2rx7 axis in mouse hippocampal neuronal cells. *American Journal of Physiology. Cell Physiology*, *318*(6), C1123-C1135. https://doi.org/10.1152/ajpcell.00070.2019

Gornicka, A.; Bragoszewski, P.; Chroscicki, P.; Wenz, L.-S.; Schulz, C.; Rehling, P., & Chacinska, A. (2014). A discrete pathway for the transfer of intermembrane space proteins across the outer membrane of mitochondria. *Molecular Biology of the Cell*, *25*(25), 3999–4009. https://doi.org/10.1091/mbc.E14-06-1155

Grice, G. L.; Lobb, I. T.; Weekes, M. P.; Gygi, S. P.; Antrobus, R., & Nathan, J. A. (2015). The Proteasome Distinguishes between Heterotypic and Homotypic Lysine-11-Linked Polyubiquitin Chains. *Cell Reports*, *12*(4), 545–553. https://doi.org/10.1016/j.celrep.2015.06.061

Gruhler, A.; Ono, H.; Guiard, B [B.]; Neupert, W., & Stuart, R. A. (1995). A novel intermediate on the import pathway of cytochrome b2 into mitochondria: Evidence for conservative sorting. *The EMBO Journal*, *14*(7), 1349–1359. https://doi.org/10.1002/j.1460-2075.1995.tb07121.x

Appendix

Harper, J. W.; Ordureau, A., & Heo, J.-M. (2018). Building and decoding ubiquitin chains for mitophagy. *Nature Reviews. Molecular Cell Biology*, *19*(2), 93–108. https://doi.org/10.1038/nrm.2017.129

Harper, S.; Gratton, H. E.; Cornaciu, I.; Oberer, M.; Scott, D. J.; Emsley, J., & Dreveny, I. (2014). Structure and catalytic regulatory function of ubiquitin specific protease 11 N-terminal and ubiquitin-like domains. *Biochemistry*, *53*(18), 2966–2978. https://doi.org/10.1021/bi500116x

Hasson, S. A.; Damoiseaux, R.; Glavin, J. D.; Dabir, D. V.; Walker, S. S., & Koehler, C. M. (2010). Substrate specificity of the TIM22 mitochondrial import pathway revealed with small molecule inhibitor of protein translocation. *Proceedings of the National Academy of Sciences*, *107*(21), 9578–9583. https://doi.org/10.1073/pnas.0914387107

Heath, O.; Del Caño-Ochoa, F.; Baris, S.; Carrozzo, R.; Coman, D.; Distelmaier, F.; Ellaway, C.; Feichtinger, R. G.; Finocchi, A.; Guerrero-Castillo, S.; Halligan, R.; Hannibal, I.; Kritzer, A.; Lichter-Konecki, U.; Merkevicius, K.; Panis, B.; Pitceathly, R. D. S.; Pizzamiglio, C.; Iwanicka-Pronicka, K., . . . Wortmann, S. B. (2026). From genotype to outcome: Zygosity-specific insights in 63 cases of CLPB-related mitochondrial disease. *Molecular Genetics and Metabolism*, *147*(4), 109752. https://doi.org/10.1016/j.ymgme.2026.109752

Heo, J.-M.; Ordureau, A.; Paulo, J. A.; Rinehart, J., & Harper, J. W. (2015). The PINK1-PARKIN Mitochondrial Ubiquitylation Pathway Drives a Program of OPTN/NDP52 Recruitment and TBK1 Activation to Promote Mitophagy. *Molecular Cell*, *60*(1), 7–20. https://doi.org/10.1016/j.molcel.2015.08.016

Hönlinger, A.; Bömer, U.; Alconada, A.; Eckerskorn, C.; Lottspeich, F.; Dietmeier, K., & Pfanner, N [N.] (1996). Tom7 modulates the dynamics of the mitochondrial outer membrane translocase and plays a pathway-related role in protein import. *The EMBO Journal*, *15*(9), 2125–2137. https://doi.org/10.1002/j.1460-2075.1996.tb00566.x

Horibe, T., & Hoogenraad, N. J. (2007). The chop gene contains an element for the positive regulation of the mitochondrial unfolded protein response. *PloS One*, *2*(9), e835. https://doi.org/10.1371/journal.pone.0000835

Horner, S. M.; Liu, H. M.; Park, H. S.; Briley, J., & Gale, M. (2011). Mitochondrial-associated endoplasmic reticulum membranes (MAM) form innate immune synapses and are targeted by hepatitis C virus. *Proceedings of the National Academy of Sciences*, *108*(35), 14590–14595. https://doi.org/10.1073/pnas.1110133108

Horvath, S. E.; Rampelt, H [Heike]; Oeljeklaus, S.; Warscheid, B.; van der Laan, M., & Pfanner, N [Nikolaus] (2015). Role of membrane contact sites in protein import into

mitochondria. *Protein Science : A Publication of the Protein Society*, *24*(3), 277–297. https://doi.org/10.1002/pro.2625

Hoseini, H.; Pandey, S.; Jores, T.; Schmitt, A.; Franz-Wachtel, M.; Macek, B.; Buchner, J.; Dimmer, K. S., & Rapaport, D. (2016). The cytosolic cochaperone Sti1 is relevant for mitochondrial biogenesis and morphology. *The FEBS Journal*, *283*(18), 3338–3352. https://doi.org/10.1111/febs.13813

Hospenthal, M. K.; Freund, S. M. V., & Komander, D. (2013). Assembly, analysis and architecture of atypical ubiquitin chains. *Nature Structural & Molecular Biology*, *20*(5), 555–565. https://doi.org/10.1038/nsmb.2547

Hospenthal, M. K.; Mevissen, T. E. T., & Komander, D. (2015). Deubiquitinase-based analysis of ubiquitin chain architecture using Ubiquitin Chain Restriction (UbiCRest). *Nature Protocols*, *10*(2), 349–361. https://doi.org/10.1038/nprot.2015.018

Hsu, M.-C.; Kinefuchi, H.; Lei, L.; Kikuchi, R.; Yamano, K., & Youle, R. J. (2025). Mitochondrial YME1L1 governs unoccupied protein translocase channels. *Nature Cell Biology*, *27*(2), 309–321. https://doi.org/10.1038/s41556-024-01571-z

Huang, F.; Zeng, X.; Kim, W.; Balasubramani, M.; Fortian, A.; Gygi, S. P.; Yates, N. A., & Sorkin, A. (2013). Lysine 63-linked polyubiquitination is required for EGF receptor degradation. *Proceedings of the National Academy of Sciences*, *110*(39), 15722–15727. https://doi.org/10.1073/pnas.1308014110

Huang, H.; Jeon, M.-S.; Liao, L.; Yang, C.; Elly, C.; Yates, J. R., & Liu, Y.-C. (2010). K33-linked polyubiquitination of T cell receptor-zeta regulates proteolysis-independent T cell signaling. *Immunity*, *33*(1), 60–70. https://doi.org/10.1016/j.immuni.2010.07.002

Huang, S.-Y.; Gong, S.; Zhao, Y [Yin]; Ye, M.-L.; Li, J.-Y.; He, Q.-M.; Qiao, H.; Tan, X.-R.; Wang, J.-Y.; Liang, Y.-L.; Huang, S.-W.; He, S.-W.; Li, Y.-Q [Ying-Qin]; Xu, S.; Li, Y.-Q [Ying-Qing], & Liu, N. (2024). Pja1-mediated suppression of pyroptosis as a driver of docetaxel resistance in nasopharyngeal carcinoma. *Nature Communications*, *15*(1), 5300. https://doi.org/10.1038/s41467-024-49675-2

Hughes, A. L.; Hughes, C. E.; Henderson, K. A.; Yazvenko, N., & Gottschling, D. E. (2016). Selective sorting and destruction of mitochondrial membrane proteins in aged yeast. *ELife*, *5.* https://doi.org/10.7554/eLife.13943

Hutu, D. P.; Guiard, B [Bernard]; Chacinska, A.; Becker, D.; Pfanner, N [Nikolaus]; Rehling, P., & van der Laan, M. (2008). Mitochondrial protein import motor: Differential role of Tim44 in the recruitment of Pam17 and J-complex to the presequence translocase. *Molecular Biology of the Cell*, *19*(6), 2642–2649. https://doi.org/10.1091/mbc.e07-12-1226

Appendix

Ilik, İ. A.; Malszycki, M.; Lübke, A. K.; Schade, C.; Meierhofer, D., & Aktaş, T. (2020). Son and SRRM2 are essential for nuclear speckle formation. *ELife*, *9.* https://doi.org/10.7554/eLife.60579

Ishii, T.; Funakoshi, M., & Kobayashi, H. (2006). Yeast Pth2 is a UBL domain-binding protein that participates in the ubiquitin-proteasome pathway. *The EMBO Journal*, *25*(23), 5492–5503. https://doi.org/10.1038/sj.emboj.7601418

Iwai, K. (2021). Discovery of linear ubiquitination, a crucial regulator for immune signaling and cell death. *The FEBS Journal*, *288*(4), 1060–1069. https://doi.org/10.1111/febs.15471

Jahan, A. S.; Elbæk, C. R., & Damgaard, R. B. (2021). Met1-linked ubiquitin signalling in health and disease: Inflammation, immunity, cancer, and beyond. *Cell Death and Differentiation*, *28*(2), 473–492. https://doi.org/10.1038/s41418-020-00676-w

Jain, S.; Paz, E., & Azem, A [Abdussalam] (2024). Hotspots for Disease-Causing Mutations in the Mitochondrial TIM23 Import Complex. *Genes*, *15*(12). https://doi.org/10.3390/genes15121534

Johnsson, N., & Varshavsky, A. (1994). Split ubiquitin as a sensor of protein interactions in vivo. *Proceedings of the National Academy of Sciences of the United States of America*, *91*(22), 10340–10344. https://doi.org/10.1073/pnas.91.22.10340

Jonckheere, A. I.; Smeitink, J. A. M., & Rodenburg, R. J. T. (2012). Mitochondrial ATP synthase: Architecture, function and pathology. *Journal of Inherited Metabolic Disease*, *35*(2), 211–225. https://doi.org/10.1007/s10545-011-9382-9

Jores, T.; Lawatscheck, J.; Beke, V.; Franz-Wachtel, M.; Yunoki, K.; Fitzgerald, J. C.; Macek, B.; Endo, T [Toshiya]; Kalbacher, H.; Buchner, J., & Rapaport, D. (2018). Cytosolic Hsp70 and Hsp40 chaperones enable the biogenesis of mitochondrial β-barrel proteins. *The Journal of Cell Biology*, *217*(9), 3091–3108. https://doi.org/10.1083/jcb.201712029

Kamadurai, H. B.; Qiu, Y.; Deng, A.; Harrison, J. S.; Macdonald, C.; Actis, M.; Rodrigues, P.; Miller, D. J.; Souphron, J.; Lewis, S. M.; Kurinov, I.; Fujii, N.; Hammel, M.; Piper, R.; Kuhlman, B., & Schulman, B. A. (2013). Mechanism of ubiquitin ligation and lysine prioritization by a HECT E3. *ELife*, *2*, e00828. https://doi.org/10.7554/eLife.00828

Karnkowska, A.; Vacek, V.; Zubáčová, Z.; Treitli, S. C.; Petrželková, R.; Eme, L.; Novák, L.; Žárský, V.; Barlow, L. D.; Herman, E. K.; Soukal, P.; Hroudová, M.; Doležal, P.; Stairs, C. W.; Roger, A. J.; Eliáš, M.; Dacks, J. B.; Vlček, Č., & Hampl, V. (2016). A Eukaryote without a Mitochondrial Organelle. *Current Biology : CB*, *26*(10), 1274–1284. https://doi.org/10.1016/j.cub.2016.03.053

Khaminets, A.; Behl, C., & Dikic, I. (2016). Ubiquitin-Dependent And Independent Signals In Selective Autophagy. *Trends in Cell Biology*, *26*(1), 6–16. https://doi.org/10.1016/j.tcb.2015.08.010

Kilgas, S., & Ramadan, K. (2023). Inhibitors of the ATPase p97/VCP: From basic research to clinical applications. *Cell Chemical Biology*, *30*(1), 3–21. https://doi.org/10.1016/j.chembiol.2022.12.007

Kim, I.; Rodriguez-Enriquez, S., & Lemasters, J. J. (2007). Selective degradation of mitochondria by mitophagy. *Archives of Biochemistry and Biophysics*, *462*(2), 245–253. https://doi.org/10.1016/j.abb.2007.03.034

Kim, J.; Goldstein, M.; Zecchel, L.; Ghorayeb, R.; Maxwell, C. A., & Weidberg, H. (2024). Atad1 prevents clogging of TOM and damage caused by un-imported mitochondrial proteins. *Cell Reports*, *43*(8), 114473. https://doi.org/10.1016/j.celrep.2024.114473

Kim, M.-S.; Ramakrishna, S.; Lim, K.-H.; Kim, J.-H., & Baek, K.-H. (2011). Protein stability of mitochondrial superoxide dismutase SOD2 is regulated by USP36. *Journal of Cellular Biochemistry*, *112*(2), 498–508. https://doi.org/10.1002/jcb.22940

Kirkpatrick, D. S.; Weldon, S. F.; Tsaprailis, G.; Liebler, D. C., & Gandolfi, A. J. (2005). Proteomic identification of ubiquitinated proteins from human cells expressing His-tagged ubiquitin. *Proteomics*, *5*(8), 2104–2111. https://doi.org/10.1002/pmic.200401089

Kizmaz, B.; Nutz, A.; Egeler, A., & Herrmann, J. M. (2024). Protein insertion into the inner membrane of mitochondria: Routes and mechanisms. *FEBS Open Bio*, *14*(10), 1627–1639. https://doi.org/10.1002/2211-5463.13806

Kohler, V.; Kohler, A.; Berglund, L. L.; Hao, X.; Gersing, S.; Imhof, A.; Nyström, T.; Höög, J. L.; Ott, M.; Andréasson, C., & Büttner, S. (2024). Nuclear Hsp104 safeguards the dormant translation machinery during quiescence. *Nature Communications*, *15*(1), 315. https://doi.org/10.1038/s41467-023-44538-8

Kölliker, A. von. (1856). *Einige Bemerkungen über die Endigungen der Hautnerven und den Bau der Muskeln*. *Zeitschrift für wissenschaftliche Zoologie: Vol. 8* [Online-PDF]. Engelmann. https://www.zobodat.at/pdf/Zeitschrift-fuer-wiss-Zoologie_8_0311-0325.pdf

Komander, D., & Rape, M. (2012). The ubiquitin code. *Annual Review of Biochemistry*, *81*, 203–229. https://doi.org/10.1146/annurev-biochem-060310-170328

Kondadi, A. K.; Anand, R.; Hänsch, S.; Urbach, J.; Zobel, T.; Wolf, D. M.; Segawa, M.; Liesa, M.; Shirihai, O. S.; Weidtkamp-Peters, S., & Reichert, A. S. (2020). Cristae undergo continuous cycles of membrane remodelling in a MICOS-dependent manner. *EMBO Reports*, *21*(3), e49776. https://doi.org/10.15252/embr.201949776

Appendix

Kondadi, A. K.; Anand, R., & Reichert, A. S. (2020). Cristae Membrane Dynamics - A Paradigm Change. *Trends in Cell Biology*, *30*(12), 923–936. https://doi.org/10.1016/j.tcb.2020.08.008

König, T., & McBride, H. M. (2024). Mitochondrial-derived vesicles in metabolism, disease, and aging. *Cell Metabolism*, *36*(1), 21–35. https://doi.org/10.1016/j.cmet.2023.11.014

König, T.; Nolte, H.; Aaltonen, M. J.; Tatsuta, T.; Krols, M.; Stroh, T.; Langer, T., & McBride, H. M. (2021). Miros and DRP1 drive mitochondrial-derived vesicle biogenesis and promote quality control. *Nature Cell Biology*, *23*(12), 1271–1286. https://doi.org/10.1038/s41556-021-00798-4

Krais, J. J.; Wang, Y [Yifan]; Patel, P.; Basu, J.; Bernhardy, A. J., & Johnson, N. (2021). Rnf168-mediated localization of BARD1 recruits the BRCA1-PALB2 complex to DNA damage. *Nature Communications*, *12*(1), 5016. https://doi.org/10.1038/s41467-021-25346-4

Krakowczyk, M.; Lenkiewicz, A. M.; Sitarz, T.; Malinska, D.; Borrero, M.; Mussulini, B. H. M.; Linke, V.; Szczepankiewicz, A. A.; Biazik, J. M.; Wydrych, A.; Nieznanska, H.; Serwa, R. A.; Chacinska, A., & Bragoszewski, P. (2024). Oma1 protease eliminates arrested protein import intermediates upon mitochondrial depolarization. *The Journal of Cell Biology*, *223*(5). https://doi.org/10.1083/jcb.202306051

Krämer, L.; Dalheimer, N.; Räschle, M.; Storchová, Z.; Pielage, J.; Boos, F., & Herrmann, J. M. (2022). *MitoStores: Chaperone-controlled protein granules store mitochondrial precursors in the cytosol.* https://doi.org/10.1101/2022.08.02.502474

Krämer, L.; Dalheimer, N.; Räschle, M.; Storchová, Z.; Pielage, J.; Boos, F., & Herrmann, J. M. (2023). Mitostores: Chaperone-controlled protein granules store mitochondrial precursors in the cytosol. *The EMBO Journal*, *42*(7), e112309. https://doi.org/10.15252/embj.2022112309

Kremer, L. S., & Rehling, P. (2024). Coordinating mitochondrial translation with assembly of the OXPHOS complexes. *Human Molecular Genetics*, *33*(R1), R47-R52. https://doi.org/10.1093/hmg/ddae025

Kubitz, L.; Bitsch, S.; Zhao, X [Xiyan]; Schmitt, K.; Deweid, L.; Roehrig, A.; Barazzone, E. C.; Valerius, O.; Kolmar, H., & Béthune, J. (2022). Engineering of ultraID, a compact and hyperactive enzyme for proximity-dependent biotinylation in living cells. *Communications Biology*, *5*(1), 657. https://doi.org/10.1038/s42003-022-03604-5

Kücükköse, C.; Taskin, A. A.; Marada, A.; Brummer, T.; Dennerlein, S., & Vögtle, F.-N [Friederike-Nora] (2021). Functional coupling of presequence processing and degradation in human mitochondria. *The FEBS Journal*, *288*(2), 600–613. https://doi.org/10.1111/febs.15358

Kumar, A. V.; Mills, J., & Lapierre, L. R. (2022). Selective Autophagy Receptor p62/SQSTM1, a Pivotal Player in Stress and Aging. *Frontiers in Cell and Developmental Biology*, *10*, 793328. https://doi.org/10.3389/fcell.2022.793328

Kumar, A., & Shaha, C. (2018). Rbx1-mediated ubiquitination of SESN2 promotes cell death upon prolonged mitochondrial damage in SH-SY5Y neuroblastoma cells. *Molecular and Cellular Biochemistry*, *446*(1-2), 1–9. https://doi.org/10.1007/s11010-017-3267-7

Kunová, N.; Havalová, H.; Ondrovičová, G.; Stojkovičová, B.; Bauer, J. A.; Bauerová-Hlinková, V.; Pevala, V., & Kutejová, E. (2022). Mitochondrial Processing Peptidases-Structure, Function and the Role in Human Diseases. *International Journal of Molecular Sciences*, *23*(3). https://doi.org/10.3390/ijms23031297

Kutejová, E.; Kučera, T.; Matušková, A., & Janata, J. (2013). Mitochondrial Processing Peptidase. In *Handbook of Proteolytic Enzymes* (pp. 1435–1442). Elsevier. https://doi.org/10.1016/B978-0-12-382219-2.00323-9

Lazarou, M.; Jin, S. M.; Kane, L. A., & Youle, R. J. (2012). Role of PINK1 binding to the TOM complex and alternate intracellular membranes in recruitment and activation of the E3 ligase Parkin. *Developmental Cell*, *22*(2), 320–333. https://doi.org/10.1016/j.devcel.2011.12.014

Lechado-Terradas, A.; Schepers, S.; Zittlau, K. I.; Sharma, K.; Ok, O.; Fitzgerald, J. C.; Geimer, S.; Westermann, B.; Macek, B., & Kahle, P. J. (2022). Parkin-dependent mitophagy occurs via proteasome-dependent steps sequentially targeting separate mitochondrial sub-compartments for autophagy. *Autophagy Reports*, *1*(1), 576–602. https://doi.org/10.1080/27694127.2022.2143214

Lee, S [Sangho]; Tsai, Y. C.; Mattera, R.; Smith, W. J.; Kostelansky, M. S.; Weissman, A. M.; Bonifacino, J. S., & Hurley, J. H. (2006). Structural basis for ubiquitin recognition and autoubiquitination by Rabex-5. *Nature Structural & Molecular Biology*, *13*(3), 264–271. https://doi.org/10.1038/nsmb1064

Li, C [Chuhan]; Yan, Y.; Stork, O.; Shen, R., & Behnisch, T. (2025). The E3 Ubiquitin Ligase PRAJA1: A Key Regulator of Synaptic Dynamics and Memory Processes with Implications for Alzheimer's Disease. *International Journal of Molecular Sciences*, *26*(7). https://doi.org/10.3390/ijms26072909

Li, J [Jiaming]; Cai, Z.; Vaites, L. P.; Shen, N.; Mitchell, D. C.; Huttlin, E. L.; Paulo, J. A.; Harry, B. L., & Gygi, S. P. (2021). Proteome-wide mapping of short-lived proteins in human cells. *Molecular Cell*, *81*(22), 4722-4735.e5. https://doi.org/10.1016/j.molcel.2021.09.015

Li, Q [Qiang]; Gao, S.; Kang, Z.; Zhang, M.; Zhao, X [Xin]; Zhai, Y.; Huang, J.; Yang, G.-Y.; Sun, W., & Wang, J [Jian] (2018). Rapamycin Enhances Mitophagy and Attenuates

Apoptosis After Spinal Ischemia-Reperfusion Injury. *Frontiers in Neuroscience*, *12*, 865. https://doi.org/10.3389/fnins.2018.00865

Li, W [Wen]; Zhang, X [Xingli]; Zhuang, H.; Chen, H [He-ge]; Chen, Y [Yinqin]; Tian, W.; Wu, W.; Li, Y [Ying]; Wang, S [Sijie]; Zhang, L [Liangqing]; Chen, Y [Yusen]; Li, L [Longxuan]; Zhao, B.; Sui, S.; Hu, Z., & Du Feng (2014). Microrna-137 is a novel hypoxia-responsive microRNA that inhibits mitophagy via regulation of two mitophagy receptors FUNDC1 and NIX. *The Journal of Biological Chemistry*, *289*(15), 10691–10701. https://doi.org/10.1074/jbc.M113.537050

Li, X.; Straub, J.; Medeiros, T. C.; Mehra, C.; Brave, F. den; Peker, E.; Atanassov, I.; Stillger, K.; Michaelis, J. B.; Burbridge, E.; Adrain, C.; Münch, C.; Riemer, J.; Becker, T., & Pernas, L. F. (2022). Mitochondria shed their outer membrane in response to infection-induced stress. *Science*, *375*(6577), eabi4343. https://doi.org/10.1126/science.abi4343

Li, Y [Yanchang]; Dammer, E. B.; Gao, Y.; Lan, Q.; Villamil, M. A.; Duong, D. M.; Zhang, C [Chengpu]; Ping, L.; Lauinger, L.; Flick, K.; Xu, Z [Zhongwei]; Wei, W [Wei]; Xing, X.; Chang, L.; Jin, J.; Hong, X.; Zhu, Y [Yunping]; Wu, J.; Deng, Z [Zixin], . . . Xu, P. (2019). Proteomics Links Ubiquitin Chain Topology Change to Transcription Factor Activation. *Molecular Cell*, *76*(1), 126-137.e7. https://doi.org/10.1016/j.molcel.2019.07.001

Liao, Y.; Sumara, I., & Pangou, E. (2022). Non-proteolytic ubiquitylation in cellular signaling and human disease. *Communications Biology*, *5*(1), 114. https://doi.org/10.1038/s42003-022-03060-1

Liess, A. K. L.; Kucerova, A.; Schweimer, K.; Yu, L.; Roumeliotis, T. I.; Diebold, M.; Dybkov, O.; Sotriffer, C.; Urlaub, H.; Choudhary, J. S.; Mansfeld, J., & Lorenz, S. (2019). Autoinhibition Mechanism of the Ubiquitin-Conjugating Enzyme UBE2S by Autoubiquitination. *Structure (London, England : 1993)*, *27*(8), 1195-1210.e7. https://doi.org/10.1016/j.str.2019.05.008

Lignitto, L.; Carlucci, A.; Sepe, M.; Stefan, E.; Cuomo, O.; Nisticò, R.; Scorziello, A.; Savoia, C.; Garbi, C.; Annunziato, L., & Feliciello, A. (2011). Control of PKA stability and signalling by the RING ligase praja2. *Nature Cell Biology*, *13*(4), 412–422. https://doi.org/10.1038/ncb2209

Lim, G. G., & Lim, K.-L. (2017). Parkin-independent mitophagy-FKBP8 takes the stage. *EMBO Reports*, *18*(6), 864–865. https://doi.org/10.15252/embr.201744313

Lin, D. Y.; Diao, J.; Zhou, D [Daoguo], & Chen, J [Jue] (2011). Biochemical and structural studies of a HECT-like ubiquitin ligase from Escherichia coli O157:H7. *The Journal of Biological Chemistry*, *286*(1), 441–449. https://doi.org/10.1074/jbc.M110.167643

Lin, M.; Zhao, Z.; Yang, Z.; Meng, Q.; Tan, P.; Xie, W.; Qin, Y [Yunfei]; Wang, R.-F., & Cui, J [Jun] (2016). Usp38 Inhibits Type I Interferon Signaling by Editing TBK1 Ubiquitination through NLRP4 Signalosome. *Molecular Cell*, *64*(2), 267–281. https://doi.org/10.1016/j.molcel.2016.08.029

Lin, Y.-C.; Nihongaki, Y.; Liu, T.-Y.; Razavi, S.; Sato, M., & Inoue, T. (2013). Rapidly reversible manipulation of molecular activity with dual chemical dimerizers. *Angewandte Chemie (International Ed. In English)*, *52*(25), 6450–6454. https://doi.org/10.1002/anie.201301219

Lithgow, T., & Schneider, A. (2010). Evolution of macromolecular import pathways in mitochondria, hydrogenosomes and mitosomes. *Philosophical Transactions of the Royal Society of London. Series B, Biological Sciences*, *365*(1541), 799–817. https://doi.org/10.1098/rstb.2009.0167

Liu, C.; Liu, W [Weixiao]; Ye, Y., & Li, W [Wei] (2017). Ufd2p synthesizes branched ubiquitin chains to promote the degradation of substrates modified with atypical chains. *Nature Communications*, *8*, 14274. https://doi.org/10.1038/ncomms14274

Lofrumento, D. D.; La Piana, G.; Abbrescia, D. I.; Palmitessa, V.; La Pesa, V.; Marzulli, D., & Lofrumento, N. E. (2011). Valinomycin induced energy-dependent mitochondrial swelling, cytochrome c release, cytosolic NADH/cytochrome c oxidation and apoptosis. *Apoptosis : An International Journal on Programmed Cell Death*, *16*(10), 1004–1013. https://doi.org/10.1007/s10495-011-0628-7

Lv, X.-B.; Xie, F.; Hu, K.; Wu, Y [Yuanzhong]; Cao, L.-L.; Han, X.; Sang, Y.; Zeng, Y.-X., & Kang, T. (2010). Damaged DNA-binding protein 1 (DDB1) interacts with Cdh1 and modulates the function of APC/CCdh1. *The Journal of Biological Chemistry*, *285*(24), 18234–18240. https://doi.org/10.1074/jbc.M109.094144

MacKenzie, J. A., & Payne, R. M. (2007). Mitochondrial protein import and human health and disease. *Biochimica Et Biophysica Acta*, *1772*(5), 509–523. https://doi.org/10.1016/j.bbadis.2006.12.002

Madiraju, C.; Novack, J. P.; Reed, J. C., & Matsuzawa, S.-I. (2022). K63 ubiquitination in immune signaling. *Trends in Immunology*, *43*(2), 148–162. https://doi.org/10.1016/j.it.2021.12.005

Maniccia, A. W.; Lewis, C.; Begum, N.; Xu, J [Jingyao]; Cui, J [Jianqi]; Chipitsyna, G.; Aysola, K.; Reddy, V.; Bhat, G.; Fujimura, Y.; Henderson, B.; Reddy, E. S. P., & Rao, V. N. (2009). Mitochondrial localization, ELK-1 transcriptional regulation and growth inhibitory functions of BRCA1, BRCA1a, and BRCA1b proteins. *Journal of Cellular Physiology*, *219*(3), 634–641. https://doi.org/10.1002/jcp.21708

Mårtensson, C. U.; Priesnitz, C.; Song, J [Jiyao]; Ellenrieder, L.; Doan, K. N.; Boos, F.; Floerchinger, A.; Zufall, N.; Oeljeklaus, S.; Warscheid, B., & Becker, T. (2019).

Mitochondrial protein translocation-associated degradation. *Nature*, *569*(7758), 679–683. https://doi.org/10.1038/s41586-019-1227-y

Martinez-Caballero, S.; Grigoriev, S. M.; Herrmann, J. M.; Campo, M. L., & Kinnally, K. W. (2007). Tim17p regulates the twin pore structure and voltage gating of the mitochondrial protein import complex TIM23. *The Journal of Biological Chemistry*, *282*(6), 3584–3593. https://doi.org/10.1074/jbc.M607551200

Maruszczak, K. K.; Draczkowski, P.; Wnorowski, A., & Chacinska, A. (2024). Structure prediction analysis of human core TIM23 complex reveals conservation of the protein translocation mechanism. *FEBS Open Bio*, *14*(10), 1656–1667. https://doi.org/10.1002/2211-5463.13840

Mathieson, T.; Franken, H.; Kosinski, J.; Kurzawa, N.; Zinn, N.; Sweetman, G.; Poeckel, D.; Ratnu, V. S.; Schramm, M.; Becher, I.; Steidel, M.; Noh, K.-M.; Bergamini, G.; Beck, M.; Bantscheff, M., & Savitski, M. M. (2018). Systematic analysis of protein turnover in primary cells. *Nature Communications*, *9*(1), 689. https://doi.org/10.1038/s41467-018-03106-1

Matouschek, A.; Azem, A [A.]; Ratliff, K.; Glick, B. S.; Schmid, K., & Schatz, G. (1997). Active unfolding of precursor proteins during mitochondrial protein import. *The EMBO Journal*, *16*(22), 6727–6736. https://doi.org/10.1093/emboj/16.22.6727

Matsuda, N.; Sato, S.; Shiba, K.; Okatsu, K.; Saisho, K.; Gautier, C. A.; Sou, Y.-S.; Saiki, S.; Kawajiri, S.; Sato, F.; Kimura, M.; Komatsu, M.; Hattori, N., & Tanaka, K. (2010). Pink1 stabilized by mitochondrial depolarization recruits Parkin to damaged mitochondria and activates latent Parkin for mitophagy. *The Journal of Cell Biology*, *189*(2), 211–221. https://doi.org/10.1083/jcb.200910140

Mauro-Lizcano, M.; Esteban-Martínez, L.; Seco, E.; Serrano-Puebla, A.; Garcia-Ledo, L.; Figueiredo-Pereira, C.; Vieira, H. L. A., & Boya, P. (2015). New method to assess mitophagy flux by flow cytometry. *Autophagy*, *11*(5), 833–843. https://doi.org/10.1080/15548627.2015.1034403

McFarquhar, M.; Elliott, R.; McKie, S.; Thomas, E.; Downey, D.; Mekli, K.; Toth, Z. G.; Anderson, I. M.; Deakin, J. F. W., & Juhasz, G. (2014). Tomm40 rs2075650 may represent a new candidate gene for vulnerability to major depressive disorder. *Neuropsychopharmacology : Official Publication of the American College of Neuropsychopharmacology*, *39*(7), 1743–1753. https://doi.org/10.1038/npp.2014.22

Meisinger, C [C.]; Ryan, M. T.; Hill, K.; Model, K.; Lim, J. H.; Sickmann, A [A.]; Müller, H.; Meyer, H. E [H. E.]; Wagner, R., & Pfanner, N [N.] (2001). Protein import channel of the outer mitochondrial membrane: A highly stable Tom40-Tom22 core structure differentially interacts with preproteins, small tom proteins, and import receptors.

Molecular and Cellular Biology, *21*(7), 2337–2348. https://doi.org/10.1128/MCB.21.7.2337-2348.2001

Metzger, M. B.; Pruneda, J. N.; Klevit, R. E., & Weissman, A. M. (2014). Ring-type E3 ligases: Master manipulators of E2 ubiquitin-conjugating enzymes and ubiquitination. *Biochimica Et Biophysica Acta*, *1843*(1), 47–60. https://doi.org/10.1016/j.bbamcr.2013.05.026

Meurant, S.; Mauclet, L.; Dieu, M.; Arnould, T.; Eyckerman, S., & Renard, P. (2023). Endogenous TOM20 Proximity Labeling: A Swiss-Knife for the Study of Mitochondrial Proteins in Human Cells. *International Journal of Molecular Sciences*, *24*(11). https://doi.org/10.3390/ijms24119604

Meyer, H.-J., & Rape, M. (2014). Enhanced protein degradation by branched ubiquitin chains. *Cell*, *157*(4), 910–921. https://doi.org/10.1016/j.cell.2014.03.037

Meylan, E.; Curran, J.; Hofmann, K.; Moradpour, D.; Binder, M.; Bartenschlager, R., & Tschopp, J. (2005). Cardif is an adaptor protein in the RIG-I antiviral pathway and is targeted by hepatitis C virus. *Nature*, *437*(7062), 1167–1172. https://doi.org/10.1038/nature04193

Michel, M. A.; Elliott, P. R.; Swatek, K. N.; Simicek, M.; Pruneda, J. N.; Wagstaff, J. L.; Freund, S. M. V., & Komander, D. (2015). Assembly and specific recognition of k29- and k33-linked polyubiquitin. *Molecular Cell*, *58*(1), 95–109. https://doi.org/10.1016/j.molcel.2015.01.042

Michel, M. A.; Swatek, K. N.; Hospenthal, M. K., & Komander, D. (2017). Ubiquitin Linkage-Specific Affimers Reveal Insights into K6-Linked Ubiquitin Signaling. *Molecular Cell*, *68*(1), 233-246.e5. https://doi.org/10.1016/j.molcel.2017.08.020

Mishra, G.; Wang, X [Xiaowen]; Fitzpatrick, E.; Ghosh, A., & Chen, X. J. (2025). The Mitochondrial F-box protein 1 and DJ-1 homolog HSP31 support cellular proteostasis during mitochondrial protein import clogging. *BioRxiv : The Preprint Server for Biology.* Advance online publication. https://doi.org/10.1101/2025.10.13.682092

Miyahara, K.; Takano, N.; Yamada, Y.; Kazama, H.; Tokuhisa, M.; Hino, H.; Fujita, K.; Barroga, E.; Hiramoto, M.; Handa, H.; Kuroda, M.; Ishikawa, T., & Miyazawa, K. (2021). Brca1 degradation in response to mitochondrial damage in breast cancer cells. *Scientific Reports*, *11*(1), 8735. https://doi.org/10.1038/s41598-021-87698-7

Miyata, N.; Tang, Z [Zhiye]; Conti, M. A.; Johnson, M. E.; Douglas, C. J.; Hasson, S. A.; Damoiseaux, R.; Chang, C.-E. A., & Koehler, C. M. (2017). Adaptation of a Genetic Screen Reveals an Inhibitor for Mitochondrial Protein Import Component Tim44. *The Journal of Biological Chemistry*, *292*(13), 5429–5442. https://doi.org/10.1074/jbc.M116.770131

Appendix

Mossmann, D.; Meisinger, C [Chris], & Vögtle, F.-N [F-Nora] (2012). Processing of mitochondrial presequences. *Biochimica Et Biophysica Acta*, *1819*(9-10), 1098–1106. https://doi.org/10.1016/j.bbagrm.2011.11.007

Moura, J. P.; Oliveira, P. J., & Urbano, A. M. (2025). Mitochondria: An overview of their origin, genome, architecture, and dynamics. *Biochimica Et Biophysica Acta. Molecular Basis of Disease*, *1871*(5), 167803. https://doi.org/10.1016/j.bbadis.2025.167803

Murschall, L. M.; Peker, E.; MacVicar, T.; Langer, T., & Riemer, J. (2021). Protein Import Assay into Mitochondria Isolated from Human Cells. *Bio-Protocol*, *11*(12), e4057. https://doi.org/10.21769/BioProtoc.4057

Muthukumar, G., & Weissman, J. S. (2025). Shaping the composition of the mitochondrial outer membrane. *Nature Cell Biology*, *27*(6), 890–901. https://doi.org/10.1038/s41556-025-01683-0

Nargund, A. M.; Fiorese, C. J.; Pellegrino, M. W.; Deng, P., & Haynes, C. M. (2015). Mitochondrial and nuclear accumulation of the transcription factor ATFS-1 promotes OXPHOS recovery during the UPR(mt). *Molecular Cell*, *58*(1), 123–133. https://doi.org/10.1016/j.molcel.2015.02.008

Nauerz, C.; Pines, O., & Herrmann, J. M. (2025). Biogenesis and function of the mitochondrial solute carrier (SLC25) family in yeast. *Biological Chemistry.* Advance online publication. https://doi.org/10.1515/hsz-2025-0152

Needs, H. I.; Glover, E.; Pereira, G. C.; Witt, A.; Hübner, W.; Dodding, M. P.; Henley, J. M., & Collinson, I. (2024). Rescue of mitochondrial import failure by intercellular organellar transfer. *Nature Communications*, *15*(1), 988. https://doi.org/10.1038/s41467-024-45283-2

Neuspiel, M.; Schauss, A. C.; Braschi, E.; Zunino, R.; Rippstein, P.; Rachubinski, R. A.; Andrade-Navarro, M. A., & McBride, H. M. (2008). Cargo-selected transport from the mitochondria to peroxisomes is mediated by vesicular carriers. *Current Biology : CB*, *18*(2), 102–108. https://doi.org/10.1016/j.cub.2007.12.038

Nguyen, T. N [Thanh N.]; Padman, B. S., & Lazarou, M. (2016). Deciphering the Molecular Signals of PINK1/Parkin Mitophagy. *Trends in Cell Biology*, *26*(10), 733–744. https://doi.org/10.1016/j.tcb.2016.05.008

Nibe, Y.; Oshima, S.; Kobayashi, M.; Maeyashiki, C.; Matsuzawa, Y.; Otsubo, K.; Matsuda, H.; Aonuma, E.; Nemoto, Y.; Nagaishi, T.; Okamoto, R.; Tsuchiya, K.; Nakamura, T.; Nakada, S., & Watanabe, M. (2018). Novel polyubiquitin imaging system, PolyUb-FC, reveals that K33-linked polyubiquitin is recruited by SQSTM1/p62. *Autophagy*, *14*(2), 347–358. https://doi.org/10.1080/15548627.2017.1407889

Nicolas, E.; Tricarico, R.; Savage, M.; Golemis, E. A., & Hall, M. J. (2019). Disease-Associated Genetic Variation in Human Mitochondrial Protein Import. *American Journal of Human Genetics*, *104*(5), 784–801. https://doi.org/10.1016/j.ajhg.2019.03.019

Niu, K.; Fang, H.; Chen, Z.; Zhu, Y [Yuqi]; Tan, Q.; Di Wei; Li, Y [Yueyang]; Balajee, A. S., & Zhao, Y [Yongliang] (2020). Usp33 deubiquitinates PRKN/parkin and antagonizes its role in mitophagy. *Autophagy*, *16*(4), 724–734. https://doi.org/10.1080/15548627.2019.1656957

Niyazov, D. M.; Kahler, S. G., & Frye, R. E. (2016). Primary Mitochondrial Disease and Secondary Mitochondrial Dysfunction: Importance of Distinction for Diagnosis and Treatment. *Molecular Syndromology*, *7*(3), 122–137. https://doi.org/10.1159/000446586

Nowinski, S. M.; Solmonson, A.; Rusin, S. F.; Maschek, J. A.; Bensard, C. L.; Fogarty, S.; Jeong, M.-Y.; Lettlova, S.; Berg, J. A.; Morgan, J. T.; Ouyang, Y.; Naylor, B. C.; Paulo, J. A.; Funai, K.; Cox, J. E.; Gygi, S. P.; Winge, D. R.; DeBerardinis, R. J., & Rutter, J. (2020). Mitochondrial fatty acid synthesis coordinates oxidative metabolism in mammalian mitochondria. *ELife*, *9.* https://doi.org/10.7554/eLife.58041

Nsiah-Sefaa, A., & McKenzie, M. (2016). Combined defects in oxidative phosphorylation and fatty acid β-oxidation in mitochondrial disease. *Bioscience Reports*, *36*(2). https://doi.org/10.1042/BSR20150295

Ohtake, F.; Tsuchiya, H.; Saeki, Y., & Tanaka, K. (2018). K63 ubiquitylation triggers proteasomal degradation by seeding branched ubiquitin chains. *Proceedings of the National Academy of Sciences*, *115*(7), E1401-E1408. https://doi.org/10.1073/pnas.1716673115

Oikawa, D.; Sato, Y.; Ito, H., & Tokunaga, F. (2020). Linear Ubiquitin Code: Its Writer, Erasers, Decoders, Inhibitors, and Implications in Disorders. *International Journal of Molecular Sciences*, *21*(9). https://doi.org/10.3390/ijms21093381

Okamoto, M.; Kouwaki, T.; Fukushima, Y., & Oshiumi, H. (2017). Regulation of RIG-I Activation by K63-Linked Polyubiquitination. *Frontiers in Immunology*, *8*, 1942. https://doi.org/10.3389/fimmu.2017.01942

Okumoto, K.; Noda, H., & Fujiki, Y. (2014). Distinct modes of ubiquitination of peroxisome-targeting signal type 1 (PTS1) receptor Pex5p regulate PTS1 protein import. *The Journal of Biological Chemistry*, *289*(20), 14089–14108. https://doi.org/10.1074/jbc.M113.527937

Ono, H.; Gruhler, A.; Stuart, R. A.; Guiard, B [B.]; Schwarz, E., & Neupert, W. (1995). Sorting of cytochrome b2 to the intermembrane space of mitochondria. Kinetic analysis of

intermediates demonstrates passage through the matrix. *Journal of Biological Chemistry*, *270*(28), 16932–16938. https://doi.org/10.1074/jbc.270.28.16932

Oshiumi, H.; Matsumoto, M.; Hatakeyama, S., & Seya, T. (2009). Riplet/rnf135, a RING finger protein, ubiquitinates RIG-I to promote interferon-beta induction during the early phase of viral infection. *Journal of Biological Chemistry*, *284*(2), 807–817. https://doi.org/10.1074/jbc.M804259200

Otera, H.; Taira, Y.; Horie, C.; Suzuki, Y.; Suzuki, H.; Setoguchi, K.; Kato, H.; Oka, T., & Mihara, K. (2007). A novel insertion pathway of mitochondrial outer membrane proteins with multiple transmembrane segments. *The Journal of Cell Biology*, *179*(7), 1355–1363. https://doi.org/10.1083/jcb.200702143

Palicharla, V. R., & Maddika, S. (2015). Hace1 mediated K27 ubiquitin linkage leads to YB-1 protein secretion. *Cellular Signalling*, *27*(12), 2355–2362. https://doi.org/10.1016/j.cellsig.2015.09.001

Palikaras, K.; Lionaki, E., & Tavernarakis, N. (2018). Mechanisms of mitophagy in cellular homeostasis, physiology and pathology. *Nature Cell Biology*, *20*(9), 1013–1022. https://doi.org/10.1038/s41556-018-0176-2

Parenteau, J.; Tsang, J.; Downs, S. R.; Zhou, D [Delong]; Scott, M. S.; Pleiss, J. A., & Abou Elela, S. (2025). Cells resist starvation through a nutrient stress splice switch. *Nucleic Acids Research*, *53*(12). https://doi.org/10.1093/nar/gkaf525

Park, G. H.; Park, H. in; Shin, D., & Chung, K. C. (2025). Ubiquitin-Specific Protease 20 Promotes CCCP-Induced Mitophagy Through Deubiquitination and Stabilization of Serine/Threonine Protein Kinase PINK1. *Journal of Molecular Neuroscience : MN*, *75*(4), 162. https://doi.org/10.1007/s12031-025-02457-x

Peker, E.; Weiss, K.; Song, J [Jiyao]; Zarges, C.; Gerlich, S.; Boehm, V.; Trifunovic, A.; Langer, T.; Gehring, N. H.; Becker, T., & Riemer, J. (2023). A two-step mitochondrial import pathway couples the disulfide relay with matrix complex I biogenesis. *The Journal of Cell Biology*, *222*(7). https://doi.org/10.1083/jcb.202210019

Peng, J.; Schwartz, D.; Elias, J. E.; Thoreen, C. C.; Cheng, D.; Marsischky, G.; Roelofs, J.; Finley, D [Daniel], & Gygi, S. P. (2003). A proteomics approach to understanding protein ubiquitination. *Nature Biotechnology*, *21*(8), 921–926. https://doi.org/10.1038/nbt849

Pettersen, E. F.; Goddard, T. D.; Huang, C. C.; Couch, G. S.; Greenblatt, D. M.; Meng, E. C., & Ferrin, T. E. (2004). Ucsf Chimera--a visualization system for exploratory research and analysis. *Journal of Computational Chemistry*, *25*(13), 1605–1612. https://doi.org/10.1002/jcc.20084

Pfanner, N [Nikolaus]; den Brave, F., & Becker, T. (2025). Mitochondrial protein import stress. *Nature Cell Biology*, *27*(2), 188–201. https://doi.org/10.1038/s41556-024-01590-w

Phipson, B.; Lee, S [Stanley]; Majewski, I. J.; Alexander, W. S., & Smyth, G. K. (2016). Robust hyperparameter estimation protects against hypervariable genes and improves power to detect differential expression. *The Annals of Applied Statistics*, *10*(2), 946–963. https://doi.org/10.1214/16-AOAS920

Phu, L.; Rose, C. M.; Tea, J. S.; Wall, C. E.; Verschueren, E.; Cheung, T. K.; Kirkpatrick, D. S., & Bingol, B. (2020). Dynamic Regulation of Mitochondrial Import by the Ubiquitin System. *Molecular Cell*, *77*(5), 1107-1123.e10. https://doi.org/10.1016/j.molcel.2020.02.012

Picca, A.; Faitg, J.; Auwerx, J.; Ferrucci, L., & D'Amico, D. (2023). Mitophagy in human health, ageing and disease. *Nature Metabolism*, *5*(12), 2047–2061. https://doi.org/10.1038/s42255-023-00930-8

Pizzorno, J. (2014). Mitochondria-Fundamental to Life and Health. *Integrative Medicine (Encinitas, Calif.)*, *13*(2), 8–15.

Pruneda, J. N., & Damgaard, R. B. (2021). Ester-linked ubiquitination by HOIL-1 controls immune signalling by shaping the linear ubiquitin landscape. *The FEBS Journal*, *288*(20), 5903–5908. https://doi.org/10.1111/febs.16118

Puri, R.; Cheng, X.-T.; Lin, M.-Y.; Huang, N., & Sheng, Z.-H. (2020). Defending stressed mitochondria: Uncovering the role of MUL1 in suppressing neuronal mitophagy. *Autophagy*, *16*(1), 176–178. https://doi.org/10.1080/15548627.2019.1687216

Qin, Y [Yue]; Zhou, M.-T.; Hu, M.-M.; Hu, Y.-H.; Zhang, J [Jing]; Guo, L.; Zhong, B., & Shu, H.-B. (2014). Rnf26 temporally regulates virus-triggered type I interferon induction by two distinct mechanisms. *PLoS Pathogens*, *10*(9), e1004358. https://doi.org/10.1371/journal.ppat.1004358

Radford, A. (1991). Methods in Yeast Genetics — A Laboratory Course Manual. *Biochemical Education*, *19*(2), 101–102. https://doi.org/10.1016/0307-4412(91)90039-B

Rao, D. M.; Horton, E. R.; Barrington, C. L.; Briney, C. A.; Henriksen, J. C.; Martinez-Seidel, F.; Morrison, E. J.; Sterling, E. M.; Provencio, E. D.; Harris, M.; Allen, E.; Hesselberth, J. R., & Rissland, O. S. (2025). Systematic identification and characterization of eukaryotic and viral 2A peptide-bond-skipping sequences. *Cell Reports*, *44*(7), 115822. https://doi.org/10.1016/j.celrep.2025.115822

Rappsilber, J.; Ishihama, Y., & Mann, M. (2003). Stop and go extraction tips for matrix-assisted laser desorption/ionization, nanoelectrospray, and LC/MS sample pretreatment in proteomics. *Analytical Chemistry*, *75*(3), 663–670. https://doi.org/10.1021/ac026117i

Appendix

Rassow, J.; Guiard, B [B.]; Wienhues, U.; Herzog, V.; Hartl, F. U [F. U.], & Neupert, W. (1989). Translocation arrest by reversible folding of a precursor protein imported into mitochondria. A means to quantitate translocation contact sites. *Journal of Cell Biology*, *109*(4 Pt 1), 1421–1428. https://doi.org/10.1083/jcb.109.4.1421

Rath, S.; Sharma, R.; Gupta, R.; Ast, T.; Chan, C.; Durham, T. J.; Goodman, R. P.; Grabarek, Z.; Haas, M. E.; Hung, W. H. W.; Joshi, P. R.; Jourdain, A. A.; Kim, S. H.; Kotrys, A. V.; Lam, S. S.; McCoy, J. G.; Meisel, J. D.; Miranda, M.; Panda, A., . . . Mootha, V. K. (2021). Mitocarta3.0: An updated mitochondrial proteome now with sub-organelle localization and pathway annotations. *Nucleic Acids Research*, *49*(D1), D1541-D1547. https://doi.org/10.1093/nar/gkaa1011

Raval, P. K.; Martin, W. F., & Gould, S. B. (2023). Mitochondrial evolution: Gene shuffling, endosymbiosis, and signaling. *Science Advances*, *9*(32), eadj4493. https://doi.org/10.1126/sciadv.adj4493

Ravanelli, S.; Brave, F. den, & Hoppe, T. (2020). Mitochondrial Quality Control Governed by Ubiquitin. *Frontiers in Cell and Developmental Biology*, *8*, 270. https://doi.org/10.3389/fcell.2020.00270

Renz, C.; Asimaki, E.; Meister, C.; Albanèse, V.; Petriukov, K.; Krapoth, N. C.; Wegmann, S.; Wollscheid, H.-P.; Wong, R. P.; Fulzele, A.; Chen, J.-X.; Léon, S., & Ulrich, H. D. (2024). Ubiquiton-An inducible, linkage-specific polyubiquitylation tool. *Molecular Cell*, *84*(2), 386-400.e11. https://doi.org/10.1016/j.molcel.2023.11.016

Ries, L. K.; Sander, B.; Deol, K. K.; Letzelter, M.-A.; Strieter, E. R [Eric Robert], & Lorenz, S. (2019). Analysis of ubiquitin recognition by the HECT ligase E6AP provides insight into its linkage specificity. *The Journal of Biological Chemistry*, *294*(15), 6113–6129. https://doi.org/10.1074/jbc.RA118.007014

Rieusset, J. (2018). The role of endoplasmic reticulum-mitochondria contact sites in the control of glucose homeostasis: An update. *Cell Death & Disease*, *9*(3), 388. https://doi.org/10.1038/s41419-018-0416-1

Roberts, R. F.; Bayne, A. N.; Goiran, T.; Lévesque, D.; Boisvert, F.-M.; Trempe, J.-F., & Fon, E. A. (2021). Proteomic Profiling of Mitochondrial-Derived Vesicles in Brain Reveals Enrichment of Respiratory Complex Sub-assemblies and Small TIM Chaperones. *Journal of Proteome Research*, *20*(1), 506–517. https://doi.org/10.1021/acs.jproteome.0c00506

Roger, A. J.; Muñoz-Gómez, S. A., & Kamikawa, R. (2017). The Origin and Diversification of Mitochondria. *Current Biology : CB*, *27*(21), R1177-R1192. https://doi.org/10.1016/j.cub.2017.09.015

Rojo, E. E.; Guiard, B [B.]; Neupert, W., & Stuart, R. A. (1998). Sorting of D-lactate dehydrogenase to the inner membrane of mitochondria. Analysis of topogenic signal

and energetic requirements. *The Journal of Biological Chemistry*, *273*(14), 8040–8047. https://doi.org/10.1074/jbc.273.14.8040

Ryan, T. A.; Phillips, E. O.; Collier, C. L.; Jb Robinson, A.; Routledge, D.; Wood, R. E.; Assar, E. A., & Tumbarello, D. A. (2020). Tollip coordinates Parkin-dependent trafficking of mitochondrial-derived vesicles. *The EMBO Journal*, *39*(11), e102539. https://doi.org/10.15252/embj.2019102539

Sakaue, H.; Shiota, T.; Ishizaka, N.; Kawano, S.; Tamura, Y.; Tan, K. S.; Imai, K.; Motono, C.; Hirokawa, T.; Taki, K.; Miyata, N.; Kuge, O.; Lithgow, T., & Endo, T [Toshiya] (2019). Porin Associates with Tom22 to Regulate the Mitochondrial Protein Gate Assembly. *Molecular Cell*, *73*(5), 1044-1055.e8. https://doi.org/10.1016/j.molcel.2019.01.003

Sap, K. A.; Guler, A. T.; Bury, A.; Dekkers, D.; Demmers, J. A. A., & Reits, E. A. (2021). Identification of Full-Length Wild-Type and Mutant Huntingtin Interacting Proteins by Crosslinking Immunoprecipitation in Mice Brain Cortex. *Journal of Huntington's Disease*, *10*(3), 335–347. https://doi.org/10.3233/JHD-210476

Sayson, S. L.; Fan, J.-N.; Ku, C.-L.; Lo, J.-F., & Chou, S.-H. (2024). Dnaja3 regulates B cell development and immune function. *Biomedical Journal*, *47*(2), 100628. https://doi.org/10.1016/j.bj.2023.100628

Scaglione, K. M.; Bansal, P. K.; Deffenbaugh, A. E.; Kiss, A.; Moore, J. M.; Korolev, S.; Cocklin, R.; Goebl, M.; Kitagawa, K., & Skowyra, D. (2007). Scf E3-mediated autoubiquitination negatively regulates activity of Cdc34 E2 but plays a nonessential role in the catalytic cycle in vitro and in vivo. *Molecular and Cellular Biology*, *27*(16), 5860–5870. https://doi.org/10.1128/MCB.01555-06

Schäfer, J. A.; Bozkurt, S.; Michaelis, J. B.; Klann, K., & Münch, C. (2022). Global mitochondrial protein import proteomics reveal distinct regulation by translation and translocation machinery. *Molecular Cell*, *82*(2), 435-446.e7. https://doi.org/10.1016/j.molcel.2021.11.004

Schiefer, S., & Hale, B. G. (2024). Proximal protein landscapes of the type I interferon signaling cascade reveal negative regulation by PJA2. *Nature Communications*, *15*(1), 4484. https://doi.org/10.1038/s41467-024-48800-5

Schiff, M.; Haberberger, B.; Xia, C.; Mohsen, A.-W.; Goetzman, E. S.; Wang, Y [Yudong]; Uppala, R.; Zhang, Y [Yuxun]; Karunanidhi, A.; Prabhu, D.; Alharbi, H.; Prochownik, E. V.; Haack, T.; Häberle, J.; Munnich, A.; Rötig, A.; Taylor, R. W.; Nicholls, R. D.; Kim, J.-J., . . . Vockley, J. (2015). Complex I assembly function and fatty acid oxidation enzyme activity of ACAD9 both contribute to disease severity in ACAD9 deficiency. *Human Molecular Genetics*, *24*(11), 3238–3247. https://doi.org/10.1093/hmg/ddv074

Appendix

Schifferer, M.; Feng, S.; Stein, F [F.], & Schultz, C. (2017). Reversible Chemical Dimerization by rCD1. *Methods in Enzymology*, *583*, 173–195. https://doi.org/10.1016/bs.mie.2016.10.035

Schmidt, O.; Pfanner, N [Nikolaus], & Meisinger, C [Chris] (2010). Mitochondrial protein import: From proteomics to functional mechanisms. *Nature Reviews. Molecular Cell Biology*, *11*(9), 655–667. https://doi.org/10.1038/nrm2959

Schneider-Poetsch, T.; Ju, J.; Eyler, D. E.; Dang, Y.; Bhat, S.; Merrick, W. C.; Green, R.; Shen, B., & Liu, J. O. (2010). Inhibition of eukaryotic translation elongation by cycloheximide and lactimidomycin. *Nature Chemical Biology*, *6*(3), 209–217. https://doi.org/10.1038/nchembio.304

Schuberth, C.; Richly, H.; Rumpf, S., & Buchberger, A. (2004). Shp1 and Ubx2 are adaptors of Cdc48 involved in ubiquitin-dependent protein degradation. *EMBO Reports*, *5*(8), 818–824. https://doi.org/10.1038/sj.embor.7400203

Sekine, S., & Youle, R. J. (2018). Pink1 import regulation; a fine system to convey mitochondrial stress to the cytosol. *BMC Biology*, *16*(1), 2. https://doi.org/10.1186/s12915-017-0470-7

Shakya, V. P.; Barbeau, W. A.; Xiao, T.; Knutson, C. S.; Schuler, M. H., & Hughes, A. L. (2021). A nuclear-based quality control pathway for non-imported mitochondrial proteins. *ELife*, *10.* https://doi.org/10.7554/eLife.61230

Shearer, R. F.; Typas, D.; Coscia, F.; Schovsbo, S.; Kruse, T.; Mund, A., & Mailand, N. (2022). K27-linked ubiquitylation promotes p97 substrate processing and is essential for cell proliferation. *The EMBO Journal*, *41*(9), e110145. https://doi.org/10.15252/embj.2021110145

Shen, K.; Pender, C. L.; Bar-Ziv, R.; Zhang, H [Hanlin]; Wickham, K.; Willey, E.; Durieux, J.; Ahmad, Q., & Dillin, A. (2022). Mitochondria as Cellular and Organismal Signaling Hubs. *Annual Review of Cell and Developmental Biology*, *38*, 179–218. https://doi.org/10.1146/annurev-cellbio-120420-015303

Shi, H.-X.; Liu, X.; Wang, Q.; Tang, P.-P.; Liu, X.-Y.; Shan, Y.-F., & Wang, C. (2011). Mitochondrial ubiquitin ligase MARCH5 promotes TLR7 signaling by attenuating TANK action. *PLoS Pathogens*, *7*(5), e1002057. https://doi.org/10.1371/journal.ppat.1002057

Shiota, T.; Maruyama, M.; Miura, M.; Tamura, Y.; Yamano, K.; Esaki, M [Masatoshi], & Endo, T [Toshiya] (2012). The Tom40 assembly process probed using the attachment of different intramitochondrial sorting signals. *Molecular Biology of the Cell*, *23*(20), 3936–3947. https://doi.org/10.1091/mbc.E12-03-0202

Sideris, D. P.; Petrakis, N.; Katrakili, N.; Mikropoulou, D.; Gallo, A.; Ciofi-Baffoni, S.; Banci, L.; Bertini, I., & Tokatlidis, K. (2009). A novel intermembrane space-targeting

signal docks cysteines onto Mia40 during mitochondrial oxidative folding. *The Journal of Cell Biology*, *187*(7), 1007–1022. https://doi.org/10.1083/jcb.200905134

Sloper-Mould, K. E.; Jemc, J. C.; Pickart, C. M., & Hicke, L. (2001). Distinct functional surface regions on ubiquitin. *Journal of Biological Chemistry*, *276*(32), 30483–30489. https://doi.org/10.1074/jbc.M103248200

Sobhian, B.; Shao, G.; Lilli, D. R.; Culhane, A. C.; Moreau, L. A.; Xia, B.; Livingston, D. M., & Greenberg, R. A. (2007). Rap80 targets BRCA1 to specific ubiquitin structures at DNA damage sites. *Science*, *316*(5828), 1198–1202. https://doi.org/10.1126/science.1139516

Sokhi, S.; Lewis, C. W.; Bukhari, A. B.; Hadfield, J.; Xiao, E. J.; Fung, J.; Yoon, Y. J.; Hsu, W.-H.; Gamper, A. M., & Chan, G. K. (2023). Myt1 overexpression mediates resistance to cell cycle and DNA damage checkpoint kinase inhibitors. *Frontiers in Cell and Developmental Biology*, *11*, 1270542. https://doi.org/10.3389/fcell.2023.1270542

Song, J [Jihe]; Han, B.; Du, X.; Chen, H [Hongping]; Li, M.; Tang, Z [Zhanbin]; Xu, C.; Wei, W [Wan]; Jia, F.; Wang, X [Xinrui]; Sun, S [Shuanghong], & Di Zhong (2025). Ubiquitination of ALOX15 regulates endoplasmic reticulum stress in Schwann cells and experimental autoimmune neuritis (EAN) models. *Free Radical Biology & Medicine*, *234*, 141–150. https://doi.org/10.1016/j.freeradbiomed.2025.04.018

Soubannier, V.; McLelland, G.-L.; Zunino, R.; Braschi, E.; Rippstein, P.; Fon, E. A., & McBride, H. M. (2012). A vesicular transport pathway shuttles cargo from mitochondria to lysosomes. *Current Biology : CB*, *22*(2), 135–141. https://doi.org/10.1016/j.cub.2011.11.057

Soubannier, V.; Rippstein, P.; Kaufman, B. A.; Shoubridge, E. A., & McBride, H. M. (2012). Reconstitution of mitochondria derived vesicle formation demonstrates selective enrichment of oxidized cargo. *PloS One*, *7*(12), e52830. https://doi.org/10.1371/journal.pone.0052830

Sperka-Gottlieb, C. D.; Hermetter, A.; Paltauf, F., & Daum, G. (1988). Lipid topology and physical properties of the outer mitochondrial membrane of the yeast, Saccharomyces cerevisiae. *Biochimica Et Biophysica Acta*, *946*(2), 227–234. https://doi.org/10.1016/0005-2736(88)90397-5

Srinivasan, V.; Soliymani, R.; Ivanova, L.; Eriksson, O.; Peitsaro, N.; Lalowski, M.; Karelson, M., & Lindholm, D. (2025). Usp14 is crucial for proteostasis regulation and α-synuclein degradation in human SH-SY5Y dopaminergic cells. *Heliyon*, *11*(3), e42031. https://doi.org/10.1016/j.heliyon.2025.e42031

Appendix

Stefansson, O. A., & Esteller, M. (2012). Brca1 as a tumor suppressor linked to the regulation of epigenetic states: Keeping oncomiRs under control. *Breast Cancer Research : BCR*, *14*(2), 304. https://doi.org/10.1186/bcr3119

Su, J.; Liu, D [Desheng]; Yang, F.; Zuo, M.-Q.; Li, C [Chang]; Dong, M.-Q.; Sun, S [Shan], & Sui, S.-F. (2022). Structural basis of Tom20 and Tom22 cytosolic domains as the human TOM complex receptors. *Proceedings of the National Academy of Sciences of the United States of America*, *119*(26), e2200158119. https://doi.org/10.1073/pnas.2200158119

Sung, H.-M.; Schott, J.; Boss, P.; Lehmann, J. A.; Hardt, M. R.; Lindner, D.; Messens, J.; Bogeski, I.; Ohler, U., & Stoecklin, G. (2023). Stress-induced nuclear speckle reorganization is linked to activation of immediate early gene splicing. *The Journal of Cell Biology*, *222*(12). https://doi.org/10.1083/jcb.202111151

Suomalainen, A., & Nunnari, J. (2024). Mitochondria at the crossroads of health and disease. *Cell*, *187*(11), 2601–2627. https://doi.org/10.1016/j.cell.2024.04.037

Suryo Rahmanto, A.; Blum, C. J.; Scalera, C.; Heidelberger, J. B.; Mesitov, M.; Horn-Ghetko, D.; Gräf, J. F.; Mikicic, I.; Hobrecht, R.; Orekhova, A.; Ostermaier, M.; Ebersberger, S.; Möckel, M. M.; Krapoth, N.; Da Silva Fernandes, N.; Mizi, A.; Zhu, Y [Yajie]; Chen, J.-X.; Choudhary, C., . . . Beli, P. (2023). K6-linked ubiquitylation marks formaldehyde-induced RNA-protein crosslinks for resolution. *Molecular Cell*, *83*(23), 4272-4289.e10. https://doi.org/10.1016/j.molcel.2023.10.011

Swatek, K. N., & Komander, D. (2016). Ubiquitin modifications. *Cell Research*, *26*(4), 399–422. https://doi.org/10.1038/cr.2016.39

Sy, S. M. H.; Huen, M. S. Y., & Chen, J [Junjie] (2009). Palb2 is an integral component of the BRCA complex required for homologous recombination repair. *Proceedings of the National Academy of Sciences*, *106*(17), 7155–7160. https://doi.org/10.1073/pnas.0811159106

Tang, J. X.; Thompson, K.; Taylor, R. W., & Oláhová, M. (2020). Mitochondrial OXPHOS Biogenesis: Co-Regulation of Protein Synthesis, Import, and Assembly Pathways. *International Journal of Molecular Sciences*, *21*(11). https://doi.org/10.3390/ijms21113820

Terešak, P.; Lapao, A.; Subic, N.; Boya, P.; Elazar, Z., & Simonsen, A. (2022). Regulation of PRKN-independent mitophagy. *Autophagy*, *18*(1), 24–39. https://doi.org/10.1080/15548627.2021.1888244

Thrower, J. S.; Hoffman, L.; Rechsteiner, M., & Pickart, C. M. (2000). Recognition of the polyubiquitin proteolytic signal. *The EMBO Journal*, *19*(1), 94–102. https://doi.org/10.1093/emboj/19.1.94

Timper, K.; Paeger, L.; Sánchez-Lasheras, C.; Varela, L.; Jais, A.; Nolte, H.; Vogt, M. C.; Hausen, A. C.; Heilinger, C.; Evers, N.; Pospisilik, J. A.; Penninger, J. M.; Taylor, E. B.; Horvath, T. L.; Kloppenburg, P., & Brüning, J. C. (2018). Mild Impairment of Mitochondrial OXPHOS Promotes Fatty Acid Utilization in POMC Neurons and Improves Glucose Homeostasis in Obesity. *Cell Reports*, *25*(2), 383-397.e10. https://doi.org/10.1016/j.celrep.2018.09.034

Tomar, D.; Prajapati, P.; Lavie, J.; Singh, K.; Lakshmi, S.; Bhatelia, K.; Roy, M.; Singh, R [Rochika]; Bénard, G., & Singh, R [Rajesh] (2015). Trim4; a novel mitochondrial interacting RING E3 ligase, sensitizes the cells to hydrogen peroxide (H2O2) induced cell death. *Free Radical Biology & Medicine*, *89*, 1036–1048. https://doi.org/10.1016/j.freeradbiomed.2015.10.425

Tong, Z.; Wu, X.; Cai, H.; Wu, S.; Zhang, T [Tianyi]; Deng, Z [Zhiheng]; Xu, Z [Ziyu]; Yuan, R.; Ai, H.; Liu, L., & Pan, M. (2025). Structural basis for E4 enzyme Ufd2-catalyzed K48/K29 branched ubiquitin chains. *Nature Chemical Biology.* Advance online publication. https://doi.org/10.1038/s41589-025-01985-2

Tracz, M., & Bialek, W. (2021). Beyond K48 and K63: Non-canonical protein ubiquitination. *Cellular & Molecular Biology Letters*, *26*(1), 1. https://doi.org/10.1186/s11658-020-00245-6

Truscott, K. N [K. N.]; Kovermann, P.; Geissler, A [A.]; Merlin, A.; Meijer, M.; Driessen, A. J.; Rassow, J.; Pfanner, N [N.], & Wagner, R. (2001). A presequence- and voltage-sensitive channel of the mitochondrial preprotein translocase formed by Tim23. *Nature Structural Biology*, *8*(12), 1074–1082. https://doi.org/10.1038/nsb726

Tucker, K., & Park, E. (2019). Cryo-EM structure of the mitochondrial protein-import channel TOM complex at near-atomic resolution. *Nature Structural & Molecular Biology*, *26*(12), 1158–1166. https://doi.org/10.1038/s41594-019-0339-2

Uoselis, L.; Nguyen, T. N [Thanh Ngoc], & Lazarou, M. (2023). Mitochondrial degradation: Mitophagy and beyond. *Molecular Cell*, *83*(19), 3404–3420. https://doi.org/10.1016/j.molcel.2023.08.021

Utsugi, Y.; Nishimura, K.; Yamanaka, S.; Nishino, K.; Kosako, H.; Sawasaki, T.; Shigemori, H.; Wandless, T. J., & Miyamae, Y. (2024). Ubiquitin-Derived Fragment as a Peptide Linker for the Efficient Cleavage of a Target Protein from a Degron. *ACS Chemical Biology*, *19*(2), 497–505. https://doi.org/10.1021/acschembio.3c00670

Vakifahmetoglu-Norberg, H.; Ouchida, A. T., & Norberg, E. (2017). The role of mitochondria in metabolism and cell death. *Biochemical and Biophysical Research Communications*, *482*(3), 426–431. https://doi.org/10.1016/j.bbrc.2016.11.088

Appendix

Valenti, D., & Vacca, R. A. (2022). Primary and Secondary Mitochondrial Diseases: Etiologies and Therapeutic Strategies. *Journal of Clinical Medicine*, *11*(14). https://doi.org/10.3390/jcm11144209

Valkevich, E. M.; Sanchez, N. A.; Ge, Y., & Strieter, E. R [Eric R.] (2014). Middle-down mass spectrometry enables characterization of branched ubiquitin chains. *Biochemistry*, *53*(30), 4979–4989. https://doi.org/10.1021/bi5006305

van der Laan, M.; Wiedemann, N [Nils]; Mick, D. U.; Guiard, B [Bernard]; Rehling, P., & Pfanner, N [Nikolaus] (2006). A role for Tim21 in membrane-potential-dependent preprotein sorting in mitochondria. *Current Biology : CB*, *16*(22), 2271–2276. https://doi.org/10.1016/j.cub.2006.10.025

van Huizen, M., & Kikkert, M. (2019). The Role of Atypical Ubiquitin Chains in the Regulation of the Antiviral Innate Immune Response. *Frontiers in Cell and Developmental Biology*, *7*, 392. https://doi.org/10.3389/fcell.2019.00392

Varughese, J. T.; Buchanan, S. K., & Pitt, A. S. (2021). The Role of Voltage-Dependent Anion Channel in Mitochondrial Dysfunction and Human Disease. *Cells*, *10*(7). https://doi.org/10.3390/cells10071737

Vijay-Kumar, S.; Bugg, C. E., & Cook, W. J. (1987). Structure of ubiquitin refined at 1.8 A resolution. *Journal of Molecular Biology*, *194*(3), 531–544. https://doi.org/10.1016/0022-2836(87)90679-6

Voos, W [W.]; Gambill, B. D.; Guiard, B [B.]; Pfanner, N [N.], & Craig, E. A. (1993). Presequence and mature part of preproteins strongly influence the dependence of mitochondrial protein import on heat shock protein 70 in the matrix. *Journal of Cell Biology*, *123*(1), 119–126. https://doi.org/10.1083/jcb.123.1.119

Wagner, S. A.; Beli, P.; Weinert, B. T.; Nielsen, M. L.; Cox, J.; Mann, M., & Choudhary, C. (2011). A proteome-wide, quantitative survey of in vivo ubiquitylation sites reveals widespread regulatory roles. *Molecular & Cellular Proteomics : MCP*, *10*(10), M111.013284. https://doi.org/10.1074/mcp.M111.013284

Wallin, I. E. (1927). *Symbionticism and the Origin of Species*. Baillière, Tindall & Cox.

Wang, L.; Zhou, X., & Lu, T. (2025). Role of mitochondria in physiological activities, diseases, and therapy. *Molecular Biomedicine*, *6*(1), 42. https://doi.org/10.1186/s43556-025-00284-5

Wang, S [Shouliang]; Long, H.; Hou, L.; Feng, B.; Ma, Z.; Wu, Y [Ying]; Zeng, Y.; Cai, J.; Zhang, D.-W., & Zhao, G. (2023). The mitophagy pathway and its implications in human diseases. *Signal Transduction and Targeted Therapy*, *8*(1), 304. https://doi.org/10.1038/s41392-023-01503-7

Wang, Z.; Yu, C [Cheng]; Xie, G [Gengchen]; Tao, K.; Yin, Z., & Lv, Q. (2025). Usp14 inhibits mitophagy and promotes tumorigenesis and chemosensitivity through

deubiquitinating BAG4 in microsatellite instability-high colorectal cancer. *Molecular Medicine (Cambridge, Mass.)*, *31*(1), 163. https://doi.org/10.1186/s10020-025-01182-w

Warren, G. D.; Kitao, T.; Franklin, T. G.; Nguyen, J. V.; Geurink, P. P.; Kubori, T.; Nagai, H., & Pruneda, J. N. (2023). Mechanism of Lys6 poly-ubiquitin specificity by the L. Pneumophila deubiquitinase LotA. *Molecular Cell*, *83*(1), 105-120.e5. https://doi.org/10.1016/j.molcel.2022.11.022

Wauer, T.; Simicek, M.; Schubert, A., & Komander, D. (2015). Mechanism of phospho-ubiquitin-induced PARKIN activation. *Nature*, *524*(7565), 370–374. https://doi.org/10.1038/nature14879

Wegmann, S.; Meister, C.; Renz, C.; Yakoub, G.; Wollscheid, H.-P.; Takahashi, D. T.; Mikicic, I.; Beli, P., & Ulrich, H. D. (2022). Linkage reprogramming by tailor-made E3s reveals polyubiquitin chain requirements in DNA-damage bypass. *Molecular Cell*, *82*(8), 1589-1602.e5. https://doi.org/10.1016/j.molcel.2022.02.016

Weidberg, H., & Amon, A. (2018). Mitocpr-A surveillance pathway that protects mitochondria in response to protein import stress. *Science*, *360*(6385). https://doi.org/10.1126/science.aan4146

Weith, M.; Weiss, K.; Stobbe, D., & Riemer, J. (2025). The mitochondrial intermembrane space - a permanently proteostasis-challenged compartment. *Biological Chemistry*, *406*(5-7), 263–294. https://doi.org/10.1515/hsz-2025-0108

Welsh, K. A.; Bolhuis, D. L.; Nederstigt, A. E.; Boyer, J.; Temple, B. R. S.; Bonacci, T.; Gu, L.; Ordureau, A.; Harper, J. W.; Steimel, J. P.; Zhang, Q.; Emanuele, M. J.; Harrison, J. S., & Brown, N. G. (2022). Functional conservation and divergence of the helix-turn-helix motif of E2 ubiquitin-conjugating enzymes. *The EMBO Journal*, *41*(3), e108823. https://doi.org/10.15252/embj.2021108823

Wen, H.; Deng, H.; Li, B.; Chen, J [Junyu]; Zhu, J [Junye]; Zhang, X [Xian]; Yoshida, S., & Zhou, Y. (2025). Mitochondrial diseases: From molecular mechanisms to therapeutic advances. *Signal Transduction and Targeted Therapy*, *10*(1), 9. https://doi.org/10.1038/s41392-024-02044-3

Wickliffe, K. E.; Lorenz, S.; Wemmer, D. E.; Kuriyan, J., & Rape, M. (2011). The mechanism of linkage-specific ubiquitin chain elongation by a single-subunit E2. *Cell*, *144*(5), 769–781. https://doi.org/10.1016/j.cell.2011.01.035

Wickliffe, K. E.; Williamson, A.; Meyer, H.-J.; Kelly, A., & Rape, M. (2011). K11-linked ubiquitin chains as novel regulators of cell division. *Trends in Cell Biology*, *21*(11), 656–663. https://doi.org/10.1016/j.tcb.2011.08.008

Appendix

Wiedemann, N [N.]; Pfanner, N [N.], & Ryan, M. T. (2001). The three modules of ADP/ATP carrier cooperate in receptor recruitment and translocation into mitochondria. *The EMBO Journal*, *20*(5), 951–960. https://doi.org/10.1093/emboj/20.5.951

Williams, C. C.; Jan, C. H., & Weissman, J. S. (2014). Targeting and plasticity of mitochondrial proteins revealed by proximity-specific ribosome profiling. *Science*, *346*(6210), 748–751. https://doi.org/10.1126/science.1257522

Wolf, L. M.; Lambert, A. M.; Haenlin, J., & Boutros, M. (2021). Evi/wls function is regulated by ubiquitylation and is linked to ER-associated degradation by ERLIN2. *Journal of Cell Science*, *134*(16). https://doi.org/10.1242/jcs.257790

Wu, T.; Merbl, Y.; Huo, Y.; Gallop, J. L.; Tzur, A., & Kirschner, M. W. (2010). Ube2s drives elongation of K11-linked ubiquitin chains by the anaphase-promoting complex. *Proceedings of the National Academy of Sciences*, *107*(4), 1355–1360. https://doi.org/10.1073/pnas.0912802107

Xia, P.; Zhou, L [Liankui]; Guan, J.; Ding, W., & Liu, Y [Ying] (2022). Splicing factor PRP-19 regulates mitochondrial stress response. *Life Metabolism*, *1*(1), 81–93. https://doi.org/10.1093/lifemeta/loac009

Xian, H., & Liou, Y.-C. (2021). Functions of outer mitochondrial membrane proteins: Mediating the crosstalk between mitochondrial dynamics and mitophagy. *Cell Death and Differentiation*, *28*(3), 827–842. https://doi.org/10.1038/s41418-020-00657-z

Xiao, B.; Goh, J.-Y.; Xiao, L.; Xian, H.; Lim, K.-L., & Liou, Y.-C. (2017). Reactive oxygen species trigger Parkin/PINK1 pathway-dependent mitophagy by inducing mitochondrial recruitment of Parkin. *The Journal of Biological Chemistry*, *292*(40), 16697–16708. https://doi.org/10.1074/jbc.M117.787739

Xie, G [Guofeng]; Xie, Y [Yongping], & Xu, X [Xichao] (2025). Multifaceted functions of Y-box binding protein 1 in RNA methylated modifications (Review). *Molecular Medicine Reports*, *32*(6). https://doi.org/10.3892/mmr.2025.13707

Yamamoto, H.; Fukui, K.; Takahashi, H.; Kitamura, S.; Shiota, T.; Terao, K.; Uchida, M.; Esaki, M [Masatoshi]; Nishikawa, S.; Yoshihisa, T.; Yamano, K., & Endo, T [Toshiya] (2009). Roles of Tom70 in import of presequence-containing mitochondrial proteins. *The Journal of Biological Chemistry*, *284*(46), 31635–31646. https://doi.org/10.1074/jbc.M109.041756

Yamano, K.; Yatsukawa, Y.-I.; Esaki, M [Masatoshi]; Hobbs, A. E. A.; Jensen, R. E., & Endo, T [Toshiya] (2008). Tom20 and Tom22 share the common signal recognition pathway in mitochondrial protein import. *The Journal of Biological Chemistry*, *283*(7), 3799–3807. https://doi.org/10.1074/jbc.M708339200

Yan, M.; Mei, Y.; Zhang, T [Tianjun]; Liu, Z.; Su, L.; Xiao, Y [Yang]; Zhong, X., & Lu, Y. (2024). Usp7 cardiomyocyte specific knockout causes disordered mitochondrial

biogenesis and dynamics and early neonatal lethality in mice. *International Journal of Cardiology*, *408*, 132149. https://doi.org/10.1016/j.ijcard.2024.132149

Young, J. C.; Hoogenraad, N. J., & Hartl, F. U [F. Ulrich] (2003). Molecular chaperones Hsp90 and Hsp70 deliver preproteins to the mitochondrial import receptor Tom70. *Cell*, *112*(1), 41–50. https://doi.org/10.1016/s0092-8674(02)01250-3

Yu, W.; Zhuang, S.; Zhan, M.; Chen, Y [Yong]; Zhang, J [Jieping]; Chen, L [Ling]; Tu, C.; Zheng, L., & Chen, S [Shi] (2024). Deubiquitinating Enzyme USP19 Regulates Ferroptosis and Mitochondrial Damage in SH-SY5Y Cells by Targeting the NOX4 Protein. *Journal of Alzheimer's Disease : JAD*, *100*(3), 799–808. https://doi.org/10.3233/JAD-231193

Yu, Y.; Zheng, Q.; Erramilli, S. K.; Pan, M.; Park, S.; Xie, Y [Yuan]; Li, J [Jingxian]; Fei, J.; Kossiakoff, A. A.; Liu, L., & Zhao, M. (2021). K29-linked ubiquitin signaling regulates proteotoxic stress response and cell cycle. *Nature Chemical Biology*, *17*(8), 896–905. https://doi.org/10.1038/s41589-021-00823-5

Zervopoulos, S. D.; Boukouris, A. E.; Saleme, B.; Haromy, A.; Tejay, S.; Sutendra, G., & Michelakis, E. D. (2022). Mfn2-driven mitochondria-to-nucleus tethering allows a non-canonical nuclear entry pathway of the mitochondrial pyruvate dehydrogenase complex. *Molecular Cell*, *82*(5), 1066-1077.e7. https://doi.org/10.1016/j.molcel.2022.02.003

Zhang, D.; Hua, Z., & Li, Z. (2024). The role of glutamate and glutamine metabolism and related transporters in nerve cells. *CNS Neuroscience & Therapeutics*, *30*(2), e14617. https://doi.org/10.1111/cns.14617

Zhang, L [Lingxiao]; Su, N.; Luo, Y.; Chen, S [Siyin], & Zhao, T. (2021). Trap1 inhibits MIC60 ubiquitination to mitigate the injury of cardiomyocytes and protect mitochondria in extracellular acidosis. *Cell Death Discovery*, *7*(1), 389. https://doi.org/10.1038/s41420-021-00786-5

Zhang, X [Xinyu]; Fan, Y., & Tan, K. (2024). A bird's eye view of mitochondrial unfolded protein response in cancer: Mechanisms, progression and further applications. *Cell Death & Disease*, *15*(9), 667. https://doi.org/10.1038/s41419-024-07049-y

Zhu, K.; Chatrin, C.; Suskiewicz, M. J.; Aucagne, V.; Foster, B.; Kessler, B. M.; Gibbs-Seymour, I.; Ahel, D., & Ahel, I. (2024). Ubiquitylation of nucleic acids by DELTEX ubiquitin E3 ligase DTX3L. *EMBO Reports*, *25*(10), 4172–4189. https://doi.org/10.1038/s44319-024-00235-1

Zhu, Z.; Mallik, S.; Stevens, T. A.; Huang, R.; Levy, E. D., & Shan, S.-O. (2025). Principles of cotranslational mitochondrial protein import. *Cell*, *188*(20), 5605-5617.e14. https://doi.org/10.1016/j.cell.2025.07.021

Appendix

Zimorski, V.; Ku, C.; Martin, W. F., & Gould, S. B. (2014). Endosymbiotic theory for organelle origins. *Current Opinion in Microbiology*, *22*, 38–48. https://doi.org/10.1016/j.mib.2014.09.008

Zong, Y.; Li, H [Hao]; Liao, P.; Chen, L [Long]; Pan, Y.; Zheng, Y.; Zhang, C [Changqing]; Liu, D [Delin]; Zheng, M., & Gao, J [Junjie] (2024). Mitochondrial dysfunction: Mechanisms and advances in therapy. *Signal Transduction and Targeted Therapy*, *9*(1), 124. https://doi.org/10.1038/s41392-024-01839-8

Zorova, L. D.; Popkov, V. A.; Plotnikov, E. Y.; Silachev, D. N.; Pevzner, I. B.; Jankauskas, S. S.; Babenko, V. A.; Zorov, S. D.; Balakireva, A. V.; Juhaszova, M.; Sollott, S. J., & Zorov, D. B. (2018). Mitochondrial membrane potential. *Analytical Biochemistry*, *552*, 50–59. https://doi.org/10.1016/j.ab.2017.07.009

Zou, S.; Wang, B.; Yi, K.; Su, D.; Chen, Y [Yukai]; Li, N., & Geng, Q. (2024). The critical roles of STING in mitochondrial homeostasis. *Biochemical Pharmacology*, *220*, 115938. https://doi.org/10.1016/j.bcp.2023.115938

Zucchelli, S.; Codrich, M.; Marcuzzi, F.; Pinto, M.; Vilotti, S.; Biagioli, M.; Ferrer, I., & Gustincich, S. (2010). Traf6 promotes atypical ubiquitination of mutant DJ-1 and alpha-synuclein and is localized to Lewy bodies in sporadic Parkinson's disease brains. *Human Molecular Genetics*, *19*(19), 3759–3770. https://doi.org/10.1093/hmg/ddq290